UNIVERSIDADE DE SÃO PAULO
Instituto de Ciências Matemáticas e de Computação

Modeling high-dimensional time series from large scale brain networks

Diego Carvalho do Nascimento

Tese de Doutorado do Programa Interinstitucional de Pós-Graduação em Estatística (PIPGEs)

ICMC USP
SÃO CARLOS

Diego Carvalho do Nascimento

Modeling high-dimensional time series from large scale brain networks

Thesis submitted to the Institute of Mathematics and Computer Sciences – ICMC-USP and to the Department of Statistics – DEs-UFSCar – in accordance with the requirements of the Statistics Interagency Graduate Program, for the degree of Doctor in Statistics. *EXAMINATION BOARD PRESENTATION COPY*

Concentration Area: Statistics

Advisor: Prof. Dr. Francisco Louzada Neto
Co-advisor: Prof. Dr. Osvaldo Anacleto

USP – São Carlos
March 2020

Ficha catalográfica elaborada pela Biblioteca Prof. Achille Bassi
e Seção Técnica de Informática, ICMC/USP,
com os dados inseridos pelo(a) autor(a)

N244m

Nascimento, Diego Carvalho do
Modeling high-dimensional time series from large scale brain networks / Diego Carvalho do Nascimento; orientador Francisco Louzada Neto; coorientador Osvaldo Anacleto. -- São Carlos, 2020.
198 p.

Tese (Doutorado - Programa Interinstitucional de Pós-graduação em Estatística) -- Instituto de Ciências Matemáticas e de Computação, Universidade de São Paulo, 2020.

1. Multivariate Time Series. 2. Dynamic Models. 3. High-dimensional data analysis. 4. Graphical models. I. Louzada Neto, Francisco , orient. II. Anacleto, Osvaldo, coorient. III. Título.

Bibliotecários responsáveis pela estrutura de catalogação da publicação de acordo com a AACR2:
Gláucia Maria Saia Cristianini - CRB - 8/4938
Juliana de Souza Moraes - CRB - 8/6176

Diego Carvalho do Nascimento

Modelagem de séries temporais de alta dimensão a partir de redes cerebrais de larga escala

Tese apresentada ao Instituto de Ciências Matemáticas e de Computação – ICMC-USP e ao Departamento de Estatística – DEs-UFSCar, como parte dos requisitos para obtenção do título de Doutor em Estatística – Programa Interinstitucional de Pós-Graduação em Estatística. *EXEMPLAR DE DEFESA*

Área de Concentração: Estatística

Orientador: Prof. Dr. Francisco Louzada Neto
Coorientador: Prof. Dr. Osvaldo Anacleto

USP – São Carlos
Março de 2020

This work results is dedicated first to my parents, José Deoclécio do Nascimento and Josineide Maria Carvalho do Nascimento, whom have always encouraged me to study, providing unconditional support, necessary for the success of it. Also to my sisters Daniele, Debora and Dayanne.

–

O fruto deste trabalho é dedicado primeiramente aos meus pais, José Deoclécio do Nascimento e Josineide Maria Carvalho do Nascimento, que sempre me incentivaram a estudar, fornecendo apoio incondicional, necessário para o êxito do mesmo. Bem como as minhas irmãs Daniele, Débora e Dayanne.

ACKNOWLEDGEMENTS

Ao meu mentor, Professor Dr. Francisco Louzada Neto, pelos ensinamentos transmitidos, verdadeiros momentos valiosos que levarei tanto para a vida profissional quanto pessoal. Assim, possibilitando que o meu sonho de si tornar cientista fosse realizado. Agradecimento especial a pesquisadora e professora Dra. Taiza Santos (FMRP/USP), pela sua colaboração e parceria, disponibilizando os dados que motivaram e deram origem a esta pesquisa.

A toda banca, pelas valiosas contribuições que possibilitaram a evolução deste trabalho doutoral. De uma maneira especial à professora Lilia Costa, que me auxiliou trazendo grandes debates e direcionamento ao que diz respeito a estatística aplicada à neurociência. Aos professores, pesquisadores e funcionários do Instituto de Ciências Matemáticas e de Computação (ICMC) que fazem desse lugar um ambiente propício a ciência. Ao professor Dr. Marinho Gomes de Andrade Filho sou grato pelas orientações informais, e conversas na cantina, que motivaram o início das análises deste trabalho.

Também gostaria de deixar registrado os meus sinceros agradecimentos aos amigos que o doutorado no apresentou, em especial, a Pedro Ramos, Wesley Bertoli, Camila Bolzani, Fábio Felix, Marcos Jardel e Oilson Gonzatto seja pelas horas de estudos ou parceria de pesquisas, mas especialmente (mais importante) pelos momentos compartilhados ao longo dessa difícil jornada.

Por fim, porém não menos importante, gostaria de agradecer o apoio financeiro da Coordenação de Aperfeiçoamento de Pessoal de Nível Superior (CAPES), bem como a pesquisa está sendo desenvolvida com utilização dos recursos computacionais do Centro de Ciências Matemáticas Aplicadas à Indústria (CeMEAI), financiados pela FAPESP (proc. 2013/07375-0).

"As invenções são, sobretudo,
o resultado de um trabalho de teimoso."
(Santos Dumont)

ABSTRACT

NASCIMENTO, D.C. **Modeling high-dimensional time series from large scale brain networks**. 2020. 198 p. Tese (Doutorado em Estatística – Programa Interinstitucional de Pós-Graduação em Estatística) – Instituto de Ciências Matemáticas e de Computação, Universidade de São Paulo, São Carlos – SP, 2020.

Neuroscientists have an urge to understand the effective brain connectivity, through the direction/correlation of the brain areas, using biosignals, although this task demands to consider the spatiotemporal dependence and some computational constraints. Naturally, the use of large Vector Autoregression (VARs) would be appropriated if did not present a high-dimensionality curse, where the number of parameters is vastly representative. Additionally, shrinkage either in the data or parameter spaces is not trivial towards maintaining its interpretation. Therefore, some modifications were discussed, towards the graph-based model and entropy analysis, adopting the Bayesian approach, addressed by the estimate of the human brain connectivity using electroencephalogram (EEG) signals. As a motivation, we used a study case of neurorehabilitation, regarding the manipulation of human verticality, we are using high-definition transcranial direct current stimulation (HD-tDCS) as a non-invasive modulation.

Keywords: Multivariate Time Series, Dynamic Models, High-dimensional data analysis, Graphical models.

RESUMO

NASCIMENTO, D.C. **Modelagem de séries temporais de alta dimensão a partir de redes cerebrais de larga escala**. 2020. 198 p. Tese (Doutorado em Estatística – Programa Interinstitucional de Pós-Graduação em Estatística) – Instituto de Ciências Matemáticas e de Computação, Universidade de São Paulo, São Carlos – SP, 2020.

Neste projeto focamos na necessidade de compreender sobre a conectividade cerebral, através da direção/correlação entre as áreas cerebrais, por meio de biossinais, embora essa tarefa apresente dificuldades como dependência espaço-temporal e algumas restrições computacionais. Naturalmente, o uso de *large vector autoregression* (VAR) seria apropriado se não apresentassem problema de alta dimensionalidade, onde o espaço paramétrico é largamente representativo. Além disso, o encolhimento nos espaços de dados/parâmetros não é uma tarefa trivial, essencialmente demandando mantendo interpretabilidade nos resultados. Portanto, algumas modificações foram discutidas, em relação ao modelo via gráfos e análise de entropia, adotando uma abordagem Bayesiana, motivada por estimatar a conectividade do cérebro humano usando sinais de eletroencefalograma (EEG). Assim, a motivação que este utilizou foi proveniente de um estudo de caso de neuro-reabilitação, no que se refere à manipulação da verticalidade humana, nele utilizamos a estimulação transcraniana de corrente direta de alta definição (HD-tDCS) como modulação não invasiva visando a recuperação de pacientes pós-AVC.

Palavras-chave: Séries Temporais Multivariadas, modelos dinâmicos, Dados de alta-dimensionalidade, Modelos de grafos.

LIST OF FIGURES

LIST OF TABLES

CONTENTS

CHAPTER

1

INTRODUCTION

Human brain connectivity is a complex phenomenon of substantial relevance, e.g. in neuropsychology and clinical studies of postural and vertical perception (NASCIMENTO *et al.*, in press). For instance, brain activation can be monitor under different stimulation conditions targeting some neurorehabilitation (EDWARDS, 2009), which responses may varies within participants (LIAO *et al.*, 2017; MATTAR *et al.*, 2018). Some elements may influence the brain connectivity changes, and physiological structure, such as stroke and epilepsy seizure.

Stroke is the third global leading cause of disability, and evidence-based rehabilitation intervention to improve the burden from stroke remains limited (FEIGIN *et al.*, 2014). The numbers about the problematic on the world population with stroke is 70%, whereas 87% are related with some physical disability or deaths both in low- and middle-income countries and, over the last four decades, the stroke incidence has more than doubled (JOHNSON *et al.*, 2016). The consequences are immeasurable mainly affecting individuals at the peak of their productive life, in people living in low-and middle-income countries when compared to those in high-income countries (HIC). Despite its enormous impact on the socioeconomic conjuncture of developing countries, this rising crisis has received very little attention to date.

One silent but critical symptom after stroke for which there is no present treatment and is observed in more than half of stroke survivors, is the visual vertical disorder that can occur with lesions in either hemisphere. Since vertical alignment in relation to gravitational forces is required for most of daily activities, the impact on functionality of vertical disorders is devastating (JOHNSTON; MENDIS; MATHERS, 2009). Generally, the error in the perception of visual vertical is tilted to the contralesional side (coronal plane) leading to postural imbalance and higher risk of falls after supratentorial lesions. Reduced visual vertical disorder is associated with better clinical function. Yet to date, there are no methods to therapeutically improve this highly prevalent disorder.

In this manner, this work is part of the Transcranial Electrical Stimulation (TES) research

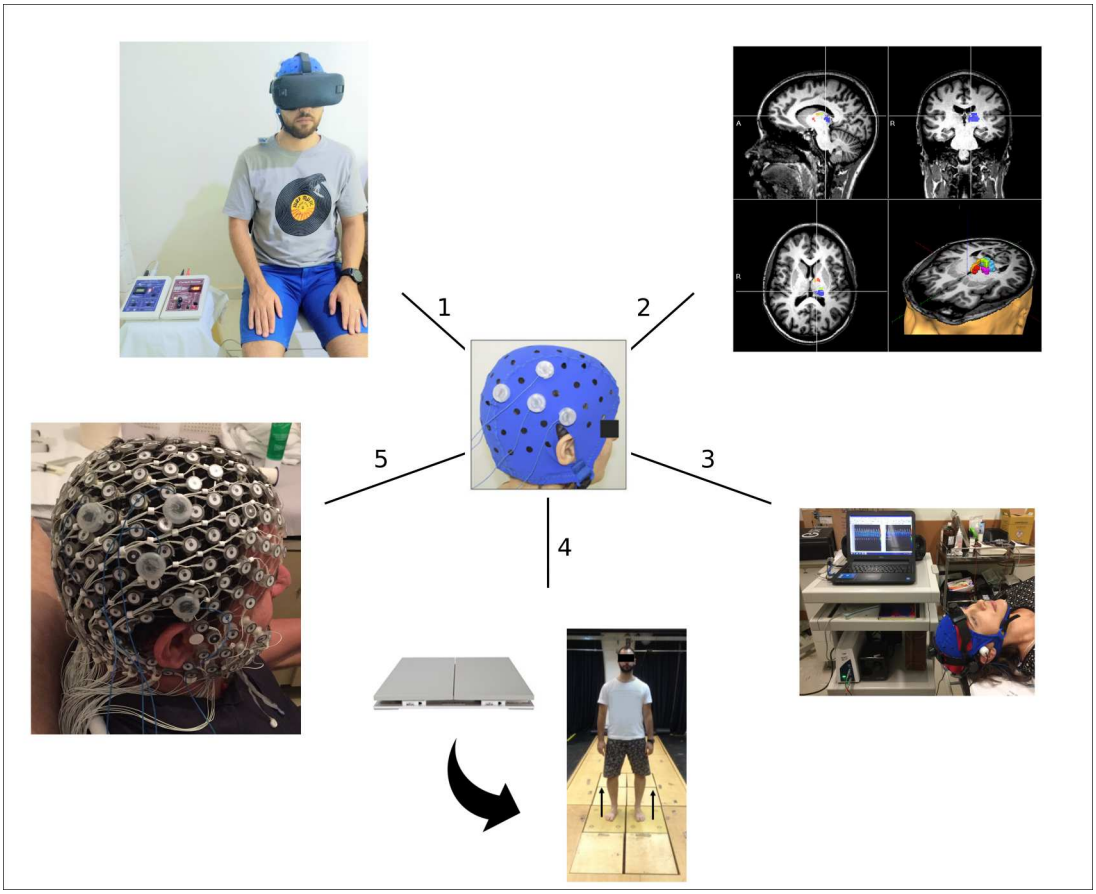

Figure 1 – Visual vertical disorder neurorehabilitation project. Five ongoing studies; (Clockwise) 1.Error in perception visual vertical (EPVV), 2.Diffusion tensor imaging (DTI), 3.Doppler (MCA-CBFv), 4.Weight-bearing asymmetry (WBA), and 5.Electroencephalography (EEG).

trials project which aims to develop a non-invasive post-stroke treatment. Figure 1 describes the five ongoing clinical studies, related to the TES project, (Error in perception visual vertical (EPVV), Diffusion tensor imaging (DTI), Doppler (MCA-CBFv), Weight-bearing asymmetry (WBA), and Electroencephalography (EEG)). TES activation may impacts on the connectivity of the region implying on activities of daily living, physical and cognitive functioning, in people. Wherein each experiment deals with great, and different, data complexity (e.g. high-dimensional multivariate time series and longitudinal data), bringing relevant contributions to the neuroscience/medical field and statistics as well.

Thereby, this dissertation aimed to test and develop new statistical approaches, facing a Big Data problematic (given the equipment's high resolution), moreover, addressed by the estimate the human brain connectivity using only the electroencephalogram (EEG) signals. As a motivation, we used a study case of neurorehabilitation, regarding the manipulation of human verticality, we are using high-definition transcranial direct current stimulation (HD-tDCS) as a non-invasive modulation.

This work intends to analyze some class of statistical models, related with multivariate time series analysis, using entropy and graph-based models. Such methods are capable of estimate

complexity and network topology (from their structure up to dynamic), in order make feasible the estimation process considering the space-time dependencies; that is, i) To compare different approach, for EEG signal data, pre-existed in the time series theory, and ii) To present the Bayesian Dynamic Graphical and Dynamic Chain Graph models, as an extension of the vector autoregressive models, incorporating mixed/random effects with dynamic graphical structure, aiming to compare the conditions and structural relations (effective and functional connectivity).

Therefore, the study experimentation was motivated stems from the dynamic brain communication behavior, whereas we were targeting the vertical perception manipulation for later to be applied on the recovery of patients with stroke records (SANTOS *et al.*, 2018), using a non-invasive promising method in the neuroscience field (ZHOU *et al.*, 2014; BABYAR *et al.*, 2016). In this manner, it is important to analyze a large number of time series, and its dependence, estimating not only the effects on an individual, but the common impact and connectivity of the applied condition.

Entropy analysis is a measurement of the complexity and may identify intervention-related change as a useful "summary" statistic in non-linear dynamical systems (NASCIMENTO *et al.*, 2019). In addition, dynamical graph helps understanding human brain' dynamic, which could provide hints about disorder, related with brain activity, therefore suggesting some types of localized stimulation as treatment (RUBIN *et al.*, 1991; PAAKKI *et al.*, 2010; COSTA *et al.*, 2017).

Modeling high-dimensional graphical time series present a limitation, like the Bayesian Network, by suppressing its temporal links evolution, in the process of estimating networks or graphs (important for understanding brain connectivity) (COSTA *et al.*, 2017). Nonetheless, there are some existent methods regarding the networks structure, but usually they are based on strong assumptions towards the observed series, for instance *vector autoregressive* or *multiregression dynamic* models (FIECAS; OMBAO, 2011; GORROSTIETA *et al.*, 2012; PRADO; WEST; KRYSTAL, 2001; GRUBER; WEST, 2017). In this case, the need arises to develop methods capable of estimating connectivity while allowing the inclusion of the dynamics of brain activity, affected by the different conditions of the experiment.

1.1 Research goals and main results

Therefore, this project was motivated by the data analysis given the ever-increasing need for developing statistical novel for analyzing high-dimensional brain activity data, motivated by a large-scale experiment related with post-stroke recovery.

- Analyze the complexity of the brain network, by discussing entropy measure and maximum likelihood estimation, aiming to summarize Time Series as complexity values.
- Analyze the brain connectivity dynamic, using a Dynamic Graphical Model, under the

Bayesian paradigm which combines with the Hamiltonian Monte Carlo. Moreover, it was extend the Multiregression Dynamic Model (MDM) with its hierarchical version.

- Compare some alternatives towards graph-based structure estimation.
- Developed a new distribution called Inverse Nakagami-m (INK) distribution.
- Propose an alternative towards the threshold tolerance for accepting similar patterns between two subsequences of the Approximate Entropy parameter (r).
- Propose an extension for the Symbolic Data Analysis, regarding interval data, as a dynamic regression approach.
- Analyze susceptible of sparse dynamic models and filtering decomposition, combined with multiplex network, towards EEG signal.
- Analyze the acquired EEG data from the protocol (SANTOS *et al.*, 2018), used in health participant, towards vertical manipulation perception. Then, this therapeutic method may be proposed as a post-stroke treatment.

In this manner, this project targets to analyze the stimulation protocol results aiming, as a next step, to propose a non-invasive method towards the post-Stroke verticality recovery. That is, this study Phase #1 analyzed different dose-responses reactions on young health participants, using a neuromodulation, seeking to understand better its electrical dynamic given a brain stimulation.

1.2 Thesis Organization

This dissertation is a result of seven separate works, as describes Figure 2, that is, five as chapters and one as appendix.

Chapter 2 presents the article published at *Brain Science Journal* which discuss the high-dimensionality of the data, through its complexity, work entitle as "Entropy analysis of High-definition transcranial electric stimulation effects on EEG dynamics".

Chapter 3 relates with a new methodological contribution, computational efficiency (using the Hamiltonian Monte Carlo (HMC)) and improvement of the existent MDM such as its hierarchical version, as "Bayesian Dynamic Graphical Models: Analyzing brainwave data from fixed parameters to hierarchical design". Then, later an other chapter 4 extend the understanding of Bayesian Network structural estimation and numerical approximation for Bayesian inference towards MDM, as "Brain Graph Complexity: Revealing common cerebral waves pattern".

Chapter 5 is a published article, at *Information Sciences*, called "Dynamic Time Series Smoothing for Symbolic Interval Data applied to Neuroscience", focus in the reduction of the

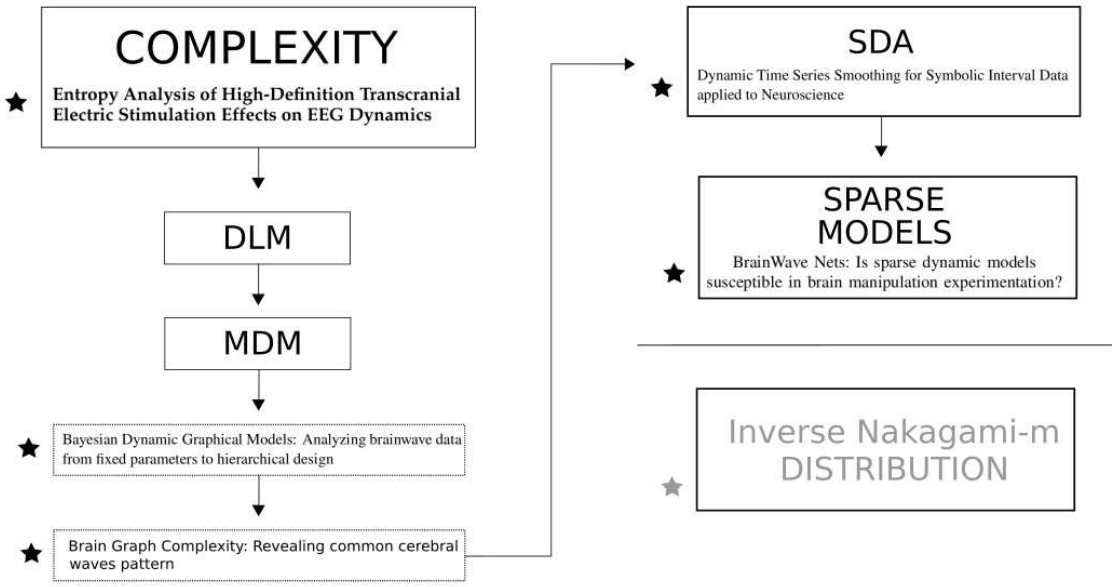

Figure 2 – Thesis scope. The preface/organization of the thesis, as a chart-flow, where each star represents a developed article.

data dimension using Symbolic Data Analysis (SDA) methodology – Lower-upper intervals e Center & range – which enhance a new methodological version using dynamic models.

Chapter 6 is an article, named "BrainWave Nets: Are sparse dynamic models susceptible to brain manipulation experimentation?", that presents the need of filtering process in EEG data, combined with multiplex network and its structure estimation, imposing sparsity in the dynamic model, and comparing different existent models in order to reduce the amount of false-positive link estimation.

Lastly, Chapter 7 presents this work discussion and conclusion, as well the future steps of this research. The appendix A presented the developed Inverse Nakagami-m distribution, published at IEEE Transaction in Reliability.

CHAPTER

2

ENTROPY ANALYSIS OF HIGH-DEFINITION TRANSCRANIAL ELECTRIC STIMULATION EFFECTS ON EEG DYNAMICS

This chapter corresponds to a manuscript published at *Brain Sciences* journal, in which presents the discussion towards complexity analysis, using entropy as a measure, upon EEG signal data. This work had as co-authors: Gabriela Depetri (Google Enterprise, Ireland), Luiz H Stefano (FMRP-USP, Brazil), Osvaldo Anacleto (ICMC-USP, Brazil), Joao P Leite (FMRP-USP, Brazil), Dylan Edwards (MOSS, USA and Edith Cowan University, Australia), Taiza E G Santos (FMRP-USP, Brazil), Francisco Louzada (ICMC-USP, Brazil).

Within the medical field it is standard practice to use the statistical mean as a summary statistic for observed time series (a common sight in the field) and then perform standard statistical tests. However, this procedure relies on the assumption that the analyzed time series are stationary, which often is not the case. This chapter follows an improved approach to the summary statistic in the context of Neuroscience, and discusses the use of entropy as a measurement of complexity of time series due to the non-stationary characteristic of the data. To elucidate our discussion, we use entropy to analyze recorded data from EEG signals, analyzing by statistics for difference aiming to establish a safe and effective protocol to address human verticality through the application of non-invasive brain stimulation.

2.1 Introduction

Following Prigogine (PRIGOGINE, 1987), entropy is a measurement of complexity, among time series or signal data, which associates the amount of information to a probability distribution. Prior to the 1990s, given computational technological constraints, early entropy measure calculations were neglected because they required a great amount of data (PINCUS,

1991; RICHMAN; MOORMAN, 2000).

Time series data could be defined as oriented data in time. An illustrative example of entropy can be expressed by two simple time series. The first one is perfectly regular, alternating between 0 and 1, such as 0,1,0,1,0,1,0,1,0,1,..., whereas the second one is constructed by randomly drawing 0 and 1 with probability $1/2$ each, for example 0,1,0,0,1,1,0,1,1,1,0,1,0,1,1,0,.... In this example, moments of this example such as mean and standard deviation will not distinguish them: both series have mean and deviation equal to 1/2. However, the first one is a periodic time series, while the second one is not, this exemplification was inspired in Pincus (PINCUS; GLADSTONE; EHRENKRANZ, 1991).

In the medical field, most of the data that is acquired as time series is modeled through its mean (may also be complemented with its variance) that enables the application of the usual statistical methods. According to the definition of a stationary process relies on the unconditional joint probability distribution time-invariant. Therefore, stationarity is required in order to get a good summarization of a process via its mean, and this often is not the case in real data with temporal dependence.

Statistical analyses of time series require methods to incorporate the description of all moments associated with the process, with the purpose of differing regularity from chaos in data. Entropy has been used to describe the changes in gene expression (HEINTZMAN *et al.*, 2009), cardiac signals (PINCUS; GLADSTONE; EHRENKRANZ, 1991), postural control sway (YENTES *et al.*, 2018), blood oximetry (BHOGAL; MANI, 2017), and to characterize epileptic seizure using electroencephalographic (EEG) data (CUESTA-FRAU *et al.*, 2017), however, much more could be explored using complex outcome measures.

The objective of the present study was to apply a robust methodology into a biological data set considering its complex structure in the statistical estimation processes. Given the nature of the EEG (or any brain waveform) data, where its known that electrical connections are present, it would be natural to describe it in entropy form.

However, this work innovates in the sense of combine the right entropy with the appropriate statistical analysis, mixed effects models, due a presence of unobserved variables. This work is divided into two parts, the statistical robustness discussion, and the clinical gain by its adoption.

The data set analyzed in the current study was originated from a randomized double blinded sham controlled clinical trial that aimed to investigate a polarity and intensity-dependent shift in high-density EEG signal following an intervention using high-definition transcranial direct current stimulation applied over the temporo-parietal junction in healthy subjects (for protocol details read (SANTOS *et al.*, 2018)).

We will adopt two different statistical methods related to entropy for summarizing time series as a single number: the Kullback-Leibler (KL) divergence and the Approximate Entropy

(ApEn). Both incorporate all the generated moments of the process, and enable the use of traditional models such as regression, while the independence assumption on the observations is not violated. In this way, it is possible to compare regularity contained in data, taking into account computational feasibility, without losing valuable information. The Approximate Entropy emerged in the medical field by Pincus (PINCUS; GLADSTONE; EHRENKRANZ, 1991) as a method to discriminate biosignals events. Its first application aimed to analyze the difference between healthy and sick heartbeats in infants, through its electrocardiograms (ECGs), since it is known that sick individuals have more regular heartbeats. We now investigate its applicability in the context of Neuroscience.

2.2 Methods

The paper is organized as follows. In Section 2 we present an overview of both the experimental protocol and the concepts behind the definition of entropy. In Section 3 we use numerical simulations to establish a comparison between representing a TS process using its mean versus its entropy, in a controlled scheme. In Section 4 we apply the use of entropy to our data analysis. We aim at an efficient summarization of our TS, using a hierarchical model to distinguish between stimulation types versus intensity, as well as quantifying the differences in regularity among them. Finally, some concluding comments are given in Section 5.

2.3 Background Theory

The Kullback-Leibler (KL) divergence is the most commonly presented in statistics, and the Approximate Entropy (ApEn), useful in the case of non-stationary Time Series. This application is experimental neurology makes use of an established technique of transcranial stimulation (NASSERI; NITSCHE; EKHTIARI, 2015), which has been a powerful experimental tool over the last two decades, although there are there are few reproduced studies reported in the literature. Therefore our research findings are perhaps the first in vertical perception, using electrical stimulation to generate a ‘virtual lesion’, corroborating with proving the protocol presented in (SANTOS *et al.*, 2018) as a safe procedure.

2.3.1 Experimental rationale

The data acquisition belongs from a novel approach to systematically analyze the dose-response effects of a focal electrical stimulation, concerning around the dynamic of the brain connectivity outcome. The study protocol centered the stimulations over the right *TemporoParietal Junction*, as shown Figure 41, in healthy subjects, based on prior results that postural perception could be manipulated (SANTOS-PONTELLI *et al.*, 2016), which is of primary

clinical importance in adult falls and post-stroke recovery (PÉRENNOU, 2006; BONAN *et al.*, 2007), and thus has potential clinical utility.

Figure 3 – Left image represents the tDCS (dark blue dots) and EEG channels (light blue dots). Right image presents the stimulated area highlighted in red.

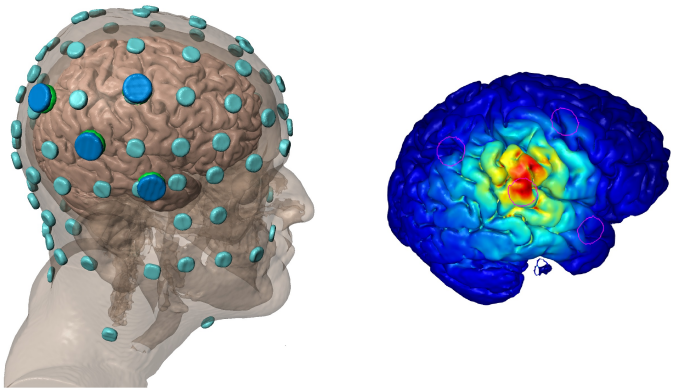

The systems' imbalance and degeneration related to postural control, lead new research towards their origin and pathophysiology (WINTER, 1995). The different sensory information is used as pathways in the brain to posture maintain upright position (DAY; COLE, 2002). Thus, the postural imbalance is one of the most common findings found after stroke (BAGGIO *et al.*, 2016; CHERN *et al.*, 2010). However, increasing knowledge about the effects of this strategy is essential for the development of more effective rehabilitation protocols.

Transcranial direct current electrical stimulation protocols were suggested to influence changes in postural control also in post-stroke patients (BABYAR *et al.*, 2016; ZHOU *et al.*, 2014). However, even with current evidence and decades of experimentation on transcranial direct current stimulation, few protocols have achieved robust scientific acceptance. Therefore, it is essential to investigate the dose-response effects of brain stimulation in order to devise more effective protocols for rehabilitation.

In this manner, the experimentation submitted each patient to three trials, which included a distinctive sample population naive and blind. In this first phase, the studied candidates were healthy subjects with no evidence of brain, nor balance dysfunction. The trial included seven healthy right-handed subjects, mean age 34.7 ± 7.6 years, four men. The experimentation was conducted in a seated position, participants received three electrical stimulation conditions (anode center, cathode center, and sham) on three different days, with an interval of at least 24 hours.

Noninvasive techniques of brain stimulation are current therapeutic resources related to the pathophysiology and behavior of the mechanisms that guide the human mind. In the field of neuroscience, the clinical application of these tools has gained greater repercussion in the last two decades, resulting in an eventual increase in the number of studies and clinical trials in this area (ROSSINI; ROSSI, 2007; ROSSI *et al.*, 2009). Several studies have indicated the therapeutic efficacy of the use of non-invasive stimulus in psychiatric, neurological, and motor

disorders (BRUNONI *et al.*, 2012; BASHIR *et al.*, 2010; SIEBNER *et al.*, 2009).

Dense array EEG was assessed with electrical stimulation conditions and was acquired using a 256-channel sensor net, from Electrical Geodesics Inc, with a sampling frequency of 500Hz (observation points per second). All channels were referenced to the vertex with electrical impedance reduced. The EEG was recorded continuously before and after the stimulation, including ramp-up and ramp-down periods, lasting in total between 120 minutes.

To-date, only two studies are reporting the dose-response effects of electrical stimulation in human adults (SHEKHAWAT *et al.*, 2016; CASTILLO-SAAVEDRA *et al.*, 2016). The crossover trial of (SHEKHAWAT *et al.*, 2016) investigated 1mA and 2mA applied for 10 and 20 minutes, applied over the left temporoparietal area or the dorsolateral prefrontal region in patients with tinnitus; describing positive effects of both intensities and most effective tinnitus relief after 2mA for 20 minutes.

2.3.1.1 Transcranial direct current electrical stimulation

Transcranial direct current electrical stimulation(TDCS) is a non-invasive neuromodulation technique that allows modeling the cerebral function with a safe profile. Consists of electrodes unleashing weak electrical current in the scalp, inducing cortical changes: It rises or lowers the neuronal membrane potential activation depending on the electrical current polarity.

The idea of applying electrical current for modulate brain function dates from the classical era when the Roman physician Scribonius Largus recommended the application of a living electric torpedo fish in his patients head for treat ”melancholia” (KELLAWAY, 1946).

Back to at least 200 years, Giovani Aldini used rudimentary batteries with a constant voltage applied in the head of people with personality disorders, with good reported results (PARENT, 2004).

Over the 20th century, direct voltage studies remain with less new researches until the remarkable studies of (NITSCHE; PAULUS, 2000) and (PRIORI *et al.*, 1998) who demonstrated changes in cortical response to transcranial magnetic stimulation using weak direct current stimulation, thereby indicating that TDCS could change neuronal membrane excitability: cathodal stimulation induces a decrease in cortical excitability, whereas anodal stimulation induces an increase in cortical excitability. This lead to new protocols in high definition transcranial direct current stimulation(HD-tDCS), allowing a more specific activation area with less adverse effects.

2.3.1.2 Neurophysiology background

At the neuronal level, HD-tDCS promotes a polarization of the rest membrane potential as mentioned above, and this effect is responsible for the acute effects of tDCS in cortical excitability (PRIORI *et al.*, 1998). Other mechanisms also contribute to modifying the electrical neuronal

membrane potential and maintenance of membrane changes at least one hour (NITSCHE *et al.*, 2003).

They consist of a modification of the synaptic microenvironment, changing GABAergic activity or altering synaptic strength NMDA receptor-dependently. It seems that the excitatory effects of anodal TDCS are mediated at least in part by the reduction of GABAergic inhibition in addition to an NMDA receptor-dependency, while the inhibitory effects of cathodal are mediated by a reduction in excitatory glutamatergic neurotransmission (LIEBETANZ *et al.*, 2002; STAGG *et al.*, 2009). Studies with peripheral nerve and spinal cord stimulation showed that direct current effects are also non-synaptic, with transient changes in the density of protein channels below the stimulation area (ARDOLINO *et al.*, 2005; COGIAMANIAN *et al.*, 2008).

In addition to this tDCS direct effects, "indirect" effects come from connective-driven alterations of distant cortical and sub-cortical areas (BRUNONI *et al.*, 2012). Lang and others (LANG *et al.*, 2005) revealed that stimulating the right frontopolar cortex (M1) with tDCS also activate several connected areas. They assessed the changes in brain activity after the TDCS session measuring regional cerebral blood flow, with sequential H152O PET scan. Besides, under the area of the stimulus, that is, several motor areas such as the caudal portion of the anterior cingulate cortex, cerebellum and superior temporal sulcus, were activated. Maybe in part, due to a modulation of the functional interaction between M1 and these areas via cortico-cortical and cortico-subcortical connections.

Other studies using transcranial magnetic stimulation (TMS) describes the increased activity of the homologous area, contralateral to the stimuli (SIEBNER *et al.*, 2000; LEE *et al.*, 2003). The last reduction in left can explain it to the right transcallosal inhibition between the two cortices (GILIO *et al.*, 2003; PLEWNIA; LOTZE; GERLOFF, 2003).

These "indirect" changes on cerebral function are fundamental issues regarding the objective of the present study, that evaluated the effects of TDCS in the temporoparietal junction, the area related to postural control in humans"[29]". Inter-hemispheric interactions may contribute to defining the temporal and spatial features of voluntary movements and consequently, postural control (MEYER; RÖRICHT; WOICIECHOWSKY, 1998). There is a balance between these inter-hemispheric interactions, where each human cortex exerts inhibitory influences on the opposite motor cortex in normal conditions (FERBERT *et al.*, 1992).

Lesions of the corpus callosum, a structure that links homonymous areas of both cerebral hemispheres, results in impaired coordination and deficits of inter-hemispheric inhibition (MEYER; RÖRICHT; WOICIECHOWSKY, 1998). The inter-hemispheric inhibition is also affected by unilateral hemispheric lesions, like a stroke, leading to increased excitability of the opposite intact cortex (LIEPERT; HAMZEI; WEILLER, 2000). Thus, develop non-invasive techniques that modulate this balance will be a significant advance in the rehabilitation setting of stroke patients and other postural control disorders, after more profound knowledge of these techniques effects on the human brain.

2.3.1.3 Stimulation Protocol

In the present study was applied the HD-tDCS with the modulation montage in the right temporoparietal junction area, as reported above. A Soterix® NY-USA HD-tDCS was used, with a constant current from the anode to cathode. There were 3 stimulation conditions: 1- anode center, 2- cathode center, and 3- Sham, where each subject was stimulated with one condition at a time, on an interval at least 24 hours between the sessions.

Four electrodes were fixed with a Soterix® cap, and the central electrode was placed over the circumcenter of the EEG coordinates. The three peripheries electrodes were placed at a distance of 3 centimeters from the central electrode. After the electrodes positioning, an accommodation was made, with the intensity of stimulation varying from 1 to 3mA and then initiated the stimulation with 1, 2 and 3mA. At the same time, an EEG recording was made, allowing detect ongoing changes on the raw EEG in response to tDCS. The total duration of each session was about 120 minutes.

2.3.2 Entropy Background

As an alternative to analyzing and modeling the entire TS, one can use summary statistics, which could be the average of the processor, for example, some measure of its regularity. The last one is commonly used as an index to quantify the complexity of the TS, considering all of its generated moments. Let us start by discussing the relation between maximum likelihood estimation and information entropy.

Consider a random sample $X = \{X_1, \cdots, X_n\}$ of random variables, all with a common (but unknown) density $f(x|\theta_0)$. From the data, it is possible to estimate its associated unknown parameter θ, and then associate to it a density function (pdf) family (e.g., normal, gamma, beta etc.). Our goal is to estimate θ through a robust statistic T, using the data $X_1, \cdots, X_n$, that is, $\hat{\theta} = T(X_1, \cdots, X_n)$. As an illustration of a statistic we could have, for example, the sample mean, in the case the times series under analysis are stationary,

$$T(X) = \bar{X} = \frac{1}{n}\sum_{i=1}^{n} X_i.$$

Then, using the maximum likelihood estimation (MLE), one could obtain $\hat{\theta}$ as a joint density of the random sample, and using a traditional result known by the (Strong or Weak) Law of Large Numbers, we know that the sample negative log-likelihood converges to its expected value (almost surely or in quadratic mean). Moreover, by the asymptotic equipartition theorem (further details in McMillan (MCMILLAN, 1953)), this will converge to the differential entropy of X. If x denotes the sample observations, then

$$h[f(x|\theta_0)] = -E[\log f(X|\theta_0)] = -\int_{\mathbb{R}} f_X(x|\theta_0) \log f_X(x|\theta_0) dx$$

Notice that using the expectation of the parameter, does not fix θ at θ_0, and does not give us any information about the conversion of the sample negative log-likelihood, and how it should behave (the only assumption of the asymptotic equipartition theorem is related to θ_0). Therefore, adding and subtracting the log-likelihood under the true model,

$$\begin{aligned} -\frac{1}{n}\sum_{i=1}^{n}[\log f(X_i|\theta)+\log f(X_i|\theta_0)-\log f(X_i|\theta_0)] = \\ = \frac{1}{n}\sum_{i=1}^{n}\log\left[\frac{f(X_i|\theta_0)}{f(X_i|\theta)}\right]-\frac{1}{n}\sum_{i=1}^{n}\log f(X_i|\theta_0) = \\ = f(x|\theta_0,\theta)-f(x|\theta_0) \end{aligned}$$

Now the divergence of this estimator will be denoted as

$$D_{KL}(f(x|\theta_0)||f(x|\theta)) = h[f(x|\theta_0,\theta)]-h[f(x|\theta_0)]$$

where

$$D_{KL}(f(x|\theta_0)||f(x|\theta)) = \int_{\mathbb{R}} f(x|\theta_0)\log\frac{f(x|\theta_0)}{f(x|\theta)}dx$$

known as the Kullback-Leibler divergence or relative entropy between $f(x|\theta_0)$ and $f(x|\theta)$. Notice that the mean negative log-likelihood converges to the differential entropy under the true distribution plus the Kullback-Leibler divergence between the true distribution and the assumed distribution.

It is also possible to show that the Kullback-Leibler divergence is non-negative and is zero only when $f(x|\theta_0)$=$f(x|\theta)$ almost surely. Consider that to minimize the mean negative log-likelihood, implies that it is needed to choose means $\theta = \theta_0$ which minimizes this limiting function.

Moreover, after a bit of a detour through information theory, we have seen a sketch as to why Maximum Likelihood Estimation makes sense as a procedure for estimating a parameter θ. The mean negative log-likelihood converges to a non-random function, as so takes its minimum at the correct answer to our question. It is fully proving the consistency of the Maximum Likelihood Estimator it is out of this work scope.

Limitation among regularity in TS data is presented among the usage on entropy, where stationarity is also recurrently needed. Despite it, the regularity statistic suggested by Pincus (PINCUS, 1991) uses the capability to discern the changing of the complexity from such a relatively small amount of data.

Simplistically, the proposed solution to summarize the TS, in one representative statistic, is based on a recurrent calculation of conditional probabilities at the i-th time-window. The result is an average obtained from the numbers of distance superior to the filter (r), $d[x,x^*] = \max|u(a)-u^*(a)|$, therefore calculating through $C_i^m(r)$ as a relative frequency of generated vector.

Let us consider the vector u a vector of collected data, u(i) is the i-th observation of u, and x is an element of a partition as following. Considering $x(1) = \{u(1), \ldots, u(m)\}, x(2) = \{u(m+1), \ldots, u(2m)\}, \ldots, x(N-m+1) = \{u((N-m)m+1), \ldots, u((N-m+1)m)\}$.

STEP 1. Consider a TS, equally spaced in time, contained N raw data values (u), from each series. Then u(1), u(2), ..., u(N).

STEP 2. Adopt a length of compared runs of data (m), and a filtering level (r). Implying in a new vector of data x(1), x(2), ..., x($N-m+1$).

STEP 3. For each i, $1 < i < N-m+1$, to construct $C_i^m(r) = (cardinal\ d[x(i), x(j)] \leq r)/(N-m+1)$ where $i \neq j$

STEP 4. Then, $\Phi^m(r) = \sum_{i=1}^{N-m+1} \ln C_i^m(r)/(N-m+1)$

STEP 5. Calculate the average over i of ln towards conditional probability as $ApEn = \Phi^m(r) - \Phi^{m+1}(r)$

The choice towards m affects the conditional probabilities directly well achieved with between 10^m and 30^m observations. The filter level (r) suggested is at least three times the estimated mean noise amplitude. Important to point out about the consistency, even ApEn not been an absolute measure, theoretic analyses, whenever $entropy(A) \leq entropy(B)$ for noiseless systems, then $ApEn(A) \leq ApEn(B)$.

2.4 Simulation

The mean estimator could be a good statistic to summarize a collection of the observation given some mild behavior, e.g., in TS under the presence of stationarity. Although, in medical data often this is not the case. In order to illustrate a simulated case, four models were considered, as follows, which 100 simulated series of each were calculated then its mean and Approximated Entropy were estimated, considering different sample size (n) as $n = \{70, 100, 250, 500, 1000\}$. Whereas Autoregressive (AR) model and Generalized AutoRegressive Conditional Heteroskedasticity (GARCH) model.

$$
\begin{aligned}
Y_t^{(1)} &= \phi_1 Y_{t-1} + \varepsilon, \quad [AR(1)] \\
Y_t^{(2)} &= \gamma_0 + Y_t^{(1)} + \alpha_0 + \alpha_1 \varepsilon_{t-1}^2 + \beta_1 h_{t-1}^2, \quad [Inter. + AR(1) + GARCH(1,1)] \\
Y_t^{(3)} &= \gamma * t + Y_t^{(1)}, \quad [Linear\ Trend + AR(1)] \\
Y_t^{(4)} &= \frac{\gamma * t^2}{1000} + Y_t^{(1)} + \alpha_0 + \alpha_1 \varepsilon_{t-1}^2 + \beta_1 h_{t-1}^2, \quad [Quadratic\ Trend + AR(1) + GARCH(1,1)]
\end{aligned}
$$

where $\phi_1 = 0.7, 0.9$ as the autoregressive with different parameters, $\gamma_0 = 2$ as an intercept, $\gamma = 0.02, 0.2$ as parameters for the deterministic trends (linear and quadratic). The γ parameter gives the series the strength (influence) of its deterministic part.

As expected, Figure 4 shows that the mean estimator is very sensible given where the series sample was taken. Although, primarily they are all generated from the same AR(1). As the sample size grows both trends influence more on its estimation.

Figure 4 – Each figure represents a simulated scenario, with their respective parameters (in the top). Each class (color) is associated with a given model. In the x-axis shows different sample size, and y-axis the **mean** statistic.

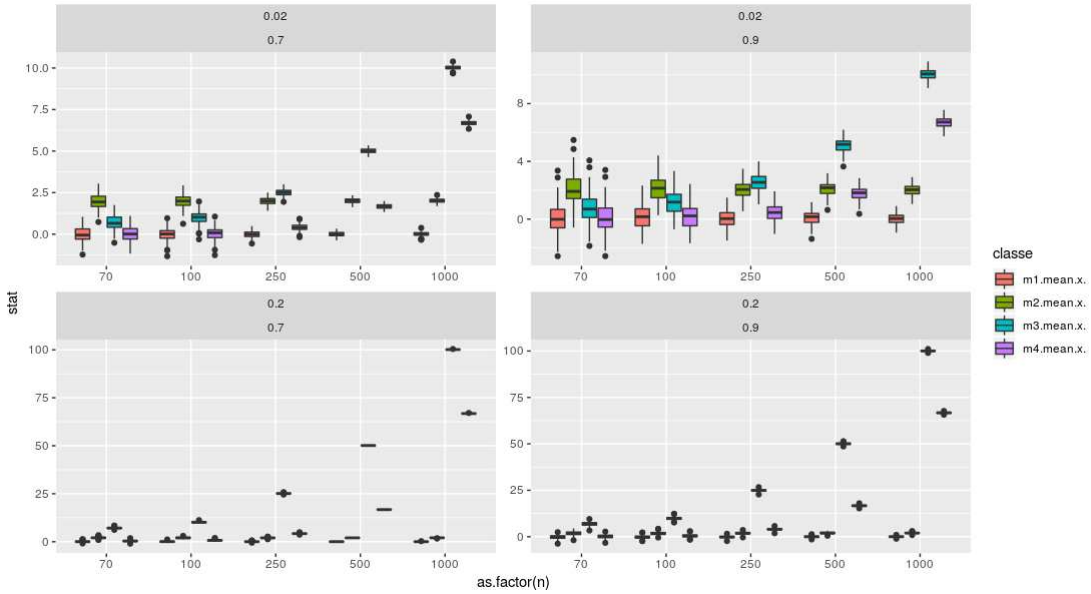

Considering the EEG montages (set), a standard methodology is to use a *common reference montage* which compare every electrode in the head against a referenced one (usually the central, Cz). Therefore, each patient will present a different unit amplitude wave, regardless of the channel, given this recording methodology uses a central channel to take an amplitude difference as a reference. Then becoming extremely sensitive to each patients' characteristic, so it can be bypassed using, for example, an Approximate Entropy.

Fixing the parameters, for the entropy calculation, considering $m = 2$ and $r = 0.2$. Figure 5 explicit the simulated scenarios. Top figures considering $\gamma = 0.02$ and $\phi_1 = 0.7,\ 0.9$ shows stability for models m3 and m4 (the ones containing deterministic part) versus m1 and m2 as the sample size grows. The bottom figures, which considered $\gamma = 0.2$, turning up describing better given the increase of the deterministic part in models 3 and 4, kept both ApEn close and in a lower range regardless of its sample size process (closer to zero, which presents a great deterministic component in the series).

Figure 5 – Each figure represents a simulated scenario, with their respective parameters (in the top). Each class (color) is associated with a given model. In the x-axis shows different sample size, and y-axis the **Approximate Entropy** statistic.

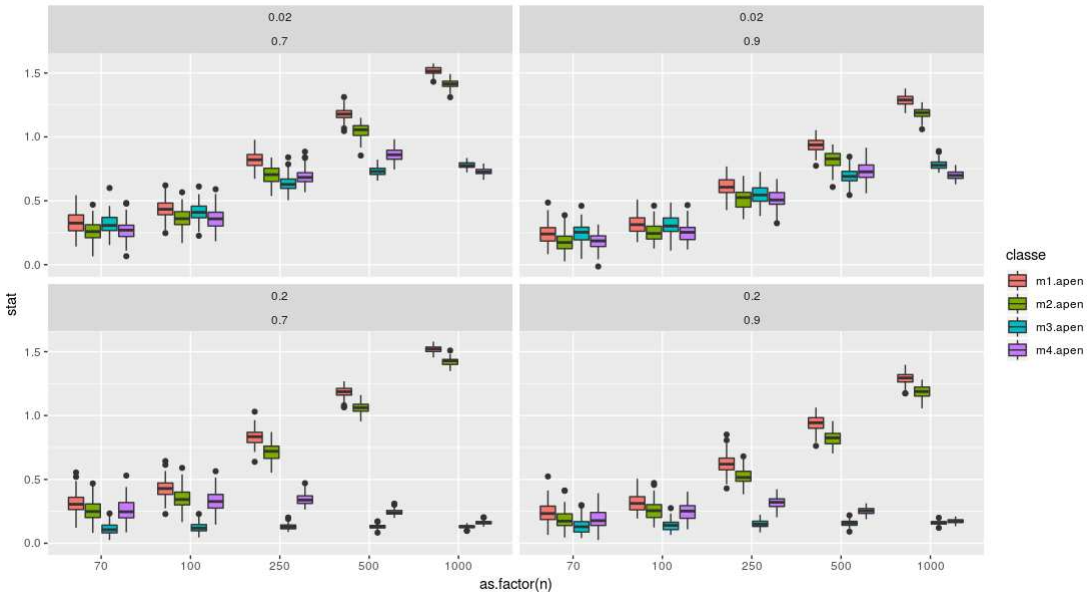

It is important to mention, as Pincus (PINCUS, 1991) elucidates, that ApEn stability it is conditioned to the fixed parameter m where the number of observations (n) needs to be between $10^m < n < 30^m$. Thereby, samples below this will not guarantee its efficiency.

The influences observed in the estimations of the mean exemplifies this statistic is non-robust to under non-stationarity TS. Dealing with Electroencephalography signal is very challenge given its scale conditional to its subject and brain region. The record is made using the technology of a differential amplifier, which takes the difference of two inputs and displays only one output, as their difference, useful to small electrical impulse systems. Therefore, EEG signals are not something absolute, but somewhat relative to a difference between inputs and may be too noisy.

2.5 Results

In order to test the condition-intensity equivalence, we designed (SANTOS *et al.*, 2018) an experiment in which we compare the effect of electrical stimulation modulation (Anodal and Cathodal) in different phases (baseline, 1mA, 2mA, and 3mA). Data is acquired via Electroencephalogram technique and then its time series process was summarized using entropy indices.

The dynamic across the brain network connectivity is a complex phenomenon of substantial relevance which could help neurologists to understand better some pathologies and help on the development of new treatments. Different brain areas could be compared using complexity as a measurement among neural group communication.

Our analysis is divided into two parts. First, we will illustrate one single case, to compare brain regions activation (as channels) using relative entropy, and then we consider the entire dynamic of the experiment (dose-response *versus* conditions).

2.5.1 Analyzing complexity within channels

We propose an Information Theoretic Approach to Neuroscience, with the application of the Kullback-Leibler divergence and the Approximate Entropy to the analysis of time series. Our goal is to compare different processes taking into account all their distribution moments (considering much more than only their average), thus enabling further analysis between neural events (PÉREZ-CRUZ, 2008; CHIANG *et al.*, 2007; JOSHI *et al.*, 2011; AFGANI; SINANOVIC; HAAS, 2008).

To illustrate the previous discussion, let us consider the *Kullback-Leibler* divergence (KL) between channels. For simplicity, we examined just a single trial of one subject, giving the possibility to analyze the process' synergy difference between the 51 channels located in the central region (left and right motor brain area). All the analyzes consider the smoothed TS, that is, with one observation point per the second resolution, with only 300 observations per phase (dose-response).

Let us bear in mind that the KL divergence is not symmetric. To make it asymmetric distance measure, we use the average shown below,

$$KL_{DIST}(p,q) = \frac{KL(p,q) + KL(q,p)}{2}. \tag{2.1}$$

In our case, the probability distributions represent electrical activity from each EEG channel.

In Figure 6 we use the pairwise complexity measurement (2.1). Due to the imposed symmetry, it suffices to visualize only the bottom right to perform a comparison among the channels through the brain hemisphere (25 first channels refer to the left brain side [left motor + left temporal] and right respectively). This is particularly important because we needed to know if across each intervention there exists a change in the dynamics of system complexity (if one stimulation region is impacting/connected to another). As well, this helps in describing the activation areas and its structural relations.

Figure 6 – Each matrix represents the stage of the experimentation. Due to the matrix symmetry, it was considered only the lower triangular part of it (light gray). The red color scale correlates the energy dynamics synergy of each EEG channel, being the dark red of greater intensity and the light of lesser.

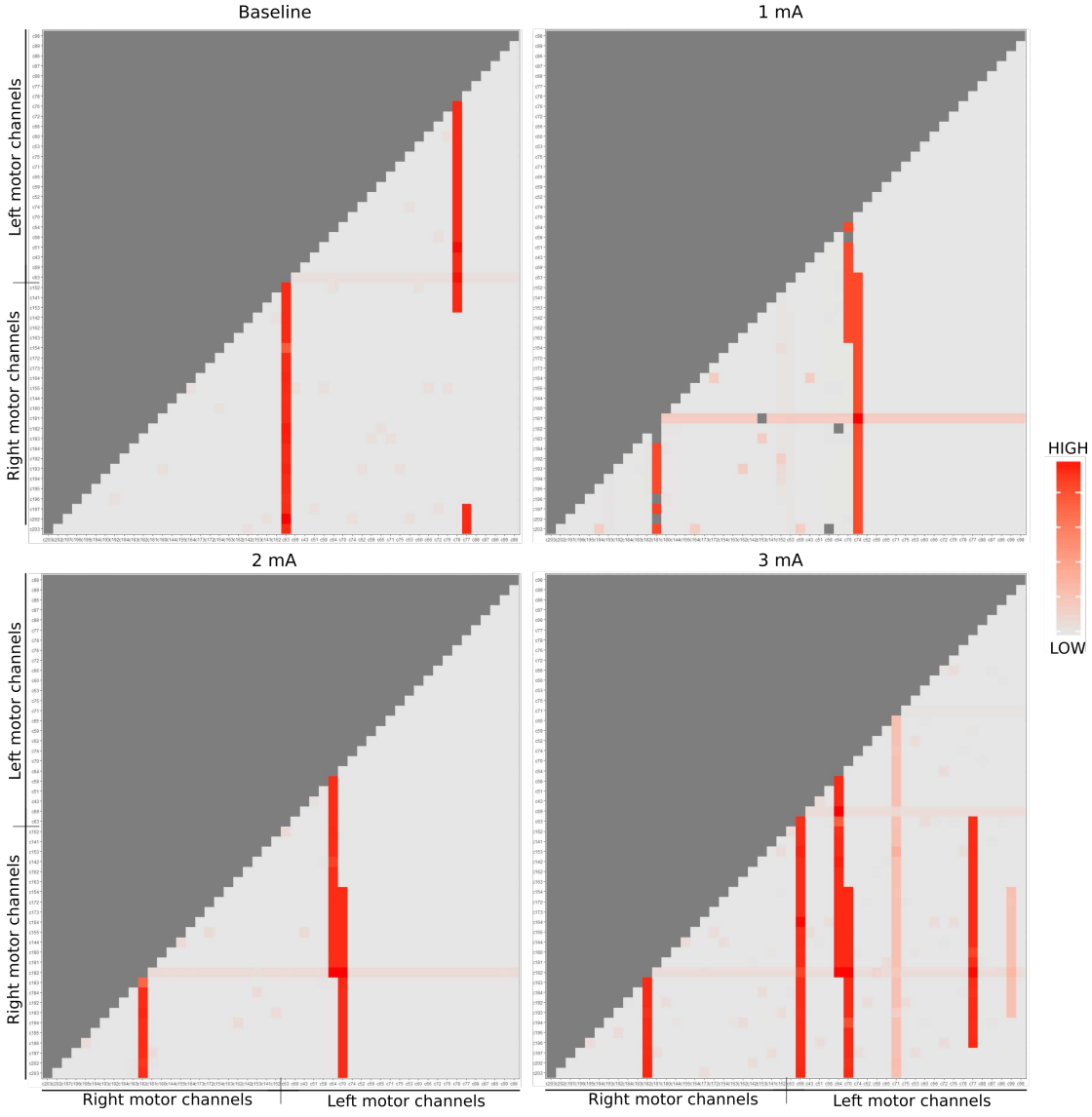

Notice that during baseline state (top left figure), channel 63, placed in the right side motor, reacted remarkably, as well as channels 77 and 78 with some other channels. Due to the electrical stimulus at 1mA (top right figure), it is possible to notice some change in the dynamic according to the stimulation regions: especially channels 181 (stimulation tDCS point), 70 and 74 (the equivalent points in the other hemisphere) present a larger entropy. In the 2mA stimulation (bottom left figure), the activity in channels 182, 70, and 64 (the neighbor of the stimulation tDCS point and the equivalent points in the other hemisphere) is highlighted. Finally, in the 3mA (bottom right figure), the channels 182, 69, 64, 70, and 77 are emphasized concerning the others, while channels 71 and 99 also point out, but present smaller statistics.

Therefore, this approach enables the comparison between brain regions in each dose-

response, by summarizing its complexity. It is worth mentioning that in the case of a non-stationary process, the class of entropy must take this fact into account.

2.5.2 Analyzing complexity across dose-response effect

Pincus (PINCUS; GLADSTONE; EHRENKRANZ, 1991) presented the so-called *Approximate Entropy* (ApEn) as a technique to quantify the amount of regularity, and the unpredictability of fluctuations, over time-series data not conditional to its stationarity. This entropy is particularly interesting for this application given the main questions are settled discerning about the regularity of the dose-response across the montages. Therefore, aiming to test the patient recovery, the entropy approach target is to summarize the comparison towards the induced neuromodulation, that is, the electrical stimulation.

Given the presence of repetitive patterns, in a time series, its predictability renders conditionally to its fluctuation. ApEn can be interpreted as the likelihood that similar patterns of observations will not be followed by additional similar observations, calculated by

$$ApEn = \Phi^m(r) - \Phi^{m+1}(r),\ where\ \Phi^m(r) = (N-m+1)^{-1} \sum_{i=1}^{N-m+1} ln(C_i^m(r))$$

where N is raw data values from a equally spaced in time, m is the length of compared time-window data, r is filtering level and $C_i^m(r)$ measures within a tolerance r the regularity of patterns similar to a given pattern.

In this manner, $m = 2$ and $r = 0.2 \times sd(TS)$ were adopted, and the ApEn were used to summarize the time series block experimentation and then adjusted a mixed-effect model in other to verify its similarity. A Time Series which contains many repetitive patterns has a relatively small ApEn; a less predictable process has a higher ApEn. Figure 7 describes the fluctuations over time-series data in each dose-response respectively.

Figure 7 – Each group is related to one condition (Anodal, Cathodal, Sham-Anodal, Sham-Cathodal). Visually the boxplots seem to present equivalence results among the brain stimulation conditions also considering amid their different intensities.

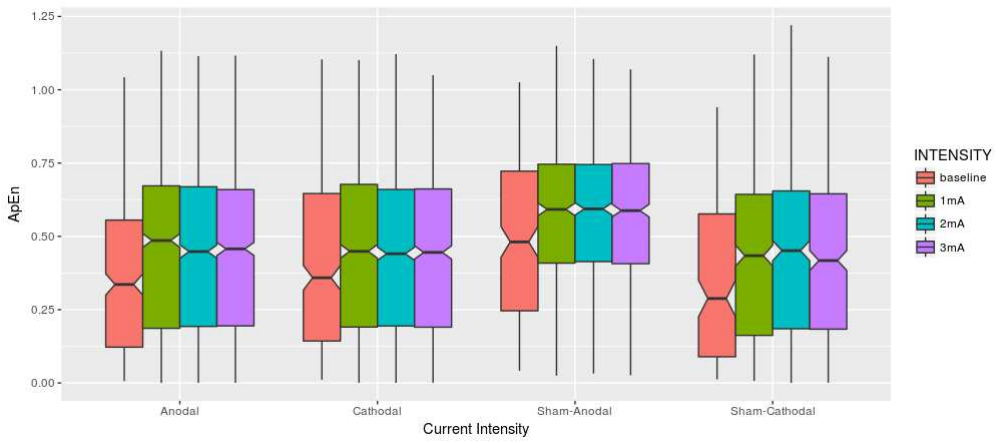

Complementing the descriptive analysis, Table 1 brings the basics statistical descriptive under the optic of the Approximate Entropy among dose-response within Conditions. It is to be noticed that both mean and median increased once the stimulus is applied although remaining quite similar among them, sharing a similar range of standard deviation. One thing we would like to highlight is that the 3mA intensity in the Cathodal condition has the smallest maximum ApEn.

Table 1 – ApEn summary among Stimulus versus Intensity

Condition	Intensity	MEAN	SD	MIN	MEDIAN	MAX
Anodal	base	0.365	0.260	0.0064	0.336	1.043
	1mA	0.452	0.280	0.0004	0.486	1.133
	2mA	0.445	0.278	0.0006	0.448	1.115
	3mA	0.444	0.279	0.0006	0.457	1.116
Cathodal	base	0.397	0.284	0.0108	0.359	1.104
	1mA	0.447	0.281	0.0006	0.449	1.101
	2mA	0.433	0.276	0.0006	0.441	1.121
	3mA	0.440	0.273	0.0006	0.445	1.050
Sham	base	0.430	0.283	0.0121	0.418	1.026
	1mA	0.512	0.264	0.0068	0.536	1.150
	2mA	0.514	0.260	0.0005	0.534	1.220
	3mA	0.510	0.259	0.0008	0.532	1.112

The theoretical adopted mixed model is explicit by Equation 2.2, represented as

$$\boldsymbol{Y} = \boldsymbol{X\beta} + \boldsymbol{Z\gamma} + \boldsymbol{\varepsilon} \tag{2.2}$$

where the $\boldsymbol{Y}$ is a vector of the ApEn containing 51 channels, per patient, $\boldsymbol{X}$ and $\boldsymbol{Z}$ are design matrices, $\boldsymbol{\beta}$ refers to the fixed-effects related to the intercept, montage (stimulation), intensity and their interaction, and $\boldsymbol{\gamma}$ is a matrix including the random-effects been channel and condition nested patient.

The number associated with the intention stage (configured by each dose-response - 1, 2 and 3mA) is equivalent to ten periods in total (baseline + 3 replicas of each dose-response). Due to the number of condition is three (Anodal, Cathodal, and Sham), per patient which are seven, then twenty-one obtained trials. All this combination summarizes in a total of 10,710 observations (given that a scalar number - ApEn represents each TS). Therefore, the model's fixed effects were converted into dummies variables (Stimulations versus Intensity).

According to Table 2, which presents the estimations relating the variances of each random component, a similar variance among the different stimulus are observed conditioned to the subjects (involving personal characteristic).

Analyzing the estimates associated with the fixed effects, in Table 3 and considering a significance level of 5%, shows the differences among the complexity across the intensity effects (not distinguish the stimulus). No difference was shown cross stimulus (regardless of

Table 2 – Mixed model - Random effects estimations

Groups		Variance	Std.Dev.
Channel	(Intercept)	0.0012	0.0348
Key	Anodal	0.0119	0.1089
	Cathodal	0.0113	0.1063
	Sham	0.0165	0.1283
Residual		0.0634	0.2519

electrical stimulation) using the Anodal stimulus as a reference to compare the conditions. Then, observing the iteration among stimulus versus intensity, only Cathodal with 2mA presented to be statistically different between condition (Anodal vs. Cathodal).

Table 3 – Mixed model - Fixed effects estimations

	Estimate	Std. Error	t value	p-value	
(Intercept)	0.365	0.044	8.373	5.13E-05	***
INTENSITY 1mA-Baseline	0.088	0.015	5.706	1.19E-08	***
INTENSITY 2mA-Baseline	0.080	0.015	5.221	1.82E-07	***
INTENSITY 3mA-Baseline	0.079	0.015	5.153	2.61E-07	***
CONDITION Sham-Anodal	0.066	0.052	1.266	0.2425	
CONDITION Cathodal-Anodal	0.033	0.044	0.735	0.482	
INTENSITY 1mA : Sham-Anodal	-0.006	0.022	-0.298	0.7656	
INTENSITY 2mA : Sham-Anodal	0.003	0.022	0.137	0.8913	
INTENSITY 3mA : Sham-Anodal	0.000	0.022	-0.006	0.9951	
INTENSITY 1mA : Cathodal-Anodal	-0.038	0.022	-1.730	0.0837	.
INTENSITY 2mA : Cathodal-Anodal	-0.044	0.022	-2.029	0.0425	*
INTENSITY 3mA : Cathodal-Anodal	-0.037	0.022	-1.693	0.0905	.

— Signif. codes: 0 ’***’ 0.001 ’**’ 0.01 ’*’ 0.05 ’.’ 0.1 ’ ’ 1

These results are quite close to the obtained (SANTOS *et al.*, 2018) which considered only channels 164 and 66, and now extended to the motor brain region composed mainly by 51 channels, where robust results were bypassed through non-parametric techniques. The Kruskal-Wallis test revealed intensity-dependent effects on the cathode center condition in the gamma frequency band, and the Tukey post-hoc test indicated a significant difference between 2 and 3 mA ($p = 0.044$).

Furthermore, Table 4 presents the correlation of fixed effects matrix, consider Sham (S), Anodal (A) and Cathodal (C).

Results, as expected, showed similarities with the protocol paper (SANTOS *et al.*, 2018), where only two (among our 51) channels were considered. The results presented in the Subsection 5.2 agree with Bikson, Perennou and others (BIKSON *et al.*, 2016; PÉRENNOU, 2006), where the importance of a safe protocol is highlighted. It is important to point out that the condition-intensity equivalence shown in this past results, may be successfully applied in patients with vertical disorder (e.g. post cerebral vascular accident).

Table 4 – Mixed model - Correlation of fixed effects estimations

	(Intr)	1mA	2mA	3mA	S:A	C:A	S:A1mA	S:A2mA	S:A3mA	C:A1mA	C:A2mA
1mA	-0.265										
2mA	-0.265	0.750									
3mA	-0.265	0.750	0.750								
S:A	-0.461	0.222	0.222	0.22							
C:A	-0.721	0.260	0.260	0.26	0.535						
S:A1mA	0.187	-0.707	-0.530	-0.53	-0.314	-0.184					
S:A2mA	0.187	-0.530	-0.707	-0.53	-0.314	-0.184	0.75				
S:A3mA	0.187	-0.530	-0.530	-0.707	-0.314	-0.184	0.75	0.75			
C:A1mA	0.187	-0.707	-0.530	-0.53	-0.157	-0.368	0.5	0.375	0.375		
C:A2mA	0.187	-0.530	-0.707	-0.53	-0.157	-0.368	0.375	0.5	0.375	0.75	
C:A3mA	0.187	-0.530	-0.530	-0.707	-0.157	-0.368	0.375	0.375	0.5	0.75	0.75

2.6 Conclusions

This work aimed to discuss the use of an appropriate statistic in the summarization of time series processes, preserving the information contained therein. Thus, entropy was suggested (in Section 5) as a robust alternative replacing the average since the processes observed in real life do not show stationarity. In the medical field, traditional statistical models are commonly adopted, which generally depart from the principle of independence between data, then time series are pre-processed (summarized) in an attempt to fit data into these types of models.

By using entropy, in the area of neuroscience, it has a straightforward interpretation which is associated with the energetic dynamics of the process then statistical hypothesis tests comparing their equivalences. Moreover, in this study, under this approach, we could discuss the feasibility of the protocol, and its safety, towards treatment as a vertical human manipulation task presented in, e.g. post-stroke patients.

Future works shall explore the time-varying dynamic across stimulus (voltage) versus conditions (treatment). Other approaches shall be further explored adapting different metrics, such as Mahalanobis or Geodesic distance, in the complexity calculation used in the approximate entropy measure, as well as incorporate a time-varying filter level parameter.

CHAPTER

3

BAYESIAN DYNAMIC GRAPHICAL MODELS: ANALYZING BRAINWAVE DATA FROM FIXED PARAMETERS TO HIERARCHICAL DESIGN

This chapter corresponds to a white paper, in which presents the discussion towards Bayesian dynamic networks, using the robust Hamiltonian Monte Carlo (HMC), aiming to estimate the brain dynamic-stimulation. This work had as co-authors: Lilia Costa (IME-UFBA, Brazil), Joao P Leite (FMRP-USP, Brazil), Dylan Edwards (MOSS, USA and Edith Cowan University, Australia), Taiza E G Santos (FMRP-USP, Brazil), Francisco Louzada (ICMC-USP, Brazil).

A dynamic linear model can be used in graphical modeling, enabling a complex problem to be split up into simpler components, through some plausible assumptions, aiming to ensure stable inference and computational feasibility. In this work, we analyzed the assessment of Multiregression Dynamic Models (MDMs) using the Hamiltonian Monte Carlo (HMC) numerical approximation, and its multivariate version, aiming to estimate the dynamic electrical accommodation associated with a human brain stimulation intervention. These dynamic graphical models can be an alternative to solve the challenge in analyzing/forecasting high-dimensional data. The motivation came from a brain neuromodulation intervention, assessed using EEG signals, from clinical study trials regarding understanding causal mechanisms that underpin neural communication, considering different subjects, and regarding the dose-response from the electrical stimulation.

3.1 Introduction

Unraveling human brain activity and how its architecture is related to a complex function and nontrivial task is of paramount importance in the neuroscience field. Mathematical models can contribute to enhance the interpretation of the brain dynamics and facilitate the development of therapeutic strategies to prevent, manage, and treat brain diseases, such as Alzheimer, Parkinson, and psychiatric disorders, such as schizophrenia (COSTA *et al.*, 2017; PRADO; WEST; KRYSTAL, 2001; GORROSTIETA *et al.*, 2013). Human brain connectivity is a substantial phenomenon relevant for clinical neuropsychological challenges such as postural and vertical perception (SANTOS *et al.*, 2018).

Brain activation and internal communication can be collected as biosignals in different ways, such as electroencephalography (EEG), functional magnetic resonance imaging (fMRI), diffusion tensor imaging (DTI). Nevertheless, all these biosignal tend to present a large dataset, given its sample rate and complexity (i.e. a EEG recording can reach up to millisecond resolution or a DTI observe billions of connections simultaneously). These oriented data address information regarding the brain activation usually characterized by non-regular behaviors and non-linear patterns. Therefore, computational constraints are presented in any applications and the spatiotemporal dependence is crucial to be incorporated in the model (FRISTON *et al.*, 2002; SHINKAREVA *et al.*, 2006; CRANSTOUN *et al.*, 2002). It is expected that mathematical models present the high-dimensional curse in neuroscience experimentation (GORROSTIETA *et al.*, 2013; SHEN; BAINGANA; GIANNAKIS, 2016).

Naturally, to adopt a paradigm that incorporates the flexibility in the dynamic of this estimation process, it is necessary to reckon modifications conditionally to the time evolution (WEST; HARRISON, 1989). These models presents time varying parameters. Consequentially, adopting the Bayesian paradigm can assist the incorporation of information prior to the parameter estimation process over time.

Hierarchical models allow the description of a complex phenomenon, dismembered in a smaller dimensions, breaking a complex problem into small ones. By assigning a conditional independence structure and adding different levels of parameter, the complex problem borrows in different stages common information added by small contributions assumed in the description of the problem (ANACLETO; QUEEN; ALBERS, 2013b).

This Bayesian time-varying multilevel model targets to model high-dimensional time series which present some challenges given its temporal interdependence. For instance, the estimation of brain network connectivity must incorporate its dynamics. State-space models are competitive in estimating brain networks (FIECAS; OMBAO, 2011; GORROSTIETA *et al.*, 2012; PRADO; WEST; KRYSTAL, 2001; GRUBER; WEST, 2017), which is a wide class of models able to incorporate even non-stationary series, for instance, as a *vector autoregressive*. Traditional methods in state-space models (usually) only describe the casual relation across

covariates (time series). Alternatively, Costa and coworkers (COSTA *et al.*, 2017) used *multi-regression dynamic* model (MDM) to estimate the brain connectivity graph from fMRI data, including the brain dynamics to indicate a resolution for the brain structure estimation.

The present study innovates in the literature by using the graphical representation of it (see (QUEEN; SMITH, 1993)), as MDM which uses a conditional independence supposition. In addition, dynamical graph helps understanding human behavior, through brain's dynamic, that can provide hints about types of localized electrical stimulation toward a solution (or soften) disorder related with brain activity (RUBIN *et al.*, 1991; PAAKKI *et al.*, 2010; COSTA *et al.*, 2017).

Here we analyze MDM variations related to multivariate time series, using a directed acyclic graphical (DAG) model combined with a Bayesian paradigm (Hamiltonian Monte Carlo), aiming to estimate cerebral connectivity dynamic under a robust and feasible estimation process.

3.2 Methodology

This work is divided into five main sections; In a methodological Section which contains the subsections 3.2.1 briefly detailing about the structure of the adopted biosignal, electroencephalogram (EEG) and its modeling challenges, and 6.2.1 describing the origin of the problem which motivated this work as well its data acquisition. Section 6.2.2 presents the theoretical background needed to analysis the considered clinical study. Then, Section 6.3 discuss the empirical results towards the estimated brain connectivity across subjects over time. Finally, Section 6.4 brings some final remarks about this work and some guidelines for further studies and this work limitations.

3.2.1 EEG signal structure & its challenges

Electroencephalogram (EEG) is a technique which measures brain activity by recording the electrical signals of the neurons. It results of summation of potentials derived from the mixture of extracellular currents generated by populations of neurons. The appearance of EEG rhythmic activity in scalp recordings is only possible as a result of the synchronized activation of massifs of neurons, the summed synaptic events of which become sufficiently large (WINDHORST; JOHANSSON, 2012).

EEG provides a very detailed and exact picture of brain structures involved in normal functioning or when damaged by pathological processes. The record is made using the technology of differential amplifier, which takes the difference of two inputs and displays only one output, as their difference, useful to small electrical impulse systems. Therefore, EEG signals are not something absolute, but rather relative to a difference between inputs called montage, illustrated by Figure 8. EEG recording is displayed in different montages, and among them the *common*

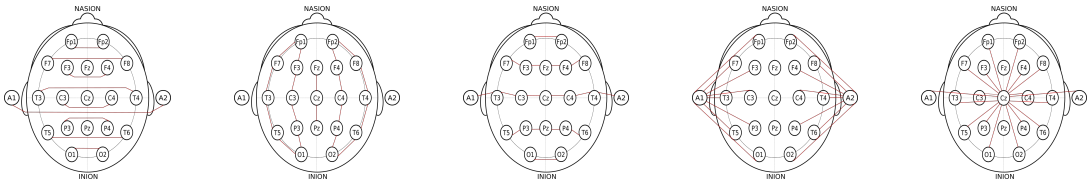

Figure 8 – Typical EEG montage maps described in the literature, the Czr, is discuss in the present paper. The adopted form of mapping the EEG data signal depends directly on its structure, moreover each participant has their own reference value (carrying out an individual structure), therefore EEG signal comparison is nontrivial across participants.

reference montage compares every placed electrode in the head against a single point, e.g. the central (Cz), displaying each difference as a single tracing named as channel or derivation.

Electroencephalography explicit discover the circuitry of brain processes, revealing not only “where” but “how” information is processed in the brain. This approach is essential for the solution of the mind-brain connectivity problem. As EEG spectrum may reflect particular cognitive conditions, the EEG recording can be used for on-line diagnostics of cognitive operations with a possible detection of thinking errors. The EEG based biofeedback may be applied for correction of brain malfunction, including the signaling in wrong mental operations. It is essential in high technological processes where a value of the error is high.

Thus, EEG, which previously was treated as a result of simple and almost occasional summation of the activity of huge masses of neurons, is now an effective tool in exploring the intimate mechanisms of information processing in human brain (WINDHORST; JOHANSSON, 2012). EEG has a high time resolution, and rather simple in use, cheap and almost does not disturb a subject. The EEG can be recorded near the subject’s bed and used for long-term monitoring of sleep stages or epilepsy. EEG also is a convenient tool for psychophysiological research when the subject has to perform some behavioral tasks or is out of the laboratory. One may expect, therefore, those innovative EEG methods have a good perspective in future neuroscience.

3.2.2 Brief on Motivation & Data Acquisition

The dynamic of a brain network connectivity is a complex phenomenon of substantial relevance which could help neurologists to understand better some pathology and help on the development of new treatments. In this manner, brain network activity could be observed as biosignals, measure in different ways such as Electroencephalogram (EEG) or Functional Magnetic Resonance Imaging (fMRI).

Electroencephalogram (EEG) is a technique which measures brain activity by recording the electrical signals of the neurons, as mentioned in subsection 3.2.1. It results of the differentiation of summations which potentially derived from the mixture of extracellular currents generated by populations of neurons. The appearance of EEG rhythmic activity in scalp recordings is only

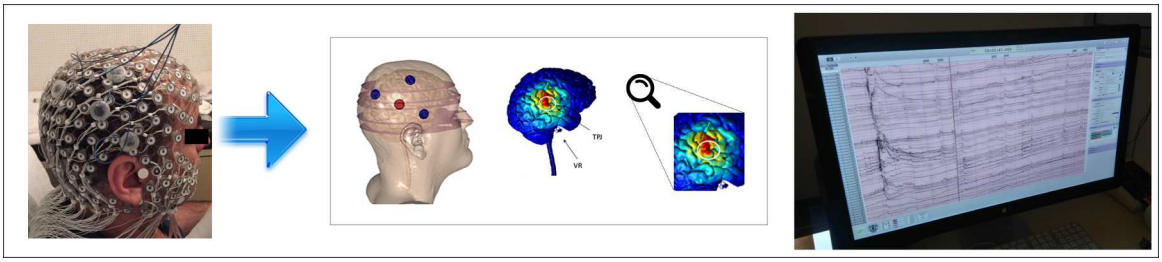

Figure 9 – Illustration of the acquisition of EEG data used in the present paper [see (SANTOS *et al.*, 2018)]. Left image shows EEG cap with small electrode array covering the scalp, while the large electrodes identifiable as a triangle configuration (4 electrodes total) represents the tDCS stimulating electrodes. The central panel shows the predicted cortical electric field from this tDCS montage. The right-hand image shows stacked single channel EEG potentials with time, from the Czr montage.

possible as a result of the synchronized activation of massifs of neurons, the summed synaptic events of which become sufficiently large (WINDHORST; JOHANSSON, 2012).

The data acquisition belongs from a novel approach to systematically analyze the dose-response effects of a focal electrical stimulation, transcranial Direct-Current Stimulation (tDCS), connected in the EEG cap. The adopted HD-tDCS condition comprised of three electrical stimulation electrodes where the center was placed on the right hemisphere as circumcircle of a triangle with vertices on C4, T4, P4. T8. All channels were referenced to the vertex (electrode CZ) with electrical impedance 128 reduced.

The studied protocol (SANTOS *et al.*, 2018) adopted the tDCS over the right TemporoParietal Junction (TPJ), as shown Figure 41, in healthy subjects. Based on prior results that postural perception could be manipulated (SANTOS-PONTELLI *et al.*, 2016), which is of major clinical importance in adult falls and post-stroke recovery (PÉRENNOU, 2006; BONAN *et al.*, 2007), and thus has potential clinical utility.

The systems' imbalance and degeneration related to postural control, lead new researches towards their origin and pathophysiology (WINTER, 1995). The different sensory information is used as pathways in the brain to posture maintain upright position (DAY; COLE, 2002). Thus, the postural imbalance is one of the most common findings found after stroke (BAGGIO *et al.*, 2016; CHERN *et al.*, 2010). However, increasing knowledge about the effects of this strategy is essential for the development of more effective rehabilitation protocols.

Transcranial direct current electrical stimulation protocols were suggested to influence changes in postural control also in post-stroke patients (BABYAR *et al.*, 2016; ZHOU *et al.*, 2014). However, even with current evidence and decades of experimentation on transcranial direct current stimulation, few protocols have achieved robust scientific acceptance. Therefore, it is essential to investigate the dose-response effects of brain stimulation in order to devise more effective protocols for rehabilitation.

In this study, the main goal as said is to verify the dynamic polarity-intensity-dependent

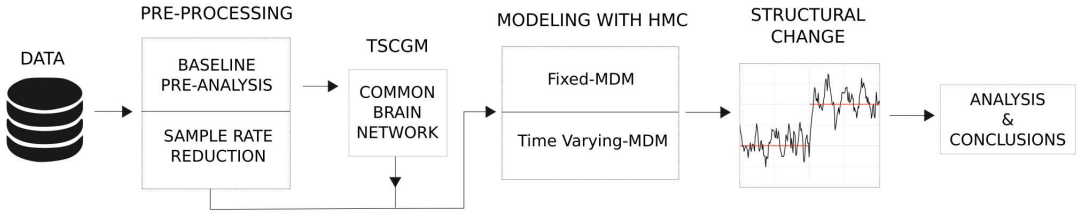

Figure 10 – Visual summary of the methodological framework. Acquired data were divided into two parts, the first being baseline only, to estimate the common brain network structure among the six participants (later explained in Fig. 16). Using this baseline structure together with that acquired from a post-tDCS collection, and considering the acquisition rate (500Hz), and the duration (300sec), we used the median value per second, for a total of 300 observations. We then modeled its dissipation with across time (post tDCS EEG, relative to pre tDCS; using two models, Fixed- and Time Varying-MDM). Then, structural changes across time were analyzed and conclusions were drawn. Acronyms are Time Series Chain Graphical Model (TSCGM), Hamiltonian Monte Carlo (HMC), and Multiregression Dynamic Model (MDM).

effect in the asymmetry of spontaneous posture after the application of HD-tDCS, applied to the temporoparietal junction region of the right cerebral hemisphere, in healthy young adults.

3.2.3 Visual Chain of Methods

In this subsection we describe the approach employed for EEG signals analysis. First, the observed clinical trial (from a single participant, 500Hz sample rate) seeking for pre-analysis related to the participant baseline (resting-stage) only. Later, we pursued a common resting-stage structure among six participants resting-stage, using the Time Series Chain Graphical Model (TSCGM) (ABEGAZ; WIT, 2013; NASCIMENTO *et al.*, in press). Then, combining the reduced data (per median second observation, 1Hz sample rate) with the common estimated connectivity structure, used as reference structure on the multivariate time series model, the so called Multiregression Dynamic Model (MDM) (QUEEN; SMITH, 1993) accommodated the post-stimulus towards its energetically time dissipation, then later analyzed its structural time series change (BAI, 1994).

Carrying on, Figure 10 represents visually the adopted methodology framework, from importing data to extracting its information. Next section will present the statistical theoretical models used to accommodate the dynamical process.

3.3 Recalling Dynamic Graphical Models

Graphical models describes the dependence structure among sets of random variables. There is, describe and manipulate conditional independence relations between variables in multivariate data. For instance, let's consider the case where one variable is regarded as response and the others as explanatory variables. Then, a model selection problem is created to generate

inferences towards the conditional correlations.

For a given related structure as pairwise objects, called graph, constraints under its parametrization are often claimed (desired to be estimated). An important work developed initially by Whittle (WHITTLE, 1953; WHITTLE, 1954) estimate than determined Gaussian graphical models, by equations similar, using maximum likelihood estimates (MLEs). This parametrization, using autoregressive models, allows terms to describe the contemporaneous relation (assotiated with the inverse covariance of the process) and dynamic relation obtained by the autoregressive coefficients.

In the analysis of neurophysiological data, correlation analysis is still an important, widely used tool (MELSSEN; EPPING, 1987; GORROSTIETA *et al.*, 2013). The advantage of such time domain based methods, compared with the frequency approach, is the interpretability of the links, which yield information concomitantly about the direction and the type of brain connections over time (EICHLER, 1999).

Given that all inference will be leaded by the information contained only in the data, Kullback-Leibler (KL) information is a natural candidate in the estimation process. Nevertheless, Akaike (AKAIKE, 1973) pointed out that the KL information is related to the method of maximum likelihood. Because MLE gives a nice interpretation, that is, maximizing the likelihood of data under our estimate is equal to minimizing the difference between our estimate and the real data distribution. We can see MLE as a proxy for fitting our estimate to the real distribution, which alternatively can be done indirectly as the real distribution is unknown.

In model selection, using the final prediction error instead of the KL distance, one focus on predicting future values of the sampled process by the past. We therefore would like to use only those variables which lead to a substantial reduction of the prediction error. But this is just the definition of causality (Pearl, 1990). It therefore seems to be natural to consider causal graphical time series models when choosing models for prediction.

In this manner, dynamic models are a powerful class of models whose structure changes over time are based on non-stationary or time-varying differential (difference equations) (ANACLETO; QUEEN; ALBERS, 2013b; COSTA *et al.*, 2017). This implies that a given phenomenon which presents change of structure, under this class, are continually maximized. In this manner, class of multiregression dynamic model (MDM) uses a graph to represent multivariate time series, which is a particular case of state-space model. This work explored its application in the neurophysiological data from the fixed to the time-varying parameters extension, as well as its multivariate version.

From now on in this section we will adopted the notation of uppercase, for convenience, related to random vector and lowercase for the observed vector.

3.3.1 Multiregression Dynamic Model (MDM)

Within the large class of Dynamic Graphical Models (DGMs), the flexible State-space model represented as a graph was discussed by Queen and Smith (QUEEN; SMITH, 1993) and it will be adopted in this work. This models are called Multiregression dynamic model (MDM). But first let's present some the primarily elements needed to understand this models functionality and challenges.

Consider a Global optimization as a collection of large finite amount of variables and add a real valued function, with finitely imposed constraints, which requires an objective function, assigning a value to all feasible points (HECKERMAN; GEIGER; CHICKERING, 1995). This will lead into finding those feasible observations, whose objective function value is minimal (maximal) among all feasible points. Nevertheless, this will leads in to a NP-hard problem (CHICKERING, 1996b).

Moreover, global optimization problem are often represented as a directed acyclic graph (DAG), which without changing it can be accommodated through various algorithms (SACHS *et al.*, 2005); i) aiming the local optimization, most compact form with the smallest number of variables and number of non-linear equalities, ii) problem definition, interpreting all named vertices as variables leads to a representation equivalent to the problem, and iii) increasing sparsity and dimension, to improve the sparsity pattern of the Hessian, that is, additional vertices can be regarded as variables.

(SCANAGATTA *et al.*, 2015) described that often a DAG structural learning may be plotted by its parent set identification and structure optimization. The node (variable) depends on only of its ancestor, also called parent. And this work understands as structure optimization the result of one structure which maximize the information, assigning an acyclic relation towards the variables.

Consider $Y_t = [Y_t(1), ..., Y_t(p)]$ as an p-dimensional time series array, i.e. each time series vector $Y_t(i)$ has $i = 1, ..., p$ observed values. Let $\theta_t = [\theta_t(1), ..., \theta_t(p)]$ be the state vectors of Y_t, where $dim(\theta_t(i)) = s_i$, $i = 1, ..., p$.

Under mild conditions, the conditional independence relationships fulfill the Markov Conditions and split a complex multivariate data problem into simpler ones. Then, a representative causal structure is a DAG. Let's consider for each time $t \in \mathbf{N}$, for $i = 2, ..., n$

$$Y_t(i) \text{ independent } Y_t^i | Parent(Y_t(i))$$

where Y_t^i is the set of all variables, except for node i, its parents and its descendants.

This type of graphs don't have any cycles, which presents no path for information to return to the nodes on the left of each diagram without doubling back and hitting a node that has already been encountered. In this manner, its is feasible to optimize its structure. This result is often applied in Bayesian network models where probabilistic dependence relationships among

multiple interacting components, which sometimes be interpreted as causal influence connections when interventional data are used (SACHS *et al.*, 2005).

Using the conditional independence assumption, DAG structure is convenient among the estimation of a graphical model structure by reducing its complexity. This implies that all necessary information will be available only a part of the data (not need to use the entire set all the time). In order to estimate this structure, this work adopted a class of models, the dynamic linear model.

The Gaussian linear state space models are also known as Dynamic linear model (DLM) is specified by a normal probability distribution for the p-dimensional state vector and m-dimensional observed vector. The model is composed of the observation equation (distribution of observations) and state equation (evolution of the parameters through time). At the time $t = 0$,

$$\theta_0 \sim N(\theta_0, \sigma_0^2)$$

after the time $t \geq 1$ then,

$$\underbrace{Y_t = F_t\theta_t + \upsilon_t}_{\text{observation equation}}, \quad \upsilon_t \sim N(0, V_t),$$
$$\underbrace{\theta_t = G_t\theta_{t-1} + \omega_t}_{\text{state equation}}, \quad \omega_t \sim N(0, W_t)$$

where G_t and F_t are known matrices ($p \times p$ and $m \times p$) and the disturbance terms υ_t and ω_t are two independent Gaussian random vectors with mean zero and known variance matrices V_t and W_t.

Considering a $\mathbf{R}^p$-valued and $\mathbf{R}^m$-valued time series satisfying

1. (θ_t) is a Markov chain
2. Conditionally on (θ_t), the observed time series (Y_t) are independent and depends only on (θ_t).

That is, allowing the time-varying parameters and incorporating more complex structures adding the composition of latent variable in the estimation process. That is, to estimate the state Vector we compute the conditional density $\pi(\theta_s \mid Y)$, where $t = 1, ..., T$. Consider θ_t as the mean parameter at the time t of a process, from a series $Y_t = \{y_1, ..., y_t\}$, under the Bayesian approach Figure 33 presents, as a DAG, the posterior (post.) and prior conditional densities as DLM performing upgrade inference procedure.

Evolution or update steps, related with the state equation, may consider consecutive stages, which is nominated as parametric hierarchy structure. Figure 12, for instance, illustrates a MDM representation.

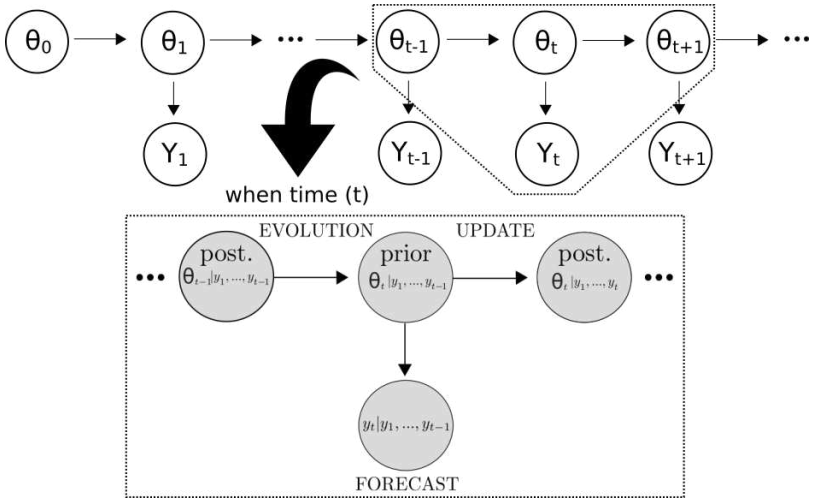

Figure 11 – Here we show a dynamic linear model (DLM), demonstrating how accuracy of the model increases by each new observed value. The model comprises three stages: evolution, forecast and updates. These processes revise the model information [from the Unobserved/predicted values (θ's)], extracting from each new inputted observation (Y's), across time.

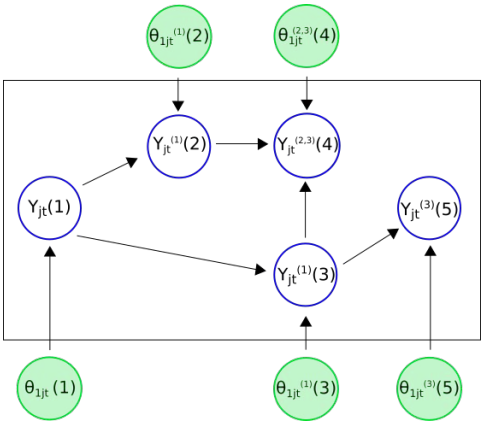

Figure 12 – Multiregression dynamic model (MDM) graph representation, containing the observed time series represented by nodes (Y's in blue) and non-observed or hidden states (θ's in green), where t refers to time and j to the elements (participants). This representation shows the conditional independence structure of each node.

Before continuing, to distinguish estimation problems where s is the recursive period and t is the current period, is needed where filtering ($s = t$), smoothing ($s < t$) and state prediction ($s > t$). Filtering is a procedure that aims to update the current estimates as new data are observed $\pi(\theta_t \mid y_{1:t})$. Smoothing is a retrospective analysis which compute the conditional distribution θ given in once the data $\pi(\theta_t \mid y_{1:T})$, starting from $\pi(\theta_T \mid y_{1:T})$ estimating the states backward. Prediction is a forecast procedure which estimate the next observation based on the distribution $\pi(\theta_{t+1} \mid y_{1:t})$. Further details about Bayesian Forecasting and Dynamic Models (WEST; HARRISON, 1989; PETRIS; PETRONE; CAMPAGNOLI, 2009).

Notice that this general case is can be a vector autoregressive (VAR) model as a static parameters, that is, if the parameters are time-invariant.

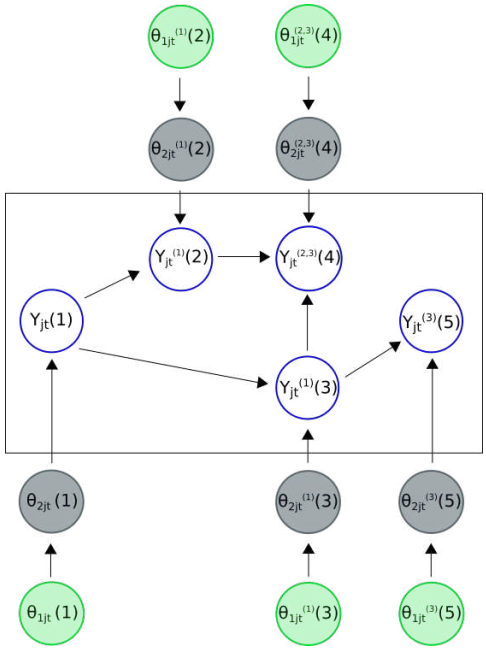

Figure 13 – Second order latent structure (multi-level) of the multiregression dynamic model (MDM) graph representation containing the observed time series represented by nodes (Y's in blue), added by the hidden structure (in gray), and states (θ's in green). Time is represented by t and participants are represented by j. This parameterization allows the estimation towards the sharing information across elements (participants) as a common structure, still maintaining their respective personal characteristics.

The Multivariate dynamic linear model were extended to its version, based on Gamerman & Migon (GAMERMAN; MIGON, 1993) dynamic models where they presented as a state estimation problem considering multiple parameter layers, equivalent to hidden unobserved stage, now considering three equation components

$$
\begin{aligned}
\text{observation equation} &\left\{ Y_t = F_{1,t}\theta_{1,t} + \upsilon_{1,t}, \qquad \upsilon_{1,t} \sim N(0, V_{1,t}), \right. \\
\text{structure equation} &\left\{ \begin{array}{ll} \theta_{1,t} = F_{2,t}\theta_{2,t} + \upsilon_{2,t} & , \upsilon_{2,t} \sim N(0, V_{2,t}), \\ \ldots & \\ \theta_{p,t} = F_{(p+1),t}\theta_{(p+1),t} + \upsilon_{(p+1),t} & , \upsilon_{(p+1),t} \sim N(0, V_{(p+1),t}), \end{array} \right. \\
\text{state equation} &\left\{ \theta_{(p+1),t} = G_t\theta_{(p+1),t-1} + \omega_t, \qquad \omega_t \sim N(0, W_t) \right.
\end{aligned}
$$

Figure 13 exemplifies a system which considers a Two-Stage model. For instance, this simple model illustrates, by adding one more hierarchical layer, that the structure equation is added aiming to extract from the experiments a common latent measurement (on a collection) related but from different units.

Thus, common latent structures are enable to be included, on the estimation process, aiming to share information towards similar patterns. Regarding this work motivation, which deals

with different participants electrical structures, given the EEG spectrum nature, by considering consecutive latent stages we address common brain process information.

Through a multivariate approach estimation procedure, under a high-dimensional parameterized model, is feasible to condition the existence with just a few data points. Shrinkage in parameter space is only doable if appropriated priors, although is not a trivial task. Using the multilevel prior approach allows us to "learn the priors" by sharing information across units of observation, based in conditional independence.

3.3.2 Hamiltonian Monte Carlo (HMC)

Under the Bayesian paradigm, statistical models can be calculated analytically from their posterior distributions, with reference to their parameters. However, deterministic integration methods are usually used to approximate this posterior distributions, which present a high complexity especially under the presence of high dimensions.

Any unknown parameter (θ) is associated to a probability function ($\pi(.)$) can be determined by Bayes' theorem

$$\pi(\theta|Data) = \frac{\pi(\theta)\pi(Data|\theta)}{\pi(Data)} = \frac{\pi(\theta)\pi(Data|\theta)}{\int \pi(\theta)\pi(Data|\theta)d\theta}$$

The first study to proposed a numerical approximation to $\pi(Data)$ relating this integration problem using as solution the states of molecules systems simulation proposed by Metropolis (METROPOLIS *et al.*, 1953) as its updates is done as a random-walk, is known as Markov chain Monte Carlo (MCMC). It says that a large identically and independent sample $(T_1, ..., T_n)$, where $T_i \sim \pi(t|Data)$, from the posterior distribution results that for any function g forthcoming from the law of large numbers

$$\mathrm{E}(g(T_i)) = \int g(t)\pi(t|Data)dt = \int g(\theta)\pi(\theta|Data)d\theta = \mathrm{E}(g(\theta)|Data)$$

Later combining with the idea, presented by Alder & Wainwright (ALDER; WAINWRIGHT, 1959), which this states are deterministical following Newton's laws of motion as Hamiltonian dynamics, originated the hybrid Monte Carlo method or Hamiltonian Monte Carlo (HMC). In order to search the position of the variables, to obtain inferences towards θ, the method adds an auxiliary variable (φ) called "momentum" so the parameter space is explored through partial derivatives of the Hamilton's equation converging much faster. For deeper investigations mind the see Brooks and other (BROOKS *et al.*, 2011).

First, Hamiltonian function can be defined in terms of the probability distribution we wish to sample from. Then, HMC method alternates simple updates for these momentum variables with Metropolis updates in which a new state is proposed by computing a trajectory according to Hamiltonian dynamics (using the concept of energy and gradient), implemented with the leapfrog numerical method (Discretizing Hamilton's Equation). That is, the non-linear update

state may be distant from the current state although presenting a high probability of acceptance. The steps are as follows

Algorithm 1 – Hamiltonian Monte Carlo (HMC)

Sample $\varphi_1^* \sim Normal(0, \Sigma)$
for *i in* $2 : N$ **do**
  $\varphi_i^* \leftarrow \varphi_i^* + \varepsilon \frac{\partial \pi(\theta|x)}{\partial \theta}(\theta_{i-1})$
  $\theta_i^* \leftarrow \theta_{i-1} + \varepsilon \Sigma^{-1} \varphi_i^*$
  $\varphi_i^* \leftarrow \varphi_i^* + \varepsilon \frac{\partial \pi(\theta|x)}{\partial \theta}(\theta_i^*)$
  if $Uniform(0,1) \leq \frac{\pi(\varphi_i^*)\pi(\theta_i^*|x)}{\pi(\varphi_{i-1})\pi(\theta_{i-1}|x)}$ **then**
    $(\theta_i, \varphi_i) = (\theta_i^*, \varphi_i^*)$
  else
    $(\theta_i, \varphi_i) = (\theta_{i-1}, \varphi_{i-1})$
  end if
end for

where N is the sample size (leapfrog steps), φ represents the position parameter, θ the momentum parameter, where as φ^* and θ^* are the new proposed parameters, Σ the variance, and ε is step-size for leapfrog steps. The process computes the partial derivatives of the log of the density function.

This HMC algorithm performance is based in two steps; the first step, new values for the momentum variables are randomly drawn from their Gaussian distribution, independently of the current values of the position variables. In the second step, a Metropolis update is performed, using Hamiltonian dynamics to propose a new state. If the proposed state is not accepted, the next state is the same as the current.

Some major differences comparing Metropolis to HMC are

1. The calculated distances which conduce the parameter(s) updates usually are “large", then less iterations are needed obtain a representative sampling;

2. HMC presents a greater acceptance rate towards new calculated states;

3. Computational demands of a single iteration is higher, although more efficient;

4. HMC may be limited if sampling from distributions with isolated local minimums is required;

This work used the R packages called *rstan* & *rstanarm*, which connect R software with Stan, which contains the partials derivatives calculation implemented. Stan’s software enabled the application of HMC in different applications due to its simplicity, and this helped the spread of Hamiltonian numerical approximation based on its computational efficiency, compiling/working in C language.

3.4 Empirical Analysis

Considering the protocol study (SANTOS *et al.*, 2018), which aims to study the manipulation of human verticality non-invasively via tDCS dose-response. A visual representation of clinical study trial can be seen based on the dynamic from a single subject EEG channel 147. Figure 14 illustrates an example of EEG amplitude, among the experiment, where the light blue shade area refers to the baseline phase (5 min duration) and the light gray refers to the moment after the HD-tDCS dose-response (also 5 min each).

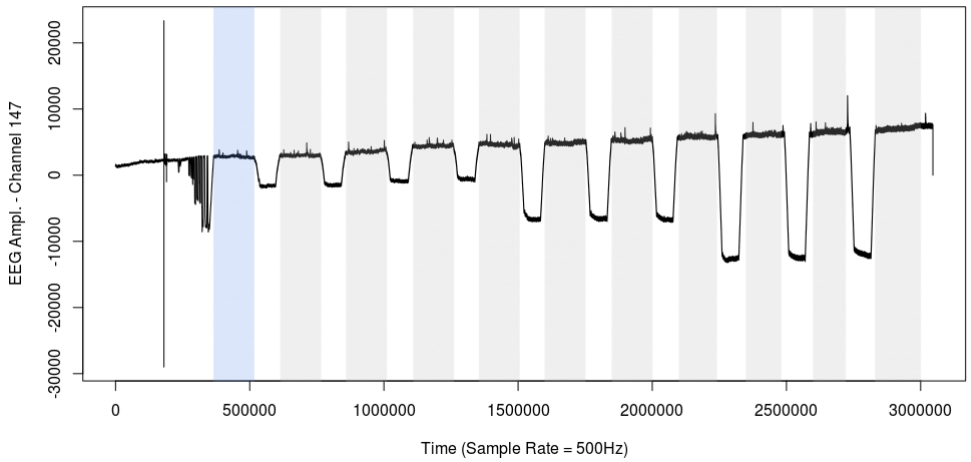

Figure 14 – Single participant EEG channel 147 full trial representation of EEG amplitude over time in a 500Hz sample rate. Light blue shade area represents the 5 min baseline response. Light gray area refers to the 5 min post HD-tDCS dose-response.

Initially, we observed only the brainwave baseline dynamic of a single subject to highlight their different patterns. For that, channels 164, 66 and 147 were selected respectively. Channels 164 and 66 represents an important brain spot, given that they are places at the right and left motor regions, responsible for advanced motor functions such as motor planning and bilateral coordination. Channel 147 because it is less sensible to noise. Figure 15 display, during baseline, their high-resolution behavior across 5 minutes time-window.

All of them have 300-second window total, considering a frequency of 500Hz (sample rate), then returning 150.000 observations each “resting time”. Continuing with Figure 15, it is noticeable during “resting” time-window that non-linearity patterns are presented. Some heteroscedastic behavior is also visually notable, as well the presence of structure break in a form of “peaks” among time.

Personal characteristic are intrinsically presented on the EEG signals, given its recording methods (presented in Section 3.2.1). Then a personalized model needs to by used, for each subject responses. Based on Nascimento (NASCIMENTO *et al.*, in press) results, a common brain connectivity was estimated using the Time Series Chain Graphical Model (TSCGM),

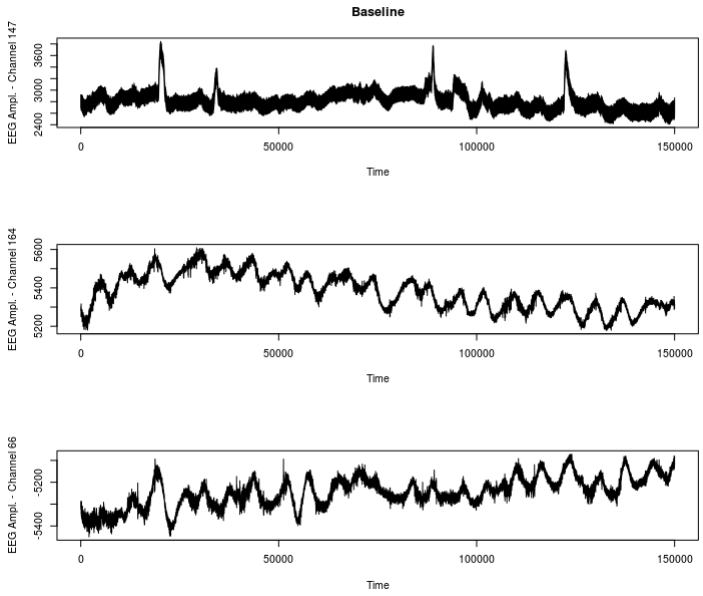

Figure 15 – Three dynamic EEG responses of a single participant showing channels 164, 66, and 147, during the baseline period. The EEG channels indicate different patterns between each brain location.

considering a SCAD penalization, on each 6 subjects during baseline condition, with 7 channels (164, 173, 183, 66, 71, 72, and 147). Then based on its estimated autoregressive parameters, it was calculated the median relating a common dynamic connectivity behaviour, then illustrated by Figure 16 shows a median graph behavior (among the patients).

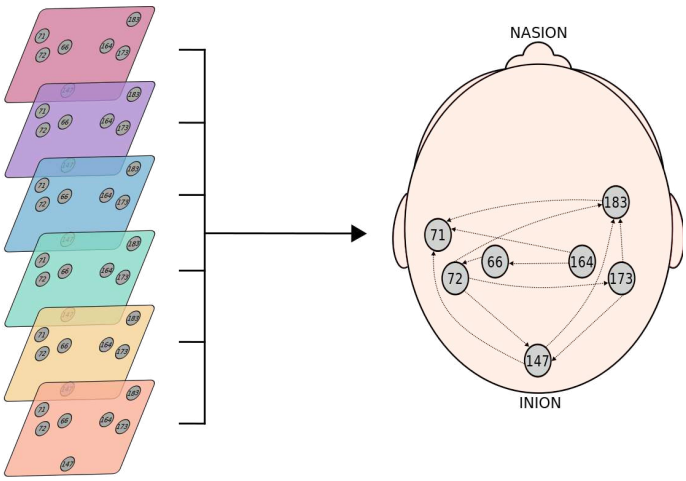

Figure 16 – Common resting-stage Network Structure estimation representation (right figure), based on data from six participants (each participant represented by a different color in the left figures). The structure starts on the EEG channel 164 (root node) and ends at the channel 71 (leaf node), showing the information flowing across the right and left hemispheres. Each arc (arrow) represents a casual relationship across the channels. This estimated network as a directed acyclic graph (DAG) was used as a common structure in the Multiregression Dynamic Models aiming to describe the electrical dynamic across the time.

Once we established a pre-defined brain network, a dynamic model can be adjusted based

Table 5 – The selected priors distributions.

Parameter	Prior Distribution
$\alpha^*_{t,i,s}$	Normal(0,10.000)
$\beta^*_{*,t,i,s}$	Normal(0,10.000)
$\sigma^*_{t,i,s}$	Uniform(0,100)

on a preliminary structure. Adopting the Multiregression Dynamic Models (MDMs), moreover, a first order random walk evolution and seasonal behavior of simpler state-space model as a DGM, in which we are interest to model the dynamic connectivity after a HD-tDCS dose-response. Thereby, we are looking how its behaviour is changing over time (or preserved). For that, the theoretical model for each EEG channel as

$$
\begin{aligned}
Y^{(164)}_{t,i,s} &\sim N(\mu^{(164)}_{t,i,s}, \tau^{(164)}_{t,i,s}),\\
Y^{(66)}_{t,i,s} &\sim N(\mu^{(66)}_{t,i,s}, \tau^{(66)}_{t,i,s}),\\
Y^{(71)}_{t,i,s} &\sim N(\mu^{(71)}_{t,i,s}, \tau^{(71)}_{t,i,s}),\\
Y^{(72)}_{t,i,s} &\sim N(\mu^{(72)}_{t,i,s}, \tau^{(72)}_{t,i,s}),\\
Y^{(147)}_{t,i,s} &\sim N(\mu^{(147)}_{t,i,s}, \tau^{(147)}_{t,i,s}),\\
Y^{(173)}_{t,i,s} &\sim N(\mu^{(173)}_{t,i,s}, \tau^{(173)}_{t,i,s}),\\
Y^{(183)}_{t,i,s} &\sim N(\mu^{(183)}_{t,i,s}, \tau^{(183)}_{t,i,s}),
\end{aligned}
$$

where t is related with the time-point, i with subject, and s section number. Moreover, their respectfully mean distributions is

$$
\begin{aligned}
\mu^{(164)}_{t,i,s} &= \alpha^{(164)}_{t,i,s} + \beta^{(164)}_{1,t,i,s} Y^{(164)}_{t-1,i,s}\\
\mu^{(66)}_{t,i,s} &= \alpha^{(66)}_{t,i,s} + \beta^{(66)}_{1,t,i,s} Y^{(164)}_{t,i,s}\\
\mu^{(71)}_{t,i,s} &= \alpha^{(71)}_{t,i,s} + \beta^{(71)}_{1,t,i,s} Y^{(66)}_{t,i,s}\\
\mu^{(72)}_{t,i,s} &= \alpha^{(72)}_{t,i,s} + \beta^{(72)}_{1,t,i,s} Y^{(147)}_{t,i,s} + \beta^{(72)}_{2,t,i,s} Y^{(164)}_{t,i,s} + \beta^{(72)}_{3,t,i,s} Y^{(173)}_{t,i,s} + \beta^{(72)}_{4,t,i,s} Y^{(183)}_{t,i,s}\\
\mu^{(147)}_{t,i,s} &= \alpha^{(147)}_{t,i,s} + \beta^{(147)}_{1,t,i,s} Y^{(71)}_{t,i,s} + \beta^{(147)}_{2,t,i,s} Y^{(173)}_{t,i,s}\\
\mu^{(173)}_{t,i,s} &= \alpha^{(173)}_{t,i,s} + \beta^{(173)}_{1,t,i,s} Y^{(71)}_{t,i,s}\\
\mu^{(183)}_{t,i,s} &= \alpha^{(183)}_{t,i,s} + \beta^{(183)}_{1,t,i,s} Y^{(147)}_{t,i,s} + \beta^{(183)}_{2,t,i,s} Y^{(71)}_{t,i,s} + \beta^{(183)}_{3,t,i,s} Y^{(173)}_{t,i,s}
\end{aligned}
$$

when $t = 1$ then $\mu^{(164)}_{t,i,s} = \alpha^{(164)}_{t,i,s} + \beta^{(164)}_{1,t,i,s} Y^{(164)}_{t,i,s}$, for a feasible first draw.

All used prior distribution, for parameters, were little or non-informative. The priors distributions, in Table 5 considered in the estimation process are

and transformed parameters were also adopted such as $\tau^*_{t,i,s} = 1/(\sigma^*_{t,i,s})^2$.

Thus high-frequency signals, naturally was required a smoothing transformation, targeting data simplification, but also preserving interpretability of the time series, given the

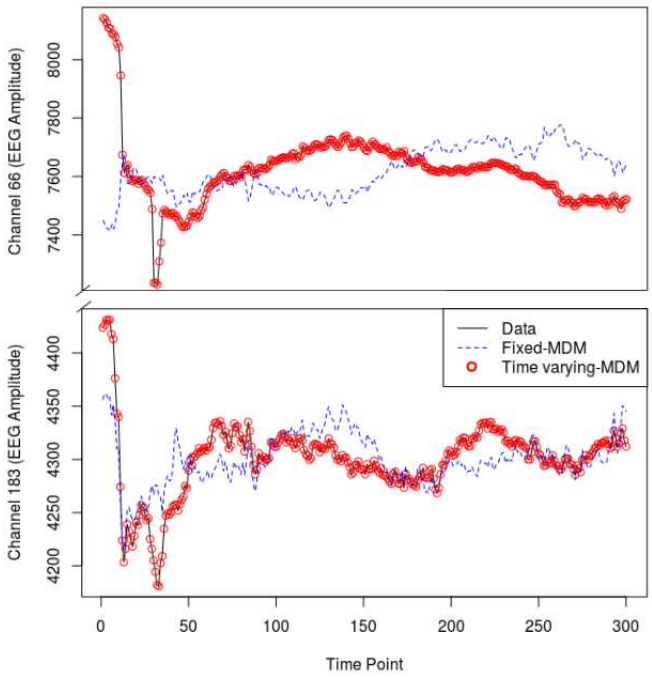

Figure 17 – EEG signal from channels 66 (top) and 183 (bottom) containing the observed data (in black solid line), their model estimations from the Multiregression Dynamic Model (MDM) with Fixed parameters (in blue dashed line), and Time Varying parameters (in red dots). In both cases, the post-electrical perturbation is noticeable in the beginning of the series, followed by their accommodation. The Time Varying-MDM shows to be more flexible through its fitting along the observed values.

hyperparametrization of the MDM. Each 500 observations was taken the median, reducing the sample size rate to its median single point observation per second. In this manner, the time series representation would preserved such behavior and reduce its noise, as a modification of the segmented transformation (YI; FALOUTSOS, 2000).

In this work, when we refer as MDM fix parameters implies that t, i, s will be constants, according to the adopted notation by the theoretical model. Moreover, for MDM time-varying parameters only i, s will be considered constants, and no dimension will be constant for the multilevel MDM.

For instance, let's consider a single subject EEG signal behaviour. Figure 17 shows the performance of two channels (66 and 183), using MDMs fix versus time-varying parameters. Once the model structure was flexibilized, via MDM time-varying parameters, the accommodation of the series was shown highly competitive.

Looking closer into the estimated parameters, based on the theoretical model, by selecting only channel 66, and considering MDM time-varying parameters, Figure 18 shows the α performance along four period of time (5, 100, 200 and 300 seconds). It's noticeable that its variation follows the observed biosignal and small magnitude are given from it thus the EEG signal amplitude than associated with β parameters.

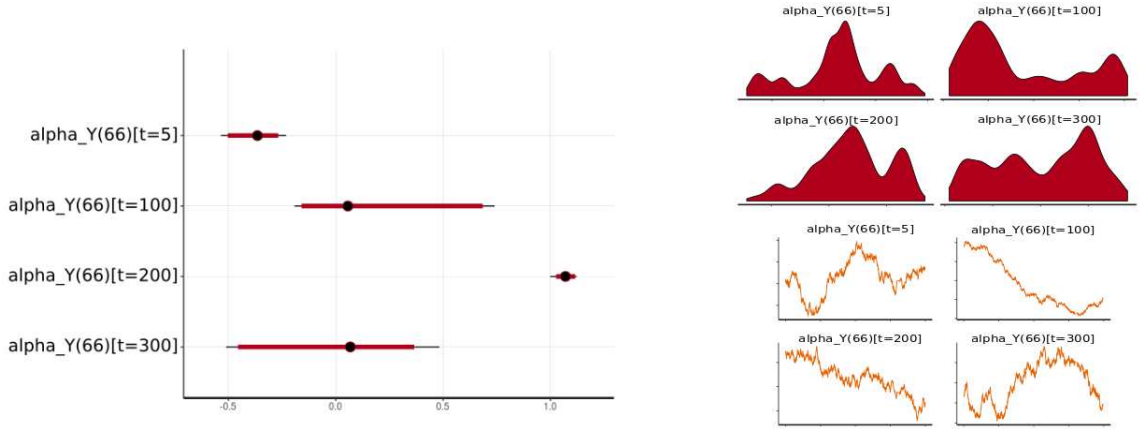

Figure 18 – Dynamic accommodation from the EEG signal (channel 66) explained by the Multiregression Dynamic Model time-varying α's estimation parameters, during time-windows 5, 100, 200 and 300 seconds. The parameters shown in the left-hand chart are related with the electrical dynamic explained by the channel' self-walk (as a process average trend), not by other channels. The electrical accommodation dynamic pattern suggesting the synergy process through tDCS post-stimulation. The Chain used, shown in right side figures, to estimate these parameters.

Figure 19 shows the performance of the β parameters from channel 66 also during four period of time (5, 100, 200 and 300 seconds). As time pass by it is noticeable a contraction, suggesting there is a influence reduction of channel 164 on channel 66.

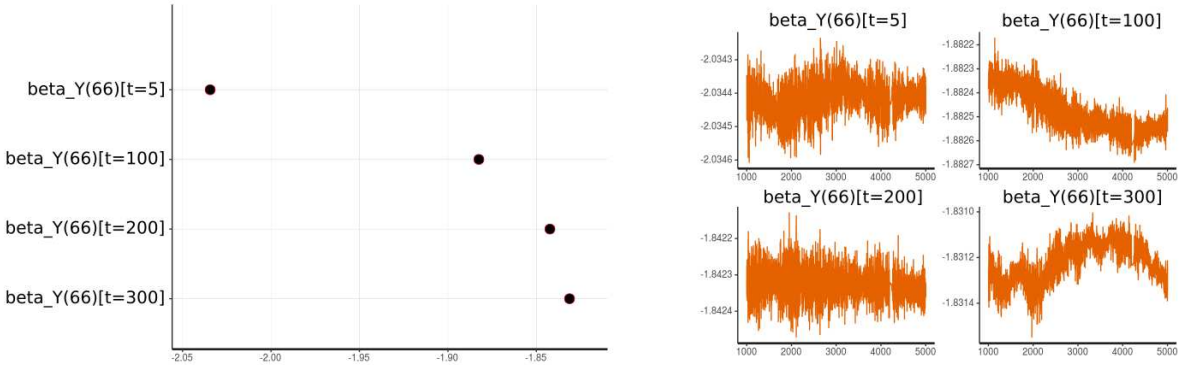

Figure 19 – Dynamic accommodation from the EEG signal (channel 66) explained by the Multiregression Dynamic Model time-varying β's estimation parameters, during time-windows 5, 100, 200 and 300 seconds. The parameters are related with the electrical dynamic explained by the related channel (164). Moreover, in the left-hand chart, the β parameters represents the electrical influence on channel 66, derivative from channel 164, losing strength among time. That is, suggesting a return to the basal stage. The Chain used, shown in right side figures, to estimate these parameters.

After comparing the models, the time-varying MDM (which is a multilevel model with parameters across time) shows to be a competitive model, given its flexibility and robustness. Figure 20 presents the accommodation of two channels, across all subjects, corroborating with its high performance.

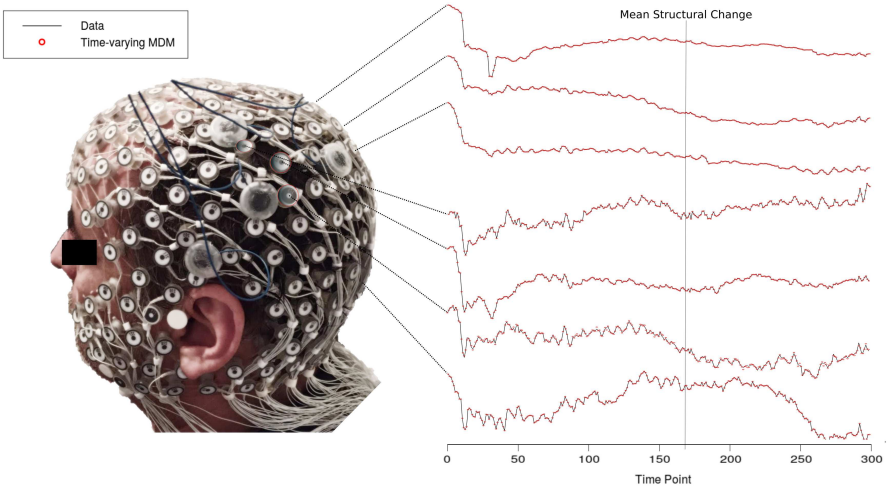

Figure 20 – Illustration of a single participant's right side (flipped picture for better representation), associated with the raw EEG signal of channels 66, 72, 72, 164, 173, 183, and 147. The black lines indicate the observed EEG signals, and the estimated behavior for each channel using MDM time-varying parameters are represented by the red points. Through their accommodation model, a mean structure break was estimated suggesting a pattern' shift after 163 seconds.

Additionally, it was also tested the dating structural changes in the adjusted mean of each EEG channel, according to Bai (BAI, 1994) using the package *strucchange*, enabling to seek for evidence related to structure break across time. Therefore, suggesting that after maximum 252 seconds all the observed areas (related to the EEG channels) starts to present a change in the electrical influence, or 163 seconds on average, that is, regarding the tDCS stimulation governable we may relate to the dynamic connectivity towards basal state.

Polarity dependence is observed, after tDCS stimulation, regarding Left and Right brain hemisphere. Figure 21 shows the seven channels mean evolution across time.

Moreover, because the EEG signal care based on a personal characteristic, when a clinical study is analyzed containing multiple subjects then flexible structures shall be introduced conditioned to each personal behaviour (response).

3.5 Final Remarks

The present study results in three main highlights upon the multivariate time series field; i) in neuroscience field, it is we are the first group, to our knowledge to use a HD-tDCS dose-response up to 3mA in human verticality manipulation, ii) a few article uses multilevel dynamic models in EEG task, dealing properly with non-linearity series and iii) moreover, a Hamiltonian Monte Carlo approach has not been much explored in statistics field, especially using time-domain time series models, alongside its computational efficiency.

In contrast to the previous studies, we developed a new methodology combining MDM with HMC broad potential associated with computational feasibility and robustness. Our statisti-

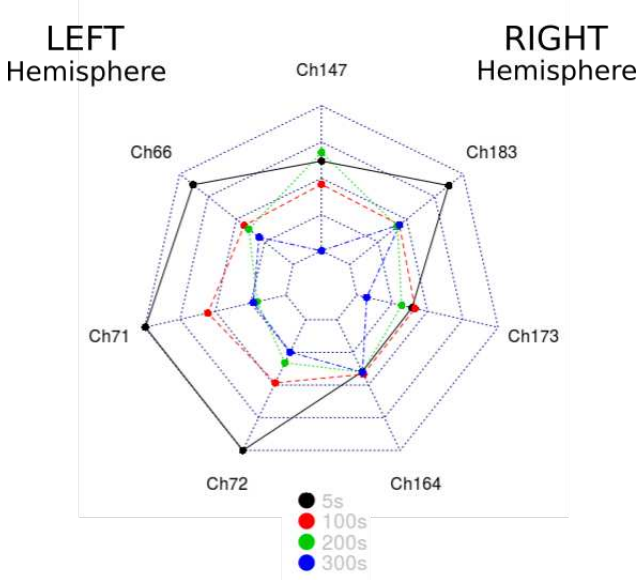

Figure 21 – Radar plot of standardized EEG signal showing the dynamic structural time-flow of four time points (5, 200, 200 and 300 seconds) from a single representative participant. Higher amplitudes can be observed in the left hemisphere (channels 66, 71 and 72) at 5 seconds (right after the stimulus), followed by a general/mutual shrinkage performance across the channels (except in channel 147 during 200 seconds) reflecting a "symmetric dispersion" across time.

cal approach is innovative also because we aggregate elements to discuss the application of this complex system analysis, using the time series approach, using a momentum variable towards estimation efficiency. As results, by analyzing the 5 minutes of EEG data after the HD-tDCS, we could identify mean structural breaks around 163 seconds, indicating a loss of HD-tDCS influence towards cortical activity (suggesting the return to the baseline state).

More specifically, dynamic linear models opens up a new class of non-trivial structure data analysis, thus enabling some types of dependence (temporal, spatial, etc.) managing to be a simpler problem given the conditional independence supposition from the state-space models.

The presented statistical approach is appropriate to human brain connectivity that is a complex phenomenon of substantial relevance, presenting results towards non-invasive brain treatment using tDCS. It has been an open question on how to deal with high-dimension data without losing relevant information in the neuroscience field. Our research group have been showing sequential evidence for the clinical and physiological effects of a non-invasive brain stimulation protocol targeting the temporo-parietal junction to understand and treat disorders of human verticality (SANTOS; EDWARDS, 2019). This context exposes the need for several time series analyzes and its dependence, estimating not only the effects individually but the impact of treatments as a whole. Understanding human neurophysiology such as the brain dynamics could provide insights about types of localized non-invasive brain stimulation toward a solution (or improvement) of the brain activity dysfunction (RUBIN *et al.*, 1991; PAAKKI *et al.*, 2010).

Furthermore, using the DLM, future works can explore the multivariate graphical models, extensions are to be included regarding the brain initial connectivity targeting a multiplex

complex system supposition. Additionally, exploring the high-dimensional data (EEG channels shrinkage) shall be considered duo will be the next step to be explored in further studies.

The application of dynamic linear model extends to the entire medical field; given that biometrics multi-sensory data fusion research displaying the technology advancement as a key facilitator of augmented quality with concurrently reduced costs (KING *et al.*, 2003). Examples can be found in the subject safety programs that use emerging technologies to automate the entire clinical continuum (PAVLOPOULOS; DELOPOULOS, 1999; SORIA-FRISCH; RIERA; DUNNE, 2010; CACAO *et al.*, 2017). Most of this data resulted from biosignals are time-oriented, therefore called time series, which present a dependence requiring special attention on modeling. Hence, the impact of this study will reach the entire medical field that needs to analyze complex data in the spatial and temporal domains.

CHAPTER

4

BRAIN GRAPH COMPLEXITY: REVEALING COMMON CEREBRAL WAVES PATTERN

This chapter corresponds to a white paper, in which presents the discussion towards the efficiency of the Bayesian Network and its dynamism, comparing structural estimations algorithms and numerical approximations towards the time-varying parameters, then later we developed a probabilistic approach to select on of the parameter related with the Approximate Entropy (ApEn) calculation. This work had as co-authors: Lilia Costa (IME-UFBA, Brazil), Oilson Gonzatto (ICMC-USP, Brazil), Joao P Leite (FMRP-USP, Brazil), Dylan Edwards (MOSS, USA and Edith Cowan University, Australia), Taiza E G Santos (FMRP-USP, Brazil), Francisco Louzada (ICMC-USP, Brazil).

Describing the behavioral actions of the human brain presents several challenges since it is a highly complex system. In particular, this system, when stimulated, is of great interest, to neuroscientists, to infer the dynamics of the brain process (or part of it). In this typical case of neurorehabilitation, the first step is to estimate the participant basal brain structure (understanding causal mechanisms that underpin neural communication) and later to summarize the dynamics of the adopted process. Thus, this work aimed to describe the brain connectivity structure adopting probabilistic graph models (e.g. Bayesian Networks) towards its spatial dependence; later, we calculate a complexity measurement of different brain locations based in a transcranial stimulation trial (positioned on the EEG cap), incorporating its estimated spatial dependence. Moreover, this work contribution is regarding the chose criteria of the parameter for the entropy calculation, which we associated with a probabilistic distribution. The results obtained from the simulation studies shown that Tabu Search Algorithm and MDM-IPA are plausible and competitive solutions towards graph structural estimation, as well we conduced three numerical estimations (MCMC, HMC and INLA) related to the BN dynamism and its computational cost; later, a probabilistic entropy calculation illustrated the efficiency of the used models. In this manner, we could use, on human brain experimentation, these techniques with more confidence

towards human brain communication and its complexity estimation.

4.1 Introduction

Stroke is the third global leading cause of disability, and evidence-based rehabilitation intervention to improve the burden from stroke remains limited (FEIGIN *et al.*, 2014). The numbers about the problematic on the world population with stroke is 70%, whereas 87% are related with some physical disability or deaths both in low- and middle-income countries and, over the last four decades, the stroke incidence has more than doubled (JOHNSON *et al.*, 2016). The consequences are immeasurable mainly affecting individuals at the peak of their productive life, in people living in low-and middle-income countries when compared to those in high-income countries (HIC). Despite its enormous impact on the socioeconomic conjuncture of developing countries, this rising crisis has received very little attention to date.

One silent but critical symptom after stroke for which there is no present treatment and is observed in more than half of stroke survivors, is the visual vertical disorder that can occur with lesions in either hemisphere. Since vertical alignment in relation to gravitational forces is required for most of daily activities, the impact on functionality of vertical disorders is devastating (JOHNSTON; MENDIS; MATHERS, 2009). Generally, the error in the perception of visual vertical is tilted to the contralesional side (coronal plane) leading to postural imbalance and higher risk of falls after supratentorial lesions. Reduced visual vertical disorder is associated with better clinical function. Yet to date there are no methods to therapeutically improve this highly prevalent disorder.

Neurorehabilitation is a functional recovery, after some neurological injury, that stimulates to obtain some neuronal restructuring (HARRIS-LOVE; COHEN, 2006). This field deals with noninvasive stimulation techniques, and targets on understanding mechanistic of the information flows. In this manner, this rehabilitation can provide insight regarding the physiologic mechanisms, for instance, as a therapeutic hospital-based rehabilitation after a stroke (AADAL *et al.*, 2013). The brain communication plays an important role in neurorehabilitation techniques, thus its structure rearrangement is composed by neural circuits synchronization. Estimation regarding this topology is a needed, baring-in-mind the existence of a complex arrangement.

Spatial dependence is often described by adopting a grid approach, nevertheless, this path presents limitations regarding a global shared information structure inter-exchange (that is, only focusing on nearest neighborhood's impact). Thereby adopting a complex topology (such as a graph) one overcome this limitation. Zanabria and others (ZANABRIA *et al.*, 2019) elucidate mainly two gains in adopting a more flexible topological structure; i) flexibility to explore between local regions, and ii) Identification of not only prevalent hotspots, but through the measure of centrality to identify information' cluster sharing.

In this manner, graph-based models, using data mining, can be seen as a dynamics of

networks measures modalities that operate on multivariate time series (TS) (COSTA; SMITH; NICHOLS, 2019; NASCIMENTO *et al.*, in press). Through the notion of (temporal) causality by Granger (GRANGER, 1969) and Sims (SIMS, 1972), the Granger causality (GC) approach has become an important part of causal inference. A word of caution regarding GC, Solo (SOLO, 2016) shows that two main issues exists are solved by combined with state-space methods: the effect of downsampling and the effect of filtering on Granger causal structure (GCS), to be overcome using Probabilistic Graphical Models (PGM).

For instance, Bayesian Network (BN) is a representation of a joint distribution of random variables as a PGM, first presented by Kim & Pearl (KIM; PEARL, 1987). In this manner, BN is a powerful tools for representing conditional independencies and dependencies between random variables, defined by some structure and parameters. The relation between variables is represented by a directed acyclic graph (DAG), if satisfying a local Markov condition, and the parameters specify as local conditional probability distributions for each variable. Costa and others (COSTA; SMITH; NICHOLS, 2019) tested different group-structure (GS) methodologies, using Bayesian Network (BN), that models heterogeneity between subjects and searches for distinct homogeneous sub-groups according to some measure that reflects the connectivity maps.

Additionally, entropy analysis is a measurement of the complexity and may identify intervention-related change as a useful "summary" statistic in non-linear dynamical systems (NASCIMENTO *et al.*, 2019). Zhang (ZHANG *et al.*, 2017) discussed that network-based analytics may increase the model structure by regulated pathways rather than common traditional analysis (univariate/multivariate). In this manner, multivariate time series analysis shall be unraveled using entropy-based on its systems' biology pathways with extra support generated by the graph-based model including some complex dependencies, nevertheless their embedded dimension are often unknown. Such methods are capable of estimate complexity and network topology, that is, combining their structure dependence up to dynamic, in order make feasible the estimation process considering the space-time dependencies.

This work aimed to describe the spatial dependence, considering individual contributions, across some brain areas, through a graph structure representation, and then using this information as a Network-based analytics to determine the complexity of the system. Thus, we first compared different methods to unravel the cerebral neural circuit connectivity, and suggest a computational feasible solution.

4.2 Methods

This work was divided into four parts. Section *Methods* contains the statistical methodology adopted on the data set. Moreover, we first bring the causal inference paradigm through the Granger Causality and its implication; its model-based, through the Bayesian Network and its dynamic version, then used this structure dependence estimation in the entropy calculation

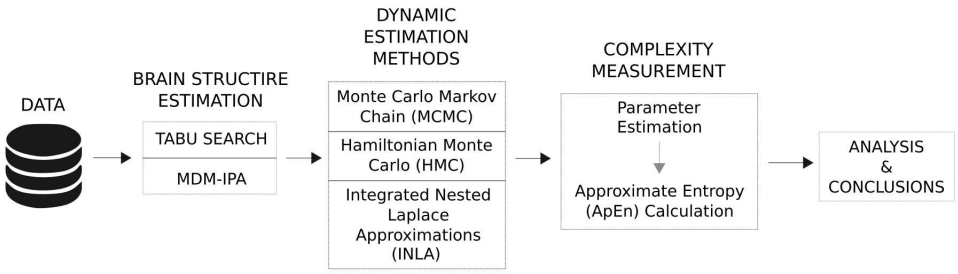

Figure 22 – Visual summary of the adopted methodological framework.

(as TS summarization), whereas we used a probabilistic function to set the entropy parameter (summarized by Figure 22). Section *Simulation Studies* presents, through synthetic data (in a controlled scheme) the comparison of this model performances, from the standpoint of statistical robustness and computational efficiency. Finally, Section *Results* elucidates the neural circuit structural estimation, considering the adopted neurorehabilitation protocol presented in Santos and others (SANTOS *et al.*, 2018), and Section *Conclusion* shows the implications related from the obtained results, and debate towards the state of art of the topic in the field.

4.2.1 Granger Causality

Granger causality is a theoretical framework which assess directional dependencies between time series, based in conditional independence (GRANGER, 1969). The problematic which influenced to fetch towards the dependencies across systems were brought into discussion by Norbet Wiener (WIENER, 1956), then unfolded by Clive Granger (GRANGER, 1963).

As a result of the model-based assessment, the concept of time series influence formulation can be inferred through maximizing the probability given the information contained in the data. That is, supported by the probability theory, random variables (e.g. time series) can be inferred unambiguously only in restricted cases, such as directed acyclic graph (DAG) models (PEARL, 2009; WHITTAKER, 2009). Amblard & Michel (AMBLARD; MICHEL, 2013) presented a review of Granger causality, over the directed information theory perspective, building links between conditional independence and causal conditioning.

In this manner, Granger causality can be seen as pair of time series variables, x_t and y_t. Let $Var(x_t|U_s)$ be the prediction error variance of x_t given U_s. Here U_s means the information set containing all the information in the universe up to time point s, and is called the universal set. For instance, Granger causality is a pair of time series variables (further details see Ozaki (OZAKI, 2012)), x_t and y_t as

- Definition 1: Causality. If $Var(x_t|U_{t1}) < Var(x_t|U_{t1}y_{t1})$, than y_t is causing x_t.
- Definition 2: Feedback. If $Var(x_t|U_{t1}) < Var(x_t|U_{t1}y_{t1})$ and $Var(y_t|U_{t1}) < Var(y_t|U_{t1}x_{t1})$

feedback occurs, which is denoted $y_t \Leftrightarrow x_t$, that is, feedback occurs when y_t causes x_t and also x_t causes y_t.

- Definition 3: Instantaneous causality. If $Var(x_t|U_{t1}, y_t) < Var(x_t|U_{t1})$, instantaneous causality occurs from y_t to x_t. In other words, the current value of x_t is better predicted if the value of y_t is included in the predictor.

- Definition 4: Causality lag. If y_t causes x_t , the causality lag is defined to be the least value of lag k such that $Var(x_t|U_t y_k) < Var(x_t|U_t y_{k+1})$. Here, knowing y_{k+1} will be of no help in improving the prediction of x_t.

The limitations towards Granger Causality come from the following:

1. The use of the nonmathematical "universal" set U_s.

2. Causality is considered on a pair-wise base.

Although the universal set U_s could be a vector variable, the comparison of the value of the prediction error variance is on a pair-wise base between $Var(x_t|U_{t1})$ and $Var(x_t|U_{t1}y_k)$. The benefit of the pair-wise base approach is to enable a direct connection to the graph-model representation, taking advantage of Markov properties assumptions. Moreover, the method for finding total causal relations between the many variables in a feedback system is not well established.

Siggiridou and others (SIGGIRIDOU *et al.*, 2019) concluded, by using model-based measures and information measures, that the Granger causality measures enhance with dimension reduction are superior and should be preferred particularly in studies involving many observed variables. In the counterpart, Zou & Feng (ZOU; FENG, 2009) made a comparative study towards Granger causality versus dynamic Bayesian network inference, discussing that the critical point is in the data length in order to choose the causality approach. For further discussion, this work will present elements in the next subsections, regarding these types of PGM, as well as present a simulation study aiming to seek the out-performance most in the next section.

4.2.2 Bayesian Networks

Bayesian Network (BN) technique was first presented by Judea Pearl, in 1985, as a mathematical probability graph model characterization; motivated by numerous variables, aiming to verify direction (as probabilistic influence) of causality of one variable to another (NEAPOLITAN, 2004). In a mild way, they can be interpreted as a visual and informative representation of the joint probability table of all the variables that involve the domain of the problem. The technology of Bayesian networks is primarily directed to the treatment of discrete

variables, such as, for example, the making of inference algorithms (KEVIN; NICHOLSON, 2004).

Let's us consider a directed graphical structure which presents root and leaf node acyclic, named as DAG, $G = (V,E)$, where the nodes in $V = \{X_1, X_2, \ldots, X_n\}$ represent the variables and E the arcs of the graph encodes conditional dependence relationships among the variables (nodes). Common terminology in the literature is (further details see (FLESCH; LUCAS, 2007)):

- **Parent:** A node is said to be a parent when there is an arc leaving it.
- **Child:** A node is said to be a child when there is an arc arriving it.
- **Parent set:** A parent set is composed by the parents and their respective parent nodes.
- **Neighbors:** Neighbors of a node are all its parents and children.
- **Markov blanket:** Markov blanket of a node is composed by its parents, its children and the other parents of its children.
- **Markov equivalence:** is an essential graphs, with the same set of Markov constraints, implying that offers an unique representations.

Bayesian Networks are DAG's that represent probability distributions. This representation, according to Gamez *et al.* (GÁMEZ; MATEO; PUERTA, 2011) has two components: graphical structure and set of numerical parameters. DAG's also have a set a numerical parameters (Θ), usually conditional probability distributions drawn from the graph structure: For each variable $X_i \in V$ we can define a conditional probability distribution $\Pr(X_i \mid pa(X_i))$, where $pa(X_i)$ is the parent set of X_i in G and represents any combination of the values of the variables in $pa(X_i)$.

4.2.2.1 Learning algorithms

The problem of training a BN can be stated as: Given a training set $D = (u_1, \ldots, u_n)$ of instances of $U = (X_1, \ldots, X_n)$, find a network B that best matches the data D (FRIEDMAN; GEIGER; GOLDSZMIDT, 1997). In this manner, BN learning algorithms can use mainly two types of approaches to find the best network, according to Scutari (SCUTARI, 2009):

- **Score-based algorithms:** for each Bayesian Network configuration a score is associated, then searching to maximize through some heuristic search algorithm aims to maximize the likelihood structure. Greedy search algorithms (such as hill-climbing or tabu search) are often used in the literature.

- **Constraint-based algorithms:** by adopting probabilistic relations based on Markov property, using conditional independence tests, and learning the network structure by constructing a graph which satisfies the corresponding d-separation statements.

The idea of these methodologies is to search the best representation network by starting from an initial solution and performing a finite number of steps. At each step, the algorithm only considers local changes, i.e. neighbor DAGs, and chooses the one resulting in the greatest improvement in the scoring metric f. Gamez *et al.* (GÁMEZ; MATEO; PUERTA, 2011) points that the algorithm stops when there is no local change yielding an improvement in f.

Many score functions f can be used as the best network decider (JIANG *et al.*, 2011), in this paper, we are going to approach the Bayesian scoring criteria. The Bayesian scoring criteria compute the posterior probability distribution, starting from a prior probability distribution on the possible DAG models, conditional on the data.

$$\text{score}_b(G:Data) = \Pr(Data \mid G) = \prod_{i=1}^{b}\prod_{j=1}^{q_i} \frac{\Gamma\left(\sum_{k=1}^{r_i} a_{ijk}\right)}{\Gamma\left(\sum_{k=1}^{r_i} a_{ijk} + \sum_{k=1}^{r_i} s_{ijk}\right)} \prod_{k=1}^{r_i} \frac{\Gamma\left(a_{ijk} + s_{ijk}\right)}{\Gamma\left(a_{ijk}\right)},$$

where r_i is the number of variables X_i, q_i is the number of different values the parents of X_i in G can jointly assume, a_{ijk} is the prior belief concerning the number of times X_i took its k-th value when the parents of X_i took their j-th value, and s_{ijk} is the number of times in the data that X_i took its k-th value when the parents of X_i took their j-th value.

It assumes that each unknown parameter in each DAG model is represented by a Dirichlet distribution, where the hyperparameters a_{ijk} are the parameters for this distribution. According to Dash *et al.* (DASH; DRUZDZEL, 1999), the disadvantage of the score-based algorithms is that they can be very slow in sense of searching through all sample space of graphs. Although any DAG can be used to initialize the search, usually the empty graph (i.e. a graph with no arcs) is used.

Inference task regarding the links' strength is straightforward if such network format is well-defined (known). Nonetheless, individual information should also be included in the estimation process (LIAO *et al.*, 2017; MATTAR *et al.*, 2018), and hierarchical architecture may be an alternative. Costa and others (COSTA *et al.*, in press) discussed the applicability of some network structure estimation methods and visualization of individual patterns (via cluster analysis), highlighting the importance of personal information. Additionally, Dynamic Bayesian Networks are also used regarding the network' dynamism, e.g. through conditional independence with state-space models may riddle it using MDM-IPA (COSTA; SMITH; NICHOLS, 2019) presented next.

Algorithm 2 – Pseudocode for TABU SEARCH

```
INPUT : TabuList_SEARCH
OUTPUT : S_best
S_best ← ConstructInicialSoluction
TabuList ← ∅
while ¬ StopCondition() do
    CandidateList ← ∅
    for S_Candidate ∈ S_best do
        if ¬ ContainAnyFeatures(S_Candidate, TabuList) then
            CandidateList ← S_Candidate
        end if
    end for
    S_Candidate ← LocateBestCandidate(CandidateList)
    if Cost(S_Candidate) ≤ Cost(S_best) then
        S_best ← S_Candidate
        TabuList ← FeatureDifferences(S_Candidate, S_best)
        while TabuList > TabuList_SIZE do
            DeleteFeature(TabuList)
        end while
    end if
end while
```

4.2.3 Dynamic Bayesian Networks

A Dynamic Bayesian Network (DBN) is an extension of a Bayesian network (BN) where the relation across the observed variables are time-varying (DAGUM; GALPER; HORVITZ, 1992). Queen & Smith (QUEEN; SMITH, 1993) also elucidated the advantages of combine state space model with graphical modeling, then developing the Multiregression Dynamic Models (MDMs). In this manner, application with the MDM, uses general probabilistic representation and inference mechanism for arbitrary nonlinear and non-normal time-dependent domains, tested in several fields such as medical (COSTA *et al.*, 2015; NASCIMENTO *et al.*, in press) and traffic (ANACLETO; QUEEN; ALBERS, 2013a).

Dynamic Linear Model (DLM) reveals to be a winning asset towards flexibility in treating non-stationary TS or modeling structural changes, nevertheless presenting easily interpretability. The class of models moves from deterministic to a stochastic system (PETRIS; PETRONE; CAMPAGNOLI, 2009); the uncertainty is always present due to forgotten variables, measurement errors, or imperfections, is supported through some probability density function (π),

$$\pi(y_{n+1}|y_{1:n}) = \frac{\pi(y_{1:n+1})}{\pi(y_{1:n})}.$$

For example, Gaussian linear state space model is a normal probability distribution for the p-dimensional State Vector (unobserved or state equation) and m-dimensional observed Vector (observation equation), moreover, it is a representation of conditional distribution given the available information (deeper details see (WEST; HARRISON, 1989)).

The Bayesian approach suits naturally for the dynamic evolution, where an important feature, regarding the DLM, is that conditional state vector (μ), compound by the observed time series (Y_t), although independent and depends only on (μ). That is,

$$\pi(\mu|y_{1:n}) = \frac{\pi(y_{1:n}|\mu)\pi(\mu)}{\pi(y_{1:n})} \propto \prod_{t=1}^{n} \pi(y_t|\mu)\pi(\mu).$$

The observation evolution and state-space update are incorporated by allowing the time-varying parameters, allowing more complex structures to be added through compounding latent variable into the estimation process. That is, to estimate the state vector, we compute the conditional density $\pi(\mu_s \mid Y)$, where $t = 1,...,T$. Consider μ_t as the mean parameter at the time t of a process, from a series $Y_t = \{y_1,...,y_t\}$, under the Bayesian approach. The DLM update process, on the time point t. The model comprises three stages (evolution, forecast and updates); then as new information approach [in the form of Unobserved/predicted values (μ's)], combined with the t-th new observed value (Y), across the time. Further details about Bayesian Forecasting and Dynamic Models can be found in (WEST; HARRISON, 1989; PETRIS; PETRONE; CAMPAGNOLI, 2009).

Related to the estimation method, s is the recursive period and t is the current period, and is called "filtering (if $s = t$), smoothing (if $s < t$) and state prediction (if $s > t$)". Filtering is a procedure that aims to update current estimates as new data is obtained $\pi(\mu_t \mid y_{1:t})$.

4.2.4 A probabilistic Approximated Entropy

Limitation among regularity in TS data is presented among the usage on entropy, where stationary is also recurrently needed. Despite it, the regularity statistic suggested by Pincus (PINCUS, 1991) uses the capability to discern the changing of the complexity from such a relatively small amount of data. Therefore, he proposed a solution, to summarize the TS, as one representative statistic, is based on a recurrent calculation of conditional probabilities at the i-th time-window. The result is an average obtained from the numbers of distance superior to the filter (r), $d[x,x^*] = \max|u(a) - u^*(a)|$, therefore calculating through $C_i^m(r)$ as a relative frequency of generated vector. ApEn algorithms is similar to K-S entropy, written as

$$ApEn = \Phi^m(r) - \Phi^{m+1}(r), \qquad \text{where} \quad \Phi^m(r) = (N-m+1)^{-1} \sum_{i=1}^{N+m+1} lnC_i^m(r).$$

ApEn calculation requires setting two parameters (m and r), related with the unknown time-series dimension, crucial towards the entropy estimation consistency; the implications of it is that for different m and r values high variability may occur. Observed time series where the "true" dimension is unknown, can be alternatively estimated by embedding its dimension, based on correlation dimension (d), where it can be defined as the nearest integer above $2d + 1$ (Takens, 1981). Chou (2014) suggested for the r value to be fixed as 0.2 times the TS' standard deviation

and m is fixed to 2. Bare in mind that for smaller embedding dimensions chaotic signals may not be distinguishable.

In order to reduce systematic errors, it is often useful to represent the attractor in a higher dimensional space than exactly necessary (Hunt, 2004). However, in higher embedding dimensions, it may not be possible to distinguish between random and chaotic signals. Restrepo and others (RESTREPO; SCHLOTTHAUER; TORRES, 2014) presented empirical discussions towards undermine the ApEn discrimination capacity through misleading parameters. Casiglioni & Rienzo (CASTIGLIONI; RIENZO, 2008) recommended solutions through some r_{MAX} (the value which maximizes the ApEn) and suggesting a search range $(0.1 < r/\sigma(TS) < 1.2)$.

To overcome these selection criteria for Approximate Entropy parameters (m and r), this work suggests incorporating, in the decision-making, the information available in the data, according to the network-based, by associating a probabilistic density function to the desired parameter. For instance, we will focus only on setting parameter (r) and adopting m=2 to all cases as often suggested in the literature (further details see (PINCUS, 1991)).

4.3 Simulation Studies

This work, as a first empirical evidence, considered some synthetic data to compare model-based performances, that is, from the standpoint of statistical robustness and computational efficiency. In this manner, first, we discussed some graph structural estimation enforcement (often presented in the neuroscience field); then later, we debate the implications towards some Bayesian dynamical graph estimation methods. Lastly, we present a solution towards setting the parameter (r) in order to calculate network-based entropy, associating a probabilistic distribution to it (Inverse Nakagami-m (INK) Distribution (LOUZADA; RAMOS; NASCIMENTO, 2018)), that is, by using the information contained in the database we aimed to maximized the information extraction contained into the data.

Graph Structural Estimation Methods

The score-based structure search algorithms, discussed in the methodological section of this work, assign a note to explore the verisimilitude topological structural which maximizes the data information representation. The time/computational demand will be conditional to the number of nodes (representation of the Time Series), whereas increases exponentially as the number of nodes increases, given the search made per each built pairwise.

In this manner, heuristic solutions, e.g. tabu search, are presented in the literature (given the greatness of the search for all possible structures) which outlines the most plausible structure search based on some Markov equivalence, although not searching through the entire space. Alternatively, Costa et. al (COSTA *et al.*, 2015) presented the MDM-IPA which delimits the par-

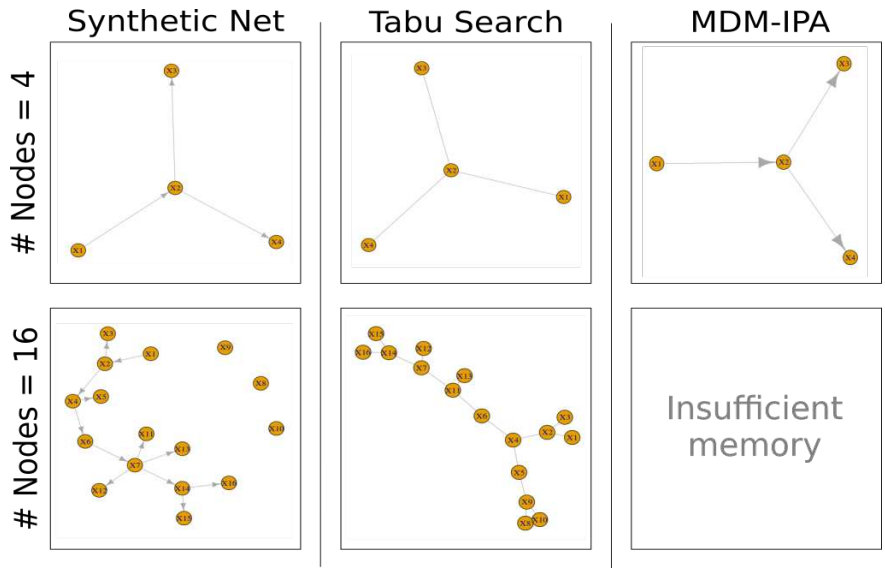

Figure 23 – Comparison of the BN structure. Left-hand side is the known network structure, center is the Tabu Search estimated network, and right-hand side the MDM-IPA estimated structure. The topology estimation performance of Tabu Search was superior than MDM-IPA, especially its time cost.

enting search space in up to 3 descendants, considering this problem as an integer programming approach, but its performance is limited by the existence of a few nodes.

This work tested the performance of Tabu and MDM-IPA algorithms, considering two synthetic databases (contain 6 and 16 time series respectively). Figure 23 describes visually the comparison through the original network and the estimated ones.

The Tabu Search routine is implemented in the *bnlearn* package in R. MDM-IPA routine combines a Bayesian Scores using R, as a first step, then through Gobnilp (program used to complete discrete/continuous data or precomputed local scores) the most likely DAG is formed. Just for illustration, Table 6 shows the obtained result, moreover it shows that node X1 is the parent of X2 and node X2 is the parent of X3 and X4.

Table 6 – BN score for the synthetic 4 nodes network.

Nodes	BN score
X1 ←	-769.99
X2 ← X1	-709.14
X3 ← X2	-655.79
X4 ← X2	-697.30
Total	-2832.23

The elements presented, so far, brought some evidences towards the BN structure estimation robustness by adopting both algorithms. The dynamic of a Network, once its structure was defined, is an easier task adopting some dynamic graphical model. Although, different numerical approximation are available in the literature, like Monte Carlo, and needed to be tested. Next

subtopic will discuss that.

4.3.1 Bayesian Numerical Approximations

Some difficulties are related with the approximation method towards time-varying parameters models were investigated and shall be discussed in the TS non-stationary context. In this manner, Synthetic data set used previously, considering only 4 nodes time points was considered. Here we describe the process of this simulation.

$$\theta_{tid}^{(k)}(r) \sim \mathcal{N}(\theta_{t-1id}^{(k)}(r), W_d^{(k)}(r)),$$

for $r = 1,\ldots,4$; $t = 1,\ldots,500$ or 5,000 or 5,000,000; $i = 1,\ldots,10$; $d = 1,2,3$; $k = 1,\ldots,p_{rd}$; and $W_d^{(k)}(r) = 0.04 \times V_d(r)$.

For this DAG, $p_{11} = 1$; $p_{21} = p_{31} = 2$ and $p_{41} = 3$. The initial values ($t = 0$) for the regression parameters were -0.5 for connections $Y(1) \rightarrow Y(2)$; 1 for $Y(2) \rightarrow Y(3)$; 1.5 for $Y(2) \rightarrow Y(4)$ and the value 0 for other θ's (intercept parameters). The observational variance ($V_1(r)$) was defined as almost one for all nodes. Observed values were then simulated using the following equations:

$$\begin{aligned}
Y_{tid}(1) &= \theta_{tid}^{(1)}(1) + v_{tid}(1); \\
Y_{tid}(4) &= \theta_{tid}^{(1)}(2) + \theta_{tid}^{(1)}(2) Y_{tid}(1) + v_{tid}(2); \\
Y_{tid}(3) &= \theta_{tid}^{(1)}(3) + \theta_{tid}^{(2)}(3) Y_{tid}(2) + v_{tid}(3); \\
Y_{tid}(4) &= \theta_{tid}^{(1)}(4) + \theta_{tid}^{(2)}(4) Y_{tid}(2) + v_{tid}(4);
\end{aligned}$$

where $d = 1$ and $v_{tid}(r) \sim \mathcal{N}(0, V_d(r))$, for $r = 1,\ldots,4$.

Considering only this BN structure with 4 nodes a analyzed about their dynamic evolution were conduced. Figure 24 describes $\theta_{tid}^{(1)}(1) + v_{tid}(1)$, visually, the Bayesian mean posterior value, through time, according three different numerical approximation (MCMC, HMC, and INLA) for a time series size of n=500 only. Table 7 shows the time cost of adopting three different time series size (n=500, 5,000, 5,000,000) as well.

Table 7 – Time cost (in minutes) adopting three different numerical approximation with time series size (n=500, 5,000, 5,000,000).

Sample Size	MCMC	HMC	INLA
500	1.035	9.305	0.172
5,000	11.04	82.315	1.333

The MDM combined with INLA approximation shows to be very promising given its computational efficiency (much less time consuming). The next step will be to analyse the residue of the adjusted models, seeking towards elements if some remaining pattern is left in the

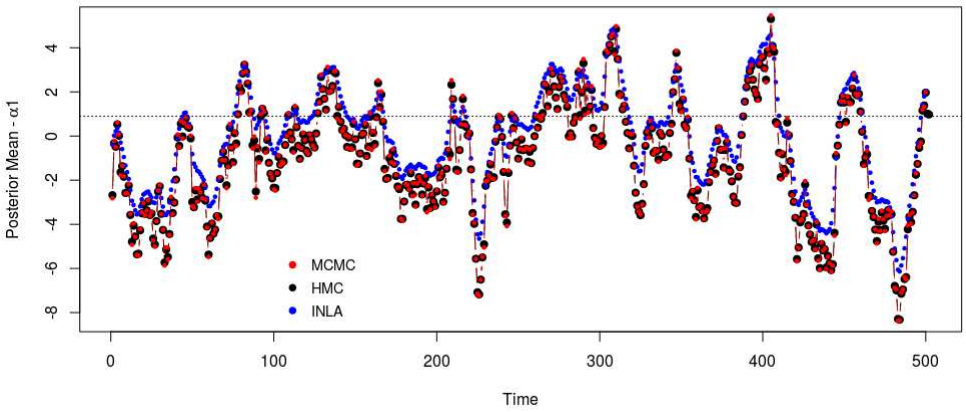

Figure 24 – MDM time-varying parameter (α_1) based on numerical estimation methods. (black dot line) Real parameter value. (red dot and dashed curved line) MCMC approximation method. (black dot and dashed curved line) HMC approximation method. (blue dot and dashed curved line) INLA approximation method. The real parameter (0.9) presents a time-varying characteristic, which incorporates a random walk from a Normal distribution with 0 mean and 1 variation.

TS noise. That is, if the presence of randomness is observed (through the TS complexity) then the BN and DBN is explaining the brain connectivity task well.

4.3.2 Probabilistic ApEn

Aproximated Entropy measures the amount of randomness in a TS, calculated based in two determined parameter m and r. Some suggestions are presented in the literature, although it remains as an open question. This work suggests to incorporate a probabilistic distribution to the r parameter, aiming to maximizing the retrieve information mining from the TS.

–Random TS drawn from a Normal distribution

The chosen distribution was the INK where some interesting mathematical properties were proven by Louzada, Ramos & Nascimento (LOUZADA; RAMOS; NASCIMENTO, 2018) related to its rth moment, mean, variance, rth central moment, and Shannon's entropy. Specially, INK distribution as a asymmetry, placing the kernel of the probability distribution on the often suggested range of the threshold tolerance for accepting similar patterns between two subsequences (parameter r).

The probabilistic look, through the ApEn parameter selection novel was motivated by the elements presented in the literature when most of works adopted r as $0.2 * sd(TS)$, nevertheless it is a reasonable to search as far as $1.2 * sd(TS)$ (CASTIGLIONI; RIENZO, 2008). Therefore, as an exemplification, we placed 99% of the INK density in the interval $[0.1, 1.2]$. The workflow of this part is described in three steps.

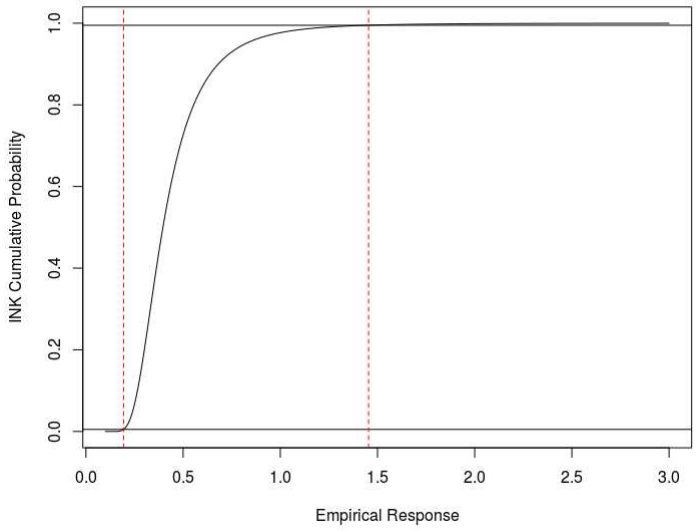

Figure 25 – Visual representation toward the optimization method on estimating parameters which live the 1% and 99% quantils of the INK distribution. Y-aes represents the accumulative INK distribution, and X-aes the empirical distribution (based on the optimization method). The vertical dashed red-lines are the correspondent quantils, and horizontal solid black-line the real quantils. Since those lines has intersections in the same quantil value, then shown the efficiency of the adopted optimization method.

STEP 1. Consider a TS, then based on the observed values, the INK's parameters calculated through a optimization method to minimize a function by a trust region method that forms quadratic models by interpolation.

The used r function was *optimr* implemented in *optimx* package. Figure 25 shows an example of a robustness of this function, where the quanties of the cumulative probability function meets with the estimated using the data.

Figure 26 illustrates the estimated probability density, based on the obtained optimum parameters (according to the data).

STEP 2. Generate values from the INK were taken, consider $i = \{1, ..., n\}$, where first generate $X_i \sim Gamma(\mu, \mu/\Omega)$, then $T_i = (\sqrt{X_i})^{-1}$.

Figure 27 shows the obtained distribution of the sampled INK.

STEP 3. Varying the r values, then calculated the ApEn in order to get a picture of the entropy behaviour. In this manner, according to some Decision Criteria, the research shall choose the r value.

Figure 28 shows the calculated ApEn, based on a vector $[0.1, 1.2]$ with 0.1 increment. Through some decision criteria, like rth central moment and quantil, the researcher will not needless have to calculate empirically the ApEn every-time, but only seek for the associated shape of the distribution (related with the data), saving computational demanding. This task

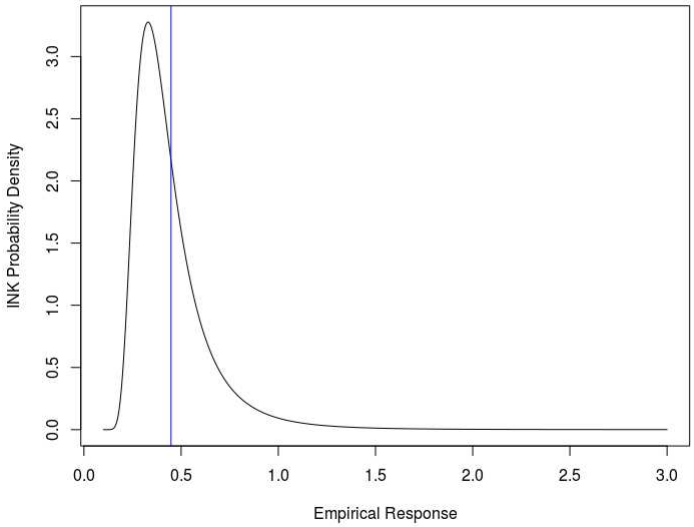

Figure 26 – Estimated the shape of the INK distribution based on the optimal parameters obtained from the *optimx* package. Blue line represents the mean of the distribution. Bare in mind the kernel of this function is around 0.2 often the suggested value for the ApEn *r* value.

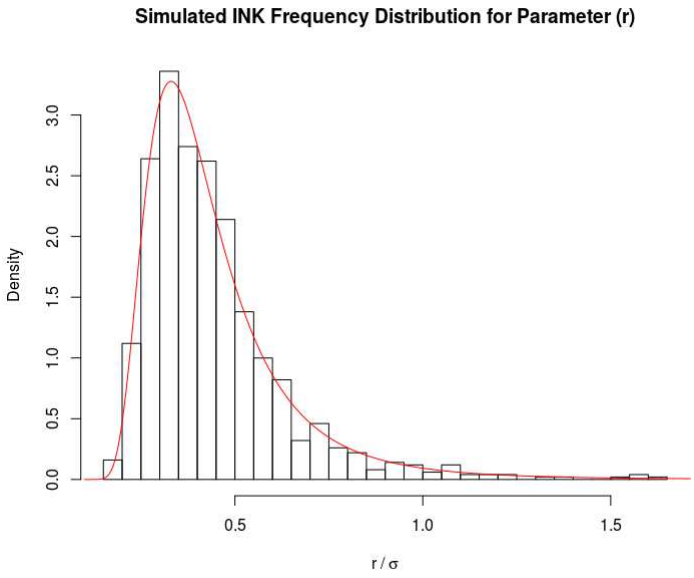

Figure 27 – Empirical distribution of a simulated value based on the estimated INK. Red curve represents the real INK distribution based on the optimal obtained parameters.

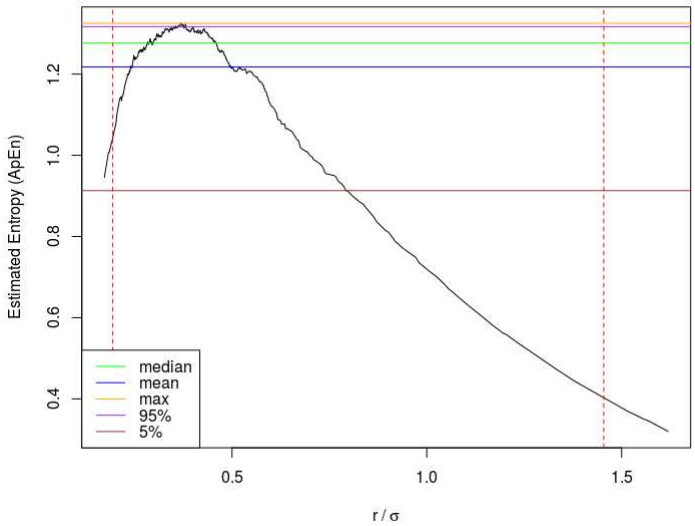

Figure 28 – Empirical ApEn calculation varying the r parameter. Different lines represent different moments from the INK distribution, enabling the ApEn maximization through the best *r* value selection criteria.

maximizes the information obtained through ApEn, as well as solves the threshold "r" influences approximate entropy analysis (see (SANTOS *et al.*, 2018)).

4.4 Results

Brain connectivity is a highly complex system, nevertheless, some neurorehabilitation task focuses on estimating structural break related to some specific brain region given a stimulation. That is, regarding a chain of neuronal pins, it is desirable to study three elements from a biosignal; i) the structural brain connection, ii) the time dynamics of the brain connectivity, and iii) the brain connectivity complexity given a stimulation per region.

The data acquisition belongs from a novel approach to systematically analyze the dose-response effects of a focal electrical stimulation, concerning around the dynamic of the brain vertical manipulation (related with the stroke recovery challenge) (SANTOS *et al.*, 2018). All of the observed biosignal (from the EEG signal) have 300-second window total, considering a frequency of 500Hz (sample rate), returned 150.000 observations in this given time period. Due the signals' high-frequency, a simple transformation was conducted to simplify the interpretation across the series. A median was taken from windows of very 500 spaced observations (the sample size-frequency), which results in a median single point per second, thus the series representation would be preserved such its behavior and reduce its noise (called smooth series, containing only 300 observations each TS). In this work, we only focused on a single Cathodal montage 2mA from a single participant.

(a) EEG cap with 6 electrodes (b) EEG cap with 16 electrodes (c) EEG cap with 64 electrodes

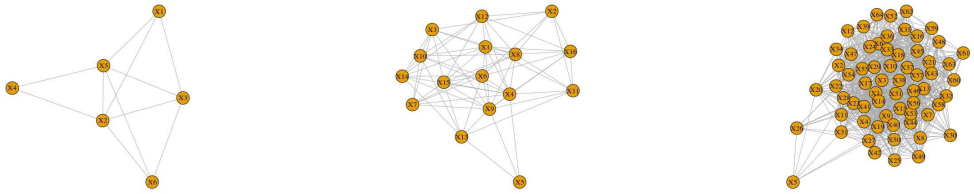

Figure 29 – Tabu Search to estimate the brain structure considering the number of 6, 16 and 64 EEG electrodes.

4.4.1 Part I – Structural brain connection estimation

After this TS transformation, based on the Tabu Search algorithm performance showed in the simulation studies, the brain network structural estimation (as a BN) was conduced considering 6, 16 and 64 nodes. Figure 29 display the estimated structure for each scenario. This worth to mention that the computational cost was not even 2 seconds for the biggest network using this heuristic.

With this estimated BN, to calculate the dynamism of each link is a straight task, using a state-space model (moreover the class of MDM). The next subsection will discuss which numerical approximation suits appropriate with the MDM.

4.4.2 Part II – Brain connectivity dynamic

Dynamic BN (DBN) may be estimated using the MDM, for the sake of illustration, let's just consider the brain EEG cap with only 6 EEG-electrodes. According to the estimated structural brain connection estimation (from part I), the theoretical equations associated with the DBN are given

$$\theta_{tid}^{(k)}(r) \sim \mathcal{N}(\theta_{t-1id}^{(k)}(r), W_d^{(k)}(r)),$$

for $r = 1,\ldots,6$; $t = 1,\ldots,300$; $i = 1$; $d = 1$; $k = 1,\ldots,p_{rd}$; and $W_d^{(k)}(r) = V_d(r)$.

For this DAG, with connections $Y(1) \leftrightarrow Y(2) \leftrightarrow Y(3) \leftrightarrow Y(5)$; for $Y(2) \leftrightarrow Y(6) \leftrightarrow Y(3) \leftrightarrow Y(5)$; for $Y(4) \rightarrow Y(2) \leftrightarrow Y(5)$ and the value 0 for other θ's (intercept parameters). The observational variance ($V_1(r)$) was defined as almost one for all nodes. Observed values were

then simulated using the following equations:

$$
\begin{aligned}
Y_{tid}(1) &= \theta_{tid}^{(1)}(1)+\theta_{tid}^{(1)}(2)Y_{tid}(2)+\theta_{tid}^{(1)}(3)Y_{tid}(3)+\theta_{tid}^{(1)}(4)Y_{tid}(5)+v_{tid}(1);\\
Y_{tid}(2) &= \theta_{tid}^{(2)}(1)+\theta_{tid}^{(2)}(2)Y_{tid}(1)+\theta_{tid}^{(2)}(3)Y_{tid}(3)+\theta_{tid}^{(2)}(4)Y_{tid}(3)+\theta_{tid}^{(2)}(5)Y_{tid}(5)\\
&\quad +\theta_{tid}^{(2)}(6)Y_{tid}(6)+v_{tid}(2);\\
Y_{tid}(3) &= \theta_{tid}^{(3)}(1)+\theta_{tid}^{(3)}(2)Y_{tid}(1)+\theta_{tid}^{(3)}(3)Y_{tid}(3)+\theta_{tid}^{(3)}(4)Y_{tid}(5)+\theta_{tid}^{(3)}(5)Y_{tid}(6)+v_{tid}(3);\\
Y_{tid}(4) &= \theta_{tid}^{(4)}(1)+\theta_{tid}^{(4)}(2)Y_{tid}(2)+\theta_{tid}^{(4)}(3)Y_{tid}(5)+v_{tid}(4);\\
Y_{tid}(5) &= \theta_{tid}^{(5)}(1)+\theta_{tid}^{(5)}(2)Y_{tid}(1)+\theta_{tid}^{(5)}(3)Y_{tid}(3)+\theta_{tid}^{(5)}(4)Y_{tid}(3)+\theta_{tid}^{(5)}(5)Y_{tid}(2)\\
&\quad +\theta_{tid}^{(5)}(6)Y_{tid}(6)+v_{tid}(5);\\
Y_{tid}(6) &= \theta_{tid}^{(6)}(1)+\theta_{tid}^{(6)}(2)Y_{tid}(2)+\theta_{tid}^{(6)}(3)Y_{tid}(3)+\theta_{tid}^{(6)}(4)Y_{tid}(5)+v_{tid}(6);
\end{aligned}
$$

where $d=1$ and $v_{tid}(r)\sim\mathcal{N}(0,V_d(r))$, for $r=1,\ldots,6$.

Figure 30 shows the model performance, considering only the TS drift of the residual, that is, after explained the BN dynamism suggesting the presence of a white noise. In this manner, MDM model describes the trajectory of the biosignal, considering neuronal connectivity, showing that the unexplained elements (pure noise), as least visually, that do not present any pattern.

In order to verify if the MDM residuals contain some pattern, the ApEn measure of complexity will be used aiming to measure of the regularity of TS. Moreover, we also incorporated the r parameter selection based on the INK probability distribution shown as follows.

4.4.3 Part III – Brain complexity

As said, using the Network-based dependence information, the parameter r will be associate with a probabilistic distribution INK then estimated each TS Approximated Entropy (AnEp). We are now able to measure each EEG selected channel randomness, by looking at the unexplained elements of each MDM adjusted equation. Moreover, given the chain information derived from the structural brain connection, we estimated its information gain as previously shown (in Part I and II).

Table 8 shows the complexity measurement, using the INK distribution versus $0.2\times\sigma$(TS), of each MDM adjusted equation unexplained part only. As their scale is closer to 1, this could be interpreted as pure noise (suggested visually in part II).

Based on the obtained results, those techniques seem to be competitive to unravel the brain connectivity and complexity helping the neuroscientists on different experiments trials. The obtained understanding is that after modeling the brain dynamic, as a BN, its remaining information, using the entropy analysis with the probabilistic approach, underlies on structure similarly from a random distribution (based on the likelihood of the noise of the originated series). In this manner, the obtained pattern recognition through the graph-based models was well accomplished.

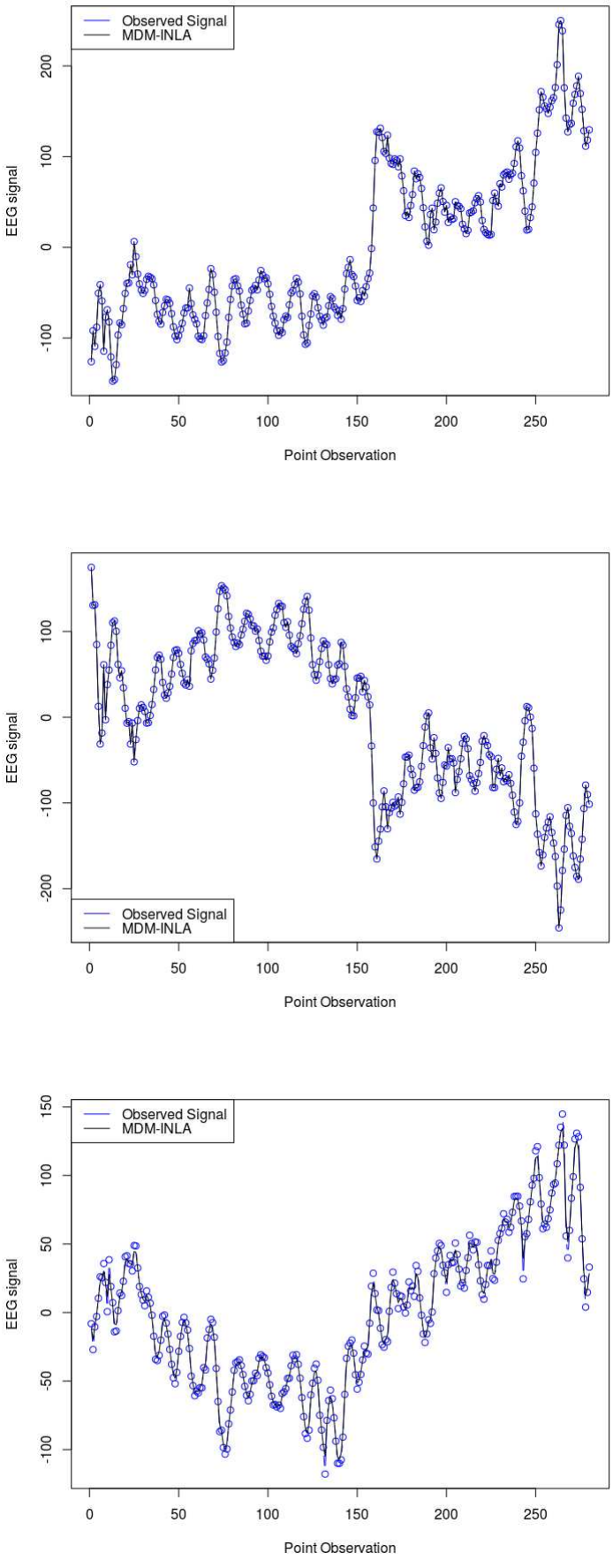

Figure 30 – Tabu Search to estimate the brain structure considering 6, 16 and 64 EEG electrodes.

Table 8 – Probabilistic ApEn (r) based on the INK quantile 1% versus $0.2\times\sigma$(TS).

	ApEn + INK	ApEn ($0.2\times\sigma$(TS))
Y1	0.8185	0.55
Y2	0.7369	0.48
Y3	0.7865	0.62
Y4	0.7221	0.53
Y5	0.7159	0.51
Y6	0.8409	0.68

4.5 Conclusion

Estimation towards network structure is not a trivial task (CHICKERING, 1996b). Nevertheless, some efforts were made in the direction of a feasible new solutions (statistical and computational per say) (COSTA *et al.*, 2015; GLOVER, 1990). Emphasizing that inference duty regarding the links' strength is straightforward if such network format is well-defined (known).

This work described the estimation of communication and recognition of brain patterns in a neuroscience experiment. The first bypassed problem referred to the estimation of the structure of a complex network, later its dynamics, and finally, it analyzed the residuals of the models in order to search for the existence of some pattern. Based on the empirical results obtained, specialists in the area confirmed the veracity of the estimated structure, supporting its usefulness. Subsequently, the extraction of relevant information from the models was confirmed (based on some results from Figures 29 and 30), since the residues presented a random characteristic (according to Table 8, TS patterns already extracted).

Previous work (LI *et al.*, 2008; IDE; ZHANG; CHIANG-SHAN, 2014) also applied Bayseian Network using VTS, CS, and IS methods to estimate the network structure, although they all recognize the importance of personal information as latent discrimination (important in the multi-participant scenario). (COSTA; SMITH; NICHOLS, 2019) extend the discussing by comparing a variety of structure estimation using MDM-IPA, where conditional independence with state-space models addresses the common network structure across Individual Estimation of Multiple Networks (IEMN) and the Marginal Estimation of Multiple Networks (MEMN) compared both from a theoretical/practical perspective using e.g. real fMRI data.

Therefore, we discussed in the paper (COSTA *et al.*, in press) a new dynamic BN structure estimation method named Hierarchical MDM (HMDM), which incorporated in the estimation process in personal/latent feature. Thus, individual information should be included in a hierarchical estimation process, regarding latent features (LIAO *et al.*, 2017; MATTAR *et al.*, 2018). Additionally, embedding projection reduction space through cluster analysis showed that the results incorporate the individual information combining with a common shared dynamic enhancing the obtained estimations.

Then as a natural future work to be extended the DBN as an hierarchical dynamic

models (specifically the HMDM) present limitations regarding the (i) large amount of parameters (over-parametrization) and (ii) non-trivial automatized selection towards the definition of a parsimonious transfer function to ensure the accuracy of the model's power prediction, that is, its lag orders and important components (DEY; RAO, 2005). As well to test some shrinkage approach towards the data high-dimensional curse presented in neuroscience experiment.

CHAPTER

5

DYNAMIC TIME SERIES SMOOTHING FOR SYMBOLIC INTERVAL DATA APPLIED TO NEUROSCIENCE

This chapter corresponds to a manuscript published at *Information Sciences* journal, in which presents the discussion towards data shrinkage dimension, using the Symbolic Data Analysis (SDA), and developing a dynamic version of smoothing a time series. This work had as co-authors: Bruno Pimentel (UFAL, Brazil), Renata Souza (UFPE, Brazil), Joao P Leite (FMRP-USP, Brazil), Dylan Edwards (MOSS, USA and Edith Cowan University, Australia), Taiza E G Santos (FMRP-USP, Brazil), Francisco Louzada (ICMC-USP, Brazil).

This work aimed to appraise a multivariate time series, high-dimensionality data-set, presented as intervals using a Symbolic Data Analysis (SDA) approach. SDA reduces data dimensionality, considering the complexity of the model information through a set-valued (interval or multi-valued). Additionally, Dynamic Linear Models (DLM) are distinguished by modeling univariate or multivariate time series in the presence of non-stationarity, structural changes and irregular patterns. We considered neurophysiological (EEG) data associated with experimental manipulation of verticality perception in humans, using transcranial electrical stimulation. The innovation of the present work is centered on use of a dynamic linear model with SDA methodology, and SDA applications for analyzing EEG data.

5.1 Introduction

Over the past few years, advances in medical technology equipment has provided a range of records containing a large volume of information, with associated effects to establish similarities and find particular patterns/characteristics. In data mining, two core tasks are similarity measurement and data segmentation, roughly classified in four fields: pattern discovery/cluster-

ing; classification; rule learning; and summarization/visualization ((FU, 2011)). We are in an era of big data which has enormous potential, presenting massive, complex and dynamic indexing information indexed in time ((CORCHADO *et al.*, 2014)). Thus, there is a growing need for investigation into new statistical models in the medical field ((GANTI; GEHRKE; RAMAKRISHNAN, 1999; JUDSON; OWEN, 1999; FERNÁNDEZ-VILLAVERDE; RUBIO-RAMÍREZ, 2007)) to analyze temporal data, using similarity measures, considering the presence of high dimensionality with nonlinear dynamics.

The characterization of cerebral physiology is fundamental in understanding the dynamics of response to an external stimulus to the brain. This type of data is developed due to the brain complexity and the high-dimensional idiosyncrasies of each neural network. Brain function can be assessed using non-invasive techniques such as electroencephalogram (EEG), transcranial Doppler, and neuroimaging techniques (e.g., functional magnetic resonance imaging). Therefore, data regarding neuroscience methods can present a high spatial dimensionality, and high frequency (being able to reach an observation per millisecond). One relevant interest in the neuroscience field is to interpret brain electric field patterns to understand mechanisms of brain information processing ((KRYSTAL; PRADO; WEST, 1999; COSTA *et al.*, 2017)).

A natural way of describing neural dynamics as a mathematical model, considering it as a high-frequency system, would be to reduce its size (e.g., by clustering) or its frequency (e.g., obtaining the median of one series every second). Data size can also be reduced using Symbolic Data Analysis (SDA) techniques ((PIMENTEL; SOUZA, 2014)). More complex information can be modeled through set-valued (interval or multi-valued) or modal (weight or probability distribution) variables also termed as 'symbolic', and extend classical data analysis techniques, such as clustering, factorial techniques, decision trees and other symbolic data. These analyses account for variability and/or uncertainty, making the symbolic data analysis more comprehensive than classical data analyses ((DIDAY; NOIRHOMME-FRAITURE, 2008)).

This paper introduces dynamic linear models to interval neuroscience data, where interval is defined as a set of real numbers that lies between two numbers. The applied idea is innovative for two reasons: i) the models are capable of incorporating dynamic events regarding more complex data, showing a competitive alternative to modeling a problem, given its flexibility and speed in data convergence; and ii) neuroscience research dynamic accommodation questions can be solved in order to reveal the pattern of brain activity. In this paper, we apply our analyses to electroencephalographic data collected in an interventional study examining effects of non-invasive brain stimulation. EEG data was collected before and after the application of anode center conditions of a high-definition transcranial direct current stimulation (HD-tDCS) applied over the temporal-parietal junction at a current intensity of 1mA in healthy subjects. This HD-tDCS protocol has proved to induce clinically relevant behavioral change (verticality perception and postural control) in healthy subjects ((SANTOS-PONTELLI *et al.*, 2016)) and assessed as a treatment in patients after stroke ((REDING *et al.*, 2017; BABYAR *et al.*, 2016)).

This paper contributes to the literature, a dynamic linear model (DLM) for interval data (SDA), where past SDA work ((BILLARD; DIDAY, 2000), (Lima Neto; De Carvalho, 2008)) only considered static models (linear model). Moreover, it underlies the change in the background that stays approximately constant over time. A Dynamic regression, with a state space approach tries to avoid some of the problems, such as stationarity. By explicitly considering variability in the regression coefficients, the proposed model allows the system properties to change with time. Moreover, the use of unobservable state variables allows direct modelling of the processes that drive the observed variability, such as external forcing, and accounts for modelling error.

Since the behavior effect is described to be a consequence of a change in neuronal activity ((TEPLAN *et al.*, 2002)), the investigators aimed to understand patterns of neuronal activation of different brain areas in relation to the stimulation protocol (i.e. spatial and temporal dimensions). The motivation for using a more appropriate mathematical strategy stems from the need for a better understanding of the activation of different brain areas after non-invasive transcranial stimulation ((SANTOS *et al.*, 2018)).

5.2 Symbolic Data Analysis

Most of the methods in the literature discuss data analysis involving numerical data only ((BOCK; DIDAY, 2012; DIDAY; NOIRHOMME-FRAITURE, 2008; NOIRHOMME-FRAITURE; BRITO, 2011)). In classical data analyses, objects are often represented as quantitative or qualitative values, where each one represents a variable. However, this representation may not be adequate to model more complex information found in applied problems ((BOCK; DIDAY, 2012)). Databases, for example, may be large and many clustering methods take time trying to extract information. A solution to execute these methods more efficiently is to summarize these data using symbolic methods ((BILLARD; DIDAY, 2006; DIDAY; NOIRHOMME-FRAITURE, 2008)).

Nowadays the concept of Data Science, considered as a science by itself, is the extraction of knowledge from data and is a new way of thinking Data Science by extending the standard input to a set of classes of individual entities ((DIDAY, 2016)). SDA handles of this type of data that may be represented as an interval, histogram, distribution and so on in order to take into account the variability and/or uncertainty innate of data ((DIDAY; NOIRHOMME-FRAITURE, 2008; BILLARD; DIDAY, 2003)). The SDA framework extends standard statistics and data mining tools to symbolic data, such as descriptive statistics, multidimensional data analysis, regression, classification, dissimilarities and clustering ((BILLARD, 2008; DIDAY; SIMON, 1976)).

In the context of linear models for interval data, some approaches have been proposed regarding the centre-range and lower-upper representations. (BILLARD; DIDAY, 2002a) proposed a regression model for interval data using the lower-upper representation, and (Lima

Neto; De Carvalho, 2008) demonstrated the superiority of the centre-range representation compared to the lower-upper range in terms of the root mean square. Regarding the lower-upper representation, (WANG; GUAN; WU, 2012) proposed a linear model which uses all interval points and (SOUZA *et al.*, 2017) introduced a lower-upper regression model which uses an interval Box-Cox transformation for the interval response variable. All models used ordinary least squares estimates.

Moreover, in the context of robust linear models for treating interval outliers, (DOMINGUES; SOUZA; CYSNEIROS, 2010) introduced an interval linear approach which builds two models assuming symmetric errors for centres and ranges of the intervals. (FAGUNDES; SOUZA; CYSNEIROS, 2013) presented a robust regression model for interval data based on centre-range representation using iterative re-weighted least-squares and (NETO; CARVALHO, 2018) proposed a robust regression using an exponential kernel to penalize the outliers in the centre and range of intervals. All of the linear models mentioned above were developed for static events, while dynamic events for interval data are still an open question in the area of SDA.

A few studies present real data applications in SDA with interval approaches. In particular, neuroscience data analysis is a type of application that has not yet been explored. Concerning the social services domain, (NETO; CARVALHO, 2002) showed an application concerning administrative management of Brazilian cities (in Pernambuco state) using interval-valued variables. (SILVA *et al.*, 2006) made experiments using information of web users whose aim is to cluster users with the same web usage behavior together. (ZUCCOLOTTO, 2007) presented Symbolic Data Analysis in a database about job satisfaction of Italian workers through the principal component analysis method. In the economic field, (GIUSTI; GRASSINI, 2008) presented cluster analysis using a symbolic data approach to cluster local areas in Italy based on their economic specialization.

Concerning the domain of engineering, (CURY; CRÉMONA, 2012) applied SDA for classifying different civil engineering structure behaviors comparing any structural behavior to the previous classification when new data became available. (GONZÁLEZ-RIVERA; ARROYO, 2012) proposed using SDA in the daily histogram time series of S&P500 intradaily returns. (PIMENTEL; SOUZA, 2014) showed an application in scientific production and educational data collected from the National Council for Scientific and Technological Development (a Brazilian agency), where a statistical analysis was carried out using SDA.

In this paper, the advantages for modelling neuroscience data in the symbolic data framework are:

- **Summarized data**: Initially, our data set contains more than 1.5 billion observations per dose-response. These data can be aggregated using cortical regions and a new reduced-size dataset can be obtained whilst preserving most of the data;
- **Use of a higher-level category**: The original data contain signals of a multi-channel

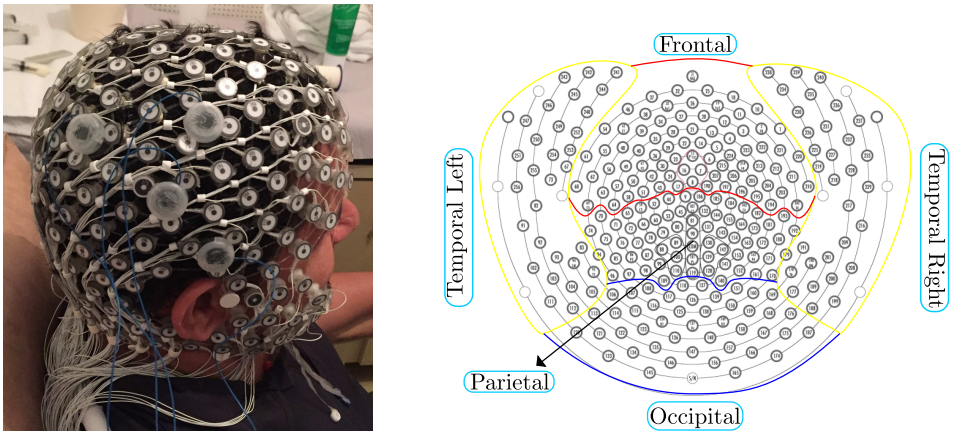

Figure 31 – The left-hand image shows the position of the $HD-tDCS_{3\times1}$ electrodes in a male participant, and the right-hand illustration dispersion of EEG electrodes demarcated by cortical areas of the brain. Written informed consent was obtained from the participant for the publication of this image.

electroencephalogram, corresponding to a frequency over time. Here, the analysis can be carried out combining the time-domain along with the frequency-domain in time series analysis. The new units obtained from the aggregation process are considered as units at a higher level of generalization than individuals.

5.3 Interval EEG data

The dataset used to describe the proposed statistical method originated from a randomized, double-blind, crossover clinical trial that investigated polarity and intensity-dependent effects of high-definition transcranial direct current stimulation (HD-tDCS) applied to the temporo-parietal junction on neuronal activity using EEG in healthy subjects (SANTOS *et al.*, 2018). Here we present the data of one participant, under an anode center condition of HD-tDCS, at a current intensity of 1mA. The outcome measure of this study was the signal of a high dimensional multi-channel electroencephalogram with 256 channels (Figure 31 left-hand side). The electrodes were grouped into 5 areas (Left Temporal, Right Temporal, Frontal, Parietal and Occipital). Hence, 31 channels were grouped in each temporal region, 81 channels in the frontal, 68 in the parietal and 45 in the occipital, as illustrated in Figure 31 right-hand side.

After grouping the respective channels per cortical region, the observations were summarized according to their tenth and ninetieth percentile (P10, and P90) configuration. This methodology seeks to group the brain waves of each region in a range, not only aiming to reduce its dimension but also as a denoising method. This interval grouping procedure was necessary due to the high-dimensionality characteristic of the data, where the experiment arrangement for each patient considering only the time-point of assessment after the HD-tDCS generates 1,500,000 observation per current intensity, in 5 minutes of observation. Consequently, 256 channels generate 1,536,000,000 observations, considering only one montage without the repetitions,

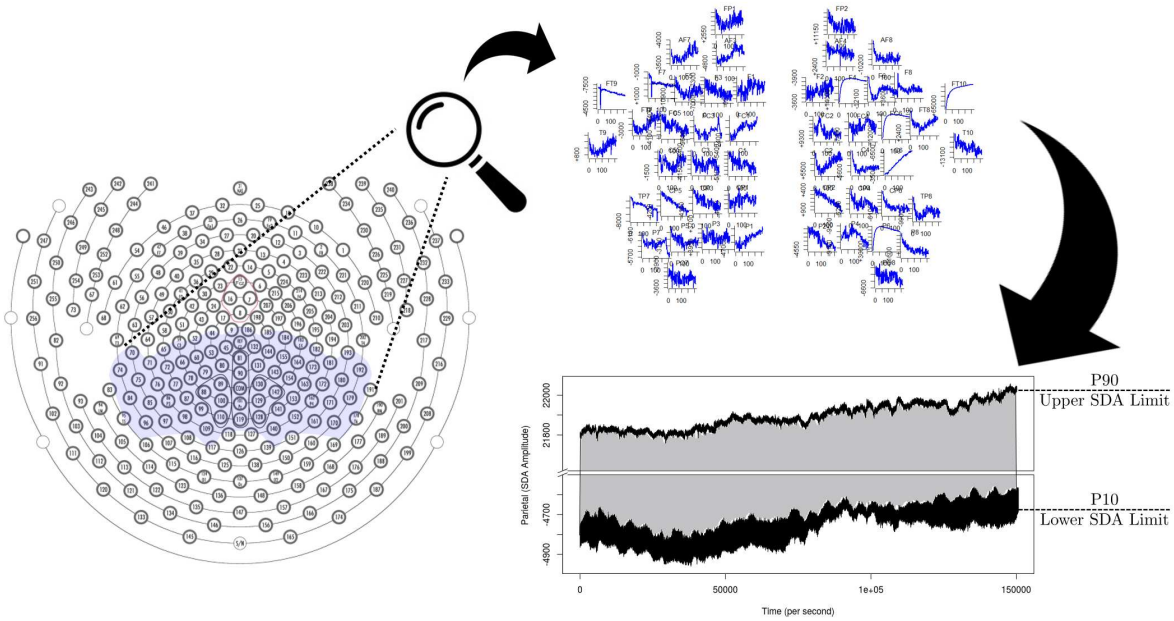

Figure 32 – Classical data transformation into symbolic interval data. (Left) Selected parietal cortical region, (Right top) Time series of some channels, and (Right bottom) Symbolic interval parietal cortical data.

and results in approximately 2.5GB of data.

By adopting the SDA methodology, instead of 256 channels, the data is reduced to 5 interval vectors (related to the 5 major cortical regions, resulting in 10 series of 1,500,000 observations) then condensed into 15,000,000 total observations, and is only 0.98% of the original data size. Figure 32 illustrates the transformation of the classical data into symbolic interval data, using SDA, for a selected region.

5.4 Dynamic linear model for interval EEG data

The interval statistical model presented in this paper is based on a dynamic linear model (DLM) that is a specific case of the space-state model, considering the centre-range and lower-upper bound representations for interval data.

5.4.1 Dynamic linear model

The Gaussian linear state space models, also known as the dynamic linear model (DLM), are specified by a normal probability distribution for the p-dimensional State Vector and m-dimensional observed Vector. At time $t = 0$,

$$\mu_0 \sim N_p(\theta_0, \sigma_0^2)$$

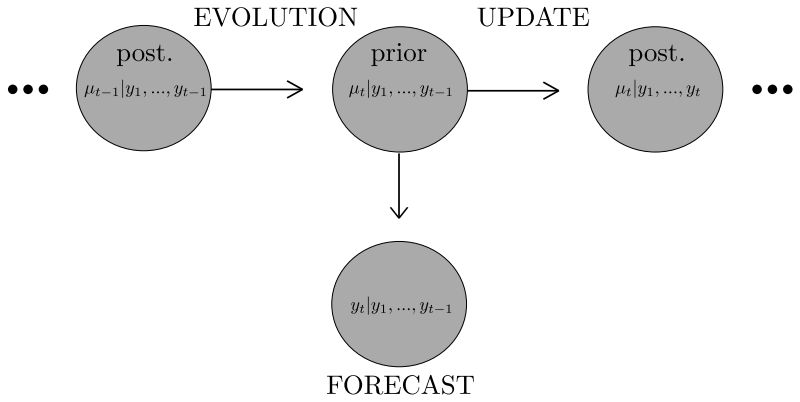

Figure 33 – This flowchart shows the dynamic linear model (DLM) update process, on the time point t. The model comprises three stages: evolution; forecast; and updates. The nodes (circles) represent the model's revision process, using the new information [from the Unobserved/predicted values (μ's)], combined with the t-th new observed value (Y), across the time.

after time $t \geq 1$ then,

$$\underbrace{Y_t = F_t\mu_t + \upsilon_t}_{\text{observation equation}}, \quad \upsilon_t \sim N_m(0, V_t), \tag{5.1}$$

$$\underbrace{\mu_t = G_t\mu_{t-1} + \omega_t}_{\text{state equation}}, \quad \omega_t \sim N_p(0, W_t) \tag{5.2}$$

where G_t and F_t are known matrices ($p \times p$ and $m \times p$) and υ_t and ω_t are two independent Gaussian random vectors with mean zero and known variance matrices V_t and W_t.

Considering a $\mathbb{R}^p$-valued and $\mathbb{R}^m$-valued time series satisfying

1. (μ_t) is a Markov chain
2. Conditionally on (μ_t), the observed time series (Y_t) are independent and depends only on (μ_t).

That is, allowing the time-varying parameters and incorporating more complex structures adding the composition of latent variable in the estimation process. That is, to estimate the state vector, we compute the conditional density $\pi(\mu_s \mid Y)$, where $t = 1, ..., T$. Consider μ_t as the mean parameter at the time t of a process, from a series $Y_t = \{y_1, ..., y_t\}$, under the Bayesian approach. Figure 33 presents the posterior (post.) and prior conditional densities.

Related to the estimation method, s is the recursive period and t is the current period, and is called "filtering (if $s = t$), smoothing (if $s < t$) and state prediction (if $s > t$)". Filtering is a procedure that aims to update current estimates as new data are observed $\pi(\mu_t \mid y_{1:t})$.

Smoothing is a retrospective analysis that computes the conditional distribution μ conditioned to the data $\pi(\mu_t \mid y_{1:T})$, starting from $\pi(\mu_T \mid y_{1:T})$, thus estimating the states backward. Prediction is a forecast procedure which estimates the next observation based on the data

$\pi(\mu_{t+1} \mid y_{1:t})$. Further details about Bayesian Forecasting and Dynamic Models can be found in (WEST; HARRISON, 1989; PETRIS; PETRONE; CAMPAGNOLI, 2009).

In the next Dynamic Linear Model, presented in this section, will extended to the two versions of SDA representation. First, we extended the static linear regression model (presented by (BILLARD; DIDAY, 2000)), called lower-upper bounds for the interval data, and later, we extended the center and range model (proposed by (Lima Neto; De Carvalho, 2008)), where for both cases we present a new methodology considering time-invariant parameters.

5.4.2 Dynamic Linear model for lower-upper representation

A prediction of the symbolic interval data using linear regression models was presented by (BILLARD; DIDAY, 2000; BILLARD; DIDAY, 2002b). Thus, the authors presented as an alternative the fitting of two independent linear regression models, one for each interval bound (lower and upper), however incorporating time-invariant parameters.

Let $E = \{e_1, \ldots, e_i, \ldots, e_n\}$ be a dataset of n examples described by $p+1$ symbolic interval-valued variables Y. Each example e_i is represented as an interval quantitative feature vector $\mathbf{z}_i = (\mathbf{x}_i, y_i)$, $\mathbf{x}_i = (x_{i1}, \ldots, x_{ij}, \ldots, x_{ip})$ where $x_{ij} = [a_{ij}, b_{ij}]$ is an interval and $[a_{ij}, b_{ij}] \in \zeta = \{[a,b] : a,b \in \Re, a \leq b\}$ and $y_i = [y_i^L, y_i^U] \in \zeta$ are the observed values X_j and Y, respectively. Thus, the proposed method considers the time-varying parameters that will minimize the errors as being:

$$\sum_{i=1}^{n} \left[(\varepsilon_{i,t}^L)^2 + (\varepsilon_{i,t}^U)^2 \right] \tag{5.3}$$

for the sake of simplicity, let us consider an autoregressive series with time dependence lag 1 (Markov Process), and the dependent variable similarly predicted as:

$$y_{i,t}^L = \beta_{0,t}^L + \beta_{1,t}^L y_{i-1,t}^L + \varepsilon_{i,t}^L$$
$$y_{i,t}^U = \beta_{0,t}^U + \beta_{1,t}^U y_{i-1,t}^U + \varepsilon_{i,t}^U$$

5.4.3 Dynamic linear model for centre-range representation

The Centre and Range representation uses the centre and range of an interval on a linear regression structure, throughout the parameters to model the contained information in the mid-points and ranges of the intervals. The time-invariant parameters ((NETO; CARVALHO, 2008)) considered a fitting a linear regression model to symbolic interval data using the mid-points and ranges of the interval values assumed by the variables through a linear regression model. For

this, the interval $[a_{jk}, b_{jk}]$ can be rewritten by:

$$y_{ij} = [a_{ij}, b_{ij}] = [c_{ij} - r_{ij}/2, c_{ij} + r_{ij}/2] \tag{5.4}$$

where $c_{ij} = (a_{ij} + b_{ij})/2$ and $r_{ij} = b_{ij} - a_{ij}$ describes, respectively, the centre and range of the interval for object i regarding variable j. Once again, incorporating the new approach, time-varying parameters (dynamic), the criterion is

$$\sum_{i=1}^{n} \left[(\varepsilon_{i,t}^{c})^2 + (\varepsilon_{i,t}^{r})^2 \right] \tag{5.5}$$

for the sake of simplicity, let us consider an autoregressive series with time dependence lag 1, and the dependent variable is similarly predicted as:

$$y_{i,t}^{c} = \beta_{0,t}^{c} + \beta_{1,t}^{c} y_{i-1,t}^{c} + \varepsilon_{i,t}^{c}$$
$$y_{i,t}^{r} = \beta_{0,t}^{r} + \beta_{1,t}^{r} y_{i-1,t}^{r} + \varepsilon_{i,t}^{r}$$

Thus, the Markovian property, i.e. time lag equal to 1, allows the use of some dynamic model classes that incorporate an optimization structure, specifically the Bayesian Networks (BN) class. For instance, (COSTA *et al.*, 2015) discuss that BN models consider a set of conditional distributions by decomposing the joint distribution derivative from the observed outcome, thereby allowing the estimation towards direct dependencies via graph structure.

Complementary, (COSTA *et al.*, 2015) also discuss that the Dynamic Bayesian Network (DBN) takes into account the dynamic nature of a process, containing certain hypotheses about the estimation of effective connectivity and embodies a particular type of Granger causality ((GRANGER, 1969)). Thus, Granger causal hypotheses shall be expressed in a state space form.

5.5 Results

Two main questions governed this work, in which researchers sought to understand the equivalence between the resting stage and post neuromodulation brain activity responses. For the first question, this work used symbolic interval data to compare the dynamic before and after the neuromodulation task. To do this, a study takes into account the lower/upper interval limits to try and identify equivalence among baseline versus post 1mA stimulus. Secondly, the study also aims to describe the stimulus' interference upon the brain activity process in each region, that is, the trace of the structural change of the process.

Figure 34 compares the resting-stage (baseline) with the post 1mA, for each major cortical brain region. The lower symbolic interval limit (left chart) shows for all brain regions the

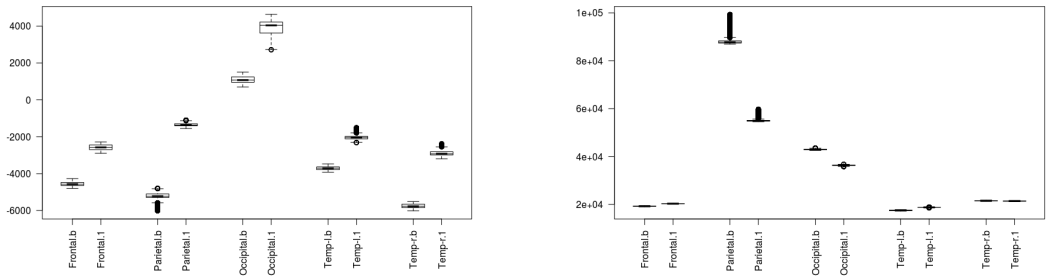

Figure 34 – Data dispersion baseline versus after 1mA per region (left) lower SDA limit and (right) upper SDA limit.

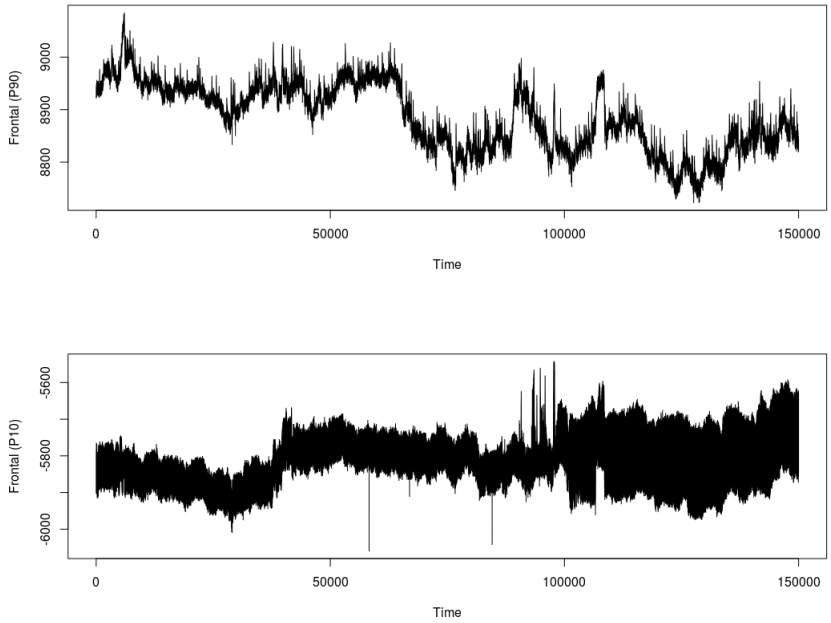

Figure 35 – Frontal time series interval (top) ninetieth-P90 and (bottom) tenth-P10 percentile or Upper/Lower SDA limits

amplitude and variation of post 1mA (represented by a suffix '1' in front of the label) are higher than the baseline (represented by a suffix 'b' in front of the label). The upper limit (right chart) presents the same pattern except for the parietal, occipital and right temporal regions, which presented post 1mA with a lower dynamic compared with the baseline.

To illustrate the analysis of the temporal evolution of each symbolic interval limit (that is, the region percentiles), the frontal cortical region -post stimulus- was selected to have its time dynamic observed regarding the 10th percentile (P10 - lower limit) and 90th (P90 - upper limit), shown in Figure 35. The P10 presents a greater variation, especially at the end, compared to P90 related to the different EEG band activation.

Some studies can be found in the literature where dynamical progress from a transformed time series is captured using SDA. (CYSARZ; EDELHÄUSER; LEEUWEN, 2015) applied

symbolic dynamics aiming to highlight dynamical properties, in physiological time series data, seeking regulation towards robustness, and thus symbolic transformation. Therefore, there is only one explicit need for variance matrices related to errors of observation and state equations, in which this work used GIBBS sampling to estimate them.

According to (VENUGOPAL; GOGATE, 2012), regarding the computational complexity of GIBBS sampling, adopted in this work, the resulting alignment algorithm is only $O(Lx)$, where Lx is the length of x, respectively. Therefore, the complexity of its model depends on the number of parameters, that is, the state vector length which is equal to the length of x. Moreover, we considered a simple structure for the DLM (order 1), in which the state equation presents only one hierarchical level, considering only the earliest past to explain the current observed outcome.

Considering the dynamic linear models, according to equation 5.1 represented by μ in the general DLM form, the state equation will be related to the modeling of the unobserved factors related to the main brain regions. That is, μ is related with the dynamic of the five upper and lower (or centre and range) bounds from the brain areas, then as a (10-dimensional) vector of trend level parameters with a corresponding 10-dimensional transpose vector as $F_t^T = (1,0,...,0)$.

In Figure 36, the time shifting structure map convolution illustrates the signal amplitude difference between each step and the one ahead (by drawing a rectangular shape out of these points). We present this interval plot with regards to the frontal region, choosing each axis to be the tenth and ninetieth percentile ranges.

Figure 36 also demonstrates the variability of both boundaries together (in rectangles), and can be compared to the marginals in Figure 35. Moreover, an increase in the color blue indicates an overlap of intervals (P10 and P90), related to step-by-step dynamics of the observed interval dynamics.

Researchers are also interested in analyzing the dynamic structure post the neuromodulation, in order to obtain information about the patterns that may be translated into a change related to the influence of the interventional electrical current. That is, we would like to verify changes in the structure of the series after the stimulus to what may be associated with the return of the patient to the baseline.

The equipment used for data acquisition has a resolution of 500Hz (sample rate), that is, it collects 500 observations per second. A data reduction was adopted, obtaining the median per second, aiming to smooth out the series and reduce the noise of the collected signals. Figure 37 shows the smoothing of a frontal cortical region, which illustrates the summarized quantile median observation time series using a 1Hz sample rate.

In this work, different SDA approaches were adopted regarding modeling using symbolic interval data, i.e. directly modeling the *centre and range* and *upper and lower limits* of the complex data. For all methods a regression structure was considered in which the best predictor of the current state (k-th stage) is only the most recent past (k-th -1 stage, so to speak following

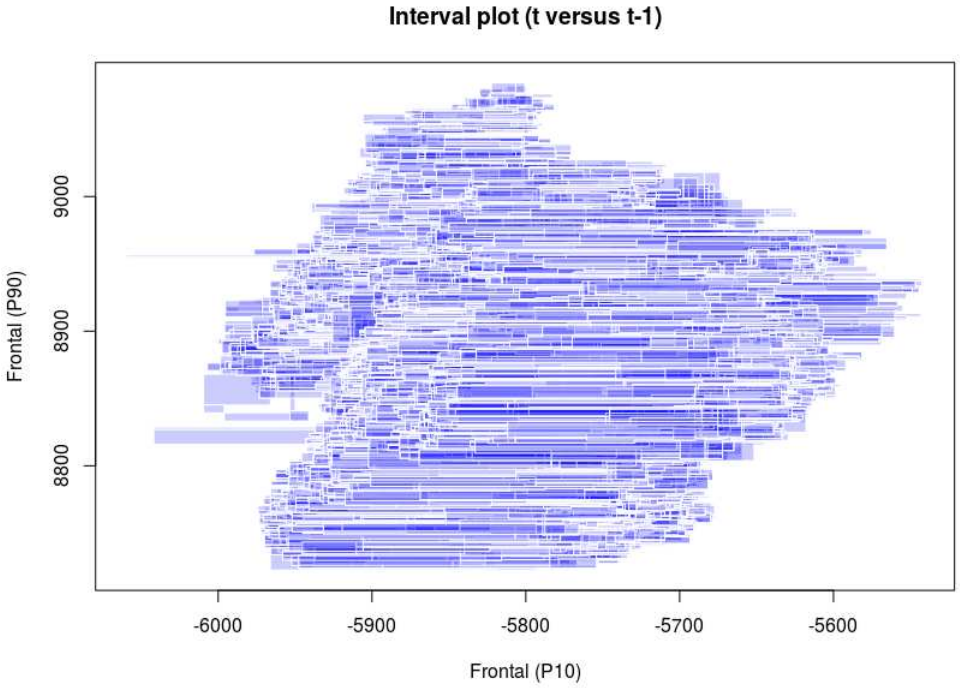

Figure 36 – Interval plot that illustrates the empirical time variation. Frontal lobe Lower (P10) $\times$ Upper (P90) SDA limits (2-millisecond variation). Amplitude variation is represented by a marginal rectangular length. The visual interval variation in time, by considering each step (rectangle) as only the time lag of 1, and also as a cross-correlation time series projection amplitude, among both dimensions (in which the symbolic data is an interval, not classic data).

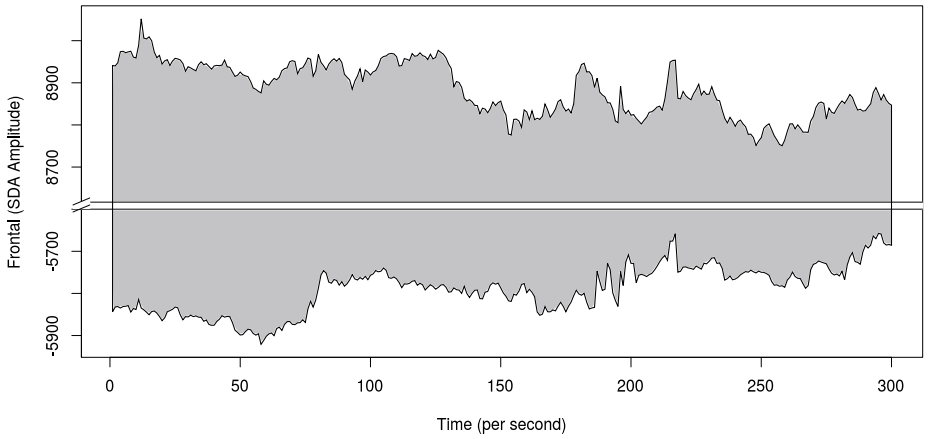

Figure 37 – Frontal lobe symbolic interval data after the time compressing.

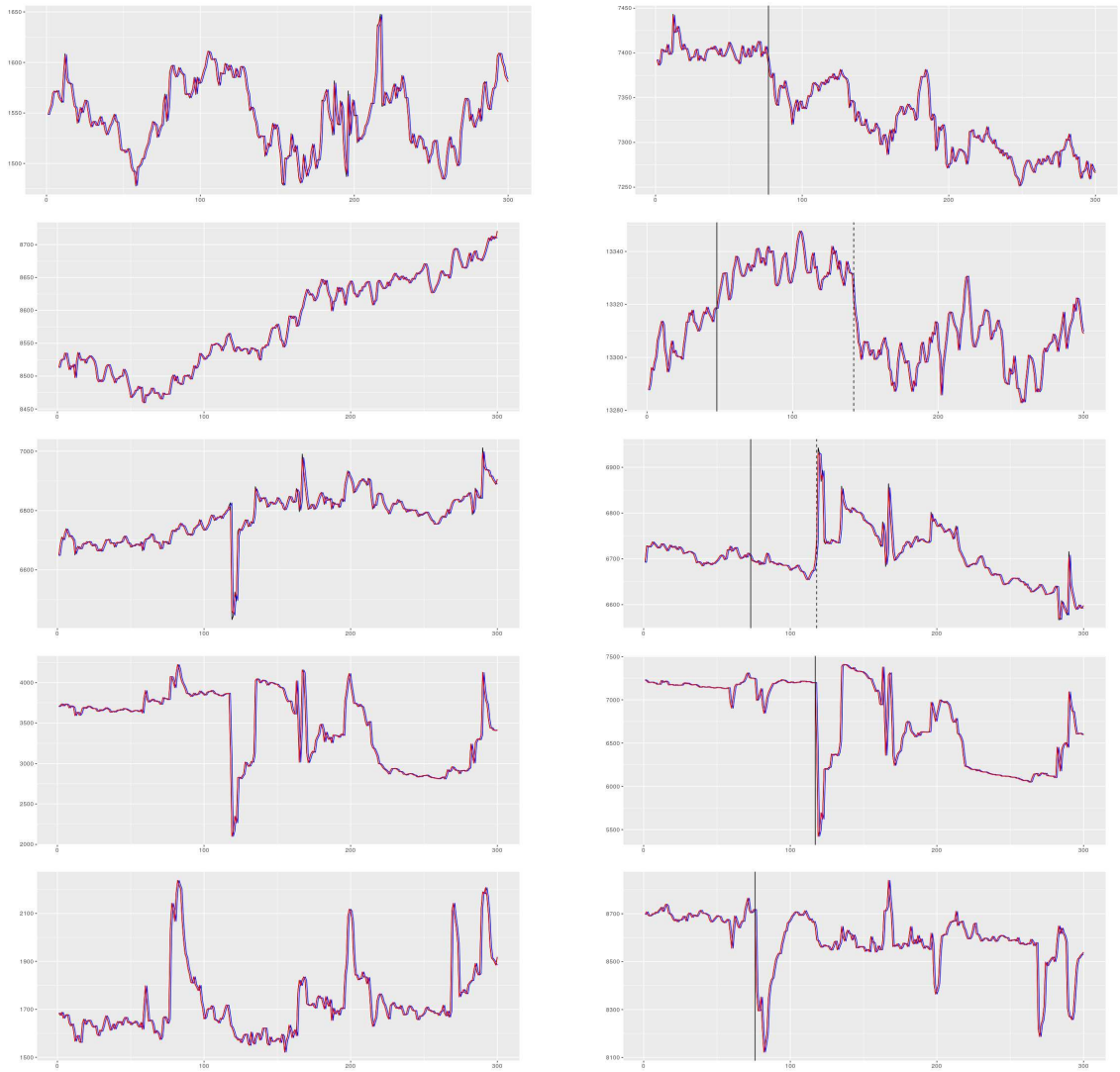

Figure 38 – (left column) Dynamic centre and (right column) dynamic range from the major cortical regions post 1mA tDCS: DLM (blue line) Smoothed, (red line) Filtered Time Series and (black vertical lines) the structure change. From the top to bottom the major cortical regions are Frontal, Parietal, Occipital, Left and Right Temporal. The centre graphs (left panels) demonstrate the different trends between the major cortical regions, and the range graphs (right panels) show the electrical dynamic across time.

a Markovian structure.

The dynamic centre and range related to each brain region dynamic was modeled using an order of 1 DLM, which describes the propagation of each area. Thus, the mean-related series in Figure 38 are associated with the median dynamics of the regions and the range with its synergy. In addition, the black vertical lines suggest the structure change (in time) of each major cortical region.

The structure change estimation adopted used the breakpoints in regression relationships (in Figure 38 as vertical solid and dashed lines). Loosely speaking, the breakpoints were based on the classical linear regression model. The aim is to detect the deviations which support the

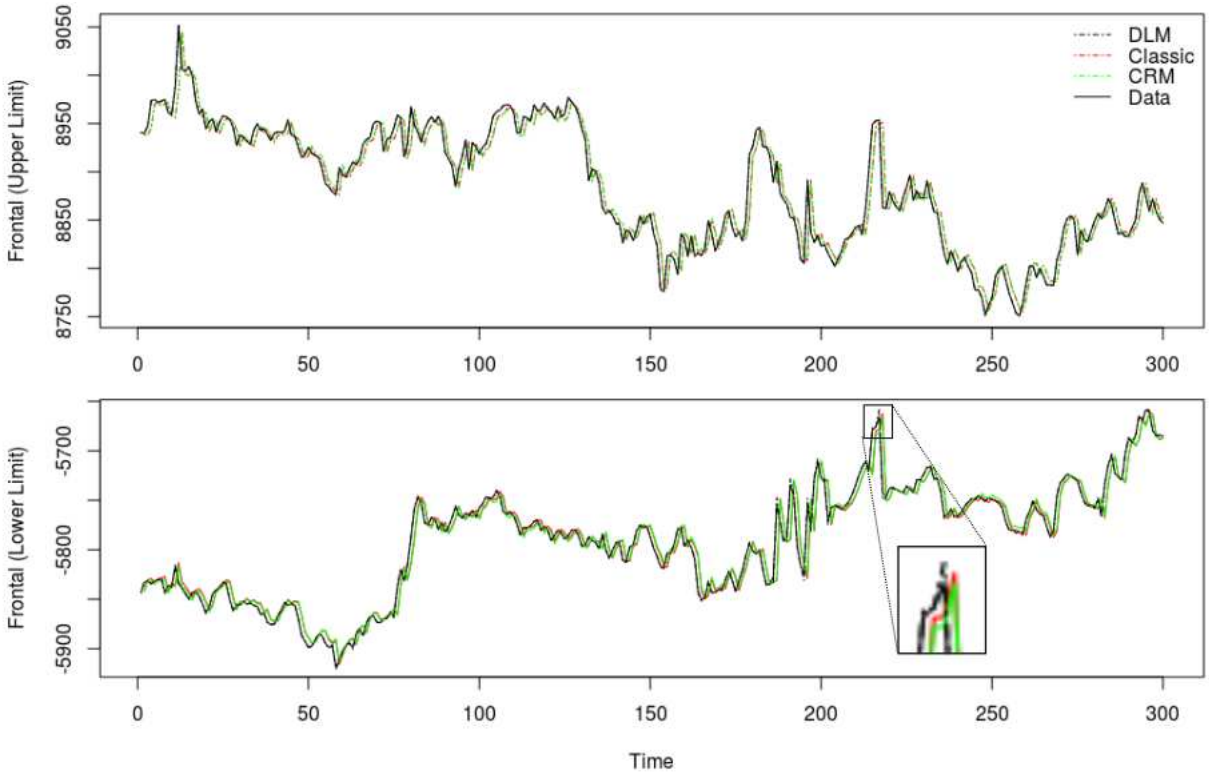

Figure 39 – Frontal cortical time series (red dashed line) the time-invariant parameters for the inferior and superior limits as an independent regression models [classic model], (green dashed line) the time-invariant centre and range method [CRM], (black dashed line) the dynamic inferior and superior limits model for each bounder [DLM], and (black solid line) the observed symbolic data. Acronyms are Dynimac Linear Model (DLM) for lower-upper SDA representation, static lower-upper SDA representation (Classic), and static centre and range SDA representation (CRM).

model stability. Thus, on average, after 106 seconds the energy dissipation introduced by the electrical stimulus begins to show a reduction/leakage.

Analyzing the dynamic upper and lower limits, Figure 39 shows the models' comparison estimations performance; (red dashed line) the time-invariant parameters for the inferior and superior limits as an independent regression models, called the classic model, (green dashed line) the time-invariant centre and range method, CRM, (black dashed line) the dynamic inferior and superior limit model for each bounder, DLM, (black solid line) and the observed symbolic data related to the frontal cortical region. It should be mentioned that the black dashed and solid lines are equal most of the time.

The performance evaluation metrics for the adjusted models will be presented only for the frontal cortical region, as shown in Table 9. These metrics are based on the comparison of the observed versus estimated values (considering each respective adjusted model), in which this comparison is made one-step ahead, aiming at measuring the accuracy of the point forecast. We used the Mean Absolute Error (MAE), Relative Absolute Error (RAE), and Mean Squared Error (MSE) respectively (further details in (HYNDMAN; ATHANASOPOULOS, 2018)). For all the

Table 9 – Evaluation metrics on the frontal cortical performance among the models. Using the dynamic methodology for point forecast, smaller errors are obtained with the proposed methods. Acronyms are Mean Absolute Error (MAE), Relative Absolute Error (RAE), Mean Squared Error (MSE), lower-upper SDA representation (Classic), centre and range SDA representation (CRM), and Dynamic Linear Model for lower-upper representation (DLM).

	MAE	RAE	MSE
lower bound			
Classic	9.7644	0.2137	0.2137
CRM	9.7882	0.2142	0.2142
DLM	**1.0050**	**0.0220**	**0.0220**
upper bound			
Classic	11.9712	0.2168	286.9932
CRM	11.9635	0.2167	283.4136
DLM	**0.0740**	**0.0013**	**0.0116**

considered errors, a better performance was noticed for the DLM compared to the other models found in the literature.

The time-invariant parameter CRM presents greater errors due to its estimation structure, regarding the SDA interval limits. Not to mention that there is a possibility of switching the interval positions (for example, the lower bound estimates are greater than the upper bound ones) given their linear structure, in both cases for the Classic and CRM models (which are time-invariant parameters). However, DLM models are those with structures that are flexible enough to incorporate non-stationary data (e.g. time series data).

Finally, the greater consideration of the question refers to the structure breakdown moment after the tDCS stimulation, where according to Figure 38, empirical evidence shows that it is reasonable to assume between 73 and 143 seconds. This means that the patient modified the energy dynamics related to stimulus towards returning the regular condition (which presented a predominance of random characteristics).

5.6 Discussion

The present study results in three main highlights relevant for this interdisciplinary field; i) in neuroscience field, it is the first work to use SDA in neuromodulation with EEG signals, ii) this is the first statistical approach described in the literature that combines a state-space (dynamic) model with symbolic interval data, and iii) this approach enables the analysis of the time-domain alongside frequency-domain in time series analysis.

Previous work described by (KELLER; LAUFFER, 2003) applied an isolated SDA methodology to detect and visualize qualitative changes of EEG data related to epileptic activity. Moreover, (RODGER, 2015) identified a clinical change in patients after traumatic brain injury by improving the data classification method using SDA. The authors showed that survival,

mortality, and morbidity rates could be derived from the superset of Medical Operations data and used for future decision-making and planning.

In contrast to the previous studies, we developed a new methodology of SDA combined with the state-space approach which opens new dynamic modeling possibilities that include several classes of models and present a broad potential associated with computational feasibility. Our statistical approach is also innovative because we aggregate elements to discuss the application of this complex system analysis, using the time series approach. For example, by analyzing 5 minutes of EEG data after the HD-tDCS intervention, we identified structural breaks around 100 seconds, indicating a loss of HD-tDCS influence towards cortical activity (suggesting the return to the baseline state) (38).

More specifically, dynamic modeling combined with symbolic interval data opens up a new class of non-trivial structure data analysis, thus enabling some types of dependence (temporal, spatial, etc.) managing to be a simpler problem, given the conditional independence supposition from the state-space models. Dynamic interval data may also incorporate multidimensional range (frequency) structures (considering the frequency and time domain approach simultaneously). Additionally, it can be seen as a denoising transformation that fits the kernel of the data at time-oriented intervals (under the time-series approach).

The presented statistical approach is appropriate for human brain connectivity analyses, a complex phenomenon of substantial relevance, presenting a big data challenge. It remains an open question on how to deal with high-dimension data without losing relevant information in the neuroscience field. Our research group has shown sequential evidence for the clinical and physiological effects of a non-invasive brain stimulation protocol targeting the temporo-parietal junction to understand and treat disorders of human verticality ((SANTOS; EDWARDS, 2019)). This context exposes the need for several time series analyses and its dependence, estimating not only the effects individually but the impact of treatments as a whole. Understanding human neurophysiology such as the brain dynamics could provide insights into types of localized non-invasive brain stimulation toward a solution (or improvement) of the brain activity disfunction ((RUBIN *et al.*, 1991; PAAKKI *et al.*, 2010)).

The dynamic models present limitations regarding the (i) large amount of parameters (over-parametrization) and (ii) non-trivial automatized selection towards the definition of a parsimonious transfer function to ensure the accuracy of the model's power prediction, that is, its lag orders and important components ((KRAVARIS; HAHN; CHU, 2013; DEY; RAO, 2005)).

Furthermore, using the DLM, future works can explore multivariate graphical models, extending to brain connectivity combined with the SDA approach, exploring the multidimensional time series relationship applied in contemporaneous interactions between brain regions with fMRI data ((COSTA *et al.*, 2015; COSTA *et al.*, 2017)). This work also has constraints in terms of the lack of exploring time and frequency domain advantages, using the developed methodology (dynamic symbolic interval analysis), as well its additional contribution to further

clinical intervention analyses.

The application of SDA with a dynamic linear model can be extended to the entire medical field (not only neuroscience) since biometric multisensory data is being disseminated and represents a technological advance that will facilitate quality of care, as well as cost reduction ((KING *et al.*, 2003)). Examples can be found in the patient safety programs that use emerging technologies to automate the entire clinical continuum ((PAVLOPOULOS; DELOPOULOS, 1999; SORIA-FRISCH; RIERA; DUNNE, 2010; CACAO *et al.*, 2017)). Most of these data resulting from biosignals are time-oriented, therefore called time series, which present a dependence requiring special attention in modeling. Hence, the impact of this study will reach the broader medical field, where these is a need to analyze complex data in the spatial and temporal domains.

CHAPTER

6

BRAINWAVE NETS: ARE SPARSE DYNAMIC MODELS SUSCEPTIBLE TO BRAIN MANIPULATION EXPERIMENTATION?

This chapter corresponds to a manuscript submitted at *Frontiers in Systems Neuroscience* journal, in which presents the discussion towards sparsity in dynamic graphical models. This work had as co-authors: Marco Pinto-Orellana (M, Norway), Joao P Leite (FMRP-USP, Brazil), Dylan Edwards (MOSS, USA and Edith Cowan University, Australia), Taiza E G Santos (FMRP-USP, Brazil), Francisco Louzada (ICMC-USP, Brazil).

Sparse time series models have shown promise for estimating contemporaneous and ongoing brain connectivity. This paper was motivated by a neuroscience experiment, using EEG signal data as the outcome of our established interventional protocol, a new method in neurorehabilitation towards the development of a treatment for visual verticality disorder in post-stroke patients. To analyze the complex outcome measure (EEG) that reflects the neural-network functioning and processing in more specific way in relation to traditional analyses, we present the comparison among sparse time series models (classic VAR, GLASSO, TSCGM, and TSCGM-modified with nonlinear and iterative optimizations) combined with the graphical approach, as a Dynamic Chain Graph Model. These dynamic graphical models were useful to assess the role of estimating the brain network structure and describing its causal relationship. Additionally, this method allowed visualization and comparison across experimental conditions and across the brain frequency domains (using finite impulse response (FIR) filter). Moreover, using multilayer networks the results corroborate with the susceptibility of sparse dynamic models, bypassing the false positives' problem in estimation algorithms. We conclude that application of sparse dynamic models to EEG data may be useful for describing intervention-relocated changes in brain connectivity.

6.1 Introduction

In the neuroscience field, tasks relating to brain network structure and its dynamics are vastly increased given the availability of the technology (high resolution and storage capacity). Notwithstanding, the field aims to understand "how" and "why" the effects/events occur based on learning probabilistic connection structure, to assume some feasible causal inference (PEARL, 2014). Therefore, an urge to map its complex organization is imminent and two types of connectivity are commonly studied: functional and dynamic. Functional connectivity is a statistical measure of the correlation within observations in the same time-lapse, and dynamic connectivity is the relationship among the measurements compared also with their previous values impact.

In this manner, the links among anatomical parcellations of the brain are described by their similarity patterns, for instance, a channel represents the activity of a group of neurons, and it is measured according to its space relation, time and frequency domains. Statistical significance tests are often conducted to estimate the existence of those links in order to project an estimated topology regarding the interaction among this observed group of neurons. For example, brain dynamics are measured as biosignals through electroencephalogram (EEG), functional magnetic resonance imaging (fMRI), diffusion tensor imaging (DTI), Doppler ultrasound etc.

Network modeling is a mathematical framework, part of graph theory, used to represent and analyze relationships in multivariate data. Recent advances in network estimation have moved the emphasis of the analysis from single-layer networks to multilayer structures facilitating the interpretation of multivariate relationships (KIVELÄ *et al.*, 2014). This shift of paradigm expands the possibilities of extracting information about complex systems, and multilayer network estimation of biosignals can incorporate the change in time and/or different frequencies.

Multilayer analysis enables to unfold of the complexity of the human brain enabling investigations to show effective functional role in brain regions activation and visual representation (DOMENICO, 2017; GRATTON *et al.*, 2018). In this context, two main approaches are often seen, multimodal connectivity or structural-functional relationships (different layers represent replicated nodes and its interaction) and time-varying networks (evolution of the temporal snapshots).

The concept of sparse multivariate time series with multiplex networks benefits the analysis of brain dynamic activation, also, by using the frequency-domain approaches as biosignal denoising that is physiologically applicable. The frequency domain is often used when adopted graphical models, as an example, (BACH; JORDAN, 2004) explicit under the presence of stationary Gaussian time series, these models are related to the elaboration of time series structured in the time domain. Moreover, sparse models deal directly with the limitations of complex high-frequency time series, such as complex structural and computational constrains.

In this paper, we describe a novel statistical method adopting the frequency domain time series combined with some sparse models approach; targeting a deeper understanding towards

an applied neuroscience research question. That is, we aimed to discuss/reveal some pattern towards brain activation, comparing the brain dynamic before and after a transcranial neuromodulation stimulation. The data was acquired following a systematic randomized controlled clinical trial protocol (SANTOS *et al.*, 2018), using a sample of the EEG signals collected *before* the application of high-definition transcranial direct current stimulation (HD-tDCS) over the temporal-parietal junction under polarity anode center condition and *post* the 2mA current intensity, in a single young healthy subject.

The motivation stems from the need for understanding neuro-activation across different brain areas, to analyze the effects of a focal transcranial brain stimulation and establish an innovative and effective neurorehabilitation strategy to treat verticality disorder after brain lesions (post-stroke). Moreover, the impact of this study will extend to the entire neuroscience/medical field that needs to adopt dynamic modeling for complex data; sparse models enable the use of large data demanding a low computational cost (shrinking the number of parameters in the model).

6.2 Methods

The paper is organized as follows. In Subsection 6.2.1, we present an overview of the adopted experimental protocol; Subsection 6.2.2, we present the theoretical background for dynamic linear models, sparse estimation, sparsity in modeling, multilayer networks, network inference, and time series from a frequency-domain approach. In Section 6.3, we discuss the empirical clinical results comparing different sparse estimations to distinguish patterns among different brain wavebands. Finally, some final comments are given in Section 6.4.

6.2.1 Protocol rational and data characterization

The neural systems' imbalance and degeneration related to postural control lead new researches towards their origin and pathophysiology (WINTER, 1995). In humans, different sensory information is used as pathways in the brain to maintain posture in the upright position (DAY; COLE, 2002), and postural imbalance is one of the most common disorders after stroke, yet is insufficiently investigated (BAGGIO *et al.*, 2016; CHERN *et al.*, 2010). Hence, increasing knowledge about the effects of this strategy is essential for the development of more effective rehabilitation protocols.

Noninvasive techniques of brain stimulation are current therapeutic resources related to the pathophysiology and behavior of the mechanisms that guide the human mind. Transcranial direct current electrical stimulation (tDCS) is a non-invasive neuromodulation technique that allows modeling the cerebral function with a safe profile (EDWARDS *et al.*, 2013). tDCS consists of electrodes unleashing weak electrical current over the scalp, inducing cortical changes; it rises or lowers the local network excitability depending on the electrical current polarity.

At the neuronal level, tDCS affects polarization of the resting membrane potential, and this effect may acutely impact cortical excitability (PRIORI *et al.*, 1998). Other mechanisms also contribute to modifying the electrical neuronal membrane potential and maintenance of membrane changes at least one hour (NITSCHE *et al.*, 2003). As well as changes in synaptic efficacy that out last the stimulation period. Studies of peripheral nerve and spinal cord stimulation have shown that direct current effects are also non-synaptic, with transient changes in the density of protein channels below the stimulation area (ARDOLINO *et al.*, 2005; COGIAMANIAN *et al.*, 2008). High definition tDCS (HD-tDCS) is a contemporary way of transcranial electrical stimulation, that promotes more focal stimulation than the conventional tDCS methods (for review see (EDWARDS *et al.*, 2013)).

In addition to this tDCS direct effects, "indirect" consequences come from connective-driven alterations of distant cortical and sub-cortical areas (BRUNONI *et al.*, 2012). (LANG *et al.*, 2005) revealed that stimulating the right frontopolar cortex (M1) with tDCS also activate several connected regions. The changes in brain activity after a tDCS session measuring regional cerebral blood flow, with sequential H152O PET scan. Besides, under the area of the stimulus, that is, several motor areas such as the caudal portion of the anterior cingulate cortex, cerebellum and superior temporal sulcus, were activated. Maybe in part, due to a modulation of the functional interaction between M1 and these areas via cortico-cortical and cortico-subcortical connections.

Other studies using transcranial magnetic stimulation (TMS), also as a non-invasive neuromodulation technique, described the increased activity of the homologous area, contralateral to the stimuli (SIEBNER *et al.*, 2000; LEE *et al.*, 2003). The last reduction in left can explain it to the right transcallosal inhibition between the two cortices (GILIO *et al.*, 2003; PLEWNIA; LOTZE; GERLOFF, 2003).

These "indirect" changes on cerebral function are fundamental issues regarding the objective of the present study, that evaluated the effects of tDCS in the temporoparietal junction, the area related to postural control in humans (WINTER, 1995). Inter-hemispheric interactions may contribute to defining the temporal and spatial features of voluntary movements and consequently, postural control (MEYER; RÖRICHT; WOICIECHOWSKY, 1998). There is a balance between these inter-hemispheric interactions, where each human cortex exerts inhibitory influences on the opposite motor cortex in normal conditions (FERBERT *et al.*, 1992). Therefore, developing non-invasive techniques which modulate this balance will be a significant advance in the rehabilitation setting of stroke patients and other postural control disorders, after more profound knowledge of the technique's effects on the human brain.

The current study derived from a randomized double-blinded sham-controlled clinical trial that aimed to investigate a polarity and intensity-dependent shift in high-density EEG signal, following an intervention using high-definition transcranial direct current stimulation applied over the temporo-parietal junction in healthy subjects (SANTOS *et al.*, 2018). The study protocol consisted of a HD-tDCS application over the right temporoparietal junction area, using

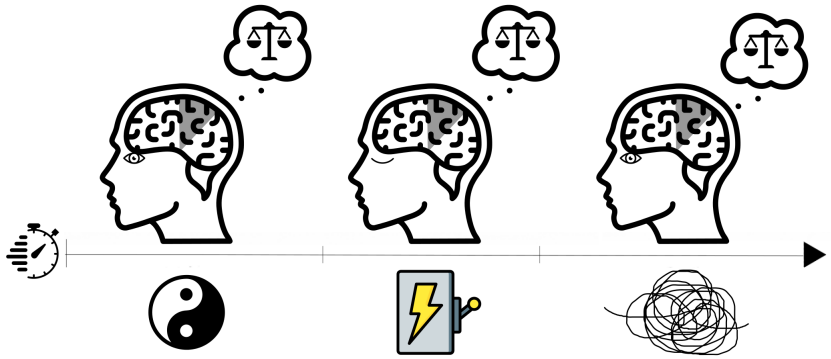

Figure 40 – Visual representation of a resting-state baseline condition (left illustration; eyes open), added by stimulation stage (eyes closed) and accommodation post-stimulus (right illustration; eyes open). The main interest in the study is to compare the resting-state versus accommodation post-stimulus.

a Soterix® NY-USA HD-tDCS with a constant current anode (active control). Four electrodes were used; the central electrode was placed over the circumcenter of P4-C4-T8 EEG coordinates, and the three peripheral electrodes were placed at a distance of 3 centimeters from the central electrode (over the EEG coordinates P4, C4 and T8). EEG recording was made before and after each stimulation period, allowing detect ongoing changes on the raw EEG signals in response to tDCS (Figure 41). The total duration was 5 minutes of resting-state baseline condition added by 1.5 minutes of stimulation plus 5 minutes of accommodation post-stimulus, as shown in Figure 40 (for protocol details read (SANTOS *et al.*, 2018)).

Dense array EEG signal was acquired using a 256-channel sensor net from Electrical Geodesics Inc. during the aforementioned electrical stimulation conditions. All channels were referenced to the vertex with reduced electrical impedance. The EEG was recorded continuously before and after the stimulation, excluding ramp-up and ramp-down periods (1.5 minutes total), lasting approximately 120 minutes the full trial experimentation. Previously, we discussed (NASCIMENTO *et al.*, 2019) some variation towards the condition Active Control (Anodal)-2mA, thereby in this work we aimed to discuss a innovative statistical analyses of only a sample of the protocol experimentation compared to its reference (baseline).

Thus, in the present study, we analyzed and discussed the data set of a single healthy adult male participant during resting-state (baseline condition) and after 45 seconds of an electrical stimulation. Each period (before and after stimulation) contains five minutes observation, whereas the EEG sample rate was 500 Hz (500 observations per second), representing a total of 300,000 observations.

6.2.2 The model

Dynamic structure modeling may be considered as an alternative to estimate brain connectivity, and additionally, it is natural to aggregate its estimated parameters into a graphical representation. Nonetheless, the class of dynamic model is overparametrised (WEST; HAR-

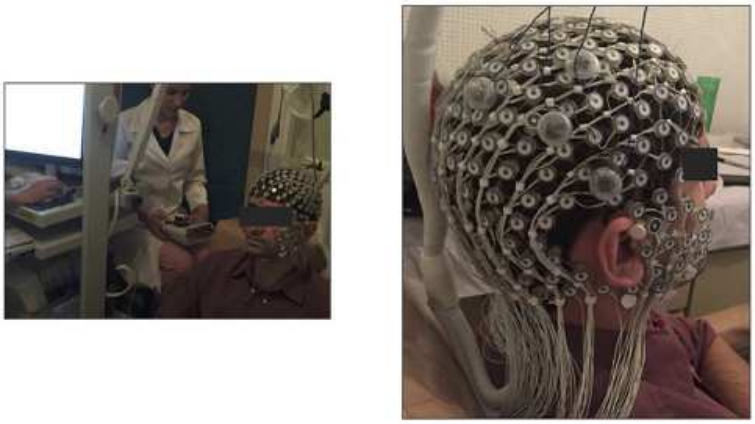

Figure 41 – Photograph of the experimental trial (left-hand side) and the EEG cap (right-hand side) with small electrode array covering the scalp, while the large electrodes identifiable as a triangle configuration (4 electrodes total) represents the tDCS stimulating electrodes (presented in article (SANTOS *et al.*, 2018)).

RISON, 1989; WEST; HARRISON; MIGON, 1985), especially in the time-varying approach, demanding some shrinkage into the parameter space (that is, by adding sparsity in the parameter vector estimation process). A word of caution must be mentioned here, search patterns in small dimensions may deal with great noise (NAKAO, 2016), added by limitations towards how to generalize the low-dimensional reduction approach (RODRIGUES *et al.*, 2016) and, for instance, brainwaves present a highly active process which comes with much noise (NATARAJAN *et al.*, 2004). Therefore, a filtering preprocessing is suggested to break the observed/raw time series signal into the frequency domain, then used the finite impulse response (FIR) filter. These elements are presented in the sequence.

6.2.2.1 Dynamic Linear Model

State space model is a flexible learning linear/nonlinear dynamical systems. As a particular case, the state transition and observation functions may be expressed as a Gaussian linear process, often called Dynamic linear model (DLM). For instance, consider a p-dimensional State Vector and m-dimensional observations, both normally distributed. At the initial time (t=0) presents mean μ_0 and variance σ_0^2,

$$\theta_0 \sim N_p(\mu_0, \sigma_0^2)$$

then for the time $t \geq 1$,

$$\underbrace{Y_t = F_t\theta_t + \upsilon_t}_{\text{observation equation}}, \quad \upsilon_t \sim N_m(0, V_t),$$

$$\underbrace{\theta_t = G_t\theta_{t-1} + \omega_t}_{\text{state equation}}, \quad \omega_t \sim N_p(0, W_t)$$

where matrices G_t (dimension $p \times p$) and F_t ($m \times p$) are known, followed by independent Gaussian random vectors υ_t and ω_t with mean equals to zero and known variance matrices V_t and W_t.

Considering a $\mathbb{R}^p$-valued and $\mathbb{R}^m$-valued time series satisfying two proper; i) (θ_t) is a Markov chain, and ii) Conditionally on (θ_t), the observed time series (Y_t) are independent and depends only on (θ_t).

Moreover, this class of models are flexible given the possibility to incorporate more complex structures (locally they are linear, but globally performs as nonlinear dynamic), by allowing the time-varying parameters, that is, compounding a latent variable in the estimation process. The estimation towards the state vector uses the conditional density $\pi(\theta_k \mid Y)$, where $t = 1, ..., T$ and Y is the observed values. Furthermore, k represents the recursive period and t is the current period, where estimation problems are filtering ($k = t$), smoothing ($k < t$) and state prediction ($k > t$).

Filtering is a procedure that aims to update the current estimates as new data are observed $\pi(\theta_t \mid Y_{1:t})$. Smoothing is a retrospective analysis which compute the conditional distribution θ given in once the data $\pi(\theta_t \mid Y_{1:T})$, starting from $\pi(\theta_T \mid Y_{1:T})$ estimating the states backward. Prediction is a forecast procedure which estimate the next observation based on the data $\pi(\theta_{t+1} \mid Y_{1:t})$. Further details about Bayesian Forecasting and Dynamic Models (WEST; HARRISON, 1989; PETRIS; PETRONE; CAMPAGNOLI, 2009).

A particular case of DLM is the Vector Autoregressive (VAR) model, when the parameters are invariant on time, implying that the parameter vector θ_t only assumes a single value $\theta_t = \theta$. VAR model is widely used in the literature (KRYSTAL; PRADO; WEST, 1999; PRADO; MOLINA; HUERTA, 2006; SCHLÖGL; SUPP, 2006; GARRISON *et al.*, 2015) and enables to recognize the nonlinear dependencies between different brain regions.

6.2.2.2 Sparse Estimation framework

Recent discoveries hone time series modeling, addressing the model order estimation challenge, that is measure complexity related to the high-dimensional resolution. For instance, it enables to rotate the eigenvalues and eigenvectors in the state-space parameter dimension, given restrictions in the parameter vector space imposing some parameters to be equal to zero. So the main question may be which is the "best" and "simpler" approximation (without losing relevant information) which corresponds to the dynamic process?

This definition of "the best" is nontrivial given the lack of knowledge regarding the joint function related to the data and parameter associated with the phenomenon under study. The only available information is from the observed data as an information base in the estimation process. Several inferential methods may be adopted; among them, the most popular are maximum likelihood and ordinary least squares.

Sparse approach is equivalent to create a bias towards sparsity, in the maximum likelihood estimator (MLE), which may reduce the minimum square error. Thus, it is setting conditions in the least squares aiming to minimize the l_1-norm producing sparsity in the parameter vector θ. Additionally, prior knowledge can be incorporated targeting only a subset of the parameter vector. That is, to minimize a specific parameterization (θ_0) problem then

$$\min_s \|\theta_0 + s\|_1$$

truncating a NP hard problem (CHICKERING, 1996a) into a linear programming (LP) problem in standard form (ZEEMERING, 2015). Loosely speaking, by adding assumptions regarding the model reparatrization where the parameter vector θ, as well the fit of the model, is represented as an error vector ($e(\theta)$, e.g. least squares criterion) that only dependents on θ.

The search space is limited by models, some of them equivalent, which produce the same value of error vector and least squares error (TIBSHIRANI *et al.*, 2012). That is, shrinkage may be applied through a singular value decomposition (SVD) to the matrix which associates the number of constraints kernel of the Jacobian ($J(\theta)$) or Hessian ($H(\theta)$) matrices.

The non-linear least squares minimization methods search direction ($s(\theta)$) to refine the parameters by successive iterations may be adopted, for example a Newton method, described as

$$s(\theta) = -\alpha H(\theta)^{-1} J(\theta)' e(\theta).$$

Based on the SVD results, this attainable to determine values that may assume to be zero, setting up a threshold if needed. A word of caution regarding the threshold, low values may bound the search space (then exclude valid directions to search for sparsity) and high values may change the model behavior.

In contrast, other solutions may be obtained by the dual or primal linear programming (LP) problem. Deviation towards the search direction accuracy during the optimization procedure, through setting up a threshold, determines the quality of the maximization procedure. As in the medical field exemplification, (ZEEMERING, 2015) applied to the class of regression and state-space models adding sparse estimation in the field of atrial fibrillation research.

The models adopted were classical VAR, Graphical Least Absolute Shrinkage and Selection Operator (GLASSO), Time Series Chain Graphical Model (TSCGM) and TSCGM-modified using Nonlinear optimization over log-likelihood and Iterative optimizing the log-likelihood. The TSCGM-modified in this work considered as optimization option towards the proportion of parameters equals to zero among the total number of model parameters with a bias towards sparsity, in MLE, which minimize through the l_1-norm of the parameter vector and the Smoothly Clipped Absolute Deviation (SCAD).

6.2.2.3 Sparsity in modeling

The classical method for estimate connectivity matrices often uses the Vector Autoregressive (VAR) Model, which is a particular case of DLM when the parameters are invariant in time. For instance, consider a vector of observed variables Y, I is a identity matrix, Matrices X represents Y lagged dependence, Γ_j are autoregressive parameters, and u is the error vector with covariance matrix Σ, using ordinary least squares (OLS) standard estimation procedure equation by equation. Its vectorized form would be expressed as

$$vec(Y) = (I_m \otimes X)\Gamma + vec(u),\ where\ vec(u) \sim N(0, \Sigma \otimes I_t)$$

where the matrix of coefficients Γ presents $m \times$ [# lagged variables + 1] dimension, that is the dynamic connectivity (also called effective connectivity), and the matrix of coefficients Σ represents the functional connectivity, where t represents the length of the Y series. The OLS estimation process can be translated by

$$\text{log-likelihood}(\hat{\Gamma}, \hat{\Sigma} | \text{observed data}) =$$
$$\underset{\Gamma,\Sigma}{argmin} \left[\frac{1}{t} tr((Y - X\Gamma)\Sigma^{-1}(Y - X\Gamma)') - log|\Sigma^{-1}| \right].$$

However, because the model also includes small linear dependencies, the number of links increases exponentially with the number of channels to include in the model, along with the analysis of complexity and the processing/interpretation rises in the results. Therefore, it is usual to use a data-dependent threshold to remove the weak connections, but the selection of an appropriate value can be different according to the experiment setting and goals (GARRISON *et al.*, 2015).

An alternative approach is to reduce the number of links during the connectivity matrices estimation, using sparse time series models. One widely used model is the GLASSO, used as a sparse VAR, proposed by (FRIEDMAN; HASTIE; TIBSHIRANI, 2008); the method takes into account the sparsity towards the estimation on the functional connectivity. Inherently, the estimated connectivity matrices often have few links, but despite to maximize the likelihood of the observed biosignals respect to the proposed theoretical model, it can lead to a distinct dynamic/effective connectivity estimation.

For instance, consider N multivariate normal observations of dimension p, with mean μ and covariance Σ. Using the empirical covariance matrix, the problem is to penalized negative log likelihood,

$$\text{log-likelihood}(\hat{\Gamma},\hat{\Sigma}|\text{observed data}) =$$
$$\underset{\Gamma,\Sigma}{argmin}[\frac{1}{t}tr((Y-X\Gamma)\Sigma^{-1}(Y-X\Gamma)') - log|\Sigma^{-1}|+$$
$$\lambda_1\sum_{i=1}^{G}\|\gamma_i\|_2+\lambda_2\sum_{k\neq k'}\|\Sigma^{-1}_{kk'}\|]$$

with λ_1 and λ_2 penalty parameters, γ_i is subvector of Γ, $G=q^2$ total number of groups and k block coordinate descent derived from Σ (that is, shrinking only in part of the covariance matrix).

A generalization of this model is found in the TSCGM, proposed by (ABEGAZ; WIT, 2013), where sparse estimations of both effective and functional connectivity matrices are obtained. In this method, both matrices are estimated interactively: first, a sparse functional connectivity estimate is calculated with a non-sparse non-concave penalty (smoothly clipped absolute deviation, SCAD); and later, sparse effective connectivity using the previous estimation as an initial value. This cycle is performed until it reaches convergence. Further details see (ABEGAZ; WIT, 2013).

TSCGM has been successfully applied to genetic data, and when applied to electroencephalograms, numerical experiments have shown a considerable reduction in the number of estimated connections. However, TSCGM also distorts the strength of some links, creating connections that were not present using a VAR model, because it relies on GLASSO for the estimation of the functional connectivity in each iteration.

The approach behind TSCGM is remarkable for increasing the sparsity of the estimations. Due to the original algorithmic implementation presented some issues during its application with biosignals, we introduced some adjustments. We also used a TSCGM-modified model that estimates the effective and functional connectivity that maximizes the loglikelihood of the model simultaneously using a Newton-type numerical optimization method. These methods are the nonlinear optimization and iterative optimization. For deeper discussions towards sparsity profile see (RAKOTOMAMONJY, 2011; BENSON; SHANNO; VANDERBEI, 2003; WIPF; NAGARAJAN, 2008).

6.2.2.4 Multilayer Networks

Graphical models are useful for describing and explore patterns of dynamic/effective and functional/contemporaneous interactions of a given phenomenon. In human neuroscience experimentation, brain network connectivity activation could be recorded from the electrical impulse aiming to highlight interaction among areas.

Given the complexity of the brain, multilayer networks incorporate the multivariate and multi-scale information scheme (DOMENICO, 2017). Generally speaking, it can be seen as a

collection of several distinct classical networks, encoding by a specific type of information about the system as a layer, compound a Multilayer network. Those layers quantify some elements of similarities such as (i) activity in different frequency bands, (ii) time-varying activity, (iii) activity of different tasks, and (iv) structural and functional connectivity.

Alongside this information, two important concepts about brain networks are essential to be pronounced; first it is the *functional connectivity* which expressed the statistical correlation within a time step, also interpreted as contemporaneous interactions, and second the *effective connectivity* that points across time from current to the previous steps, also called dynamic, indicating graphically an extra information pointing out the statistical causality (FRISTON, 2011).

6.2.2.5 Inferential Networks Analyzes

Let's consider a chain graph (or complex network) for a given network defined by a set of vertices V and a set of edges E order in pairs, then each point is represented as $P = (V, E)$. Their edges' (also called links) interpretation could be conditional within and across time steps representing the interactions between pairs.

Time series data modeling can be combining dynamic graphical models, which enables to incorporate sparsity, aiming to estimate statistical causality and correlation across series. For simplicity let's consider a Markovian dynamics (time t relates only to time $t-1$) then similar to VAR(1) as

$$(a,\ b) \in V_t \times V_{t-1} \Leftrightarrow \Gamma_{ab} \neq 0$$

where effective connectivity is represented by the link between area a and b at consecutive time steps relate to an element from Γ (points across time). Similarly, functional connectivity is represented by the link estimated from the effects of past and present corresponds from the precision matrix Σ (correlation within a time step), related to the model' errors as

$$(a,\ b) \in V_t \times V_t \Leftrightarrow \Sigma_{ab} \neq 0.$$

In this manner, a multivariate time series can be translated into a learning probabilistic connection network structure (as a graph model), targeting to estimate brain connectivity networks. Dynamic Chain Graph Model (DCGM) creates a multivariate dynamic linear model for each chain component, (WERMUTH; LAURITZEN, 1990) discuss the class of dynamic graphical models that enables to estimate of different signal phases and comparing their structural relations. For instance, the dynamic/contemporaneous interactions between brain regions, presented by (COSTA *et al.*, 2017), as a particular case of its theory in the neuroscience field.

6.2.2.6 TS Frequency Domain Approach

Brain activity can be collected as biosignals, composed by the flux of information from a group of connected neurons (called a neural circuit). Whereby seems at first to be pure noise,

but among specific ranges may lead to distinguish hidden patterns (SCHEFFER-TEIXEIRA *et al.*, 2013; PRADO; WEST, 2010). Moreover, different frequency bands can contribute towards the brain mapping functionality, by maximize the information flow through the brain regions (according to the observed and latent components).

The literature presents changes on the frequency cuts (FRANSSON, 2005; SU *et al.*, 2013), and those hubs might be very different when measured in different frequency bands. The findings concerns to the topological information measured from components in different frequency (in hertz unit - Hz). In this manner, such an enriched representation (decomposed TS signal) of is more valuable than other aggregated representation (raw TS signal). For instance, some pass band ripple filters are Butterworth, Chebyshev, Elliptic or Cauer, and Finite Impulse Response (FIR) filter (further details see (PARKS; BURRUS, 1987)).

Moreover, results presented in the literature (NEWSON; THIAGARAJAN, 2018; WOJCIK *et al.*, 2018) suggest that a healthy human brain operates at a transition point between independent and highly dependent frequency bands (e.g. represented as functional layers). EEG raw signals enable to establish encoding the connectivity between the neural circuit, and are described within five frequency bands; Then reasonable bands frequency delimitation is theta (0.01-4 Hz), delta (4-8 Hz), alpha (8-16 Hz), beta (16-32 Hz), gamma (32-49 Hz).

(DOMENICO, 2017) suggests that functional layers do not act as independent entities, then existing mechanisms for integration and segregation of brain activity within and across different frequency bands. Adopting multilayer techniques as potential non-invasive biomarkers for neurological and mental studies.

In this manner, this work adopted the finite impulse response (FIR) filter, used to filter the limit the signal coefficients given some order and frequency cutoff. Additionally, we added a correction using a Forward and Reverse filter applied on the FIR obtained signal to correct the phase distortion introduced by a one-pass filter, though it does square the magnitude response in the process. Both tools are implemented in R (OCTAVE. . . , 2007), presented in the package *signal*.

The multiplex sparse dynamic model framework enables to map the network connections, across different layers encoded as frequency bands (although integrated as (DOMENICO, 2017) suggests). Furthermore, the irreducibility of the multilayer functional representation of the human brain raises the necessity for multilayer analysis of the underlying architecture, targeting the identification of hubs.

6.3 Results

Neuroscientists seek to understand the brain connectivity through the functional and effective connectivity among the brain areas, using biosignals such as Electroencephalogram

(EEG) or functional Magnetic Resonance Imaging (fMRI). This work adopted to fathom the brain manipulation task related to the perception of verticality and posturography as a novelty targeting the development of a therapeutic approach for post-stroke patients.

For instance, (SANTOS; EDWARDS, 2019) pointed out that investigations towards the influence of cortical activity using non-invasive electromagnetic brain stimulation (NIBS) suggests to understand and treat disorders of verticality as a neurorehabilitation. Thereby, (SANTOS *et al.*, 2018) implemented a protocol towards human verticality manipulation, using neuromodulation, on healthy participants aiming to understand the recovery of this intentional artificial brain lesions, briefly introduced in section 6.2.1.

Selecting randomly a single participant, Figure 42 illustrate 5 minutes of brain response each panel (raw EEG signals), selecting only 7 channels (out of 256), and compares his signals during resting-state (top panel) versus post-2mA stimulation (bottom panel). Most of the selected EEG channels were located in the motor cortex; three channels derived from the right hemisphere (164, 173, and 183) and located nearby the region placed the tDCS four electrodes. Then, three other channels derived from the left hemisphere (66, 71, and 72), whereupon are physiologically related to those selected from the right hemisphere; additionally the EEG channel 143 placed in the parietal cortical region.

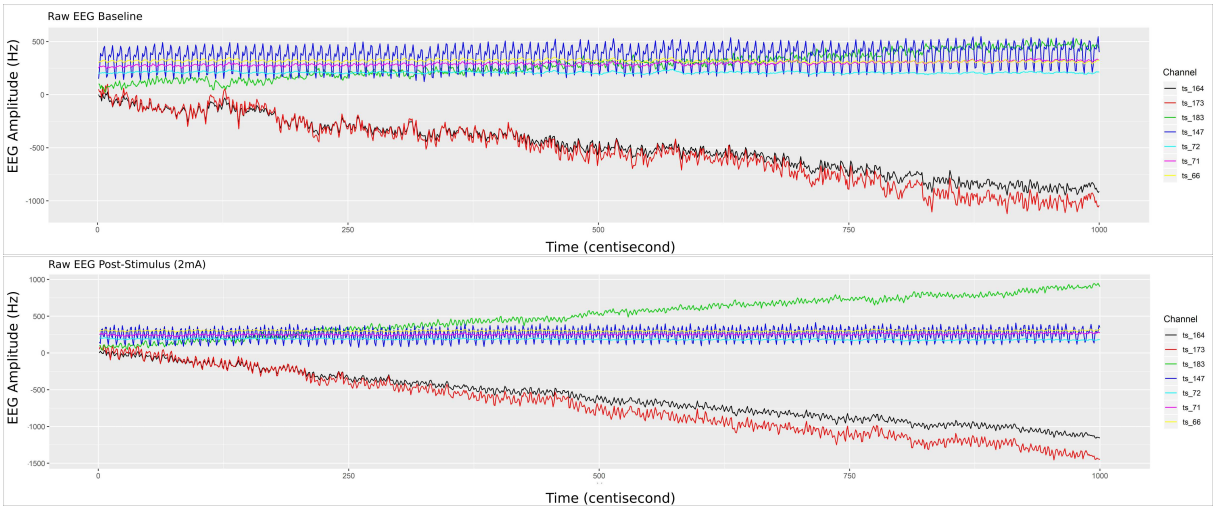

Figure 42 – Single participant EEG raw signals from 5 minutes recorded biosignals (top panel) during resting-state and (bottom panel) after HD-tDCS –Anodal Center 2mA– stimulation. The brain responses' amplitude (on the y-axis), from the raw EEG signals, increased after the stimulation.

It is noticeable in Figure 42 that post-stimulation of the brain response amplitude from the raw EEG signals increased, what is more relating with the hemisphere side to channels 183, 164, and 173 (related with the tDCS placed region). In addition, channel 66 has had its signal shifted up, which is physiologically explainable due to the polarity dependence created by the applied stimulus (directly related to channel 164, through the anodal input current electrode). Studies according to (PRADO; WEST, 2010; DOMENICO, 2017; OMBAO; HO, 2006) provide traces

that brain connectivity may be better understood using frequency bands decomposition limiting the influence of noise in the brain signal and describing different brain tasks as oscillatory bands.

Initially, we filtered the raw EEG signals, adopting the FIR with pass-band filter, utilizing 5 fundamental bands of brain waves (alpha, beta, delta, gamma, and theta). Figure 43 shows only the filtered signals related to the post-stimulation period, whereas elucidating the difference in band oscillation (signal phases) for each channel.

The channels located in the same brain hemisphere side as the neuromodulation (tDCS), presented greater oscillation. Thus, this dynamic may be translated/associated with the electrical transferred activity (energetic dissipation). This activity is expected given the rise of entropy through electrical synergy in this area (see (NASCIMENTO *et al.*, 2019)).

The study of the human brain has been developing and generates a massive amount of data, nevertheless unfolding this complex system is not trivial and, often, mishap to aggregate this information (FIECAS; OMBAO, 2011; SHEN; BAINGANA; GIANNAKIS, 2016; CASTRUCCIO; OMBAO; GENTON, 2016). Alternatively, the multilayer networks approach provides a mathematical background to model and analyze complex data with multivariate and multi-scale information (KIVELÄ *et al.*, 2014). Multiplex network shape can be formatted using (i) activity in different frequency bands, (ii) time-varying activity, (iii) activity with respect to different tasks, and (iv) structural and functional connectivity.

In this manner, estimation regarding the representation of a joint distribution of random variables is needed (the network structure). This procedure seeks to describe the causal relations across the brain regions. Thus, Vector Autoregression (VAR) model would be appropriated to describe a brain connectivity network, nonetheless, it may present a high-dimensionality curse in large sets. This class of models presents a significant number of parameters to be estimated. Additionally, shrinkage either in the data (such as PCA) or parameter spaces (like GLASSO and TSCGM) is not straightforward and may misleading information.

Graphical LASSO (GLASSO) model, proposed by (FRIEDMAN; HASTIE; TIBSHIRANI, 2008), estimates matrices tended to be different from those determined by a classical VAR method. It was noticeable that non-sparse VAR estimation not only increased the sparsity of the effective connectivity matrix, but "created links" that didn't appear before (based on our empirical analysis). Those models present a high sensibility to non-stationary series, and might mislead the estimation point connections (given the shrinkage on the covariance matrix –Contemporaneous Effect–, then changing the dynamic interactions).

Alternatively, TSCGM and TSCGM-modified was performed using a nonlinear optimization over the log-likelihood, and iterative optimizing the log-likelihood (with l_1-norm and SCAD penalization, not only in the covariance matrix) (ABEGAZ; WIT, 2013). Figure 44 shows the supra-adjacency matrix related with the functional connectivity, across 7 EEG channels, comparing seven estimation methods (classic VAR, GLASSO, TSCGM, TSCGM-nonlinear

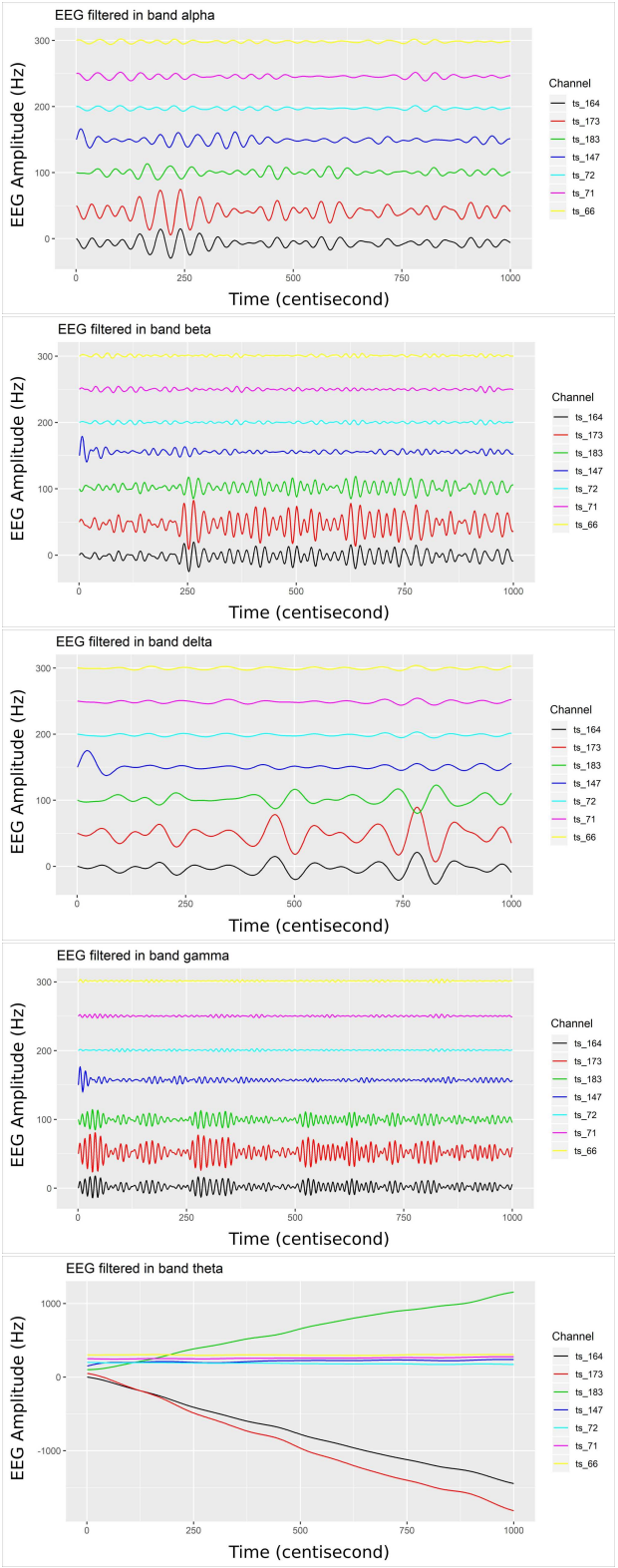

Figure 43 – Bandpower from the filtered EEG signals (top left) considering the alpha band, (top right) filter in beta band, (middle left) in delta band, (middle right) in gamma band, and (bottom center) filter in theta band. The EEG electrodes placed in the right-side brain hemisphere present higher dynamic/variation (channels 164, 173 and 183), related to post-2mA stimulation.

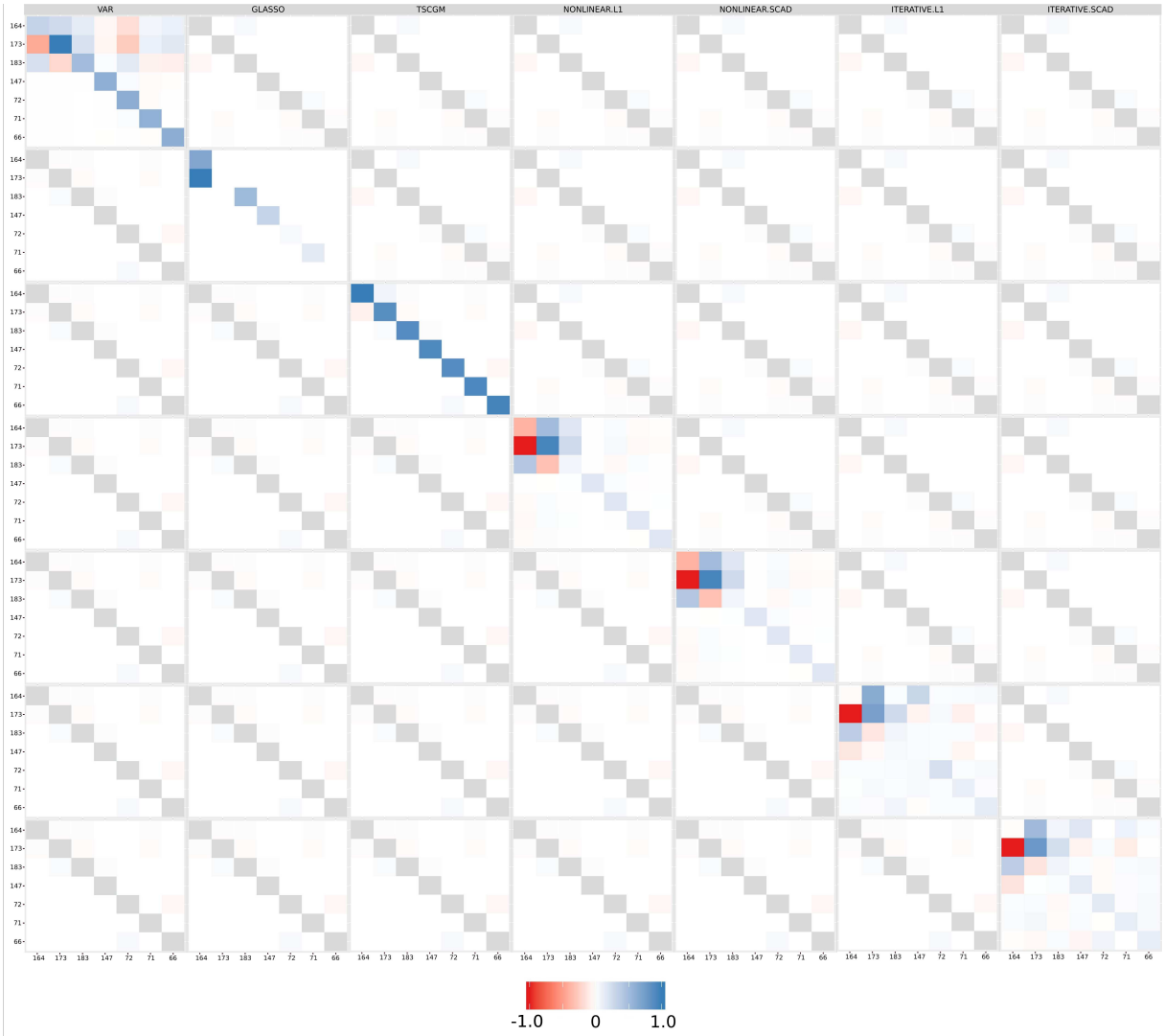

Figure 44 – Functional connectivity as supra-adjacency matrix, in-which rows and columns form group from the 7 filtered EEG alpha frequency-band signals, throughout the methods (VAR, GLASSO, TSCGM, TSCGM-nonlinear l_1-norm and SCAD, and TSCGM-iterative l_1-norm and SCAD). The VAR method is the reference, whereas the target is to maintain the strong links and remove the weak using sparsity. The TSCGM-nonlinear provided a competitive insight preserving the structure and function of the human brain.

l_1-norm, TSCGM-nonlinear SCAD, TSCGM-iterative l_1-norm and TSCGM-iterative SCAD), for instance, only the performance of a single band (alpha).

The VAR model includes weak linear dependencies, as mentioned in section 6.2.2, then it is desirable to use a data-dependent threshold to remove the weak connections without losing information. GLASSO and TSCGM led to different interpretation, compared to the VAR-estimated matrix. Nevertheless, TSCGM-modified with nonlinear optimization using both l_1-norm and SCAD penalization maintained the strong links presented in the VAR, but also eliminating the weak ones, therefore suggesting a competitive performance among the others. The same can not be said for the TSCGMs-modified with iterative optimization.

Figure 45 shows the estimated brain dynamic/effective connectivity among the seven

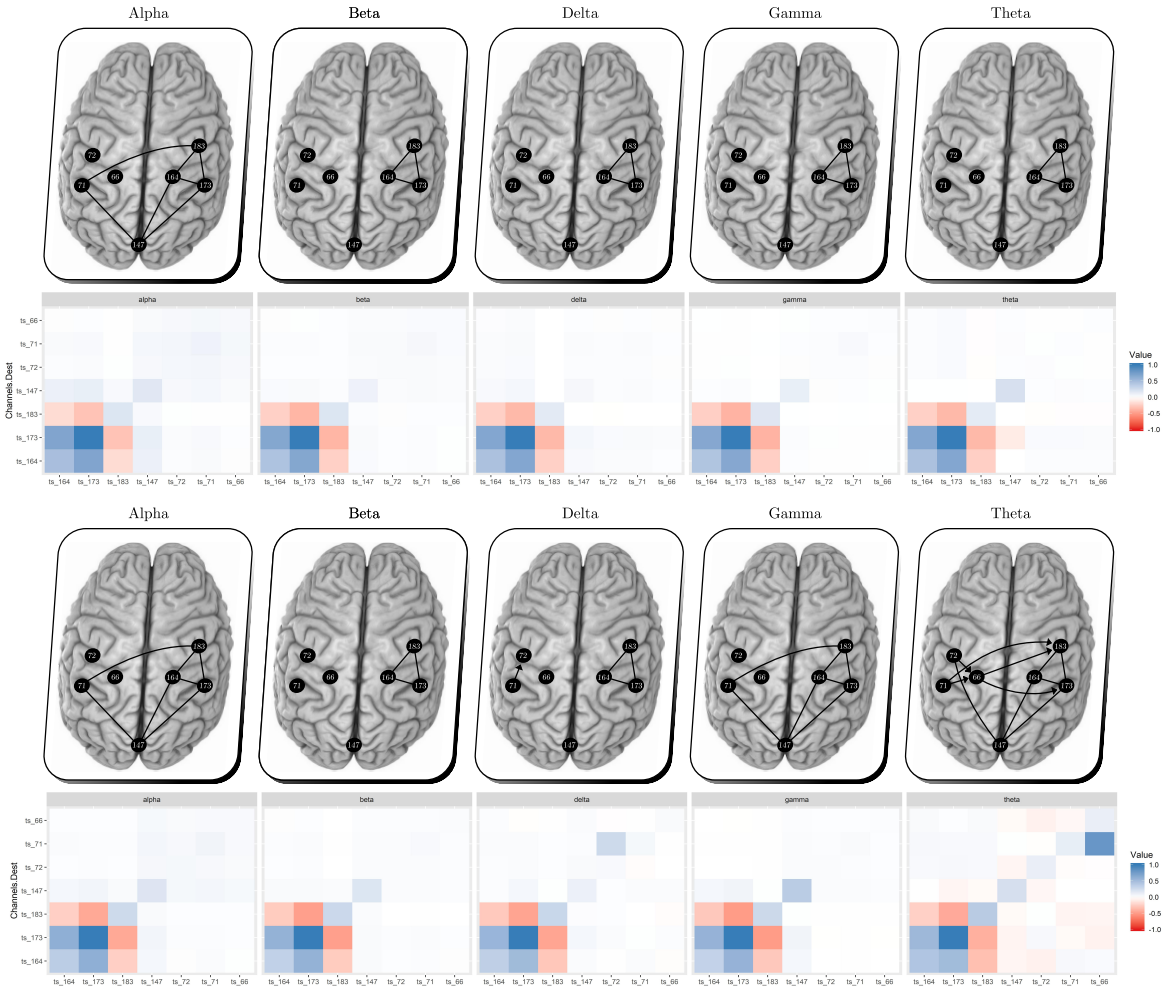

Figure 45 – Multiplex EEG signals, per bandpower, (top panels) resting-state and (bottom panels) after unilateral HD-tDCS –Anodal Center 2mA– stimulation. Comparing resting-state versus post-stimulation, we obtained additional links within the gamma and theta bands during post-stimulus suggest an outgrowth on the electrical brain dynamic.

filtered channels, (top figures) during resting-state and (bottom figures) post-stimulation, adopting the performance of TSCGM-nonlinear optimization using SCAD. That is, the brain illustrates with the correlation matrices the neuronal information floating connectivity (in different frequency-band signals).

No visual modification can be observed through the analysis of the alpha, beta and delta bands, according to Figure 45. Although gamma and theta band shows a change slightly (considering the new estimated coefficients intensity during post-stimulus). Preview results regarding the gamma band modification, after the neuromodulation, was previously discussed in agreement with (SANTOS *et al.*, 2018).

6.4 Final remarks

This work aimed to implement and discuss the comparison of sparse methods, towards parameter dimension shrinkage. Notwithstanding preserving the information, in the empirical data, aiming to develop elements towards the brain manipulation intervention related to the perception of verticality and posturography as a novelty targeting the recovery of post-stroke patients. Multilayer network approach enabled to integrate of the information retained given the electrical post-stimulus synergy (through different frequency bands).

The findings obtained in this paper help the process of estimating the neuronal circuit connections, with robust inference and computationally feasible. Estimating a network structure can be a non-trivial (CHICKERING, 1996a), highly complex task (RODRIGUES *et al.*, 2016), despite this sparse models showed to be promising bypassing the false positives' problem in estimation algorithms (results in Figure 44).

Using the sparse models (as a dynamic linear model) combined with frequency domain approach represented as multilayer network enables the neuroscience field to take advantage to interpret/estimate the dynamic of the neural circuits based on the data. Moreover, this work aimed to contribute with deeper data analysis towards the protocol (SANTOS *et al.*, 2018), discussing its feasibility, enlightening the human manipulation intervention response dynamic.

This work is limited given conclusions are based on a single participant response, whereas future works shall extend this modeling using hierarchical models and interpretation of the entire sample and protocol. (LIAO *et al.*, 2017) showed that the modular structures of brain networks completely vary across individuals. Thus, hierarchical modeling is required, in the form of a set of state vectors for each chain component, as an exchangeable sample with common mean. Therefore, future work shall explore the time-varying parameters, enclosed by the dynamic linear models, in a hierarchical version, suitable for interventions such as presented here, indexed in time.

CHAPTER

7

CONCLUSION

In this doctorate thesis we provide advances towards the neurorehabilitation data mining and its statistical analysis, towards time series dynamism and high-dimensional data. Moreover, we condensed in seven scientific work relating to the Dynamic Graph Models (DGMs) and complexity measurement, improving some of these models.

The novel starts in **chapter two** where it highlights some characteristics from these neurological data, that is the presence of high complexity. Generally, biosignals present a high spatial-temporal dependence. Naturally, one way of dealing with the structure is through the information theory, by using measures of complexity such as entropy. The main goal was to summarize/transform these data, and later, combined with classical statistical modeling (respecting its supposition). This work aimed to discuss the use of an appropriate statistic in the summarization of time series processes, preserving the information contained therein. By using entropy, in the area of neuroscience, it has a straightforward interpretation which is associated with the energetic dynamics of the process then statistical hypothesis tests comparing their equivalences. Moreover, in this study, under this approach, we could discuss the feasibility of the protocol, and its safety, towards treatment as a vertical human manipulation task presented in, e.g. post-stroke patients.

The visualization of these complex neuronal relation is needed and, commonly, explored via graph theory (complex networks). Therefore, this work adopted also the class of dynamic graph models (DGM), allowing to estimate the brain structure and dynamic, bringing more interpretation to the researchers regarding its connectivity. That is, the estimation of dynamics/evolution is a statistical problem that requires a numerical approximation towards the time-varying parameters, presented in **chapter three**. Moreover, we used the Multiregression Dynamic Models (MDM) developed by Queen & Smith (QUEEN; SMITH, 1993), recently explored in several areas such as neuroscience (COSTA *et al.*, 2015), traffic (ANACLETO; QUEEN; ALBERS, 2013a), economics (ZHAO; ZHOU, 2012) etc. As results, by analyzing the 5 minutes of EEG data after the HD-tDCS, it could identify mean structural breaks around 163

seconds, indicating a loss of HD-tDCS influence towards cortical activity (suggesting the return to the baseline state).

Further discussions were made towards the network problems require preliminary structure estimation. Estimating the structure of a network is an NP-hard complexity issue. That is, the search among all possible representations of its best structure is a highly complex task. Then, **chapter four** brings with the discussion about this structural estimation task, alternatively, using a heuristic method in comparison to the MDM-IPA, as well compares three type of numerical alternative to the MDM parameters; later, proposing a complexity measure, incorporating a probabilistic approach of the entropy parameter selection (incorporating a developed distribution, the Inverse Nakagami-m (INK) Distribution (LOUZADA; RAMOS; NASCIMENTO, 2018)), to verify the randomness of the residual of this models. It was described the estimation of communication and recognition of brain patterns in a neuroscience experiment. Subsequently, the extraction of relevant information from the models was confirmed and, since the residues presented a random characteristic, TS patterns already extracted.

The **chapter five** proposed a dynamic smoothing data compression, using a Symbolic Data Analysis approach by concatenating some TS as interval data. In this manner, this big data problem is reduced to a simpler/feasible task, where the shrinkage of this data is reduced to the decision-making granularity without further loss. In this manner, this work enables to identify some clinical change in patients after traumatic brain injury by improving the data classification method using SDA.

Finally, in **chapter six** it was discussed some filtering alternative and sparse DGM. The graph-based structure estimation may require some reduction, by imposing sparse on a complete dynamic model. In this manner, we compared (classic VAR, GLASSO, TSCGM, and TSCGM-modified with nonlinear and iterative optimizations) in order to reduce the amount of false positive link estimation combined with multilayer networks. The results were promising towards the susceptibility of sparse dynamic models. The findings obtained in this paper help the process of estimating the neuronal circuit connections, with robust inference and computationally feasible.

The chapters of this work solve, in a fraction, the complex problem that refers to the analysis of brain data from EEG signals. Presenting the discussion from the summarization of series, as complexities, to modeling their connectivity structure, as well as dynamics. Subsequently, techniques related to the reduction in data space and parametric space of DGM models were developed. The limitations regarding the results of this work refer to the fact that most of the interpretations obtained were derived from only one participant, thus it is necessary to carry out an analysis contemplating the others for generalization purposes in the area of neuroscience.

7.0.1 Perspectives

Some works that can provide continuity to the current research project are listed in the following.

- Combine all the presented adopted/developed models towards the analysis of the full EEG experiment (SANTOS *et al.*, 2018).
- To analysis other structural graph-based method, using a hybrid of Score-based and Constraint-based algorithms.
- To extend the class of DGM to the SDA approach.
- To develop a extension of the Dynamic SDA incorporating restrictions upon the boundaries estimation procedure.

BIBLIOGRAPHY

AADAL, L.; ANGEL, S.; DREYER, P.; LANGHORN, L.; PEDERSEN, B. B. Nursing roles and functions in the inpatient neurorehabilitation of stroke patients: A literature review. **Journal of Neuroscience Nursing**, LWW, v. 45, n. 3, p. 158–170, 2013. Citation on page 76.

ABEGAZ, F.; WIT, E. Sparse time series chain graphical models for reconstructing genetic networks. **Biostatistics**, Oxford University Press, v. 14, n. 3, p. 586–599, 2013. Citations on pages 58, 124, and 128.

AFGANI, M.; SINANOVIC, S.; HAAS, H. Anomaly detection using the kullback-leibler divergence metric. In: IEEE. **Applied Sciences on Biomedical and Communication Technologies, 2008. ISABEL'08. First International Symposium on**. [S.l.], 2008. p. 1–5. Citation on page 46.

AKAIKE, H. Information theory and an extension of the maximum likelihood principle,[w:] proceedings of the 2nd international symposium on information, bn petrow, f. **Czaki, Akademiai Kiado, Budapest**, 1973. Citation on page 59.

ALDER, B. J.; WAINWRIGHT, T. E. Studies in molecular dynamics. i. general method. **The Journal of Chemical Physics**, AIP, v. 31, n. 2, p. 459–466, 1959. Citation on page 64.

ALMALKI, S. J.; NADARAJAH, S. A new discrete modified weibull distribution. **IEEE Transactions on Reliability**, IEEE, v. 63, n. 1, p. 68–80, 2014. Citation on page 158.

AMBLARD, P.-O.; MICHEL, O. J. The relation between granger causality and directed information theory: A review. **Entropy**, Multidisciplinary Digital Publishing Institute, v. 15, n. 1, p. 113–143, 2013. Citation on page 78.

ANACLETO, O.; QUEEN, C.; ALBERS, C. J. Forecasting multivariate road traffic flows using bayesian dynamic graphical models, splines and other traffic variables. **Australian & New Zealand Journal of Statistics**, Wiley Online Library, v. 55, n. 2, p. 69–86, 2013. Citations on pages 82 and 133.

____. Multivariate forecasting of road traffic flows in the presence of heteroscedasticity and measurement errors. **Journal of the Royal Statistical Society: Series C (Applied Statistics)**, Wiley Online Library, v. 62, n. 2, p. 251–270, 2013. Citations on pages 54 and 59.

ARDOLINO, G.; BOSSI, B.; BARBIERI, S.; PRIORI, A. Non-synaptic mechanisms underlie the after-effects of cathodal transcutaneous direct current stimulation of the human brain. **The Journal of physiology**, Wiley Online Library, v. 568, n. 2, p. 653–663, 2005. Citations on pages 40 and 118.

BABYAR, S.; SANTOS-PONTELLI, T.; WILL-LEMOS, T.; MAZIN, S.; BIKSON, M.; TRUONG, D. Q.; EDWARDS, D.; REDING, M. Center of pressure speed changes with tdcs versus gvs in patients with lateropulsion after stroke. **Brain Stimulation: Basic, Translational, and Clinical Research in Neuromodulation**, Elsevier, v. 9, n. 5, p. 796–798, 2016. Citations on pages 31, 38, 57, and 98.

BACH, F. R.; JORDAN, M. I. Learning graphical models for stationary time series. **IEEE transactions on signal processing**, IEEE, v. 52, n. 8, p. 2189–2199, 2004. Citation on page 116.

BAGGIO, J. A.; MAZIN, S. S.; ALESSIO-ALVES, F. F.; BARROS, C. G.; CARNEIRO, A. A.; LEITE, J. P.; PONTES-NETO, O. M.; SANTOS-PONTELLI, T. E. Verticality perceptions associate with postural control and functionality in stroke patients. **PloS one**, Public Library of Science, v. 11, n. 3, p. e0150754, 2016. Citations on pages 38, 57, and 117.

BAI, J. Least squares estimation of a shift in linear processes. **Journal of Time Series Analysis**, Wiley Online Library, v. 15, n. 5, p. 453–472, 1994. Citations on pages 58 and 71.

BALAKRISHNAN, N.; HAIDARI, A.; MASOUMIFARD, K. Stochastic comparisons of series and parallel systems with generalized exponential components. **IEEE Transactions on Reliability**, IEEE, v. 64, n. 1, p. 333–348, 2015. Citation on page 158.

BALAKRISHNAN, N.; JIANG, N.; TSAI, T.-R.; LIO, Y.; CHEN, D.-G. Reliability inference on composite dynamic systems based on burr type-xii distribution. **IEEE Transactions on Reliability**, IEEE, v. 64, n. 1, p. 144–153, 2015. Citation on page 158.

BASHIR, S.; MIZRAHI, I.; WEAVER, K.; FREGNI, F.; PASCUAL-LEONE, A. Assessment and modulation of neural plasticity in rehabilitation with transcranial magnetic stimulation. **PM&R**, Elsevier, v. 2, n. 12, p. S253–S268, 2010. Citation on page 39.

BENSON, H. Y.; SHANNO, D. F.; VANDERBEI, R. J. A comparative study of large-scale nonlinear optimization algorithms. In: **High performance algorithms and software for nonlinear optimization**. [S.l.]: Springer, 2003. p. 95–127. Citation on page 124.

BHOGAL, A. S.; MANI, A. R. Pattern analysis of oxygen saturation variability in healthy individuals: Entropy of pulse oximetry signals carries information about mean oxygen saturation. **Frontiers in physiology**, Frontiers, v. 8, p. 555, 2017. Citation on page 36.

BIKSON, M.; GROSSMAN, P.; THOMAS, C.; ZANNOU, A. L.; JIANG, J.; ADNAN, T.; MOURDOUKOUTAS, A. P.; KRONBERG, G.; TRUONG, D.; BOGGIO, P. *et al.* Safety of transcranial direct current stimulation: evidence based update 2016. **Brain Stimulation: Basic, Translational, and Clinical Research in Neuromodulation**, Elsevier, v. 9, n. 5, p. 641–661, 2016. Citation on page 50.

BILLARD, L. Some analyses of interval data. **Journal of computing and information technology**, SRCE-Sveučilišni računski centar, v. 16, n. 4, p. 225–233, 2008. Citation on page 99.

BILLARD, L.; DIDAY, E. Regression analysis for interval-valued data. In: **Data Analysis, Classification, and Related Methods**. [S.l.]: Springer, 2000. p. 369–374. Citations on pages 99 and 104.

____. Symbolic regression analysis. In: **Classification, Clustering, and Data Analysis**. [S.l.]: Springer Berlin Heidelberg, 2002. p. 281–288. Citation on page 99.

____. Symbolic regression analysis. In: **Classification, Clustering, and Data Analysis**. [S.l.]: Springer, 2002. p. 281–288. Citation on page 104.

____. From the statistics of data to the statistics of knowledge: symbolic data analysis. **Journal of the American Statistical Association**, Taylor & Francis, v. 98, n. 462, p. 470–487, 2003. Citation on page 99.

____. **Symbolic Data Analysis: Conceptual Statistics and Data Mining**. [S.l.]: John Wiley & Sons, 2006. Citation on page 99.

BOCK, H.-H.; DIDAY, E. **Analysis of symbolic data: exploratory methods for extracting statistical information from complex data**. [S.l.]: Springer Science & Business Media, 2012. Citation on page 99.

BONAN, I. V.; HUBEAUX, K.; GELLEZ-LEMAN, M.; GUICHARD, J.; VICAUT, E.; YELNIK, A. Influence of subjective visual vertical misperception on balance recovery after stroke. **Journal of Neurology, Neurosurgery & Psychiatry**, BMJ Publishing Group Ltd, v. 78, n. 1, p. 49–55, 2007. Citations on pages 38 and 57.

BROOKS, S.; GELMAN, A.; JONES, G.; MENG, X.-L. **Handbook of markov chain monte carlo**. [S.l.]: CRC press, 2011. Citation on page 64.

BRUNONI, A. R.; NITSCHE, M. A.; BOLOGNINI, N.; BIKSON, M.; WAGNER, T.; MERABET, L.; EDWARDS, D. J.; VALERO-CABRE, A.; ROTENBERG, A.; PASCUAL-LEONE, A. *et al.* Clinical research with transcranial direct current stimulation (tdcs): challenges and future directions. **Brain Stimulation: Basic, Translational, and Clinical Research in Neuromodulation**, Elsevier, v. 5, n. 3, p. 175–195, 2012. Citations on pages 39, 40, and 118.

CACAO, F.; CORNELIUS, J.; FERNANDES, K.; ADEBAYO, Y.; LOZADA, M.; MARVILLE-WILLIAMS, C. Providing care in the digital way: A day in the life of a nurse in a digital intensive care unit (icu). **Canadian Journal of Critical Care Nursing**, v. 28, n. 2, 2017. Citations on pages 73 and 113.

CASTIGLIONI, P.; RIENZO, M. D. How the threshold "r" influences approximate entropy analysis of heart-rate variability. In: IEEE. **2008 Computers in Cardiology**. [S.l.], 2008. p. 561–564. Citations on pages 84 and 87.

CASTILLO-SAAVEDRA, L.; GEBODH, N.; BIKSON, M.; DIAZ-CRUZ, C.; BRANDAO, R.; COUTINHO, L.; TRUONG, D.; DATTA, A.; SHANI-HERSHKOVICH, R.; WEISS, M. *et al.* Clinically effective treatment of fibromyalgia pain with high-definition transcranial direct current stimulation: phase ii open-label dose optimization. **The Journal of Pain**, Elsevier, v. 17, n. 1, p. 14–26, 2016. Citation on page 39.

CASTRUCCIO, S.; OMBAO, H.; GENTON, M. G. A multi-resolution spatio-temporal model for brain activation and connectivity in fmri data. **arXiv preprint arXiv:1602.02435**, 2016. Citation on page 128.

CHERN, J.-S.; LO, C.-Y.; WU, C.-Y.; CHEN, C.-L.; YANG, S.; TANG, F.-T. Dynamic postural control during trunk bending and reaching in healthy adults and stroke patients. **American journal of physical medicine & rehabilitation**, LWW, v. 89, n. 3, p. 186–197, 2010. Citations on pages 38, 57, and 117.

CHIANG, M.-C.; KLUNDER, A. D.; MCMAHON, K.; ZUBICARAY, G. I. D.; WRIGHT, M. J.; TOGA, A. W.; THOMPSON, P. M. Information-theoretic analysis of brain white matter fiber orientation distribution functions. In: SPRINGER. **Biennial International Conference on Information Processing in Medical Imaging**. [S.l.], 2007. p. 172–182. Citation on page 46.

CHICKERING, D. **Learning Bayesian Networks is NP-Complete. Learning from Data: Artificial Intelligence and Statistics V. Edited by: Fisher D, Lenz HJ.** [S.l.]: Springer-Verlag, 1996. Citations on pages 122 and 132.

CHICKERING, D. M. Learning bayesian networks is np-complete. In: **Learning from data**. [S.l.]: Springer, 1996. p. 121–130. Citations on pages 60 and 94.

COGIAMANIAN, F.; VERGARI, M.; PULECCHI, F.; MARCEGLIA, S.; PRIORI, A. Effect of spinal transcutaneous direct current stimulation on somatosensory evoked potentials in humans. **Clinical Neurophysiology**, Elsevier, v. 119, n. 11, p. 2636–2640, 2008. Citations on pages 40 and 118.

CORCHADO, E.; WOZNIAK, M.; ABRAHAM, A.; CARVALHO, A. C. P. L.; SNÁSEL, V. *et al.* Recent trends in intelligent data analysis. **Neurocomputing**, Elsevier, v. 126, p. 1–2, 2014. Citation on page 98.

CORDEIRO, G. M.; KLEIN, R. Bias correction in arma models. **Statistics & Probability Letters**, Elsevier, v. 19, n. 3, p. 169–176, 1994. Citation on page 165.

COSTA, L.; ANACLETO, O.; NASCIMENTO, D. C.; SMITH, J.; LOUZADA, F.; NICHOLS, T. The hierarchical multiregression dynamic models: a brain connectivity cluster reconstruction task. **Information Sciences Journal**, Elsevier, in press. Citations on pages 81 and 94.

COSTA, L.; NICHOLS, T.; SMITH, J. Q. *et al.* Studying the effective brain connectivity using multiregression dynamic models. **Brazilian Journal of Probability and Statistics**, Brazilian Statistical Association, v. 31, n. 4, p. 765–800, 2017. Citations on pages 31, 54, 55, 59, 98, 112, and 125.

COSTA, L.; SMITH, J.; NICHOLS, T.; CUSSENS, J.; DUFF, E. P.; MAKIN, T. R. *et al.* Searching multiregression dynamic models of resting-state fmri networks using integer programming. **Bayesian Analysis**, International Society for Bayesian Analysis, v. 10, n. 2, p. 441–478, 2015. Citations on pages 82, 84, 94, 105, 112, and 133.

COSTA, L.; SMITH, J. Q.; NICHOLS, T. A group analysis using the multiregression dynamic models for fmri networked time series. **Journal of statistical planning and inference**, Elsevier, v. 198, p. 43–61, 2019. Citations on pages 77, 81, and 94.

COX, D. R.; REID, N. Parameter orthogonality and approximate conditional inference. **Journal of the Royal Statistical Society. Series B (Methodological)**, JSTOR, p. 1–39, 1987. Citation on page 165.

COX, D. R.; SNELL, E. J. A general definition of residuals. **Journal of the Royal Statistical Society. Series B (Methodological)**, JSTOR, p. 248–275, 1968. Citations on pages 158 and 165.

CRANSTOUN, S. D.; OMBAO, H. C.; SACHS, R. V.; GUO, W.; LITT, B. Time-frequency spectral estimation of multichannel eeg using the auto-slex method. **IEEE transactions on Biomedical Engineering**, IEEE, v. 49, n. 9, p. 988–996, 2002. Citation on page 54.

CUESTA-FRAU, D.; MIRÓ-MARTÍNEZ, P.; NÚÑEZ, J. J.; OLTRA-CRESPO, S.; PICÓ, A. M. Noisy eeg signals classification based on entropy metrics. performance assessment using first and second generation statistics. **Computers in biology and medicine**, Elsevier, v. 87, p. 141–151, 2017. Citation on page 36.

CURY, A.; CRÉMONA, C. Pattern recognition of structural behaviors based on learning algorithms and symbolic data concepts. **Structural Control and Health Monitoring**, Wiley Online Library, v. 19, n. 2, p. 161–186, 2012. Citation on page 100.

CYSARZ, D.; EDELHÄUSER, F.; LEEUWEN, P. V. Strategies of symbolization in cardiovascular time series to test individual gestational development in the fetus. **Philosophical Transactions of the Royal Society A: Mathematical, Physical and Engineering Sciences**, The Royal Society Publishing, v. 373, n. 2034, p. 20140087, 2015. Citation on page 106.

DAGUM, P.; GALPER, A.; HORVITZ, E. Dynamic network models for forecasting. In: ELSEVIER. **Uncertainty in artificial intelligence**. [S.l.], 1992. p. 41–48. Citation on page 82.

DASH, D.; DRUZDZEL, M. J. A hybrid anytime algorithm for the construction of causal models from sparse data. In: MORGAN KAUFMANN PUBLISHERS INC. **Proceedings of the Fifteenth conference on Uncertainty in artificial intelligence**. [S.l.], 1999. p. 142–149. Citation on page 81.

DAY, B. L.; COLE, J. Vestibular-evoked postural responses in the absence of somatosensory information. **Brain**, Oxford University Press, v. 125, n. 9, p. 2081–2088, 2002. Citations on pages 38, 57, and 117.

DEY, D. K.; RAO, C. R. **Bayesian thinking, modeling and computation**. [S.l.]: Elsevier, 2005. Citations on pages 95 and 112.

DIDAY, E. Thinking by classes in data science: the symbolic data analysis paradigm. **Wiley Interdisciplinary Reviews: Computational Statistics**, Wiley Online Library, v. 8, n. 5, p. 172–205, 2016. Citation on page 99.

DIDAY, E.; NOIRHOMME-FRAITURE, M. **Symbolic data analysis and the SODAS software**. [S.l.]: John Wiley & Sons, 2008. Citations on pages 98 and 99.

DIDAY, E.; SIMON, J. Clustering analysis. In: **Digital pattern recognition**. [S.l.]: Springer, 1976. p. 47–94. Citation on page 99.

DIDONATO, A. R.; JR, A. H. M. Computation of the incomplete gamma function ratios and their inverse. **ACM Transactions on Mathematical Software (TOMS)**, ACM, v. 12, n. 4, p. 377–393, 1986. Citation on page 160.

DOMENICO, M. D. Multilayer modeling and analysis of human brain networks. **Giga Science**, Oxford University Press, v. 6, n. 5, p. gix004, 2017. Citations on pages 116, 124, 126, and 127.

DOMINGUES, M.; SOUZA, R.; CYSNEIROS, F. A robust method for linear regression of symbolic interval data. **Pattern Recognition Letters**, v. 31, n. 13, p. 1991 – 1996, 2010. Citation on page 100.

EDWARDS, D.; CORTES, M.; DATTA, A.; MINHAS, P.; WASSERMANN, E. M.; BIKSON, M. Physiological and modeling evidence for focal transcranial electrical brain stimulation in humans: a basis for high-definition tdcs. **Neuroimage**, Elsevier, v. 74, p. 266–275, 2013. Citations on pages 117 and 118.

EDWARDS, D. J. On the understanding and development of modern physical neurorehabilitation methods: robotics and non-invasive brain stimulation. **Journal of neuroengineering and rehabilitation**, BioMed Central, v. 6, n. 1, p. 3, 2009. Citation on page 29.

EICHLER, M. **Graphical models in time series analysis**. Phd Thesis (PhD Thesis) — Universität Heidelberg, 1999. Citation on page 59.

FAGUNDES, R. A. A.; SOUZA, R. M. C. R.; CYSNEIROS, F. J. A. Robust regression with application to symbolic interval data. **Engineering Applications of Artificial Intelligence**, v. 26, n. 1, p. 564 – 573, 2013. ISSN 0952-1976. Citation on page 100.

FEIGIN, V. L.; FOROUZANFAR, M. H.; KRISHNAMURTHI, R.; MENSAH, G. A.; CONNOR, M.; BENNETT, D. A.; MORAN, A. E.; SACCO, R. L.; ANDERSON, L.; TRUELSEN, T. *et al.* Global and regional burden of stroke during 1990–2010: findings from the global burden of disease study 2010. **The Lancet**, Elsevier, v. 383, n. 9913, p. 245–255, 2014. Citations on pages 29 and 76.

FERBERT, A.; PRIORI, A.; ROTHWELL, J.; DAY, B.; COLEBATCH, J.; MARSDEN, C. Interhemispheric inhibition of the human motor cortex. **The Journal of physiology**, Wiley Online Library, v. 453, n. 1, p. 525–546, 1992. Citations on pages 40 and 118.

FERNÁNDEZ-VILLAVERDE, J.; RUBIO-RAMÍREZ, J. F. Estimating macroeconomic models: A likelihood approach. **The Review of Economic Studies**, Wiley-Blackwell, v. 74, n. 4, p. 1059–1087, 2007. Citation on page 98.

FIECAS, M.; OMBAO, H. The generalized shrinkage estimator for the analysis of functional connectivity of brain signals. **The Annals of Applied Statistics**, JSTOR, p. 1102–1125, 2011. Citations on pages 31, 54, and 128.

FLESCH, I.; LUCAS, P. J. Markov equivalence in bayesian networks. In: **Advances in probabilistic graphical models**. [S.l.]: Springer, 2007. p. 3–38. Citation on page 80.

FRANSSON, P. Spontaneous low-frequency bold signal fluctuations: An fmri investigation of the resting-state default mode of brain function hypothesis. **Human brain mapping**, Wiley Online Library, v. 26, n. 1, p. 15–29, 2005. Citation on page 126.

FRIEDMAN, J.; HASTIE, T.; TIBSHIRANI, R. Sparse inverse covariance estimation with the graphical lasso. **Biostatistics**, Oxford University Press, v. 9, n. 3, p. 432–441, 2008. Citations on pages 123 and 128.

FRIEDMAN, N.; GEIGER, D.; GOLDSZMIDT, M. Bayesian network classifiers. **Machine learning**, Springer, v. 29, n. 2-3, p. 131–163, 1997. Citation on page 80.

FRISTON, K. J. Functional and effective connectivity: a review. **Brain connectivity**, Mary Ann Liebert, Inc. 140 Huguenot Street, 3rd Floor New Rochelle, NY 10801 USA, v. 1, n. 1, p. 13–36, 2011. Citation on page 125.

FRISTON, K. J.; GLASER, D. E.; HENSON, R. N.; KIEBEL, S.; PHILLIPS, C.; ASHBURNER, J. Classical and bayesian inference in neuroimaging: applications. **Neuroimage**, Elsevier, v. 16, n. 2, p. 484–512, 2002. Citation on page 54.

FU, T.-c. A review on time series data mining. **Engineering Applications of Artificial Intelligence**, Elsevier, v. 24, n. 1, p. 164–181, 2011. Citation on page 98.

GAMERMAN, D.; MIGON, H. S. Dynamic hierarchical models. **Journal of the Royal Statistical Society: Series B (Methodological)**, Wiley Online Library, v. 55, n. 3, p. 629–642, 1993. Citation on page 63.

GÁMEZ, J. A.; MATEO, J. L.; PUERTA, J. M. Learning bayesian networks by hill climbing: efficient methods based on progressive restriction of the neighborhood. **Data Mining and Knowledge Discovery**, Springer, v. 22, n. 1-2, p. 106–148, 2011. Citations on pages 80 and 81.

GANTI, V.; GEHRKE, J.; RAMAKRISHNAN, R. Mining very large databases. **Computer**, IEEE, v. 32, n. 8, p. 38–45, 1999. Citation on page 98.

GARRISON, K. A.; SCHEINOST, D.; FINN, E. S.; SHEN, X.; CONSTABLE, R. T. The (in) stability of functional brain network measures across thresholds. **Neuroimage**, Elsevier, v. 118, p. 651–661, 2015. Citations on pages 121 and 123.

GILIO, F.; RIZZO, V.; SIEBNER, H. R.; ROTHWELL, J. C. Effects on the right motor hand-area excitability produced by low-frequency rtms over human contralateral homologous cortex. **The Journal of physiology**, Wiley Online Library, v. 551, n. 2, p. 563–573, 2003. Citations on pages 40 and 118.

GIUSTI, A.; GRASSINI, L. Cluster analysis of census data using the symbolic data approach. **Advances in Data Analysis and Classification**, Springer, v. 2, n. 2, p. 163–176, 2008. Citation on page 100.

GLASER, R. E. Bathtub and related failure rate characterizations. **Journal of the American Statistical Association**, Taylor & Francis Group, v. 75, n. 371, p. 667–672, 1980. Citation on page 161.

GLOVER, F. Tabu search: A tutorial. **Interfaces**, INFORMS, v. 20, n. 4, p. 74–94, 1990. Citation on page 94.

GONZÁLEZ-RIVERA, G.; ARROYO, J. Time series modeling of histogram-valued data: The daily histogram time series of s&p500 intradaily returns. **International Journal of Forecasting**, Elsevier, v. 28, n. 1, p. 20–33, 2012. Citation on page 100.

GOODMAN, M. S.; LI, Y.; TIWARI, R. C. Survival analysis with change point hazard functions. bepress, 2006. Citation on page 170.

GORROSTIETA, C.; FIECAS, M.; OMBAO, H.; BURKE, E.; CRAMER, S. Hierarchical vector auto-regressive models and their applications to multi-subject effective connectivity. **Frontiers in computational neuroscience**, Frontiers, v. 7, p. 159, 2013. Citations on pages 54 and 59.

GORROSTIETA, C.; OMBAO, H.; BÉDARD, P.; SANES, J. N. Investigating brain connectivity using mixed effects vector autoregressive models. **NeuroImage**, Elsevier, v. 59, n. 4, p. 3347–3355, 2012. Citations on pages 31 and 54.

GRANGER, C. W. Investigating causal relations by econometric models and cross-spectral methods. **Econometrica: Journal of the Econometric Society**, JSTOR, p. 424–438, 1969. Citations on pages 77, 78, and 105.

GRANGER, C. W. J. Economic processes involving feedback. **Information and control**, Elsevier, v. 6, n. 1, p. 28–48, 1963. Citation on page 78.

GRATTON, C.; LAUMANN, T. O.; NIELSEN, A. N.; GREENE, D. J.; GORDON, E. M.; GILMORE, A. W.; NELSON, S. M.; COALSON, R. S.; SNYDER, A. Z.; SCHLAGGAR, B. L. *et al.* Functional brain networks are dominated by stable group and individual factors, not cognitive or daily variation. **Neuron**, Elsevier, v. 98, n. 2, p. 439–452, 2018. Citation on page 116.

GRUBER, L. F.; WEST, M. Bayesian forecasting and scalable multivariate volatility analysis using simultaneous graphical dynamic linear models. **Econometrics and Statistics**, v. 3, p. 3–22, 2017. ArXiv:1606.08291. Available: <http://www.sciencedirect.com/science/article/pii/S2452306217300163>. Citations on pages 31 and 54.

HARRIS-LOVE, M. L.; COHEN, L. G. Noninvasive cortical stimulation in neurorehabilitation: a review. **Archives of Physical Medicine and Rehabilitation**, Elsevier, v. 87, n. 12, p. 84–93, 2006. Citation on page 76.

HECKERMAN, D.; GEIGER, D.; CHICKERING, D. M. Learning bayesian networks: The combination of knowledge and statistical data. **Machine learning**, Springer, v. 20, n. 3, p. 197–243, 1995. Citation on page 60.

HEINTZMAN, N. D.; HON, G. C.; HAWKINS, R. D.; KHERADPOUR, P.; STARK, A.; HARP, L. F.; YE, Z.; LEE, L. K.; STUART, R. K.; CHING, C. W. *et al.* Histone modifications at human enhancers reflect global cell-type-specific gene expression. **Nature**, Nature Publishing Group, v. 459, n. 7243, p. 108, 2009. Citation on page 36.

HYNDMAN, R. J.; ATHANASOPOULOS, G. **Forecasting: principles and practice**. [S.l.]: OTexts, 2018. Citation on page 110.

IDE, J. S.; ZHANG, S.; CHIANG-SHAN, R. L. Bayesian network models in brain functional connectivity analysis. **International Journal of Approximate Reasoning**, Elsevier, v. 55, n. 1, p. 23–35, 2014. Citation on page 94.

JIANG, X.; NEAPOLITAN, R. E.; BARMADA, M. M.; VISWESWARAN, S. Learning genetic epistasis using bayesian network scoring criteria. **BMC bioinformatics**, BioMed Central, v. 12, n. 1, p. 89, 2011. Citation on page 81.

JOHNSON, N. L.; KOTZ, S.; BALAKRISHNAN, N. Distributions in statistics: continuous univariate distributions, vol. 2. **NY: Wiley**, 1970. Citation on page 158.

JOHNSON, W.; ONUMA, O.; OWOLABI, M.; SACHDEV, S. Stroke: a global response is needed. **Bulletin of the World Health Organization**, World Health Organization, v. 94, n. 9, p. 634, 2016. Citations on pages 29 and 76.

JOHNSTON, S. C.; MENDIS, S.; MATHERS, C. D. Global variation in stroke burden and mortality: estimates from monitoring, surveillance, and modelling. **The Lancet Neurology**, Elsevier, v. 8, n. 4, p. 345–354, 2009. Citations on pages 29 and 76.

JOSHI, S. H.; BOWMAN, I.; TOGA, A. W.; HORN, J. D. V. Brain pattern analysis of cortical valued distributions. In: NIH PUBLIC ACCESS. **Proceedings/IEEE International Symposium on Biomedical Imaging: from nano to macro. IEEE International Symposium on Biomedical Imaging**. [S.l.], 2011. p. 1117. Citation on page 46.

JUDSON, R. A.; OWEN, A. L. Estimating dynamic panel data models: a guide for macroeconomists. **Economics letters**, Elsevier, v. 65, n. 1, p. 9–15, 1999. Citation on page 98.

KELLAWAY, P. The part played by electric fish in the early history of bioelectricity and electrotherapy. **Bulletin of the History of Medicine**, Johns Hopkins University Press, v. 20, p. 112, 1946. Citation on page 39.

KELLER, K.; LAUFFER, H. Symbolic analysis of high-dimensional time series. **International Journal of Bifurcation and Chaos**, World Scientific, v. 13, n. 09, p. 2657–2668, 2003. Citation on page 111.

KEVIN, B.; NICHOLSON, A. **Bayesian artificial intelligence**. [S.l.]: Chapman & Hall/CRC, 2004. Citation on page 80.

KIM, J. H.; PEARL, J. Convince: A conversational inference consolidation engine. **IEEE transactions on systems, man, and cybernetics**, IEEE, v. 17, n. 2, p. 120–132, 1987. Citation on page 77.

KING, L. A.; FISHER, J.; JACQUIN, L.; ZELTWANGER, P. The digital hospital: opportunities and challenges. **Journal of healthcare information management: JHIM**, v. 17, n. 1, p. 37–45, 2003. Citations on pages 73 and 113.

KIVELÄ, M.; ARENAS, A.; BARTHELEMY, M.; GLEESON, J. P.; MORENO, Y.; PORTER, M. A. Multilayer networks. **Journal of complex networks**, Oxford University Press, v. 2, n. 3, p. 203–271, 2014. Citations on pages 116 and 128.

KRAVARIS, C.; HAHN, J.; CHU, Y. Advances and selected recent developments in state and parameter estimation. **Computers & chemical engineering**, Elsevier, v. 51, p. 111–123, 2013. Citation on page 112.

KRYSTAL, A. D.; PRADO, R.; WEST, M. New methods of time series analysis of non-stationary eeg data: eigenstructure decompositions of time varying autoregressions. **Clinical Neurophysiology**, Elsevier, v. 110, n. 12, p. 2197–2206, 1999. Citations on pages 98 and 121.

KUNDU, D.; RAQAB, M. Z. Bayesian inference and prediction of order statistics for a type-ii censored weibull distribution. **Journal of statistical planning and inference**, Elsevier, v. 142, n. 1, p. 41–47, 2012. Citations on pages 171 and 173.

LANG, N.; SIEBNER, H. R.; WARD, N. S.; LEE, L.; NITSCHE, M. A.; PAULUS, W.; ROTHWELL, J. C.; LEMON, R. N.; FRACKOWIAK, R. S. How does transcranial dc stimulation of the primary motor cortex alter regional neuronal activity in the human brain? **European Journal of Neuroscience**, Wiley Online Library, v. 22, n. 2, p. 495–504, 2005. Citations on pages 40 and 118.

LEE, L.; SIEBNER, H. R.; ROWE, J. B.; RIZZO, V.; ROTHWELL, J. C.; FRACKOWIAK, R. S.; FRISTON, K. J. Acute remapping within the motor system induced by low-frequency repetitive transcranial magnetic stimulation. **Journal of Neuroscience**, Soc Neuroscience, v. 23, n. 12, p. 5308–5318, 2003. Citations on pages 40 and 118.

LI, J.; WANG, Z. J.; PALMER, S. J.; MCKEOWN, M. J. Dynamic bayesian network modeling of fmri: a comparison of group-analysis methods. **Neuroimage**, Elsevier, v. 41, n. 2, p. 398–407, 2008. Citation on page 94.

LIAO, X.; CAO, M.; XIA, M.; HE, Y. Individual differences and time-varying features of modular brain architecture. **Neuroimage**, Elsevier, v. 152, p. 94–107, 2017. Citations on pages 29, 81, 94, and 132.

LIEBETANZ, D.; NITSCHE, M. A.; TERGAU, F.; PAULUS, W. Pharmacological approach to the mechanisms of transcranial dc-stimulation-induced after-effects of human motor cortex excitability. **Brain**, Oxford University Press, v. 125, n. 10, p. 2238–2247, 2002. Citation on page 40.

LIEPERT, J.; HAMZEI, F.; WEILLER, C. Motor cortex disinhibition of the unaffected hemisphere after acute stroke. **Muscle & Nerve: Official Journal of the American Association of Electrodiagnostic Medicine**, Wiley Online Library, v. 23, n. 11, p. 1761–1763, 2000. Citation on page 40.

Lima Neto, E. A.; De Carvalho, F. A. T. Centre and range method for fitting a linear regression model to symbolic interval data. **Computational Statistics & Data Analysis**, v. 52, n. 3, p. 1500 – 1515, 2008. ISSN 0167-9473. Citations on pages 99, 100, and 104.

LOUZADA, F.; RAMOS, P. L.; NASCIMENTO, D. The inverse nakagami-m distribution: A novel approach in reliability. **IEEE Transactions on Reliability**, IEEE, v. 67, n. 3, p. 1030–1042, 2018. Citations on pages 84, 87, and 134.

MATTAR, M. G.; WYMBS, N. F.; BOCK, A. S.; AGUIRRE, G. K.; GRAFTON, S. T.; BASSETT, D. S. Predicting future learning from baseline network architecture. **Neuroimage**, Elsevier, v. 172, p. 107–117, 2018. Citations on pages 29, 81, and 94.

MCMILLAN, B. The basic theorems of information theory. **Annals of Mathematical Statistics**, v. 24, p. 196–219, 1953. Citation on page 41.

MELSSEN, W.; EPPING, W. Detection and estimation of neural connectivity based on crosscorrelation analysis. **Biological cybernetics**, Springer, v. 57, n. 6, p. 403–414, 1987. Citation on page 59.

METROPOLIS, N.; ROSENBLUTH, A. W.; ROSENBLUTH, M. N.; TELLER, A. H.; TELLER, E. Equation of state calculations by fast computing machines. **The journal of chemical physics**, AIP, v. 21, n. 6, p. 1087–1092, 1953. Citation on page 64.

MEYER, B.-U.; RÖRICHT, S.; WOICIECHOWSKY, C. Topography of fibers in the human corpus callosum mediating interhemispheric inhibition between the motor cortices. **Annals of neurology**, Wiley Online Library, v. 43, n. 3, p. 360–369, 1998. Citations on pages 40 and 118.

MIGON, H. S.; GAMERMAN, D.; LOUZADA, F. **Statistical inference: an integrated approach**. 2. ed. [S.l.]: Chapman and Hall/CRC press, 2014. Citation on page 165.

NAKAGAMI, N. The m-distribution a general formulation of intensity distribution of rapid fading. **Statistical Methods in Radio Wave Propagation: Proceedings of a Symposium**, Pergamon Press, p. 3–36, 1960. Citation on page 158.

NAKAHARA, H.; CARCOLÉ, E. Maximum-likelihood method for estimating coda q and the nakagami-m parameter. **Bulletin of the Seismological Society of America**, Seismological Society of America, v. 100, n. 6, p. 3174–3182, 2010. Citation on page 158.

NAKAO, H. Phase reduction approach to synchronisation of nonlinear oscillators. **Contemporary Physics**, Taylor & Francis, v. 57, n. 2, p. 188–214, 2016. Citation on page 120.

NASCIMENTO, D.; COSTA, L.; LEITE, J.; EDWARDS, D.; SANTOS, T.; LOUZADA, F. Bayesian dynamic graphical models: Analyzing brainwave data from fixed parameters to hierarchical design. **Information Sciences**, in press. Citations on pages 29, 58, and 66.

NASCIMENTO, D. C.; COSTA, L.; LEITE, J. P.; EDWARDS, D. J.; SANTOS, T.; LOUZADA, F. Bayesian dynamic graphical models: Analyzing a brainwaves task from fix parameters to the hierarchical design. **Information Sciences Journal**, Elsevier, in press. Citations on pages 77 and 82.

NASCIMENTO, D. C.; DEPETRI, G.; STEFANO, L. H.; ANACLETO, O.; LEITE, J. P.; EDWARDS, D. J.; SANTOS, T. E.; NETO, F. L. Entropy analysis of high-definition transcranial electric stimulation effects on eeg dynamics. **Brain sciences**, Multidisciplinary Digital Publishing Institute, v. 9, n. 8, p. 208, 2019. Citations on pages 31, 77, 119, and 128.

NASSERI, P.; NITSCHE, M. A.; EKHTIARI, H. A framework for categorizing electrode montages in transcranial direct current stimulation. **Frontiers in human neuroscience**, Frontiers, v. 9, p. 54, 2015. Citation on page 37.

NATARAJAN, K.; ACHARYA, R.; ALIAS, F.; TIBOLENG, T.; PUTHUSSERYPADY, S. K. Nonlinear analysis of eeg signals at different mental states. **BioMedical Engineering OnLine**, BioMed Central, v. 3, n. 1, p. 7, 2004. Citation on page 120.

NEAPOLITAN, R. E. **Learning bayesian networks: Pearson Prentice Hall Upper Saddle River**. [S.l.]: NJ, 2004. Citation on page 79.

NETO, E.; CARVALHO, F. D. Symbolic approach to analyzing administrative management. **The Electronic Journal of Symbolic Data Analysis**, v. 1, n. 1, p. 1–13, 2002. Citation on page 100.

NETO, E. A. L.; CARVALHO, F. A. T. D. An exponential-type kernel robust regression model for interval-valued variables. **Information Sciences**, v. 454-455, p. 419 – 442, 2018. ISSN 0020-0255. Citation on page 100.

NETO, E. d. A. L.; CARVALHO, F. d. A. de. Centre and range method for fitting a linear regression model to symbolic interval data. **Computational Statistics & Data Analysis**, Elsevier, v. 52, n. 3, p. 1500–1515, 2008. Citation on page 104.

NEWSON, J. J.; THIAGARAJAN, T. C. Eeg frequency bands in psychiatric disorders: a review of resting state studies. **Frontiers in human neuroscience**, Frontiers, v. 12, p. 521, 2018. Citation on page 126.

NITSCHE, M. A.; LIEBETANZ, D.; ANTAL, A.; LANG, N.; TERGAU, F.; PAULUS, W. Modulation of cortical excitability by weak direct current stimulation–technical, safety and functional aspects. In: **Supplements to Clinical neurophysiology**. [S.l.]: Elsevier, 2003. v. 56, p. 255–276. Citations on pages 40 and 118.

NITSCHE, M. A.; PAULUS, W. Excitability changes induced in the human motor cortex by weak transcranial direct current stimulation. **The Journal of physiology**, Wiley Online Library, v. 527, n. 3, p. 633–639, 2000. Citation on page 39.

NOIRHOMME-FRAITURE, M.; BRITO, P. Far beyond the classical data models: symbolic data analysis. **Statistical Analysis and Data Mining: the ASA Data Science Journal**, Wiley Online Library, v. 4, n. 2, p. 157–170, 2011. Citation on page 99.

OCTAVE Forge SourceForge Project. 2007. Available: <https://octave.sourceforge.io/>. Accessed: 10/05/2019. Citation on page 126.

OLCAY, A. H. Mean residual life function for certain types of non-monotonic ageing. **Communications in statistics. Stochastic models**, Taylor & Francis, v. 11, n. 1, p. 219–225, 1995. Citation on page 162.

OMBAO, H.; HO, M.-h. R. Time-dependent frequency domain principal components analysis of multichannel non-stationary signals. **Computational statistics & data analysis**, Elsevier, v. 50, n. 9, p. 2339–2360, 2006. Citation on page 127.

OZAKI, T. **Time series modeling of neuroscience data**. [S.l.]: CRC Press, 2012. Citation on page 78.

PAAKKI, J.-J.; RAHKO, J.; LONG, X.; MOILANEN, I.; TERVONEN, O.; NIKKINEN, J.; STARCK, T.; REMES, J.; HURTIG, T.; HAAPSAMO, H. *et al.* Alterations in regional homogeneity of resting-state brain activity in autism spectrum disorders. **Brain research**, Elsevier, v. 1321, p. 169–179, 2010. Citations on pages 31, 55, 72, and 112.

PARENT, A. Giovanni aldini: from animal electricity to human brain stimulation. **Canadian Journal of Neurological Sciences**, Cambridge University Press, v. 31, n. 4, p. 576–584, 2004. Citation on page 39.

PARKS, T. W.; BURRUS, C. S. **Digital filter design**. [S.l.]: Wiley-Interscience, 1987. Citation on page 126.

PAVLOPOULOS, S. A.; DELOPOULOS, A. N. Designing and implementing the transition to a fully digital hospital. **IEEE Transactions on information technology in biomedicine**, IEEE, v. 3, n. 1, p. 6–19, 1999. Citations on pages 73 and 113.

PEARL, J. **Causality**. [S.l.]: Cambridge university press, 2009. Citation on page 78.

____. **Probabilistic reasoning in intelligent systems: networks of plausible inference**. [S.l.]: Elsevier, 2014. Citation on page 116.

PERDONÁ, G. C.; LOUZADA-NETO, F. A general hazard model for lifetime data in the presence of cure rate. **Journal of Applied Statistics**, Taylor & Francis, v. 38, n. 7, p. 1395–1405, 2011. Citation on page 179.

PÉRENNOU, D. Postural disorders and spatial neglect in stroke patients: a strong association. **Restorative neurology and neuroscience**, IOS Press, v. 24, n. 4-6, p. 319–334, 2006. Citations on pages 38, 50, and 57.

PÉREZ-CRUZ, F. Kullback-leibler divergence estimation of continuous distributions. In: IEEE. **Information Theory, 2008. ISIT 2008. IEEE International Symposium on**. [S.l.], 2008. p. 1666–1670. Citation on page 46.

PETRIS, G.; PETRONE, S.; CAMPAGNOLI, P. Dynamic linear models. In: **Dynamic Linear Models with R**. [S.l.]: Springer, 2009. p. 31–84. Citations on pages 62, 82, 83, 104, and 121.

PIMENTEL, B. A.; SOUZA, R. M. de. A weighted multivariate fuzzy c-means method in interval-valued scientific production data. **Expert Systems with Applications**, Elsevier, v. 41, n. 7, p. 3223–3236, 2014. Citations on pages 98 and 100.

PINCUS, S. M. Approximate entropy as a measure of system complexity. **Proceedings of the National Academy of Sciences**, National Acad Sciences, v. 88, n. 6, p. 2297–2301, 1991. Citations on pages 36, 42, 45, 83, and 84.

PINCUS, S. M.; GLADSTONE, I. M.; EHRENKRANZ, R. A. A regularity statistic for medical data analysis. **Journal of clinical monitoring**, Springer, v. 7, n. 4, p. 335–345, 1991. Citations on pages 36, 37, and 48.

PLEWNIA, C.; LOTZE, M.; GERLOFF, C. Disinhibition of the contralateral motor cortex by low-frequency rtms. **Neuroreport**, LWW, v. 14, n. 4, p. 609–612, 2003. Citations on pages 40 and 118.

PRADO, R.; MOLINA, F.; HUERTA, G. Multivariate time series modeling and classification via hierarchical var mixtures. **Computational Statistics & Data Analysis**, Elsevier, v. 51, n. 3, p. 1445–1462, 2006. Citation on page 121.

PRADO, R.; WEST, M. **Time series: modeling, computation, and inference**. [S.l.]: CRC Press, 2010. Citations on pages 126 and 127.

PRADO, R.; WEST, M.; KRYSTAL, A. D. Multichannel electroencephalographic analyses via dynamic regression models with time-varying lag–lead structure. **Journal of the Royal Statistical Society: Series C (Applied Statistics)**, Wiley Online Library, v. 50, n. 1, p. 95–109, 2001. Citations on pages 31 and 54.

PRIGOGINE, I. The meaning of entropy. In: **Evolutionary Epistemology**. [S.l.]: Springer, 1987. p. 57–73. Citation on page 35.

PRIORI, A.; BERARDELLI, A.; RONA, S.; ACCORNERO, N.; MANFREDI, M. Polarization of the human motor cortex through the scalp. **Neuroreport**, LWW, v. 9, n. 10, p. 2257–2260, 1998. Citations on pages 39 and 118.

QUEEN, C. M.; SMITH, J. Q. Multiregression dynamic models. **Journal of the Royal Statistical Society: Series B (Methodological)**, Wiley Online Library, v. 55, n. 4, p. 849–870, 1993. Citations on pages 55, 58, 60, 82, and 133.

RAKOTOMAMONJY, A. Surveying and comparing simultaneous sparse approximation (or group-lasso) algorithms. **Signal processing**, Elsevier, v. 91, n. 7, p. 1505–1526, 2011. Citation on page 124.

RAMOS, P. L.; LOUZADA, F.; RAMOS, E. An efficient, closed-form map estimator for nakagami-m fading parameter. **IEEE Communications Letters**, IEEE, v. 20, n. 11, p. 2328–2331, 2016. Citations on pages 168 and 169.

READING, M.; BABYAR, S.; SANTOS-PONTELLI, T.; LEMOS, T.; EDWARDS, D. Parietal-insular-vestibular tdcs for treatment of lateropulsion following stroke. **Brain Stimulation**, Elsevier, v. 1, n. 10, p. e5, 2017. Citation on page 98.

RESTREPO, J. F.; SCHLOTTHAUER, G.; TORRES, M. E. Maximum approximate entropy and r threshold: A new approach for regularity changes detection. **Physica A: Statistical Mechanics and its Applications**, Elsevier, v. 409, p. 97–109, 2014. Citation on page 84.

REVFEIM, K. Approximation for the cumulative and inverse gamma distribution. **Statistica neerlandica**, Wiley Online Library, v. 45, n. 3, p. 327–331, 1991. Citation on page 158.

RICHMAN, J. S.; MOORMAN, J. R. Physiological time-series analysis using approximate entropy and sample entropy. **American Journal of Physiology-Heart and Circulatory Physiology**, American Physiological Society Bethesda, MD, v. 278, n. 6, p. H2039–H2049, 2000. Citation on page 36.

RODGER, J. A. Discovery of medical big data analytics: Improving the prediction of traumatic brain injury survival rates by data mining patient informatics processing software hybrid hadoop hive. **Informatics in Medicine Unlocked**, Elsevier, v. 1, p. 17–26, 2015. Citation on page 111.

RODRIGUES, F. A.; PERON, T. K. D.; JI, P.; KURTHS, J. The kuramoto model in complex networks. **Physics Reports**, Elsevier, v. 610, p. 1–98, 2016. Citations on pages 120 and 132.

ROSSI, S.; HALLETT, M.; ROSSINI, P. M.; PASCUAL-LEONE, A. Safety, ethical considerations, and application guidelines for the use of transcranial magnetic stimulation in clinical practice and research. **Clinical neurophysiology**, Elsevier, v. 120, n. 12, p. 2008–2039, 2009. Citation on page 38.

ROSSINI, P. M.; ROSSI, S. Transcranial magnetic stimulation diagnostic, therapeutic, and research potential. **Neurology**, AAN Enterprises, v. 68, n. 7, p. 484–488, 2007. Citation on page 38.

RUBIN, P.; HOLM, S.; FRIBERG, L.; VIDEBECH, P.; ANDERSEN, H. S.; BENDSEN, B. B.; STRØMSØ, N.; LARSEN, J. K.; LASSEN, N. A.; HEMMINGSEN, R. Altered modulation of prefrontal and subcortical brain activity in newly diagnosed schizophrenia and schizophreniform disorder: A regional cerebral blood flow study. **Archives of General Psychiatry**, American Medical Association, v. 48, n. 11, p. 987–995, 1991. Citations on pages 31, 55, 72, and 112.

SACHS, K.; PEREZ, O.; PE'ER, D.; LAUFFENBURGER, D. A.; NOLAN, G. P. Causal protein-signaling networks derived from multiparameter single-cell data. **Science**, American Association for the Advancement of Science, v. 308, n. 5721, p. 523–529, 2005. Citations on pages 60 and 61.

SANTOS-PONTELLI, T. E.; RIMOLI, B. P.; FAVORETTO, D. B.; MAZIN, S. C.; TRUONG, D. Q.; LEITE, J. P.; PONTES-NETO, O. M.; BABYAR, S. R.; REDING, M.; BIKSON, M. *et al.* Polarity-dependent misperception of subjective visual vertical during and after transcranial direct current stimulation (tdcs). **PloS one**, Public Library of Science, v. 11, n. 3, p. e0152331, 2016. Citations on pages 37, 57, and 98.

SANTOS, T. E.; EDWARDS, D. Non-invasive brain stimulation to treat disorders of human verticality. **Neurologie & Rehabilitation**, v. 25, p. 50–53, 2019. Citations on pages 72, 112, and 127.

SANTOS, T. E.; FAVORETTO, D. B.; TOOSTANI, I. G.; NASCIMENTO, D.; RIMOLI, B. P.; BERGONZONI, E.; LEMOS, T. W.; TRUONG, D. Q.; DELBEM, A. C.; MAKKIABADI, B.; MORAES, R.; LOUZADA, F.; BIKSON, M.; LEITE, J.; EDWARDS, D. Manipulation of human verticality using high-definition transcranial direct current stimulation. **Frontiers in neurology**, Frontiers, v. 9, p. 825, 2018. Citations on pages 16, 20, 31, 32, 36, 37, 45, 50, 54, 57, 66, 78, 90, 99, 101, 117, 118, 119, 120, 127, 131, 132, and 135.

SARKAR, S.; GOEL, N.; MATHUR, B. Performance investigation of nakagami-m distribution to derive flood hydrograph by genetic algorithm optimization approach. **Journal of Hydrologic Engineering**, American Society of Civil Engineers, v. 15, n. 8, p. 658–666, 2010. Citation on page 158.

SCANAGATTA, M.; CAMPOS, C. P. de; CORANI, G.; ZAFFALON, M. Learning bayesian networks with thousands of variables. In: **Advances in neural information processing systems**. [S.l.: s.n.], 2015. p. 1864–1872. Citation on page 60.

SCHEFFER-TEIXEIRA, R.; BELCHIOR, H.; LEAO, R. N.; RIBEIRO, S.; TORT, A. B. On high-frequency field oscillations (> 100 hz) and the spectral leakage of spiking activity. **Journal of Neuroscience**, Soc Neuroscience, v. 33, n. 4, p. 1535–1539, 2013. Citation on page 126.

SCHLÖGL, A.; SUPP, G. Analyzing event-related eeg data with multivariate autoregressive parameters. **Progress in brain research**, Elsevier, v. 159, p. 135–147, 2006. Citation on page 121.

SCHWARTZ, J.; GODWIN, R. T.; GILES, D. E. Improved maximum-likelihood estimation of the shape parameter in the nakagami distribution. **Journal of Statistical Computation and Simulation**, Taylor & Francis, v. 83, n. 3, p. 434–445, 2013. Citation on page 166.

SCUTARI, M. Learning bayesian networks with the bnlearn r package. **arXiv preprint arXiv:0908.3817**, 2009. Citation on page 80.

SHANKAR, P. M.; DUMANE, V.; REID, J. M.; GENIS, V.; FORSBERG, F.; PICCOLI, C. W.; GOLDBERG, B. B. Classification of ultrasonic b-mode images of breast masses using nakagami distribution. **IEEE transactions on ultrasonics, ferroelectrics, and frequency control**, IEEE, v. 48, n. 2, p. 569–580, 2001. Citation on page 158.

SHEKHAWAT, G. S.; SUNDRAM, F.; BIKSON, M.; TRUONG, D.; RIDDER, D. D.; STINEAR, C. M.; WELCH, D.; SEARCHFIELD, G. D. Intensity, duration, and location of high-definition transcranial direct current stimulation for tinnitus relief. **Neurorehabilitation and neural repair**, SAGE Publications Sage CA: Los Angeles, CA, v. 30, n. 4, p. 349–359, 2016. Citation on page 39.

SHEN, Y.; BAINGANA, B.; GIANNAKIS, G. B. Nonlinear structural vector autoregressive models for inferring effective brain network connectivity. **arXiv preprint arXiv:1610.06551**, 2016. Citations on pages 54 and 128.

SHINKAREVA, S. V.; OMBAO, H. C.; SUTTON, B. P.; MOHANTY, A.; MILLER, G. A. Classification of functional brain images with a spatio-temporal dissimilarity map. **Neuroimage**, Elsevier, v. 33, n. 1, p. 63–71, 2006. Citation on page 54.

SIEBNER, H.; PELLER, M.; WILLOCH, F.; MINOSHIMA, S.; BOECKER, H.; AUER, C.; DRZEZGA, A.; CONRAD, B.; BARTENSTEIN, P. Lasting cortical activation after repetitive tms of the motor cortex: a glucose metabolic study. **Neurology**, AAN Enterprises, v. 54, n. 4, p. 956–963, 2000. Citations on pages 40 and 118.

SIEBNER, H. R.; HARTWIGSEN, G.; KASSUBA, T.; ROTHWELL, J. C. How does transcranial magnetic stimulation modify neuronal activity in the brain? implications for studies of cognition. **cortex**, Elsevier, v. 45, n. 9, p. 1035–1042, 2009. Citation on page 39.

SIGGIRIDOU, E.; KOUTLIS, C.; TSIMPIRIS, A.; KUGIUMTZIS, D. Evaluation of granger causality measures for constructing networks from multivariate time series. **Entropy**, Multidisciplinary Digital Publishing Institute, v. 21, n. 11, p. 1080, 2019. Citation on page 79.

SILVA, A. D.; LECHEVALLIER, Y.; CARVALHO, F. de; TROUSSE, B. Mining web usage data for discovering navigation clusters. In: IEEE. **11th IEEE Symposium on Computers and Communications (ISCC'06)**. [S.l.], 2006. p. 910–915. Citation on page 100.

SIMS, C. A. Money, income, and causality. **The American economic review**, JSTOR, v. 62, n. 4, p. 540–552, 1972. Citation on page 77.

SOLO, V. State-space analysis of granger-geweke causality measures with application to fmri. **Neural computation**, MIT Press, v. 28, n. 5, p. 914–949, 2016. Citation on page 77.

SONG, K.-S. Globally convergent algorithms for estimating generalized gamma distributions in fast signal and image processing. **IEEE Transactions on Image Processing**, IEEE, v. 17, n. 8, p. 1233–1250, 2008. Citation on page 158.

SORIA-FRISCH, A.; RIERA, A.; DUNNE, S. Fusion operators for multi-modal biometric authentication based on physiological signals. In: IEEE. **Fuzzy Systems (FUZZ), 2010 IEEE International Conference on**. [S.l.], 2010. p. 1–7. Citations on pages 73 and 113.

SOUZA, L. C.; SOUZA, R. M.; AMARAL, G. J.; FILHO, T. M. S. A parametrized approach for linear regression of interval data. **Knowledge-Based Systems**, v. 131, p. 149 – 159, 2017. ISSN 0950-7051. Citation on page 100.

STAGG, C. J.; BEST, J. G.; STEPHENSON, M. C.; O'SHEA, J.; WYLEZINSKA, M.; KINCSES, Z. T.; MORRIS, P. G.; MATTHEWS, P. M.; JOHANSEN-BERG, H. Polarity-sensitive modulation of cortical neurotransmitters by transcranial stimulation. **Journal of Neuroscience**, Soc Neuroscience, v. 29, n. 16, p. 5202–5206, 2009. Citation on page 40.

SU, L.; WANG, L.; SHEN, H.; FENG, G.; HU, D. Discriminative analysis of non-linear brain connectivity in schizophrenia: an fmri study. **Frontiers in human neuroscience**, Frontiers, v. 7, p. 702, 2013. Citation on page 126.

TEPLAN, M. *et al.* Fundamentals of eeg measurement. **Measurement science review**, v. 2, n. 2, p. 1–11, 2002. Citation on page 99.

TIBSHIRANI, R.; BIEN, J.; FRIEDMAN, J.; HASTIE, T.; SIMON, N.; TAYLOR, J.; TIBSHIRANI, R. J. Strong rules for discarding predictors in lasso-type problems. **Journal of the Royal Statistical Society: Series B (Statistical Methodology)**, Wiley Online Library, v. 74, n. 2, p. 245–266, 2012. Citation on page 122.

TSUI, P.; HUANG, C.; WANG, S. Use of nakagami distribution and logarithmic compression in ultrasonic tissue characterization. **Journal of Medical and Biological Engineering**, WALTER H CHANG, v. 26, n. 2, p. 69, 2006. Citation on page 158.

VENUGOPAL, D.; GOGATE, V. On lifting the gibbs sampling algorithm. In: **Advances in Neural Information Processing Systems**. [S.l.: s.n.], 2012. p. 1655–1663. Citation on page 107.

WANG, H.; GUAN, R.; WU, J. Linear regression of interval-valued data based on complete information in hypercubes. **Journal of Systems Science and Systems Engineering**, v. 21, n. 4, p. 422 – 442, 2012. Citation on page 100.

WANG, N.; SONG, X.; CHENG, J. Generalized method of moments estimation of the nakagami-m fading parameter. **IEEE Transactions on Wireless Communications**, IEEE, v. 11, n. 9, p. 3316–3325, 2012. Citation on page 158.

WERMUTH, N.; LAURITZEN, S. L. On substantive research hypotheses, conditional independence graphs and graphical chain models. **Journal of the Royal Statistical Society: Series B (Methodological)**, Wiley Online Library, v. 52, n. 1, p. 21–50, 1990. Citation on page 125.

WEST, M.; HARRISON, J. **Bayesian forecasting and dynamic models**. [S.l.]: Springer Science & Business Media, 1989. Citations on pages 54, 62, 82, 83, 104, 120, and 121.

WEST, M.; HARRISON, P. J.; MIGON, H. S. Dynamic generalized linear models and bayesian forecasting. **Journal of the American Statistical Association**, Taylor & Francis Group, v. 80, n. 389, p. 73–83, 1985. Citation on page 120.

WHITTAKER, J. **Graphical models in applied multivariate statistics**. [S.l.]: Wiley Publishing, 2009. Citation on page 78.

WHITTLE, P. Estimation and information in stationary time series. **Arkiv för matematik**, Springer, v. 2, n. 5, p. 423–434, 1953. Citation on page 59.

____. **Some recent contributions to the theory of stationary processes**. [S.l.: s.n.], 1954. Citation on page 59.

WIENER, N. **Modern mathematics for the engineer, chapter The theory of prediction**. [S.l.]: MacGrawHill, 1956. Citation on page 78.

WINDHORST, U.; JOHANSSON, H. **Modern techniques in neuroscience research**. [S.l.]: Springer Science & Business Media, 2012. Citations on pages 55, 56, and 57.

WINTER, D. A. Human balance and posture control during ding and walking. **Gait & posture**, Elsevier, v. 3, n. 4, p. 193–214, 1995. Citations on pages 38, 57, 117, and 118.

WIPF, D.; NAGARAJAN, S. **Iterative Reweighted 1 and 2 Methods for Finding Sparse Solutions. UC San Francisco**. [S.l.], 2008. Citation on page 124.

WOJCIK, G. M.; MASIAK, J.; KAWIAK, A.; KWASNIEWICZ, L.; SCHNEIDER, P.; POLAK, N.; GAJOS-BALINSKA, A. Mapping the human brain in frequency band analysis of brain cortex electroencephalographic activity for selected psychiatric disorders. **Frontiers in neuroinformatics**, Frontiers Media SA, v. 12, 2018. Citation on page 126.

YENTES, J. M.; DENTON, W.; MCCAMLEY, J.; RAFFALT, P. C.; SCHMID, K. K. Effect of parameter selection on entropy calculation for long walking trials. **Gait & posture**, Elsevier, v. 60, p. 128–134, 2018. Citation on page 36.

YI, B.-K.; FALOUTSOS, C. Fast time sequence indexing for arbitrary lp norms. In: VLDB. [S.l.], 2000. Citation on page 69.

ZANABRIA, G. G.; SILVEIRA, J. A.; POCO, J.; PAIVA, A.; NERY, M. B.; SILVA, C. T.; ABREU, S. F. A. de; NONATO, L. G. Crimanalyzer: Understanding crime patterns in são paulo. **IEEE transactions on visualization and computer graphics**, IEEE, 2019. Citation on page 76.

ZEEMERING, S. **Sparse estimation: applications in atrial fibrillation**. Phd Thesis (PhD Thesis) — Maastricht University, 2015. Citation on page 122.

ZHANG, W.; CHIEN, J.; YONG, J.; KUANG, R. Network-based machine learning and graph theory algorithms for precision oncology. **NPJ precision oncology**, Nature Publishing Group, v. 1, n. 1, p. 1–15, 2017. Citation on page 77.

ZHAO, X.; ZHOU, X. Modeling gap times between recurrent events by marginal rate function. **Computational Statistics & Data Analysis**, Elsevier, v. 56, n. 2, p. 370–383, 2012. Citations on pages 133 and 179.

ZHOU, J.; HAO, Y.; WANG, Y.; JOR'DAN, A.; PASCUAL-LEONE, A.; ZHANG, J.; FANG, J.; MANOR, B. Transcranial direct current stimulation reduces the cost of performing a cognitive task on gait and postural control. **European Journal of Neuroscience**, Wiley Online Library, v. 39, n. 8, p. 1343–1348, 2014. Citations on pages 31, 38, and 57.

ZOU, C.; FENG, J. Granger causality vs. dynamic bayesian network inference: a comparative study. **BMC bioinformatics**, BioMed Central, v. 10, n. 1, p. 122, 2009. Citation on page 79.

ZUCCOLOTTO, P. Principal components of sample estimates: an approach through symbolic data analysis. **Statistical Methods and Applications**, Springer, v. 16, n. 2, p. 173–192, 2007. Citation on page 100.

GLOSSARY

Bayesian Inference: is a methodology which incorporates prior information (the specialist' expertise) with the empirical information (dataset) using Bayes' theorem..

Biosignals: is any monitored signal derived from a living been. Express as electrical, or non-electrical, signals in a given spaced time..

Complex Network: any non-trivial topological which connects events as edges through links is a graph (network)..

Dynamic Models: represents a class of models which behaves conditional the time-variant parameters giving flexibility to the model, incorporating non-linearity from the system. In contrast, static (or steady-state) model calculates the system in equilibrium, and thus is time-invariant..

Entropy: describes the amount of information which derivate from the system, considering all the moments which generates a given process. It can be thought as the accumulated energy from the system, defined by the second law of thermodynamics states..

APPENDIX

A

THE INVERSE NAKAGAMI-M DISTRIBUTION: A NOVEL APPROACH IN RELIABILITY

This chapter corresponds to a manuscript published at *IEEE Transaction in Reliability* journal, in which proposed the inverse Nakagami-m (INK) distribution. This work had as co-authors: Pedro Ramos (ICMC-USP, Brazil) and Francisco Louzada (ICMC-USP, Brazil).

Abstract

In the paper, the inverse Nakagami-m (INK) distribution is proposed. This distribution is the reciprocal of the Nakagami distribution that plays an important role in the general area of communications engineering and reliability system. The proposed model is useful to describe data that have a relatively high initial failure rate. An account of mathematical properties is presented such as the r-th moment, mean, variance, r-th central moment, survival properties and Shannon's entropy. The maximum likelihood estimators are explored under complete and censoring, but a bias correction was applied with the order $O(n^{-2})$ for obtaining nearly unbiased performance. An efficient closed-form maximum a posteriori estimator was also proposed. A simulation study compares the performance of the estimators with clear advantage for the closed-form maximum a posteriori one. We illustrate the INK distribution fitting on an aircraft survivor scope and a sugarcane harvester associated with the failure of an item given its repair, analyzing the components associated with a high failure rate after a short repair time.

Bias correction, censored data, inverse Nakagami-m distribution, maximum likelihood estimators, Nakagami-m distribution, Reliability.

Introduction

The Nakagami distribution (NAKAGAMI, 1960) plays an important role in the general area of communications engineering, such as communication range test (WANG; SONG; CHENG, 2012). This distribution has also been applied successfully in many areas such as medical image processing (SHANKAR *et al.*, 2001; TSUI; HUANG; WANG, 2006), hydrologic engineering (SARKAR; GOEL; MATHUR, 2010) and seismological analysis (NAKAHARA; CARCOLÉ, 2010). Considering X a random variable with a Nakagami-m (NK) distribution, its probability density function (PDF) is given by

$$f(x|\mu,\Omega) = \frac{2}{\Gamma(\mu)}\left(\frac{\mu}{\Omega}\right)^{\mu} x^{2\mu-1}\exp\left(-\frac{\mu x^2}{\Omega}\right) \tag{A.1}$$

for all $t > 0$, where $\mu \geq 0.5$ and $\Omega > 0$. The NK distribution is related to the gamma distribution, if $Y \sim f\Gamma(a,b)$, then $T = \sqrt{Y}$ has a NK distribution with $\mu = a$ and $\Omega = ab$. Therefore, the μ parameter can also take values on $0 < \mu < 0.5$. In this case, its hazard rate function exhibits bathtub shape.

The study of inverse distributions has provided a better comprehension of standard distributions and contributed to adding more flexibility for fitting data. For instance, if X follows a standard normal distribution then the inverse distribution of X is bimodal (JOHNSON; KOTZ; BALAKRISHNAN, 1970). Some well-known inverse distributions are the Inverse Weibull (JOHNSON; KOTZ; BALAKRISHNAN, 1970), Inverse Gamma (REVFEIM, 1991) and the inverse t distribution, to list a few.

In the paper, a new inverse distribution is proposed, named as inverse Nakagami-m (INK) distribution. The mathematical properties associated with the new INK distribution are presented, such as the r-th moment, mean, variance, r-th central moment and Shannon's entropy. Thus, the reliability properties of the INK distribution are studied in details, proving the hazard model (mean residual life) function as a unimodal (bathtub) shape. Parameter estimation is based on maximum likelihood approach. Although the maximum likelihood estimator (MLE) of Ω is an unbiased estimator, we observed the MLE of μ contains a positive bias. Therefore, we discussed a MLE bias correction based on Cox and Snell (COX; SNELL, 1968) approach. Moreover, an efficient closed-form estimator are important for practical purposes, since they can be applied to compute real time estimators in embedded technology (SONG, 2008). Besides, we considered the MLEs in the presence of randomly censored data, since it has received special attention in medical experiments and industrial lifetime testing. Recently discussions of new probability distributions can be see in (ALMALKI; NADARAJAH, 2014; BALAKRISHNAN *et al.*, 2015; BALAKRISHNAN; HAIDARI; MASOUMIFARD, 2015).

The proposed INK distribution is illustrated on a dataset related to the failure time of a given components of aircrafts and a sugarcane harvester. The variables in analysis are associated with the failure of items given its repair proving its efficiency in describing the components associated with a high failure rate after a short repair time. Hence, it can describe

well the quality of a given maintenance performed. From the practical point of view, in the first scenario, our model shows to be useful in different studies aimed at describing the lifespan of different internal cabin mechanical devices, improving consumer satisfaction and increasing the company respective profits. In the second, the improvement this heavy machine could optimize the production of a given factory.

The paper is organized as follows. Section 2 introduces the properties of the proposed distribution. Section 3 presents the inferential procedure based on MLEs for complete and censored data, as well as the bias correction. Section 4 discusses the results of a simulation studies to verify the performance of the MLEs. Section 5 illustrates the relevance of our proposed methodology in a real lifetime data. Section 6 summarizes the present study.

Inverse Nakagami-m

Let T be a random variable with an inverse Nakagami-m (INK) distribution, its probability density function (PDF) is given by

$$f(t|\mu,\Omega) = \frac{2}{\Gamma(\mu)}\left(\frac{\mu}{\Omega}\right)^{\mu} t^{-2\mu-1}\exp\left(-\frac{\mu}{\Omega t^2}\right) \tag{A.2}$$

for all $t > 0$, where $\mu > 0$ and $\Omega > 0$. This new distribution could also be named as Complementary Nakagami or Reciprocal Nakagami.

Important probability distributions can be obtained from the INK distribution such as the inverse Rayleigh distribution ($\mu = 1$), the inverse half-normal distribution ($\mu = 0.5$) and the inverse chi distribution ($\Omega = 1, \mu = \nu/2,$ and $\nu = 1,2,\ldots$). Moreover a new inverse distribution can obtained as special case, named, the inverse Hoyt distribution ($0 < \mu < 1$). The proposition bellow relates the INK with the Nakagami-m distribution.

Proposition 1. Let $T \sim fINK(\mu,\Omega)$ then $X = 1/T$ follows a Nakagami-m distribution.

Proof. Define the transformation $X = g(T) = \frac{1}{T}$ then the resulting transformation is

$$\begin{aligned} f_X(x) &= f_T\left(g^{-1}(x)\right)\left|\frac{d}{dx}g^{-1}(x)\right| \\ &= \frac{2}{\Gamma(\mu)}\left(\frac{\mu}{\Omega}\right)^{\mu} x^{2\mu+1}\exp\left(-\frac{\mu}{\Omega}x^2\right)\frac{1}{x^2} \\ &= \frac{2}{\Gamma(\mu)}\left(\frac{\mu}{\Omega}\right)^{\mu} x^{2\mu-1}\exp\left(-\frac{\mu}{\Omega}x^2\right). \end{aligned}$$

□

The cumulative distribution function (cdf) is given by

$$F(t|\Omega,\mu) = \frac{1}{\Gamma(\mu)}\Gamma\left(\mu,\frac{\mu}{\Omega t^2}\right), \tag{A.3}$$

where $\Gamma(y,x) = \int_x^\infty w^{y-1}e^{-w}dw$ is the upper incomplete gamma function.

The quantile function is obtained by inverting the cdf, i.e., solving

$$\frac{1}{\Gamma(\mu)}\Gamma\left(\mu, \frac{\mu}{\Omega t_p^2}\right) - p = 0, \tag{A.4}$$

similar to gamma distribution the inverse of incomplete gamma function does not have closed-form expression. The computation of the incomplete gamma and its inverse have been discussed earlier (DIDONATO; JR, 1986) and are implemented in many software (R, Matlab, SAS, Maple, among others). The quantile function is usually used to generated random values. However, the values of the INK distribution can be easily generated using its relation to the inversion of gamma distribution. As follow the algorithm step:

1. Generate $X_i \sim f\Gamma(\mu, \mu/\Omega)$, $i = 1,\ldots,n$
2. Then take $T_i = \frac{1}{\sqrt{X_i}}$, $i = 1,\ldots,n$

Proposition 2. For the random variable T with $fINK$ distribution, the r-th moment is given by

$$\mu_r = E[T^r] = \frac{1}{\Gamma(\mu)}\left(\frac{\mu}{\Omega}\right)^{\frac{r}{2}}\Gamma\left(\mu - \frac{r}{2}\right) \quad \text{for} \quad \mu > \frac{r}{2}. \tag{A.5}$$

Proof. We have

$$\begin{aligned}\mu_r = E[T^r] &= \int_0^\infty t^r \frac{2}{\Gamma(\mu)}\left(\frac{\mu}{\Omega}\right)^\mu t^{-2\mu-1}\exp\left(-\frac{\mu}{\Omega t^2}\right)dt \\ &= \frac{2}{\Gamma(\mu)}\left(\frac{\mu}{\Omega}\right)^\mu \int_0^\infty t^{2\left(\frac{r}{2}-\mu-\frac{1}{2}\right)}\exp\left(-\frac{\mu}{\Omega t^2}\right)dt.\end{aligned}$$

Let $x = t^2$ and $dx = 2tdt$, then

$$\begin{aligned}\mu_r = E[T^r] &= \frac{1}{\Gamma(\mu)}\left(\frac{\mu}{\Omega}\right)^\mu \int_0^\infty x^{\left(\frac{r}{2}-\mu-\frac{1}{2}\right)}\exp\left(-\frac{\mu}{\Omega x}\right)dx \\ &= \frac{1}{\Gamma(\mu)}\left(\frac{\mu}{\Omega}\right)^{\frac{r}{2}}\Gamma\left(\mu - \frac{r}{2}\right) \quad \text{for} \quad \mu > \frac{r}{2}.\end{aligned}$$

□

Proposition 3. The r-th central moment for the random variable T is given by

$$\begin{aligned}M_r =& E[T-\mu]^r = \sum_{i=0}^r \binom{r}{i}(-\mu)^{r-i}E[T^i] \\ =& \sum_{i=0}^r \binom{r}{i}\left(-\frac{1}{\Gamma(\mu)}\left(\frac{\mu}{\Omega}\right)^{\frac{1}{2}}\Gamma\left(\mu-\frac{1}{2}\right)\right)^{r-i} \times \\ &\times \left(\frac{1}{\Gamma(\mu)}\left(\frac{\mu}{\Omega}\right)^{\frac{i}{2}}\Gamma\left(\mu-\frac{i}{2}\right)\right)\end{aligned}$$

for $\mu > \frac{r}{2}$.

Proof. The result follows directly from the Proposition 2. □

From Proposition 2, the mean and variance of (A.2) are respectively given by

$$E(T) = \frac{1}{\Gamma(\mu)} \left(\frac{\mu}{\Omega}\right)^{\frac{1}{2}} \Gamma\left(\mu - \frac{1}{2}\right), \quad \text{for} \quad \mu > \frac{1}{2} \tag{A.6}$$

and

$$Var(T) = \Omega \left(1 - \left(\frac{\Gamma(\mu - 1/2)}{\Gamma(\mu)}\right)^2\right) \quad \text{for} \quad \mu > 1. \tag{A.7}$$

Reliability Properties

The reliability function that represents the probability of an observation does not fail until t is

$$R(t|\Omega,\mu) = \frac{1}{\Gamma(\mu)} \gamma\left(\mu, \frac{\mu}{\Omega t^2}\right), \tag{A.8}$$

where $\gamma(y,x) = \int_0^x w^{y-1} e^{-w} dw$ is the lower incomplete gamma function. The hazard rate function is obtained through $h(t) = f(t)/S(t)$. For the INK distribution the hazard function is given by

$$h(t|\phi,\lambda) = 2\left(\frac{\mu}{\Omega}\right)^{\mu} t^{-2\mu-1} \exp\left(-\frac{\mu}{\Omega t^2}\right) \gamma\left(\mu, \frac{\mu}{\Omega t^2}\right)^{-1}. \tag{A.9}$$

The behaviors of the hazard function (A.9) when $t \to 0$ and $t \to \infty$ are $h(0) = 0$ and $h(\infty) = 0$, respectively. Presented by Glaser (GLASER, 1980), consider the following lemma in order to obtain the shapes of the hazard function.

Lemma 1. Glaser (GLASER, 1980) Let T be a non-negative continuous random variable with twice differentiable p.d.f. f(t). Then if $\eta(t) = -\frac{d}{dt} \log f(t)$ has a unimodal shape, then $h(t)$ has a unimodal shape.

Theorem 1. The hazard rate function $h(t)$ of the INK distribution is unimodal, for all $\mu > 0$ and $\Omega > 0$.

Proof. Firstly

$$\eta(t) = -\frac{d}{dt} \log f(t) = \frac{(2\mu+1)\Omega t^2 - 2\mu}{\Omega t^3} \quad \text{and}$$

$$\eta'(t) = \frac{6\mu}{\Omega t^4} - \frac{2\mu+1}{t^2}.$$

Following Lemma 1, for all $\mu > 0$ and $\Omega > 0$, $\eta'(t) = 0$ implies that $\eta(t)$ is unimodal shaped with a global maximum at $t^* = \sqrt{\frac{6\mu}{(2\mu+1)\Omega}}$. Therefore, $h(t)$ is also unimodal shaped. □

Figure 46 presents different shapes for the density and hazard functions for the INK distribution considering different values of μ and Ω.

The mean residual life (MRL) represents the expected additional lifetime given that a component has survived until time t.

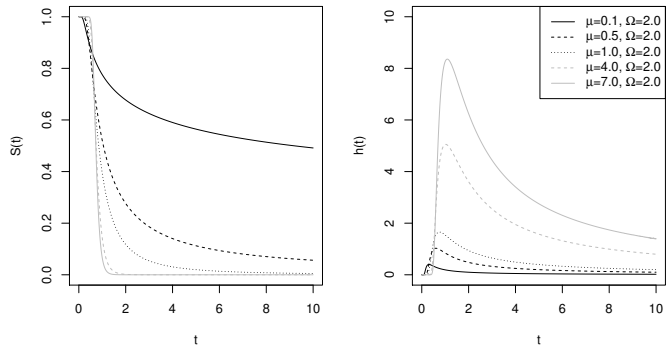

Figure 46 – Left panel: probability density function of the INK distribution. Right panel: hazard function of the INK distribution.

Proposition 4. The mean residual life function $r(t|\mu,\Omega)$ of the NK distribution is given by

$$\begin{aligned} r(t|\mu,\Omega) &= \frac{1}{S(t|\mu,\Omega)}\int_t^\infty yf(y|\lambda,\phi)dy - t \\ &= \sqrt{\frac{\mu}{\Omega}}\left(\frac{\gamma\left(\mu-\frac{1}{2},\frac{\mu}{\Omega t^2}\right)}{\gamma\left(\mu,\frac{\mu}{\Omega t^2}\right)}\right) - t. \end{aligned} \tag{A.10}$$

for $\mu > 1/2$.

The behaviors of the MRL function (A.10) when $t \to 0$ and $t \to \infty$ are, respectively

$$r(0) = \sqrt{\frac{\mu}{\Omega}}\left(\frac{\Gamma\left(\mu-\frac{1}{2}\right)}{\Gamma(\mu)}\right) \quad \text{and} \quad r(\infty) = \frac{1}{h(\infty)} = \infty.$$

The following Lemma is useful to obtain the shapes of the MRL function.

Lemma 2. Let T be non-negative continuous lifetime random variable with hazard function $h(t)$ and mean residual life function $r(t)$. If h(t) has unimodal shape and $f(0)r(0) > 1(\leq 1)$, then $r(t)$ has bathtub shape (see Gupta and Akman (OLCAY, 1995)).

Theorem 2. The mean residual life function $r(t)$ of the INK distribution is bathtub shaped for $\mu > 0.5$ and $\Omega > 0$.

Proof. For $\mu > 0.5$ and $\Omega > 0$, $h(t)$ has a bathtub shape and $f(0)r(0) > 1$. Therefore, based on Lemma 2, $r(t)$ has a unimodal shape. □

Figure 47 presents examples for the shapes of the mean residual life function for different values of μ and Ω.

Entropy

In information theory, entropy has played a central role as a measure of the uncertainty associated with a random variable. Shannon's entropy is one of the most important metrics

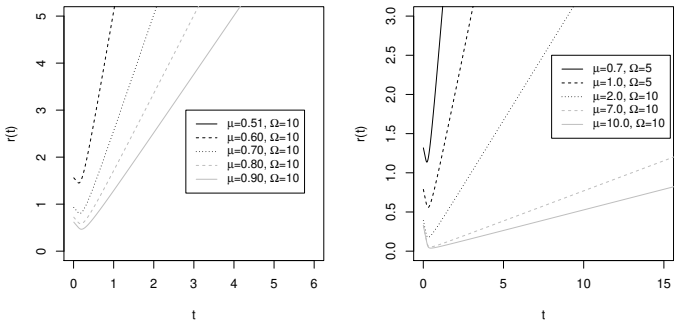

Figure 47 – Mean residual life function shapes for INK distribution considering different values of μ and Ω.

in information theory. The Shannon's entropy from INK distribution is given by solving the following equation

$$H(\mu,\Omega) = \int_0^{\infty} \log\left[\frac{2}{\Gamma(\mu)}\left(\frac{\mu}{\Omega}\right)^{\mu} t^{-2\mu-1}\exp\left(\frac{\mu}{\Omega}t^{-2}\right)\right] \times f\left(t|(\mu,\Omega)\,dt.\right. \tag{A.11}$$

Proposition 5. A random variable T with $fIWL$ distribution, has Shannon's entropy given by

$$H_S(\phi,\lambda) = \log\left(\frac{2}{\Gamma(\mu)}\right) + \mu\psi(\mu) + \frac{1}{2}\log\left(\frac{\mu}{\Omega}\right) + \frac{\psi(\mu)}{2} - \mu$$

Proof. From the equation (A.11) we have

$$H_S(\phi,\lambda) = \log\left(\frac{2}{\Gamma(\mu)}\right) + \mu\log\left(\frac{\mu}{\Omega}\right) - (2\mu+1)E\left[\log(X)\right] - \frac{\mu}{\Omega}E\left[t_i^{-2}\right].$$

Since

$$E[\log(T)] = \frac{1}{2}\left(\log\left(\frac{\mu}{\Omega}\right) - \psi(\mu)\right) \text{ and } E\left[T^{-2}\right] = \Omega$$

Then

$$H_S(\phi,\lambda) = \log\left(\frac{2}{\Gamma(\mu)}\right) + \mu\psi(\mu) + \frac{1}{2}\log\left(\frac{\mu}{\Omega}\right) + \frac{\psi(\mu)}{2} - \mu.$$

□

Inferential Procedures

In this section, we explore the maximum likelihood estimator properties for the μ and Ω, then analyzed the correction of the bias, later present some closed-form estimators and hereafter the case for censored data.

Maximum Likelihood Estimation

The maximum likelihood method, among the classical methods of statistical inference, is well preferred considering it presents better asymptotic properties. The likelihood function maximizes the estimators through the maximum likelihood method. Let $T_1,\ldots,T_n$ be a random sample such that $T \sim fNK(\Omega,\mu)$. In this case, the likelihood function from (A.2) is given by

$$\begin{aligned} L(\Omega,\mu;t) =& \frac{2^n}{\Gamma(\mu)^n}\left(\frac{\mu}{\Omega}\right)^{n\mu}\left\{\prod_{i=1}^{n} t_i^{-2\mu-1}\right\}\times \\ & \times \exp\left(-\frac{\mu}{\Omega}\sum_{i=1}^{n} t_i^{-2}\right). \end{aligned} \tag{A.12}$$

The log-likelihood function is

$$\begin{aligned} \ell(\Omega,\mu;t) =& 2\log(n) - n\log\left(\Gamma(\mu)\right) + n\mu\log\left(\frac{\mu}{\Omega}\right) \\ & - (2\mu+1)\sum_{i=1}^{n}\log(t_i) - \frac{\mu}{\Omega}\sum_{i=1}^{n} t_i^{-2}. \end{aligned} \tag{A.13}$$

From the expressions $\frac{\partial}{\partial\Omega}\ell(\Omega,\mu;t)=0$, $\frac{\partial}{\partial\mu}\ell(\Omega,\mu;t)=0$, the likelihood equations is given as

$$\begin{aligned} & n\left(1+\log\left(\mu\right)\right) - n\psi(\mu) - n\log(\Omega) \\ & -2\sum_{i=1}^{n}\log(t_i) - \frac{1}{\Omega}\sum_{i=1}^{n} t_i^{-2} = 0 \end{aligned} \tag{A.14}$$

$$-\frac{n\mu}{\Omega} + \frac{\mu}{\Omega^2}\sum_{i=1}^{n} t_i^{-2} = 0 \tag{A.15}$$

where $\psi(k) = \frac{\partial}{\partial k}\log\Gamma(k) = \frac{\Gamma'(k)}{\Gamma(k)}$ is the digamma function. The MLE for $\hat{\Omega}$ is given by

$$\hat{\Omega} = \frac{1}{n}\sum_{i=1}^{n} t_i^{-2}. \tag{A.16}$$

Note that, substituting $\hat{\Omega}_{MLE}$ in (A.14) the estimate for $\hat{\mu}_{MLE}$ can be obtained solving,

$$\begin{aligned} \xi(\mu;t) =& \log(\mu) - \psi(\mu) - \log\left(\frac{1}{n}\sum_{i=1}^{n} t_i^{-2}\right) \\ & + \frac{1}{n}\sum_{i=1}^{n}\log(t_i^{-2}) = 0. \end{aligned} \tag{A.17}$$

Theorem 3. Let $\hat{\Omega} = \frac{1}{n}\sum_{i=1}^{n} t_i^{-2}$ be the MLE of Ω. Then, the root of $\xi(\mu;t)=0$, $\hat{\mu}$, is unique.

Proof. Since $\log(\mu)-\psi(\mu)$ is strictly monotone and continuous with range in $(-\infty,0)$. Then, for $\mu>0$ there is a unique solution for

$$\log(\mu) - \psi(\mu) = \log\left(\frac{1}{n}\sum_{i=1}^{n} t_i^{-2}\right) - \frac{1}{n}\sum_{i=1}^{n}\log(t_i^{-2})$$

which completes the proof. □

Following (MIGON; GAMERMAN; LOUZADA, 2014), the MLE estimates are asymptotically normal distributed with a joint bivariate normal distribution given by

$$(\hat{\mu}_{MLE}, \hat{\Omega}_{MLE}) \sim N_2[(\mu,\Omega), I^{-1}(\mu,\Omega))] \text{ for } n \to \infty,$$

where $I(\mu,\Omega)$ is the Fisher information matrix given by

$$I(\mu,\Omega) = n \begin{bmatrix} \dfrac{(\mu\psi'(\mu)-1)}{\mu} & 0 \\ 0 & \dfrac{\mu}{\Omega^2} \end{bmatrix} \tag{A.18}$$

and $\psi'(k) = \frac{\partial}{\partial k}\psi(k)$ is the trigamma function. Importantly, this model has orthogonal parameters (ϕ,λ) in the sense discussed by Cox and Reid (COX; REID, 1987), i.e., $I_{\phi,\lambda}(\phi,\lambda) = 0$. Therefore, the covariance between ϕ and λ is equal to zero.

A1. Bias correction

Cox and Snell (COX; SNELL, 1968) showed that when the sample are independent (but not necessary identically distributed) the bias of θ_m, for $m,\ldots,p$ can be written as

$$\begin{aligned} Bias(\hat{\theta}_m) = &\sum_{i=1}^{p}\sum_{j=1}^{p}\sum_{k=1}^{p} s_{mi}(\theta)s_{jl}(\theta)\left(h_{ij,l}(\theta)+0.5h_{ijl}(\theta)\right) \\ &+O(n^{-2}) \end{aligned} \tag{A.19}$$

where s_{ij} is the (i,j)-th element of the variance-covariance matrix of $\hat{\theta}$,

$$h_{ijl}(\theta) = E\left(\frac{\partial^3 \log L}{\partial\theta_i\partial\theta_j\partial\theta_l}\right) \text{ and} \tag{A.20}$$

$$h_{ij,l}(\theta) = E\left(\frac{\partial^2 \log L}{\partial\theta_i\partial\theta_j}.\frac{\partial \log L}{\partial\theta_l}\right), \quad i,j,l = 1,\ldots,p. \tag{A.21}$$

Cordeiro and Klein (CORDEIRO; KLEIN, 1994) proved that even if the data are dependent on the expression (A.19) it can be re-written as

$$\begin{aligned} Bias(\hat{\theta}_m) = &\sum_{i=1}^{p} s_{mi}(\theta)\sum_{j=1}^{p}\sum_{k=1}^{p} s_{jl}(\theta)\left(h_{ij}^{(l)}(\theta)-0.5h_{ijl}(\theta)\right) \\ &+O(n^{-2}), \end{aligned} \tag{A.22}$$

where $h_{ij}^{(l)}(\theta) = \dfrac{\partial h_{ij}(\theta)}{\partial\theta_l}$, $i,j,l = 1,\ldots,p$. For the INK distribution the higher-order derivatives are given by

$$h_{111}(\theta) = h_{11}^{(1)}(\theta) = -\frac{n}{\mu^2} - n\psi''(\mu),$$

$$h_{122}(\theta) = h_{221}(\theta) = h_{212}(\theta) = h_{12}^{(2)}(\theta) = h_{22}^{(1)}(\theta) = -\frac{n}{\Omega^2},$$

$$h_{222}(\theta) = h_{22}^{(2)}(\theta) = 4n\frac{\mu}{\Omega^3} \quad \text{and}$$

$$h_{211}(\theta) = h_{112}(\theta) = h_{121}(\theta) = h_{12}^{(1)}(\theta) = h_{11}^{(2)}(\theta) = 0.$$

Since the MLE of Ω is unbiased. The correction approach is applied directly in the μ. After some algebraic manipulation we obtain the corrected MLE given by,

$$\hat{\mu}_{CMLE} = \hat{\mu} - \frac{\hat{\mu}\psi'(\hat{\mu}) - \hat{\mu}^2\psi''(\hat{\mu}) - 2}{2n\left(\hat{\mu}\psi'(\hat{\mu}) - 1\right)^2} \tag{A.23}$$

that is unbiased to $O(n^{-2})$.

It is important to point out that, due to the one-to-one transformation in the model, the higher-order derivatives are the same of the Nakagami-m distribution (SCHWARTZ; GODWIN; GILES, 2013).

A2. Censored Data

In reliability analysis, random censoring schemes have received special attention. Suppose that the ith individual has a lifetime T_i and a censoring time C_i, moreover the random censoring times C_is are independent of T_is and that their distribution does not depend on the parameters, then the data set is (t_i, δ_i), where $t_i = \min(T_i, C_i)$ and $\delta_i = I(T_i \leq C_i)$. This type of censoring has as special case the type I and II censoring mechanism. The likelihood function for θ is given by

$$L(\theta, t) = \prod_{i=1}^{n} f(t_i|\theta)^{\delta_i} S(t_i|\theta)^{1-\delta_i}.$$

Let $T_1, \cdots, T_n$ be a random sample of INK distribution, the likelihood function considering data with random censoring is given by

$$\begin{aligned} L(\mu, \Omega|t, \delta) = \frac{2^d}{\Gamma(\mu)^n}\left(\frac{\mu}{\Omega}\right)^{d\mu} \exp\left(-\sum_{i=1}^{n}\frac{\delta_i\mu}{\Omega t_i^2}\right) \times \\ \times \prod_{i=1}^{n}\left\{t_i^{-(2\mu+1)\delta_i}\gamma\left(\mu, \frac{\mu}{\Omega t_i^2}\right)^{1-\delta_i}\right\}. \end{aligned} \tag{A.24}$$

where $d = \sum_{i=1}^{n}\delta_i$. The logarithm of the likelihood function (A.24) is given by

$$\begin{aligned} l(\mu, \Omega|t, \delta) = d\mu\log\left(\frac{\mu}{\Omega}\right) - (2\mu+1)\sum_{i=1}^{n}\delta_i\log(t_i) - \sum_{i=1}^{n}\frac{\delta_i\mu}{\Omega t_i^2} \\ + \sum_{i=1}^{n}(1-\delta_i)\log\left(\gamma\left(\mu, \frac{\mu}{\Omega t_i^2}\right)\right) - n\log(\Gamma(\mu)). \end{aligned}$$

From $\partial l(\mu,\Omega|t,\delta)/\partial\mu = 0$ and $\partial l(\mu,\Omega|t,\delta)/\partial\Omega = 0$, the likelihood equations are given as follows

$$\begin{aligned} d\log\left(\frac{\mu}{\Omega}\right) + d - 2\sum_{i=1}^{n}\delta_i\log(t_i) + \sum_{i=1}^{n}(1-\delta_i)\Psi_1(\mu,\Omega t_i^2) \\ - n\psi(\mu) - \frac{1}{\Omega}\sum_{i=1}^{n}\frac{\delta_i}{t_i^2} = 0 \end{aligned} \tag{A.25}$$

$$\sum_{i=1}^{n}(1-\delta_i)\Psi_2(\mu,\Omega t_i^2) + \sum_{i=1}^{n}\frac{\delta_i\mu}{\Omega^2 t_i^2} - \frac{d\mu}{\Omega} = 0 \tag{A.26}$$

where

$$\Psi_1(a,b) = \frac{\partial}{\partial a}\log\gamma\left(a,\frac{a}{b}\right), \quad \Psi_2(a,b) = \frac{\partial}{\partial b}\log\gamma\left(a,\frac{a}{b}\right)$$

can be computed numerically. Numerical methods are required to find the solution of these non-linear equations.

The bias correction methodology can be extended to the censored data. Regardless the missing closed form expression, the Fisher information matrix related to the MLEs (A.28) can be considered as a bias correction as presented in A1. The approximated bias-corrected maximum likelihood estimates (ACMLE) are achieved as

$$\begin{pmatrix}\hat{\phi}_{ACMLE}\\ \hat{\lambda}_{ACMLE}\end{pmatrix} = \begin{pmatrix}\hat{\phi}_{MLE}\\ \hat{\lambda}_{MLE}\end{pmatrix} - \hat{K}^{-1}\hat{A}.vec(\hat{K}^{-1})$$

where $\hat{K} = K|_{\phi=\hat{\phi}_{MLE},\lambda=\hat{\lambda}_{MLE}}$, $\hat{A} = A|_{\phi=\hat{\phi}_{MLE},\lambda=\hat{\lambda}_{MLE}}$ and $\hat{\phi}_{MLE}$ and $\hat{\lambda}_{MLE}$ are the solutions of (A.25) and (A.26).

Generalized inverse nakagami-m

Let T be a random variable with INK distribution. Then, a generalized inverse Nakagami-m (IGNK) distribution, with a parameter vector $\theta = (\Omega,\mu,\alpha)$, can be obtained by taking $Y = T^{\frac{\alpha}{2}}$, where $\alpha > 0$ and its PDF is given by,

$$f(y|\theta) = \frac{\alpha}{\Gamma(\mu)}\left(\frac{\mu}{\Omega}\right)^{\mu} y^{-\alpha\mu-1}\exp\left(\frac{\mu}{\Omega}y^{-\alpha}\right). \tag{A.27}$$

The likelihood function from (A.27) is given by

$$\begin{aligned} L(\theta;y) = &\frac{\alpha^n}{\Gamma(\mu)^n}\left(\frac{\mu}{\Omega}\right)^{n\mu}\left\{\prod_{i=1}^{n}y_i^{-\alpha\mu-1}\right\} \\ &\times\exp\left(-\frac{\mu}{\Omega}\sum_{i=1}^{n}y_i^{-\alpha}\right). \end{aligned} \tag{A.28}$$

B1. Bayesian approach

Ramos et al. (RAMOS; LOUZADA; RAMOS, 2016) considered the Bayesian approach to derive efficient closed-form estimators for parameters of the Nakagami-m distribution. They considered the following objective prior

$$\pi(\theta) \propto \frac{1}{\Omega^{c_1}\mu^{c_2}\alpha^{c_3}} \tag{A.29}$$

where $c_i \geq 0, i = 1,2,3$ are known hyperparameters. This approach can be easily adapted for our distribution due the one-to-one invariance property. From the product of the likelihood function (A.28) and the prior distribution (A.29), the joint posterior distribution for θ is given by,

$$\begin{aligned}\pi(\theta|y) =& \frac{1}{d(y)}\frac{\alpha^{n-c_3}}{\mu^{c_2}\Omega^{c_1}\Gamma(\mu)^n}\left(\frac{\mu}{\Omega}\right)^{n\mu}\left\{\prod_{i=1}^{n} y_i^{-\alpha\mu}\right\} \\ & \times \exp\left(-\frac{\mu}{\Omega}\sum_{i=1}^{n} y_i^{-\alpha}\right),\end{aligned} \tag{A.30}$$

where $d(y)$ is the normalized constant and $\mathscr{A} = \{(0,\infty)\times(0,\infty)\times(\varepsilon, M)\}$ is the parameter space of θ, where $0 < \varepsilon < 2$ is a small constant and $M > 2$ is a large constant. We chose (ε, M) for the interval of α since the only interest is in the case where $\alpha = 2$. Therefore, any interval (ε, M) containing $\alpha = 2$ will be satisfactory for our purposes.

The maximum a posteriori probability estimator (MAP) of θ is computed through $\hat{\theta}_{MAP} = \arg\max_{\theta} \log(\pi(\theta|t))$. After some algebraic manipulation we have,

$$\hat{\Omega} = \frac{\mu\sum_{i=1}^{n} y_i^{-\hat{\alpha}}}{n\mu + c_1}. \tag{A.31}$$

Then (A.31) will be equal (A.16), if and only if $c_1 = 0$, i.e, Ω is unbiased when $\alpha = 2$. Hence we consider only that $c_1 = 0$. Note that, if $c_1 = 0$, then (A.30) is a proper posterior distribution, i.e, $d(t) < \infty$. This fact can be easily proved considering $1/Y$ instead of Y in the proof presented by Ramos et al. (RAMOS; LOUZADA; RAMOS, 2016).

The other MAP estimators are given by

$$\hat{\mu} = \frac{(n - c_3)}{\left(\frac{1}{\hat{\Omega}}\sum_{i=1}^{n} y_i^{-\alpha}\log\left(y_i^{-\alpha}\right) + \sum_{i=1}^{n}\log\left(y_i^{-\alpha}\right)\right)}, \tag{A.32}$$

and the MAP for α is obtained by solving the non-linear equation

$$\log(\hat{\mu}) - \psi(\hat{\mu}) = \log\left(\hat{\Omega}\right) - \frac{1}{n}\sum_{i=1}^{n}\log(y_i^{-\hat{\alpha}}) + \frac{c_2}{n\hat{\mu}}.$$

Therefore, for the INK distribution ($\alpha = 2$), the MAP estimator for Ω is given by $\hat{\Omega}_{MAP} = \frac{1}{n}\sum_{i=1}^{n} t_i^{-2}$ and the parameter μ can be estimated by,

$$\hat{\mu}_{fMAP} = \frac{(n - c_3)\frac{1}{n}\sum_{i=1}^{n} t_i^{-2}}{\left(\frac{1}{n}\sum_{i=1}^{n} t_i^{-2}\sum_{i=1}^{n}\log\left(t_i^2\right) - \sum_{i=1}^{n} t_i^{-2}\log\left(t_i^2\right)\right)}. \tag{A.33}$$

The asymptotic variance of μ and Ω are obtained by considering the same derivation as presented in Ramos et al. (RAMOS; LOUZADA; RAMOS, 2016). Then,

$$Var(\mu_{fMAP}) = \frac{(n-c_3)^2}{n^3}\left(\frac{1+\mu\psi'(\mu)}{\mu+\mu\psi'(\mu)-1}\right) \tag{A.34}$$

and

$$Var(\Omega_{MAP}) = \frac{\Omega^2}{n\mu}\cdot \tag{A.35}$$

Although the asymptotic variance of μ and Ω is presented in (A.34 and A.35), we observed that the variance obtained from the Fisher information matrix (A.18) provided results with better coverage probabilities. Hereafter, we considered the variances from μ and Ω obtained from this procedure.

Numerical Analysis

In this section, we studied the performance of the estimators by computing the mean relative errors (MRE) and the relative mean square errors (RMSE), comparing both scenarios with complete and censored data, given by

$$fMRE_i = \frac{1}{N}\sum_{j=1}^{N}\frac{\hat{\theta}_{i,j}}{\theta_i}\ , \quad fMSE_i = \frac{1}{N}\sum_{j=1}^{N}(\hat{\theta}_{i,j}-\theta_i)^2,$$

$ffori = 1,2$ where N is the number of estimates. As a measure instrument, it observes the MREs, with desirable levels close to one, and RMSEs, preferably the smaller levels. Given a level of confidence, the coverage probability (CP) should be close to the nominal value, considering the asymptotic confidence intervals were evaluated at a level of 95%.

Complete Data

The simulation studies consider $\theta = ((0.5,2),(2,4))$, $N = 1,000,000$ and $n = (10,15,\ldots,200)$. The presented results were analogue for different parameters values, and considering the space limitation not showed. The obtained results in the Figures 48 and 49 present the MRE, RMSE and coverage probability (CP) of the 95% asymptotic confidence intervals.

Analyzing the results was ascertain that $\hat{\Omega} = \frac{1}{n}\sum_{i=1}^{n} t_i^{-2}$ is an unbiased estimator for Ω. An important result is that $\hat{\Omega}$ showed an unbiased estimator. In addition to that, the CPs converge to the nominal value assumed when n increases.

On the other hand, the outcome also indicates that μ has a positive bias, as shown (A.23). By this fact, it was added a correction resulting in an unbiased estimator with $O(n^{-2})$ with great efficient even for small samples. Therefore, among the three proposed estimators the CMLE provided superior estimates in all cases. Additionally the coverage probability for all estimators tend to the nominal levels as n increase.

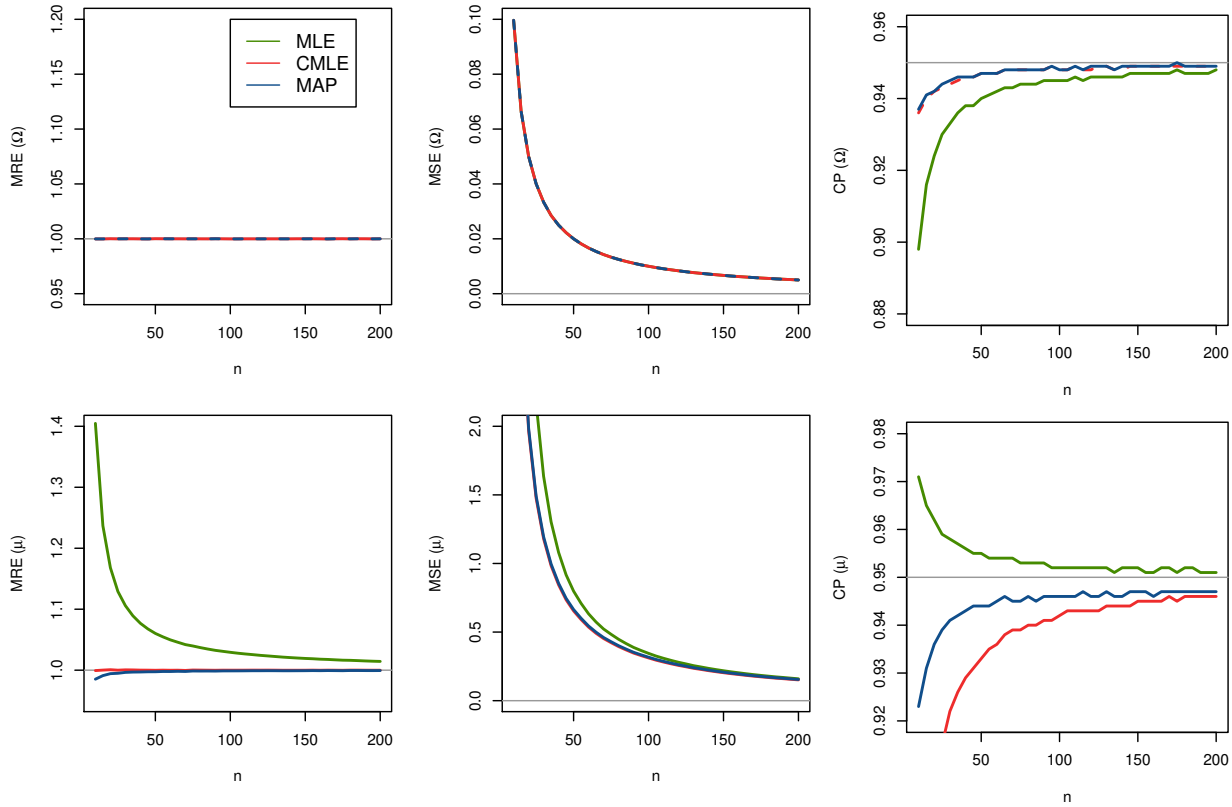

Figure 48 – MREs, MSEs and CPs related to the estimates of $\mu = 4$ and $\Omega = 2$ for $N = 1,000,000$ simulated samples, considering different values of n.

Although, the CMLE produced unbiased estimates with $O(n^{-2})$, there is a high computational cost involving non-linear equation solution and transcendental function. The MAP estimator presents similar results with a lower computational cost and can be an alternative in problems evolving embedded technology to compute real time estimators.

Censored Data

Considering censored data, used the same procedures adopted by Goodman et al. (GOODMAN; LI; TIWARI, 2006). Two scenarios were analyzed, with proportion assumed in 30% and another with 50%. The simulation study is performed considering the estimates of $\mu = 4$ and $\Omega = 2$ to $N = 1,000,000$ simulated samples, considering different values of n.

Figures 50 and 51 present the MRE, RMSE and CPs of the 95% asymptotic confidence intervals of the estimates obtained through the MLE and the CMLE.

An important aspect is that $\hat{\Omega}$ is shown as an unbiased estimator even in the presence of censoring and small sample sized data.

The outcome indicates that MLE for μ has a systematic bias, as shown Figures 50 and 51. Considering the CMLE, an improved estimation was obtained. However this corrected estimator is not equivalent to the unbiased estimator with $O(n^{-2})$, the used in the complete data, presented

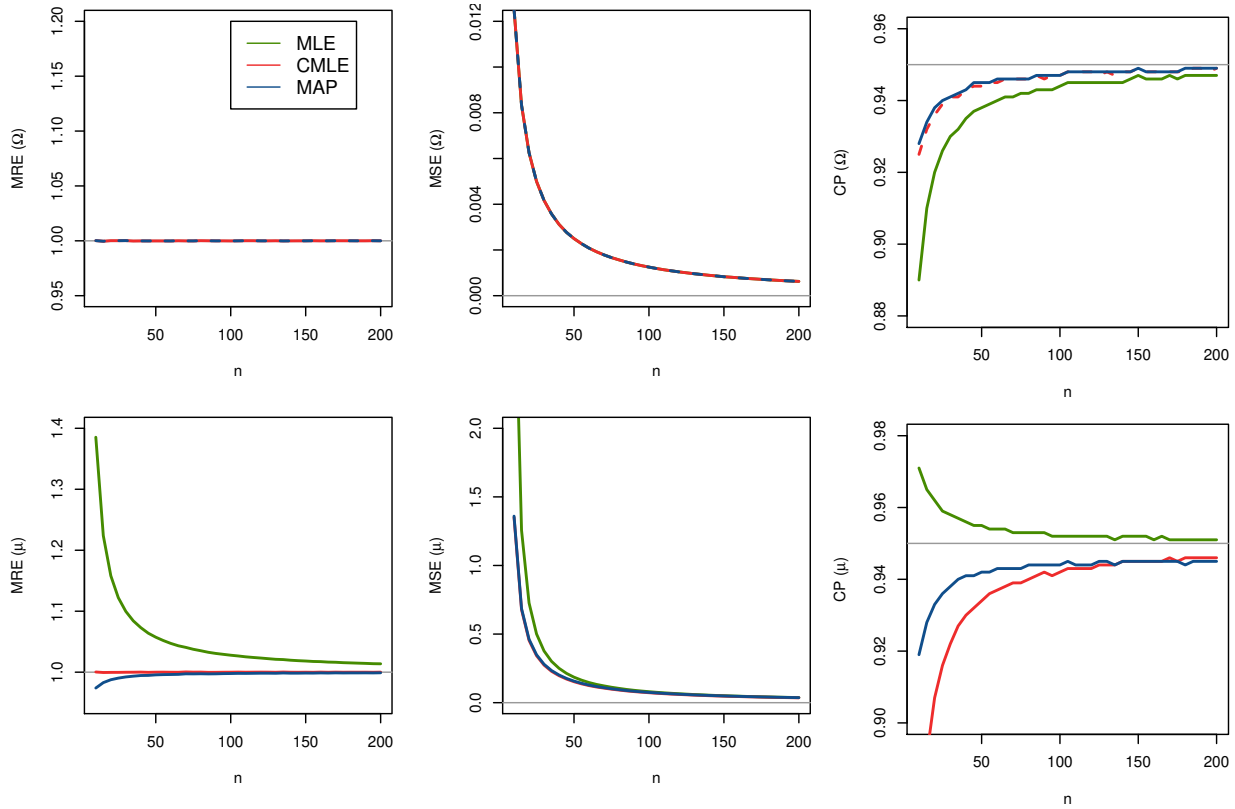

Figure 49 – MREs, MSEs and CPs related to the estimates of $\mu = 2$ and $\Omega = 0.5$ for $N = 1,000,000$ simulated samples, considering different values of n.

in the section A1. This fact derives from the argument which the bias correction was not obtained from Fisher information matrix given censored data, since it has no closed form. Finally, for both parameters, results show the coverage probabilities converge to the nominal value assumed when n increases.

Prediction analysis

Here, we consider the Bayes prediction of the INK using the observed order statistics. The Bayesian approach is considered due its facility in obtain the predictive density of the future observation. The notation and the steps assumed in this section follows Kundu and Raqab (KUNDU; RAQAB, 2012). Let $t_{(m)}$ denote the m-th order statistic, $T_{(1)} < \ldots < T_{(m)}$ be the observed sample and $T_{(m+1)} < \ldots < T_{(n)}$ be the unobserved future sample. Now, let us consider the posterior density (A.30) when $\alpha = 2$ in the presence of complete data with sample size m, that is, the posterior density of the INK distribution given by

$$\pi(\Omega,\mu|t) = \frac{1}{d(t)}\frac{1}{\mu^{c_2}\Omega^{c_1}\Gamma(\mu)^m}\left(\frac{\mu}{\Omega}\right)^{m\mu}\left\{\prod_{i=1}^{m} t_i^{-2\mu}\right\} \times \exp\left(-\frac{\mu}{\Omega}\sum_{i=1}^{m} t_i^{-2}\right), \tag{A.36}$$

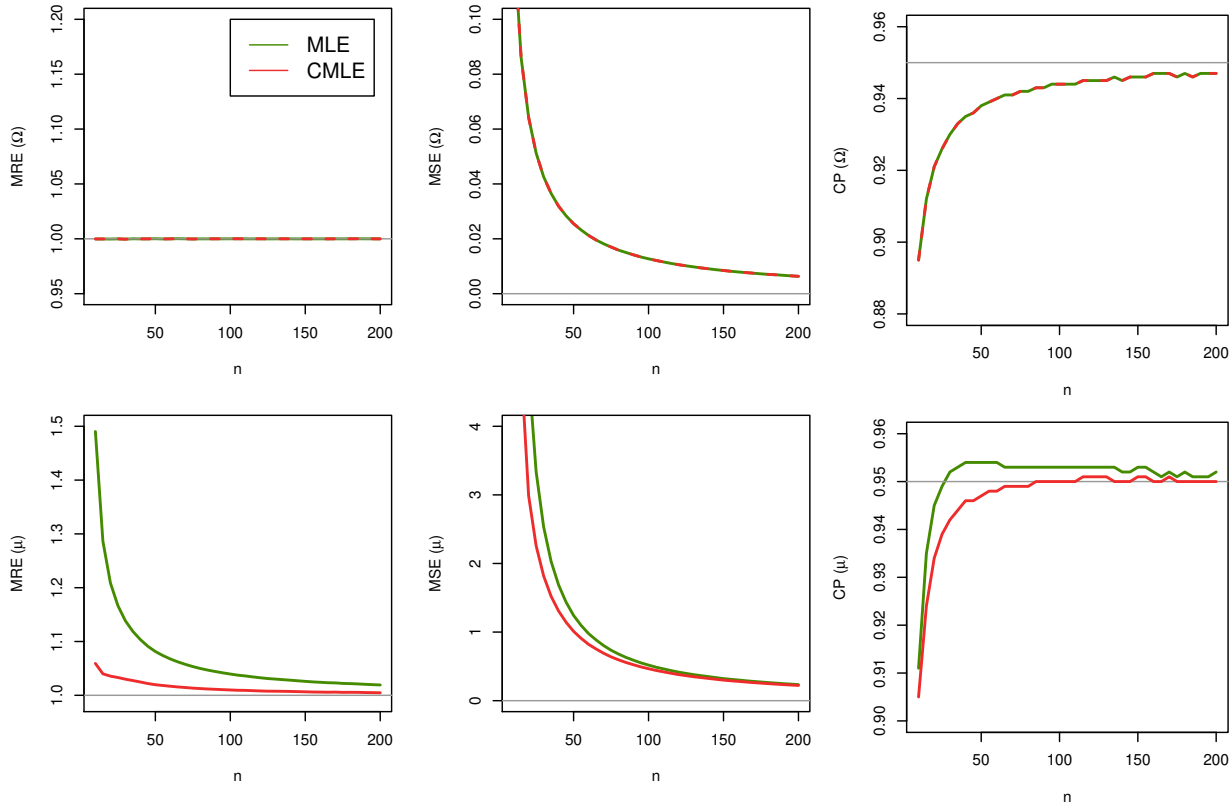

Figure 50 – MREs, MSEs and CPs related to the estimates of $\mu = 4$ and $\Omega = 2$ for $N = 1,000,000$ simulated samples, considering different values of n and 30% of censorship.

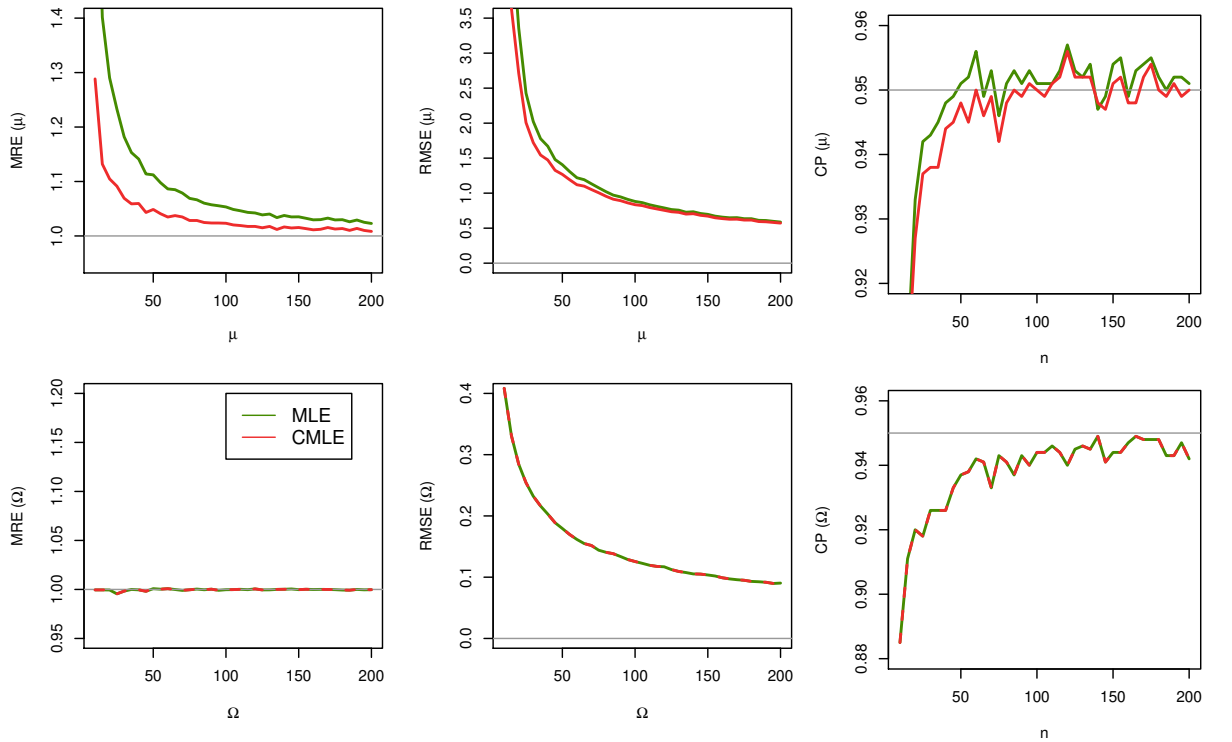

Figure 51 – MREs, MSEs and CPs related to the estimates of $\mu = 4$ and $\Omega = 2$ for $N = 10,000$ simulated samples, considering different values of n and 50% of censorship.

Table 10 – Data set related to the failure time of 194 internal cabin mechanical devices in an aircraft.

1	1	1	1	1	1	1	1	1	1	1	1	1	1	1	1	1	1
1	1	1	1	1	1	1	1	1	1	2	2	2	2	2	2	2	2
2	2	2	2	2	2	2	2	2	2	2	2	3	3	3	3	3	3
3	3	3	3	3	3	4	4	4	4	4	4	4	4	4	5	5	5
5	5	5	5	5	6	6	6	7	7	7	7	7	7	7	7	7	7
7	8	8	8	8	8	8	9	9	9	9	9	9	10	10	10	10	11
12	12	13	13	13	13	13	14	14	14	14	16	17	18	18	18	18	19
19	19	19	20	20	20	20+	21	22	25	27	29	29	31	31	32	32	34
35	37	38+	39+	40	42	43	43+	45	53	60	62+	64	65	65	70	77	78
80	85+	88	90+	90+	90+	90+	90+	90+	90+	90+	90+	90+	90+				

where c_1 and c_2 are the constants with the values given in the Section A. On the other hand, in the presence of random censoring the posterior distribution is given by

$$\begin{aligned}\pi(\Omega,\mu|t) =& \frac{1}{d(t)}\frac{1}{\mu^{c_2}\Omega^{c_1}\Gamma(\mu)^m}\left(\frac{\mu}{\Omega}\right)^{d\mu}\exp\left(-\sum_{i=1}^{m}\frac{\delta_i\mu}{\Omega t_i^2}\right)\\ &\times\prod_{i=1}^{m}\left\{t_i^{-(2\mu+1)\delta_i}\gamma\left(\mu,\frac{\mu}{\Omega t_i^2}\right)^{1-\delta_i}\right\}.\end{aligned} \tag{A.37}$$

From the Markov property of the conditional order statistics, we have

$$\begin{aligned}f_{T_{m+k}}(y|t) =& f_{T_{m+k}|T_m}(y|t) = \frac{(n-m)!}{(k-1)!(n-m-k)!}\\ &\times\frac{f(y)\,(F(y)-F(t_m))^{k-1}\,(1-F(y))^{n-m-k}}{(1-F(t_m))^{n-m}}\end{aligned} \tag{A.38}$$

for $y > t_{(m)}$. The posterior predictive density of T_{m+k} given t is

$$p_{T_{m+k}}(y|t) = \int_0^\infty\int_0^\infty f_{T_{m+k}}(y|t)\pi(\Omega,\mu|t)d\Omega d\mu. \tag{A.39}$$

Therefore, the predictive density of $T_{(m+k)}$ under the assumption of $y > t_{(m)}$ is

$$f^*_{T_{m+k}}(y|t) = \int_0^\infty\int_0^\infty f_{T_{m+k}|T_m}(y|t)\pi(\Omega,\mu|t)d\Omega d\mu. \tag{A.40}$$

An important aspect of this Bayesian predictive approach is its convenience in construct a two-sided predictive interval for T_{m+k} using the Metropolis-Hastings (MH) algorithm. For the necessary details of constructing the MH algorithm see Kundu and Raqab (KUNDU; RAQAB, 2012).

Applications

This proposed model can be useful in problems related to reliability maintenance. Thus, this model proved useful to be applied in different studies aimed at describing the lifespan of

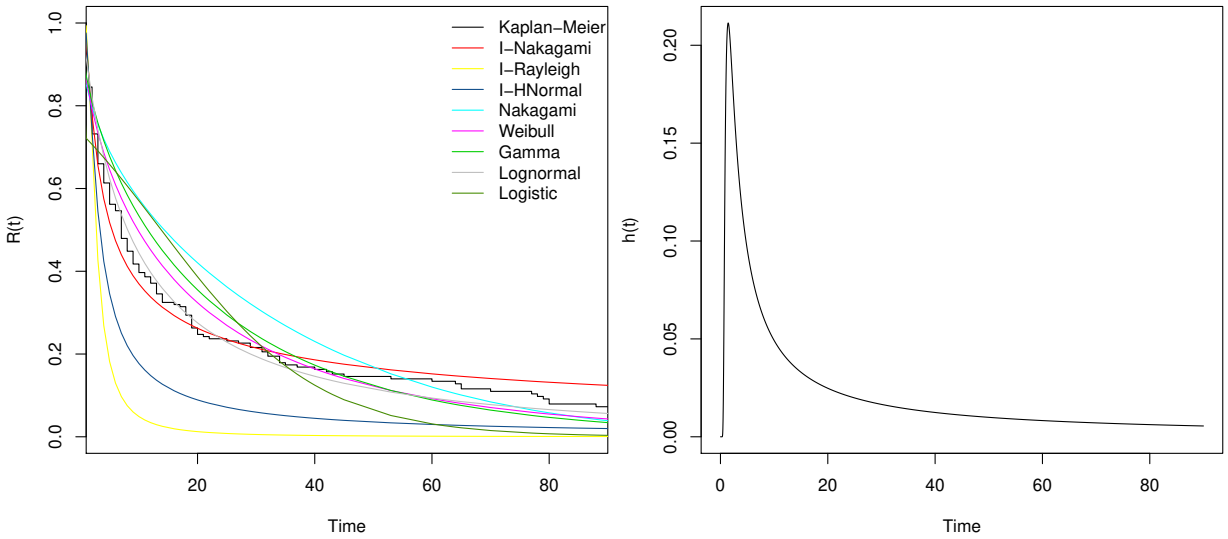

Figure 52 – Reliability function adjusted by different distributions and the Kaplan-Meier estimator (left panel) and the INK estimated hazard function (right panel) considering data set related to the failure time of 194 internal cabin mechanical devices.

different internal cabin mechanical devices, related to improving consumer satisfaction and increasing their respective profits, and in the improvement of a heavy machine (Sugarcane Harvester) optimizing the production of a given factory.

The outcome was compared to the NK, Weibull, Gamma, Lognormal, and Logistic distributions and the nonparametric reliability curve adjusted through the Kaplan-Meier estimator, regarding the INK distribution. Also it was considered the sub models of the INK distribution such as the inverse Rayleigh distribution, the inverse half-normal distribution and the inverse Hoyt distribution. As part of the analysis process, different discrimination criteria constructed under the log-likelihood function. The discrimination criterion methods are: Akaike information criterion (AIC) computed through AIC$= -2l(\hat{\theta};x)+2k$, Corrected Akaike information criterion AICC=AIC$+\frac{2k(k+1)}{(n-k-1)}$, Hannan-Quinn information criterion HQIC$= 2l(\hat{\theta};x)+2k\log(\log(n))$ and the consistent Akaike information criterion CAIC=AIC$+k\log(n)-k$, where k is the number of parameters to be fitted and $\hat{\theta}$ the estimates of θ, respectively.

Internal cabin mechanical devices in an aircraft

In this subsection, a dataset related to the failure time of a given component of aircraft of an airline company is considered. The failure of those repaired items was analyzed in 194 equipment, the failure times are reproduced in Table 1, describing a high defect rate after a short repair time, compromising the quality of the equipment. The experiment considered a period of 90 days, which the data has been censored after such given period. Censored observations with less than 90 days were also observed due to the replacement of the defective item during the experiment.

To compute the MLEs were used the equations (A.25) and (A.26), given the presence of censored data. Table 11 displays the MLEs, standard-errors and 95% confidence intervals for ϕ and λ. Table 12 presents the results of AIC, AICc, HQIC, CAIC criteria.

Table 11 – MAP, Standard deviation and 95% credibility intervals for μ, Ω and $y*$

θ	MAP	SD	$CI_{95\%}(\theta)$
μ	0.2485	0.0207	(0.2120; 0.2917)
Ω	0.2006	0.0323	(0.1565; 0.2836)
$y*$	106.2933	30.0782	(91.4465; 192.3394)

Table 12 – Results of AIC, AICc, HQIC, CAIC criteria for different probability distributions considering the data set related to the failure time of 194 of internal cabin mechanical devices in an aircraft.

Test	INK	Weibull	Gamma	Lognormal
AIC	**1322.34**	1378.71	1394.53	1338.70
AICc	**1318.40**	1374.78	1390.59	1334.76
HQIC	**1324.99**	1381.36	1397.17	1341.34
CAIC	**1330.88**	1387.25	1403.06	1347.23
Test	Logistic	Nakagami	I-Rayleigh	I-H.Normal
AIC	1695.79	1426.11	1735.49	1400.29
AICc	1691.86	1422.17	1733.51	1398.31
HQIC	1698.44	1428.76	1736.82	1401.61
CAIC	1434.64	1739.76	1403.06	1404.56

Since the inverse Hoyt distribution is as two-parameters special case of the INK distribution and the obtained estimate of μ was inside of the interval $0 < \mu < 1$, the obtained results were the same for both models. Comparing the empirical reliability function with the adjusted models available in Figure 52 we observed a goodness of fit for the INK distribution. The present data showed a hazard rate function with unimodal shape. The superior performance for the INK distribution is confirmed from the different discrimination methods since the best model is the one which provides the minimum values of those criteria. Although in this case the inverse Hoyt distribution could be used, there is no need to limit the parametric space between 0 and 1 since the MLE of the INK distribution is unique and allows more flexibility in the hazard rate. From Table 11 we see that given the last failure was observed at 90 days the prediction of the 194th failure will be at 106 days with 95% predictive interval given by $(91.4; 192.3)$. Therefore, the practical importance of the INK distribution is observed for the dataset, since it provides a better fitting in comparison with other well-known distributions.

Sugarcane Harvester

The harvest of sugarcane requires the usage of heavy equipment, which improves the process. In the following two subsections, the included dataset demonstrates two of the highest failure components from the sugarcane harvester, given its intensive operation, which is one of

the high-cost machines. Over a period of 30 months, from a given factory, the motor defaulted 66 times. In this same period of time, the elevator defaulted 54 times.

Elevator

Table 13 presents a high defect rate after a short repair time as well, compromising the cost of the production. The experiment considered a total period of 30 months. As the operating equipment had three off-seasons, these were not included in the dataset. The equipment was only observed during the time of active operation.

Table 13 – Dataset related to the sugarcane harvester's elevator.

1	1	1	1	1	1	1	1	1	1	1
1	1	1	1	1	1	2	2	2	2	2
2	3	3	3	4	4	4	5	6	7	7
7	7	9	9	11	11	11	12	17	17	17
21	23	23	24	25	31	56	61	61	122	

As the previous subsection, the same criteria to compute the MLEs were used. Table 14 displays the MLEs, standard-errors and 95% confidence intervals for and given the harvester's elevator. Table 15 presents the results of AIC, AICc, HQIC, CAIC criteria. Comparing the empirical reliability function with the adjusted models available in Figure 53 we observed a goodness of fit for the INK distribution.

Table 14 – MLE, Standard-error and 95% credibility intervals intervals for μ and Ω

θ	MAP	S. Error	$CI_{95\%}(\theta)$
μ	0.3225	0.0506	(0.2351; 0.4358)
Ω	0.3663	0.1076	(0.2492; 0.6674)
$y*$	166.6787	19.4699	(125.4677; 198.0177)

Table 15 – Results of AIC, AICc, HQIC, CAIC criteria for different probability distributions considering the data set related to the failure time of 54 related to the elevator, device in a sugarcane harvester

Test	INK	Weibull	Gamma	Lognormal
AIC	**345.99**	366.48	371.31	354.42
AICc	**342.22**	362.71	367.55	350.66
HQIC	**347.52**	368.01	372.84	355.96
CAIC	**351.96**	372.46	377.29	360.40
Test	Logistic	Nakagami	I-Rayleigh	I-H.Normal
AIC	456.57	384.90	413.14	350.95
AICc	452.81	381.14	411.22	349.03
HQIC	458.11	386.44	413.91	351.72
CAIC	462.55	390.88	416.13	353.95

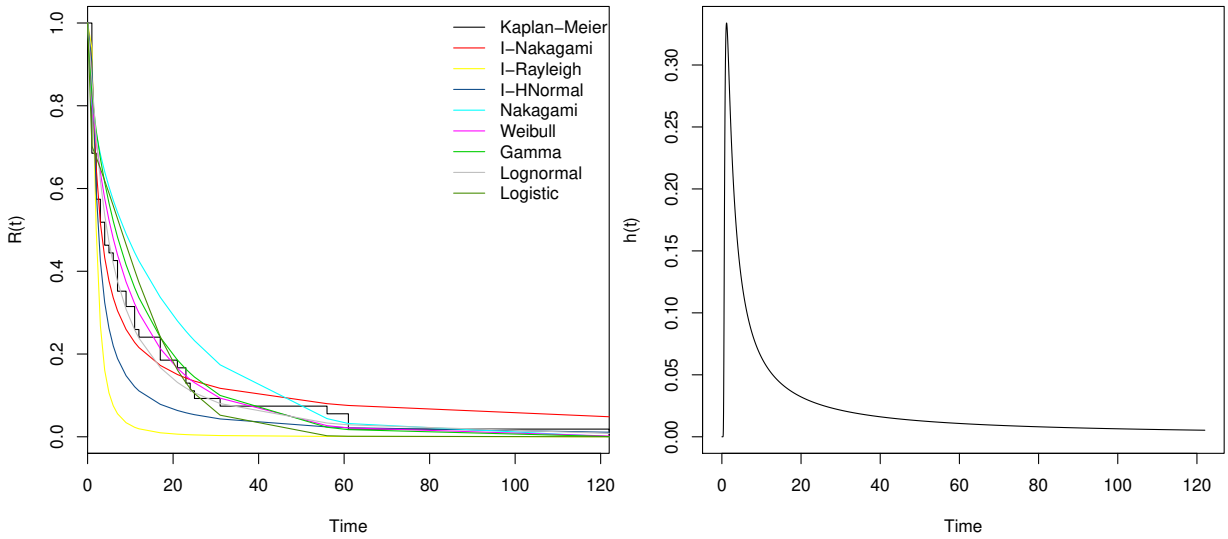

Figure 53 – Reliability function adjusted by different distributions and the Kaplan-Meier estimator (left panel) and the INK estimated hazard function (right panel) considering data set related to.

Motor

Table 16 presents likewise high defect rate related to the sugarcane harvester's motor.

Table 16 – Dataset related to the sugarcane harvester's Motor.

1	1	1	1	1	1	1	1	1	1	1
1	1	1	1	1	1	1	1	2	2	2
2	2	3	3	3	4	4	4	4	5	5
5	5	5	5	7	8	8	9	9	11	11
11	11	12	12	13	16	17	17	18	18	19
22	24	29	32	33	33	41	41	121		

Table 17 displays the MLEs, standard-errors and 95% confidence intervals for and given the harvester's motor. Table 18 presents the results of AIC, AICc, HQIC, CAIC criteria. Moreover, comparing the empirical reliability function with the adjusted models, Figure 54 explicit the goodness of fit for the INK distribution.

Table 17 – MAP, Standard-error and 95% credibility intervals intervals for μ and Ω

θ	MAP	S. Error	$CI_{95\%}(\theta)$
μ	0.3230	0.0469	(0.2434 ; 0.4289)
Ω	0.3412	0.0884	(0.2357; 0.5815)
$y*$	154.5397	23.5575	(122.9326; 207.6934)

Final remarks

In this paper the INK distribution is proposed. This distribution has a relatively high initial failure rate, such characteristic is observed in distributions that exhibits unimodal hazard

Table 18 – Results of AIC, AICc, HQIC, CAIC criteria for different probability distributions considering the data set related to the failure time of 66 related to the motor, device in a sugarcane harvester

Test	INK	Weibull	Gamma	Lognormal
AIC	**414.23**	427.49	430.99	416.70
AICc	**410.43**	423.68	427.10	412.90
HQIC	**415.93**	429.19	432.69	418.40
CAIC	**420.55**	433.81	437.30	423.02
Test	Logistic	Nakagami	I-Rayleigh	I-H.Normal
AIC	512.68	448.38	494.47	420.57
AICc	508.87	444.58	492.53	418.63
HQIC	514.38	450.08	495.32	421.42
CAIC	518.99	454.70	497.63	423.73

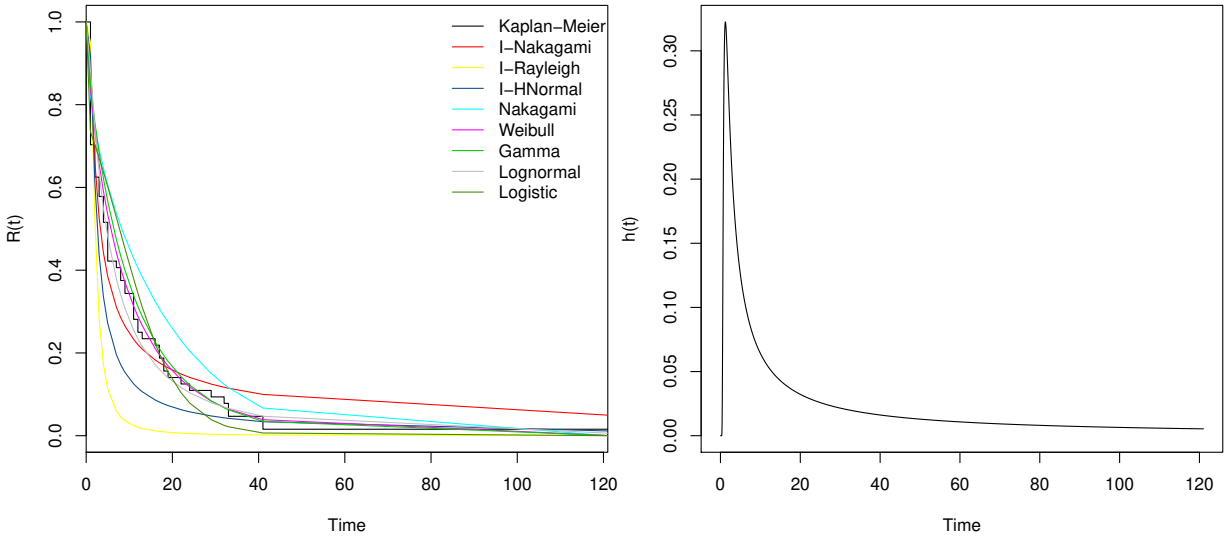

Figure 54 – Reliability function adjusted by different distributions and the Kaplan-Meier estimator (left panel) and the INK estimated hazard function (right panel) considering data set related to.

function. Furthermore, an account of mathematical properties was presented, such as the r-th moment, mean, variance, r-th central moment and Shannon's entropy.

The parameter estimators and their asymptotic intervals were explored using the maximum likelihood theory, a bias correction was proposed with the order $O(n^{-2})$ which provided nearly unbiased estimators. Efficient closed-form estimators for μ and Ω were also presented to allow problems evolving embedded technology and to compute real time estimators. Since in reliability analysis it is common the presence of incomplete data, the MLEs in the presence of random censoring were discussed as well as a bias correction approach for the parameters. The final exemplification was made by applying the INK distribution on aircraft survivor scope and a sugarcane harvester associated with the failure of items given its repairs, analyzing the components associated with a high failure rate after a short repair time.

There is a large number of possible extensions of this current work. The presence of covariates and long-term survivals are very common in practice. Our approach should be investi-

gated further in these contexts as in (PERDONÁ; LOUZADA-NETO, 2011). This distribution is also a promising distribution to be used in studies involving recurrent event data. In this case, we can consider the idea of Zhao and Zhao (ZHAO; ZHOU, 2012) to derive a rate model from nonhomogeneous Poisson process, where the parametric baseline rate function is an INK rate function.

BIBLIOGRAPHY

AADAL, L.; ANGEL, S.; DREYER, P.; LANGHORN, L.; PEDERSEN, B. B. Nursing roles and functions in the inpatient neurorehabilitation of stroke patients: A literature review. **Journal of Neuroscience Nursing**, LWW, v. 45, n. 3, p. 158–170, 2013. Citation on page 76.

ABEGAZ, F.; WIT, E. Sparse time series chain graphical models for reconstructing genetic networks. **Biostatistics**, Oxford University Press, v. 14, n. 3, p. 586–599, 2013. Citations on pages 58, 124, and 128.

AFGANI, M.; SINANOVIC, S.; HAAS, H. Anomaly detection using the kullback-leibler divergence metric. In: IEEE. **Applied Sciences on Biomedical and Communication Technologies, 2008. ISABEL'08. First International Symposium on**. [S.l.], 2008. p. 1–5. Citation on page 46.

AKAIKE, H. Information theory and an extension of the maximum likelihood principle,[w:] proceedings of the 2nd international symposium on information, bn petrow, f. **Czaki, Akademiai Kiado, Budapest**, 1973. Citation on page 59.

ALDER, B. J.; WAINWRIGHT, T. E. Studies in molecular dynamics. i. general method. **The Journal of Chemical Physics**, AIP, v. 31, n. 2, p. 459–466, 1959. Citation on page 64.

ALMALKI, S. J.; NADARAJAH, S. A new discrete modified weibull distribution. **IEEE Transactions on Reliability**, IEEE, v. 63, n. 1, p. 68–80, 2014. Citation on page 158.

AMBLARD, P.-O.; MICHEL, O. J. The relation between granger causality and directed information theory: A review. **Entropy**, Multidisciplinary Digital Publishing Institute, v. 15, n. 1, p. 113–143, 2013. Citation on page 78.

ANACLETO, O.; QUEEN, C.; ALBERS, C. J. Forecasting multivariate road traffic flows using bayesian dynamic graphical models, splines and other traffic variables. **Australian & New Zealand Journal of Statistics**, Wiley Online Library, v. 55, n. 2, p. 69–86, 2013. Citations on pages 82 and 133.

____. Multivariate forecasting of road traffic flows in the presence of heteroscedasticity and measurement errors. **Journal of the Royal Statistical Society: Series C (Applied Statistics)**, Wiley Online Library, v. 62, n. 2, p. 251–270, 2013. Citations on pages 54 and 59.

ARDOLINO, G.; BOSSI, B.; BARBIERI, S.; PRIORI, A. Non-synaptic mechanisms underlie the after-effects of cathodal transcutaneous direct current stimulation of the human brain. **The Journal of physiology**, Wiley Online Library, v. 568, n. 2, p. 653–663, 2005. Citations on pages 40 and 118.

BABYAR, S.; SANTOS-PONTELLI, T.; WILL-LEMOS, T.; MAZIN, S.; BIKSON, M.; TRUONG, D. Q.; EDWARDS, D.; REDING, M. Center of pressure speed changes with tdcs versus gvs in patients with lateropulsion after stroke. **Brain Stimulation: Basic, Translational, and Clinical Research in Neuromodulation**, Elsevier, v. 9, n. 5, p. 796–798, 2016. Citations on pages 31, 38, 57, and 98.

BACH, F. R.; JORDAN, M. I. Learning graphical models for stationary time series. **IEEE transactions on signal processing**, IEEE, v. 52, n. 8, p. 2189–2199, 2004. Citation on page 116.

BAGGIO, J. A.; MAZIN, S. S.; ALESSIO-ALVES, F. F.; BARROS, C. G.; CARNEIRO, A. A.; LEITE, J. P.; PONTES-NETO, O. M.; SANTOS-PONTELLI, T. E. Verticality perceptions associate with postural control and functionality in stroke patients. **PloS one**, Public Library of Science, v. 11, n. 3, p. e0150754, 2016. Citations on pages 38, 57, and 117.

BAI, J. Least squares estimation of a shift in linear processes. **Journal of Time Series Analysis**, Wiley Online Library, v. 15, n. 5, p. 453–472, 1994. Citations on pages 58 and 71.

BALAKRISHNAN, N.; HAIDARI, A.; MASOUMIFARD, K. Stochastic comparisons of series and parallel systems with generalized exponential components. **IEEE Transactions on Reliability**, IEEE, v. 64, n. 1, p. 333–348, 2015. Citation on page 158.

BALAKRISHNAN, N.; JIANG, N.; TSAI, T.-R.; LIO, Y.; CHEN, D.-G. Reliability inference on composite dynamic systems based on burr type-xii distribution. **IEEE Transactions on Reliability**, IEEE, v. 64, n. 1, p. 144–153, 2015. Citation on page 158.

BASHIR, S.; MIZRAHI, I.; WEAVER, K.; FREGNI, F.; PASCUAL-LEONE, A. Assessment and modulation of neural plasticity in rehabilitation with transcranial magnetic stimulation. **PM&R**, Elsevier, v. 2, n. 12, p. S253–S268, 2010. Citation on page 39.

BENSON, H. Y.; SHANNO, D. F.; VANDERBEI, R. J. A comparative study of large-scale nonlinear optimization algorithms. In: **High performance algorithms and software for nonlinear optimization**. [S.l.]: Springer, 2003. p. 95–127. Citation on page 124.

BHOGAL, A. S.; MANI, A. R. Pattern analysis of oxygen saturation variability in healthy individuals: Entropy of pulse oximetry signals carries information about mean oxygen saturation. **Frontiers in physiology**, Frontiers, v. 8, p. 555, 2017. Citation on page 36.

BIKSON, M.; GROSSMAN, P.; THOMAS, C.; ZANNOU, A. L.; JIANG, J.; ADNAN, T.; MOURDOUKOUTAS, A. P.; KRONBERG, G.; TRUONG, D.; BOGGIO, P. *et al.* Safety of transcranial direct current stimulation: evidence based update 2016. **Brain Stimulation: Basic, Translational, and Clinical Research in Neuromodulation**, Elsevier, v. 9, n. 5, p. 641–661, 2016. Citation on page 50.

BILLARD, L. Some analyses of interval data. **Journal of computing and information technology**, SRCE-Sveučilišni računski centar, v. 16, n. 4, p. 225–233, 2008. Citation on page 99.

BILLARD, L.; DIDAY, E. Regression analysis for interval-valued data. In: **Data Analysis, Classification, and Related Methods**. [S.l.]: Springer, 2000. p. 369–374. Citations on pages 99 and 104.

____. Symbolic regression analysis. In: **Classification, Clustering, and Data Analysis**. [S.l.]: Springer Berlin Heidelberg, 2002. p. 281–288. Citation on page 99.

____. Symbolic regression analysis. In: **Classification, Clustering, and Data Analysis**. [S.l.]: Springer, 2002. p. 281–288. Citation on page 104.

____. From the statistics of data to the statistics of knowledge: symbolic data analysis. **Journal of the American Statistical Association**, Taylor & Francis, v. 98, n. 462, p. 470–487, 2003. Citation on page 99.

____. **Symbolic Data Analysis: Conceptual Statistics and Data Mining**. [S.l.]: John Wiley & Sons, 2006. Citation on page 99.

BOCK, H.-H.; DIDAY, E. **Analysis of symbolic data: exploratory methods for extracting statistical information from complex data**. [S.l.]: Springer Science & Business Media, 2012. Citation on page 99.

BONAN, I. V.; HUBEAUX, K.; GELLEZ-LEMAN, M.; GUICHARD, J.; VICAUT, E.; YELNIK, A. Influence of subjective visual vertical misperception on balance recovery after stroke. **Journal of Neurology, Neurosurgery & Psychiatry**, BMJ Publishing Group Ltd, v. 78, n. 1, p. 49–55, 2007. Citations on pages 38 and 57.

BROOKS, S.; GELMAN, A.; JONES, G.; MENG, X.-L. **Handbook of markov chain monte carlo**. [S.l.]: CRC press, 2011. Citation on page 64.

BRUNONI, A. R.; NITSCHE, M. A.; BOLOGNINI, N.; BIKSON, M.; WAGNER, T.; MERABET, L.; EDWARDS, D. J.; VALERO-CABRE, A.; ROTENBERG, A.; PASCUAL-LEONE, A. *et al.* Clinical research with transcranial direct current stimulation (tdcs): challenges and future directions. **Brain Stimulation: Basic, Translational, and Clinical Research in Neuromodulation**, Elsevier, v. 5, n. 3, p. 175–195, 2012. Citations on pages 39, 40, and 118.

CACAO, F.; CORNELIUS, J.; FERNANDES, K.; ADEBAYO, Y.; LOZADA, M.; MARVILLE-WILLIAMS, C. Providing care in the digital way: A day in the life of a nurse in a digital intensive care unit (icu). **Canadian Journal of Critical Care Nursing**, v. 28, n. 2, 2017. Citations on pages 73 and 113.

CASTIGLIONI, P.; RIENZO, M. D. How the threshold "r" influences approximate entropy analysis of heart-rate variability. In: IEEE. **2008 Computers in Cardiology**. [S.l.], 2008. p. 561–564. Citations on pages 84 and 87.

CASTILLO-SAAVEDRA, L.; GEBODH, N.; BIKSON, M.; DIAZ-CRUZ, C.; BRANDAO, R.; COUTINHO, L.; TRUONG, D.; DATTA, A.; SHANI-HERSHKOVICH, R.; WEISS, M. *et al.* Clinically effective treatment of fibromyalgia pain with high-definition transcranial direct current stimulation: phase ii open-label dose optimization. **The Journal of Pain**, Elsevier, v. 17, n. 1, p. 14–26, 2016. Citation on page 39.

CASTRUCCIO, S.; OMBAO, H.; GENTON, M. G. A multi-resolution spatio-temporal model for brain activation and connectivity in fmri data. **arXiv preprint arXiv:1602.02435**, 2016. Citation on page 128.

CHERN, J.-S.; LO, C.-Y.; WU, C.-Y.; CHEN, C.-L.; YANG, S.; TANG, F.-T. Dynamic postural control during trunk bending and reaching in healthy adults and stroke patients. **American journal of physical medicine & rehabilitation**, LWW, v. 89, n. 3, p. 186–197, 2010. Citations on pages 38, 57, and 117.

CHIANG, M.-C.; KLUNDER, A. D.; MCMAHON, K.; ZUBICARAY, G. I. D.; WRIGHT, M. J.; TOGA, A. W.; THOMPSON, P. M. Information-theoretic analysis of brain white matter fiber orientation distribution functions. In: SPRINGER. **Biennial International Conference on Information Processing in Medical Imaging**. [S.l.], 2007. p. 172–182. Citation on page 46.

CHICKERING, D. **Learning Bayesian Networks is NP-Complete. Learning from Data: Artificial Intelligence and Statistics V. Edited by: Fisher D, Lenz HJ.** [S.l.]: Springer-Verlag, 1996. Citations on pages 122 and 132.

CHICKERING, D. M. Learning bayesian networks is np-complete. In: **Learning from data**. [S.l.]: Springer, 1996. p. 121–130. Citations on pages 60 and 94.

COGIAMANIAN, F.; VERGARI, M.; PULECCHI, F.; MARCEGLIA, S.; PRIORI, A. Effect of spinal transcutaneous direct current stimulation on somatosensory evoked potentials in humans. **Clinical Neurophysiology**, Elsevier, v. 119, n. 11, p. 2636–2640, 2008. Citations on pages 40 and 118.

CORCHADO, E.; WOZNIAK, M.; ABRAHAM, A.; CARVALHO, A. C. P. L.; SNÁSEL, V. *et al.* Recent trends in intelligent data analysis. **Neurocomputing**, Elsevier, v. 126, p. 1–2, 2014. Citation on page 98.

CORDEIRO, G. M.; KLEIN, R. Bias correction in arma models. **Statistics & Probability Letters**, Elsevier, v. 19, n. 3, p. 169–176, 1994. Citation on page 165.

COSTA, L.; ANACLETO, O.; NASCIMENTO, D. C.; SMITH, J.; LOUZADA, F.; NICHOLS, T. The hierarchical multiregression dynamic models: a brain connectivity cluster reconstruction task. **Information Sciences Journal**, Elsevier, in press. Citations on pages 81 and 94.

COSTA, L.; NICHOLS, T.; SMITH, J. Q. *et al.* Studying the effective brain connectivity using multiregression dynamic models. **Brazilian Journal of Probability and Statistics**, Brazilian Statistical Association, v. 31, n. 4, p. 765–800, 2017. Citations on pages 31, 54, 55, 59, 98, 112, and 125.

COSTA, L.; SMITH, J.; NICHOLS, T.; CUSSENS, J.; DUFF, E. P.; MAKIN, T. R. *et al.* Searching multiregression dynamic models of resting-state fmri networks using integer programming. **Bayesian Analysis**, International Society for Bayesian Analysis, v. 10, n. 2, p. 441–478, 2015. Citations on pages 82, 84, 94, 105, 112, and 133.

COSTA, L.; SMITH, J. Q.; NICHOLS, T. A group analysis using the multiregression dynamic models for fmri networked time series. **Journal of statistical planning and inference**, Elsevier, v. 198, p. 43–61, 2019. Citations on pages 77, 81, and 94.

COX, D. R.; REID, N. Parameter orthogonality and approximate conditional inference. **Journal of the Royal Statistical Society. Series B (Methodological)**, JSTOR, p. 1–39, 1987. Citation on page 165.

COX, D. R.; SNELL, E. J. A general definition of residuals. **Journal of the Royal Statistical Society. Series B (Methodological)**, JSTOR, p. 248–275, 1968. Citations on pages 158 and 165.

CRANSTOUN, S. D.; OMBAO, H. C.; SACHS, R. V.; GUO, W.; LITT, B. Time-frequency spectral estimation of multichannel eeg using the auto-slex method. **IEEE transactions on Biomedical Engineering**, IEEE, v. 49, n. 9, p. 988–996, 2002. Citation on page 54.

CUESTA-FRAU, D.; MIRÓ-MARTÍNEZ, P.; NÚÑEZ, J. J.; OLTRA-CRESPO, S.; PICÓ, A. M. Noisy eeg signals classification based on entropy metrics. performance assessment using first and second generation statistics. **Computers in biology and medicine**, Elsevier, v. 87, p. 141–151, 2017. Citation on page 36.

CURY, A.; CRÉMONA, C. Pattern recognition of structural behaviors based on learning algorithms and symbolic data concepts. **Structural Control and Health Monitoring**, Wiley Online Library, v. 19, n. 2, p. 161–186, 2012. Citation on page 100.

CYSARZ, D.; EDELHÄUSER, F.; LEEUWEN, P. V. Strategies of symbolization in cardiovascular time series to test individual gestational development in the fetus. **Philosophical Transactions of the Royal Society A: Mathematical, Physical and Engineering Sciences**, The Royal Society Publishing, v. 373, n. 2034, p. 20140087, 2015. Citation on page 106.

DAGUM, P.; GALPER, A.; HORVITZ, E. Dynamic network models for forecasting. In: ELSEVIER. **Uncertainty in artificial intelligence**. [S.l.], 1992. p. 41–48. Citation on page 82.

DASH, D.; DRUZDZEL, M. J. A hybrid anytime algorithm for the construction of causal models from sparse data. In: MORGAN KAUFMANN PUBLISHERS INC. **Proceedings of the Fifteenth conference on Uncertainty in artificial intelligence**. [S.l.], 1999. p. 142–149. Citation on page 81.

DAY, B. L.; COLE, J. Vestibular-evoked postural responses in the absence of somatosensory information. **Brain**, Oxford University Press, v. 125, n. 9, p. 2081–2088, 2002. Citations on pages 38, 57, and 117.

DEY, D. K.; RAO, C. R. **Bayesian thinking, modeling and computation**. [S.l.]: Elsevier, 2005. Citations on pages 95 and 112.

DIDAY, E. Thinking by classes in data science: the symbolic data analysis paradigm. **Wiley Interdisciplinary Reviews: Computational Statistics**, Wiley Online Library, v. 8, n. 5, p. 172–205, 2016. Citation on page 99.

DIDAY, E.; NOIRHOMME-FRAITURE, M. **Symbolic data analysis and the SODAS software**. [S.l.]: John Wiley & Sons, 2008. Citations on pages 98 and 99.

DIDAY, E.; SIMON, J. Clustering analysis. In: **Digital pattern recognition**. [S.l.]: Springer, 1976. p. 47–94. Citation on page 99.

DIDONATO, A. R.; JR, A. H. M. Computation of the incomplete gamma function ratios and their inverse. **ACM Transactions on Mathematical Software (TOMS)**, ACM, v. 12, n. 4, p. 377–393, 1986. Citation on page 160.

DOMENICO, M. D. Multilayer modeling and analysis of human brain networks. **Giga Science**, Oxford University Press, v. 6, n. 5, p. gix004, 2017. Citations on pages 116, 124, 126, and 127.

DOMINGUES, M.; SOUZA, R.; CYSNEIROS, F. A robust method for linear regression of symbolic interval data. **Pattern Recognition Letters**, v. 31, n. 13, p. 1991 – 1996, 2010. Citation on page 100.

EDWARDS, D.; CORTES, M.; DATTA, A.; MINHAS, P.; WASSERMANN, E. M.; BIKSON, M. Physiological and modeling evidence for focal transcranial electrical brain stimulation in humans: a basis for high-definition tdcs. **Neuroimage**, Elsevier, v. 74, p. 266–275, 2013. Citations on pages 117 and 118.

EDWARDS, D. J. On the understanding and development of modern physical neurorehabilitation methods: robotics and non-invasive brain stimulation. **Journal of neuroengineering and rehabilitation**, BioMed Central, v. 6, n. 1, p. 3, 2009. Citation on page 29.

EICHLER, M. **Graphical models in time series analysis**. Phd Thesis (PhD Thesis) — Universität Heidelberg, 1999. Citation on page 59.

FAGUNDES, R. A. A.; SOUZA, R. M. C. R.; CYSNEIROS, F. J. A. Robust regression with application to symbolic interval data. **Engineering Applications of Artificial Intelligence**, v. 26, n. 1, p. 564 – 573, 2013. ISSN 0952-1976. Citation on page 100.

FEIGIN, V. L.; FOROUZANFAR, M. H.; KRISHNAMURTHI, R.; MENSAH, G. A.; CONNOR, M.; BENNETT, D. A.; MORAN, A. E.; SACCO, R. L.; ANDERSON, L.; TRUELSEN, T. *et al.* Global and regional burden of stroke during 1990–2010: findings from the global burden of disease study 2010. **The Lancet**, Elsevier, v. 383, n. 9913, p. 245–255, 2014. Citations on pages 29 and 76.

FERBERT, A.; PRIORI, A.; ROTHWELL, J.; DAY, B.; COLEBATCH, J.; MARSDEN, C. Interhemispheric inhibition of the human motor cortex. **The Journal of physiology**, Wiley Online Library, v. 453, n. 1, p. 525–546, 1992. Citations on pages 40 and 118.

FERNÁNDEZ-VILLAVERDE, J.; RUBIO-RAMÍREZ, J. F. Estimating macroeconomic models: A likelihood approach. **The Review of Economic Studies**, Wiley-Blackwell, v. 74, n. 4, p. 1059–1087, 2007. Citation on page 98.

FIECAS, M.; OMBAO, H. The generalized shrinkage estimator for the analysis of functional connectivity of brain signals. **The Annals of Applied Statistics**, JSTOR, p. 1102–1125, 2011. Citations on pages 31, 54, and 128.

FLESCH, I.; LUCAS, P. J. Markov equivalence in bayesian networks. In: **Advances in probabilistic graphical models**. [S.l.]: Springer, 2007. p. 3–38. Citation on page 80.

FRANSSON, P. Spontaneous low-frequency bold signal fluctuations: An fmri investigation of the resting-state default mode of brain function hypothesis. **Human brain mapping**, Wiley Online Library, v. 26, n. 1, p. 15–29, 2005. Citation on page 126.

FRIEDMAN, J.; HASTIE, T.; TIBSHIRANI, R. Sparse inverse covariance estimation with the graphical lasso. **Biostatistics**, Oxford University Press, v. 9, n. 3, p. 432–441, 2008. Citations on pages 123 and 128.

FRIEDMAN, N.; GEIGER, D.; GOLDSZMIDT, M. Bayesian network classifiers. **Machine learning**, Springer, v. 29, n. 2-3, p. 131–163, 1997. Citation on page 80.

FRISTON, K. J. Functional and effective connectivity: a review. **Brain connectivity**, Mary Ann Liebert, Inc. 140 Huguenot Street, 3rd Floor New Rochelle, NY 10801 USA, v. 1, n. 1, p. 13–36, 2011. Citation on page 125.

FRISTON, K. J.; GLASER, D. E.; HENSON, R. N.; KIEBEL, S.; PHILLIPS, C.; ASHBURNER, J. Classical and bayesian inference in neuroimaging: applications. **Neuroimage**, Elsevier, v. 16, n. 2, p. 484–512, 2002. Citation on page 54.

FU, T.-c. A review on time series data mining. **Engineering Applications of Artificial Intelligence**, Elsevier, v. 24, n. 1, p. 164–181, 2011. Citation on page 98.

GAMERMAN, D.; MIGON, H. S. Dynamic hierarchical models. **Journal of the Royal Statistical Society: Series B (Methodological)**, Wiley Online Library, v. 55, n. 3, p. 629–642, 1993. Citation on page 63.

GÁMEZ, J. A.; MATEO, J. L.; PUERTA, J. M. Learning bayesian networks by hill climbing: efficient methods based on progressive restriction of the neighborhood. **Data Mining and Knowledge Discovery**, Springer, v. 22, n. 1-2, p. 106–148, 2011. Citations on pages 80 and 81.

GANTI, V.; GEHRKE, J.; RAMAKRISHNAN, R. Mining very large databases. **Computer**, IEEE, v. 32, n. 8, p. 38–45, 1999. Citation on page 98.

GARRISON, K. A.; SCHEINOST, D.; FINN, E. S.; SHEN, X.; CONSTABLE, R. T. The (in) stability of functional brain network measures across thresholds. **Neuroimage**, Elsevier, v. 118, p. 651–661, 2015. Citations on pages 121 and 123.

GILIO, F.; RIZZO, V.; SIEBNER, H. R.; ROTHWELL, J. C. Effects on the right motor hand-area excitability produced by low-frequency rtms over human contralateral homologous cortex. **The Journal of physiology**, Wiley Online Library, v. 551, n. 2, p. 563–573, 2003. Citations on pages 40 and 118.

GIUSTI, A.; GRASSINI, L. Cluster analysis of census data using the symbolic data approach. **Advances in Data Analysis and Classification**, Springer, v. 2, n. 2, p. 163–176, 2008. Citation on page 100.

GLASER, R. E. Bathtub and related failure rate characterizations. **Journal of the American Statistical Association**, Taylor & Francis Group, v. 75, n. 371, p. 667–672, 1980. Citation on page 161.

GLOVER, F. Tabu search: A tutorial. **Interfaces**, INFORMS, v. 20, n. 4, p. 74–94, 1990. Citation on page 94.

GONZÁLEZ-RIVERA, G.; ARROYO, J. Time series modeling of histogram-valued data: The daily histogram time series of s&p500 intradaily returns. **International Journal of Forecasting**, Elsevier, v. 28, n. 1, p. 20–33, 2012. Citation on page 100.

GOODMAN, M. S.; LI, Y.; TIWARI, R. C. Survival analysis with change point hazard functions. bepress, 2006. Citation on page 170.

GORROSTIETA, C.; FIECAS, M.; OMBAO, H.; BURKE, E.; CRAMER, S. Hierarchical vector auto-regressive models and their applications to multi-subject effective connectivity. **Frontiers in computational neuroscience**, Frontiers, v. 7, p. 159, 2013. Citations on pages 54 and 59.

GORROSTIETA, C.; OMBAO, H.; BÉDARD, P.; SANES, J. N. Investigating brain connectivity using mixed effects vector autoregressive models. **NeuroImage**, Elsevier, v. 59, n. 4, p. 3347–3355, 2012. Citations on pages 31 and 54.

GRANGER, C. W. Investigating causal relations by econometric models and cross-spectral methods. **Econometrica: Journal of the Econometric Society**, JSTOR, p. 424–438, 1969. Citations on pages 77, 78, and 105.

GRANGER, C. W. J. Economic processes involving feedback. **Information and control**, Elsevier, v. 6, n. 1, p. 28–48, 1963. Citation on page 78.

GRATTON, C.; LAUMANN, T. O.; NIELSEN, A. N.; GREENE, D. J.; GORDON, E. M.; GILMORE, A. W.; NELSON, S. M.; COALSON, R. S.; SNYDER, A. Z.; SCHLAGGAR, B. L. *et al.* Functional brain networks are dominated by stable group and individual factors, not cognitive or daily variation. **Neuron**, Elsevier, v. 98, n. 2, p. 439–452, 2018. Citation on page 116.

GRUBER, L. F.; WEST, M. Bayesian forecasting and scalable multivariate volatility analysis using simultaneous graphical dynamic linear models. **Econometrics and Statistics**, v. 3, p. 3–22, 2017. ArXiv:1606.08291. Available: <http://www.sciencedirect.com/science/article/pii/S2452306217300163>. Citations on pages 31 and 54.

HARRIS-LOVE, M. L.; COHEN, L. G. Noninvasive cortical stimulation in neurorehabilitation: a review. **Archives of Physical Medicine and Rehabilitation**, Elsevier, v. 87, n. 12, p. 84–93, 2006. Citation on page 76.

HECKERMAN, D.; GEIGER, D.; CHICKERING, D. M. Learning bayesian networks: The combination of knowledge and statistical data. **Machine learning**, Springer, v. 20, n. 3, p. 197–243, 1995. Citation on page 60.

HEINTZMAN, N. D.; HON, G. C.; HAWKINS, R. D.; KHERADPOUR, P.; STARK, A.; HARP, L. F.; YE, Z.; LEE, L. K.; STUART, R. K.; CHING, C. W. *et al.* Histone modifications at human enhancers reflect global cell-type-specific gene expression. **Nature**, Nature Publishing Group, v. 459, n. 7243, p. 108, 2009. Citation on page 36.

HYNDMAN, R. J.; ATHANASOPOULOS, G. **Forecasting: principles and practice**. [S.l.]: OTexts, 2018. Citation on page 110.

IDE, J. S.; ZHANG, S.; CHIANG-SHAN, R. L. Bayesian network models in brain functional connectivity analysis. **International Journal of Approximate Reasoning**, Elsevier, v. 55, n. 1, p. 23–35, 2014. Citation on page 94.

JIANG, X.; NEAPOLITAN, R. E.; BARMADA, M. M.; VISWESWARAN, S. Learning genetic epistasis using bayesian network scoring criteria. **BMC bioinformatics**, BioMed Central, v. 12, n. 1, p. 89, 2011. Citation on page 81.

JOHNSON, N. L.; KOTZ, S.; BALAKRISHNAN, N. Distributions in statistics: continuous univariate distributions, vol. 2. **NY: Wiley**, 1970. Citation on page 158.

JOHNSON, W.; ONUMA, O.; OWOLABI, M.; SACHDEV, S. Stroke: a global response is needed. **Bulletin of the World Health Organization**, World Health Organization, v. 94, n. 9, p. 634, 2016. Citations on pages 29 and 76.

JOHNSTON, S. C.; MENDIS, S.; MATHERS, C. D. Global variation in stroke burden and mortality: estimates from monitoring, surveillance, and modelling. **The Lancet Neurology**, Elsevier, v. 8, n. 4, p. 345–354, 2009. Citations on pages 29 and 76.

JOSHI, S. H.; BOWMAN, I.; TOGA, A. W.; HORN, J. D. V. Brain pattern analysis of cortical valued distributions. In: NIH PUBLIC ACCESS. **Proceedings/IEEE International Symposium on Biomedical Imaging: from nano to macro. IEEE International Symposium on Biomedical Imaging**. [S.l.], 2011. p. 1117. Citation on page 46.

JUDSON, R. A.; OWEN, A. L. Estimating dynamic panel data models: a guide for macroeconomists. **Economics letters**, Elsevier, v. 65, n. 1, p. 9–15, 1999. Citation on page 98.

KELLAWAY, P. The part played by electric fish in the early history of bioelectricity and electrotherapy. **Bulletin of the History of Medicine**, Johns Hopkins University Press, v. 20, p. 112, 1946. Citation on page 39.

KELLER, K.; LAUFFER, H. Symbolic analysis of high-dimensional time series. **International Journal of Bifurcation and Chaos**, World Scientific, v. 13, n. 09, p. 2657–2668, 2003. Citation on page 111.

KEVIN, B.; NICHOLSON, A. **Bayesian artificial intelligence**. [S.l.]: Chapman & Hall/CRC, 2004. Citation on page 80.

KIM, J. H.; PEARL, J. Convince: A conversational inference consolidation engine. **IEEE transactions on systems, man, and cybernetics**, IEEE, v. 17, n. 2, p. 120–132, 1987. Citation on page 77.

KING, L. A.; FISHER, J.; JACQUIN, L.; ZELTWANGER, P. The digital hospital: opportunities and challenges. **Journal of healthcare information management: JHIM**, v. 17, n. 1, p. 37–45, 2003. Citations on pages 73 and 113.

KIVELÄ, M.; ARENAS, A.; BARTHELEMY, M.; GLEESON, J. P.; MORENO, Y.; PORTER, M. A. Multilayer networks. **Journal of complex networks**, Oxford University Press, v. 2, n. 3, p. 203–271, 2014. Citations on pages 116 and 128.

KRAVARIS, C.; HAHN, J.; CHU, Y. Advances and selected recent developments in state and parameter estimation. **Computers & chemical engineering**, Elsevier, v. 51, p. 111–123, 2013. Citation on page 112.

KRYSTAL, A. D.; PRADO, R.; WEST, M. New methods of time series analysis of non-stationary eeg data: eigenstructure decompositions of time varying autoregressions. **Clinical Neurophysiology**, Elsevier, v. 110, n. 12, p. 2197–2206, 1999. Citations on pages 98 and 121.

KUNDU, D.; RAQAB, M. Z. Bayesian inference and prediction of order statistics for a type-ii censored weibull distribution. **Journal of statistical planning and inference**, Elsevier, v. 142, n. 1, p. 41–47, 2012. Citations on pages 171 and 173.

LANG, N.; SIEBNER, H. R.; WARD, N. S.; LEE, L.; NITSCHE, M. A.; PAULUS, W.; ROTHWELL, J. C.; LEMON, R. N.; FRACKOWIAK, R. S. How does transcranial dc stimulation of the primary motor cortex alter regional neuronal activity in the human brain? **European Journal of Neuroscience**, Wiley Online Library, v. 22, n. 2, p. 495–504, 2005. Citations on pages 40 and 118.

LEE, L.; SIEBNER, H. R.; ROWE, J. B.; RIZZO, V.; ROTHWELL, J. C.; FRACKOWIAK, R. S.; FRISTON, K. J. Acute remapping within the motor system induced by low-frequency repetitive transcranial magnetic stimulation. **Journal of Neuroscience**, Soc Neuroscience, v. 23, n. 12, p. 5308–5318, 2003. Citations on pages 40 and 118.

LI, J.; WANG, Z. J.; PALMER, S. J.; MCKEOWN, M. J. Dynamic bayesian network modeling of fmri: a comparison of group-analysis methods. **Neuroimage**, Elsevier, v. 41, n. 2, p. 398–407, 2008. Citation on page 94.

LIAO, X.; CAO, M.; XIA, M.; HE, Y. Individual differences and time-varying features of modular brain architecture. **Neuroimage**, Elsevier, v. 152, p. 94–107, 2017. Citations on pages 29, 81, 94, and 132.

LIEBETANZ, D.; NITSCHE, M. A.; TERGAU, F.; PAULUS, W. Pharmacological approach to the mechanisms of transcranial dc-stimulation-induced after-effects of human motor cortex excitability. **Brain**, Oxford University Press, v. 125, n. 10, p. 2238–2247, 2002. Citation on page 40.

LIEPERT, J.; HAMZEI, F.; WEILLER, C. Motor cortex disinhibition of the unaffected hemisphere after acute stroke. **Muscle & Nerve: Official Journal of the American Association of Electrodiagnostic Medicine**, Wiley Online Library, v. 23, n. 11, p. 1761–1763, 2000. Citation on page 40.

Lima Neto, E. A.; De Carvalho, F. A. T. Centre and range method for fitting a linear regression model to symbolic interval data. **Computational Statistics & Data Analysis**, v. 52, n. 3, p. 1500 – 1515, 2008. ISSN 0167-9473. Citations on pages 99, 100, and 104.

LOUZADA, F.; RAMOS, P. L.; NASCIMENTO, D. The inverse nakagami-m distribution: A novel approach in reliability. **IEEE Transactions on Reliability**, IEEE, v. 67, n. 3, p. 1030–1042, 2018. Citations on pages 84, 87, and 134.

MATTAR, M. G.; WYMBS, N. F.; BOCK, A. S.; AGUIRRE, G. K.; GRAFTON, S. T.; BASSETT, D. S. Predicting future learning from baseline network architecture. **Neuroimage**, Elsevier, v. 172, p. 107–117, 2018. Citations on pages 29, 81, and 94.

MCMILLAN, B. The basic theorems of information theory. **Annals of Mathematical Statistics**, v. 24, p. 196–219, 1953. Citation on page 41.

MELSSEN, W.; EPPING, W. Detection and estimation of neural connectivity based on crosscorrelation analysis. **Biological cybernetics**, Springer, v. 57, n. 6, p. 403–414, 1987. Citation on page 59.

METROPOLIS, N.; ROSENBLUTH, A. W.; ROSENBLUTH, M. N.; TELLER, A. H.; TELLER, E. Equation of state calculations by fast computing machines. **The journal of chemical physics**, AIP, v. 21, n. 6, p. 1087–1092, 1953. Citation on page 64.

MEYER, B.-U.; RÖRICHT, S.; WOICIECHOWSKY, C. Topography of fibers in the human corpus callosum mediating interhemispheric inhibition between the motor cortices. **Annals of neurology**, Wiley Online Library, v. 43, n. 3, p. 360–369, 1998. Citations on pages 40 and 118.

MIGON, H. S.; GAMERMAN, D.; LOUZADA, F. **Statistical inference: an integrated approach**. 2. ed. [S.l.]: Chapman and Hall/CRC press, 2014. Citation on page 165.

NAKAGAMI, N. The m-distribution a general formulation of intensity distribution of rapid fading. **Statistical Methods in Radio Wave Propagation: Proceedings of a Symposium**, Pergamon Press, p. 3–36, 1960. Citation on page 158.

NAKAHARA, H.; CARCOLÉ, E. Maximum-likelihood method for estimating coda q and the nakagami-m parameter. **Bulletin of the Seismological Society of America**, Seismological Society of America, v. 100, n. 6, p. 3174–3182, 2010. Citation on page 158.

NAKAO, H. Phase reduction approach to synchronisation of nonlinear oscillators. **Contemporary Physics**, Taylor & Francis, v. 57, n. 2, p. 188–214, 2016. Citation on page 120.

NASCIMENTO, D.; COSTA, L.; LEITE, J.; EDWARDS, D.; SANTOS, T.; LOUZADA, F. Bayesian dynamic graphical models: Analyzing brainwave data from fixed parameters to hierarchical design. **Information Sciences**, in press. Citations on pages 29, 58, and 66.

NASCIMENTO, D. C.; COSTA, L.; LEITE, J. P.; EDWARDS, D. J.; SANTOS, T.; LOUZADA, F. Bayesian dynamic graphical models: Analyzing a brainwaves task from fix parameters to the hierarchical design. **Information Sciences Journal**, Elsevier, in press. Citations on pages 77 and 82.

NASCIMENTO, D. C.; DEPETRI, G.; STEFANO, L. H.; ANACLETO, O.; LEITE, J. P.; EDWARDS, D. J.; SANTOS, T. E.; NETO, F. L. Entropy analysis of high-definition transcranial electric stimulation effects on eeg dynamics. **Brain sciences**, Multidisciplinary Digital Publishing Institute, v. 9, n. 8, p. 208, 2019. Citations on pages 31, 77, 119, and 128.

NASSERI, P.; NITSCHE, M. A.; EKHTIARI, H. A framework for categorizing electrode montages in transcranial direct current stimulation. **Frontiers in human neuroscience**, Frontiers, v. 9, p. 54, 2015. Citation on page 37.

NATARAJAN, K.; ACHARYA, R.; ALIAS, F.; TIBOLENG, T.; PUTHUSSERYPADY, S. K. Nonlinear analysis of eeg signals at different mental states. **BioMedical Engineering OnLine**, BioMed Central, v. 3, n. 1, p. 7, 2004. Citation on page 120.

NEAPOLITAN, R. E. **Learning bayesian networks: Pearson Prentice Hall Upper Saddle River**. [S.l.]: NJ, 2004. Citation on page 79.

NETO, E.; CARVALHO, F. D. Symbolic approach to analyzing administrative management. **The Electronic Journal of Symbolic Data Analysis**, v. 1, n. 1, p. 1–13, 2002. Citation on page 100.

NETO, E. A. L.; CARVALHO, F. A. T. D. An exponential-type kernel robust regression model for interval-valued variables. **Information Sciences**, v. 454-455, p. 419 – 442, 2018. ISSN 0020-0255. Citation on page 100.

NETO, E. d. A. L.; CARVALHO, F. d. A. de. Centre and range method for fitting a linear regression model to symbolic interval data. **Computational Statistics & Data Analysis**, Elsevier, v. 52, n. 3, p. 1500–1515, 2008. Citation on page 104.

NEWSON, J. J.; THIAGARAJAN, T. C. Eeg frequency bands in psychiatric disorders: a review of resting state studies. **Frontiers in human neuroscience**, Frontiers, v. 12, p. 521, 2018. Citation on page 126.

NITSCHE, M. A.; LIEBETANZ, D.; ANTAL, A.; LANG, N.; TERGAU, F.; PAULUS, W. Modulation of cortical excitability by weak direct current stimulation–technical, safety and functional aspects. In: **Supplements to Clinical neurophysiology**. [S.l.]: Elsevier, 2003. v. 56, p. 255–276. Citations on pages 40 and 118.

NITSCHE, M. A.; PAULUS, W. Excitability changes induced in the human motor cortex by weak transcranial direct current stimulation. **The Journal of physiology**, Wiley Online Library, v. 527, n. 3, p. 633–639, 2000. Citation on page 39.

NOIRHOMME-FRAITURE, M.; BRITO, P. Far beyond the classical data models: symbolic data analysis. **Statistical Analysis and Data Mining: the ASA Data Science Journal**, Wiley Online Library, v. 4, n. 2, p. 157–170, 2011. Citation on page 99.

OCTAVE Forge SourceForge Project. 2007. Available: <https://octave.sourceforge.io/>. Accessed: 10/05/2019. Citation on page 126.

OLCAY, A. H. Mean residual life function for certain types of non-monotonic ageing. **Communications in statistics. Stochastic models**, Taylor & Francis, v. 11, n. 1, p. 219–225, 1995. Citation on page 162.

OMBAO, H.; HO, M.-h. R. Time-dependent frequency domain principal components analysis of multichannel non-stationary signals. **Computational statistics & data analysis**, Elsevier, v. 50, n. 9, p. 2339–2360, 2006. Citation on page 127.

OZAKI, T. **Time series modeling of neuroscience data**. [S.l.]: CRC Press, 2012. Citation on page 78.

PAAKKI, J.-J.; RAHKO, J.; LONG, X.; MOILANEN, I.; TERVONEN, O.; NIKKINEN, J.; STARCK, T.; REMES, J.; HURTIG, T.; HAAPSAMO, H. *et al.* Alterations in regional homogeneity of resting-state brain activity in autism spectrum disorders. **Brain research**, Elsevier, v. 1321, p. 169–179, 2010. Citations on pages 31, 55, 72, and 112.

PARENT, A. Giovanni aldini: from animal electricity to human brain stimulation. **Canadian Journal of Neurological Sciences**, Cambridge University Press, v. 31, n. 4, p. 576–584, 2004. Citation on page 39.

PARKS, T. W.; BURRUS, C. S. **Digital filter design**. [S.l.]: Wiley-Interscience, 1987. Citation on page 126.

PAVLOPOULOS, S. A.; DELOPOULOS, A. N. Designing and implementing the transition to a fully digital hospital. **IEEE Transactions on information technology in biomedicine**, IEEE, v. 3, n. 1, p. 6–19, 1999. Citations on pages 73 and 113.

PEARL, J. **Causality**. [S.l.]: Cambridge university press, 2009. Citation on page 78.

____. **Probabilistic reasoning in intelligent systems: networks of plausible inference**. [S.l.]: Elsevier, 2014. Citation on page 116.

PERDONÁ, G. C.; LOUZADA-NETO, F. A general hazard model for lifetime data in the presence of cure rate. **Journal of Applied Statistics**, Taylor & Francis, v. 38, n. 7, p. 1395–1405, 2011. Citation on page 179.

PÉRENNOU, D. Postural disorders and spatial neglect in stroke patients: a strong association. **Restorative neurology and neuroscience**, IOS Press, v. 24, n. 4-6, p. 319–334, 2006. Citations on pages 38, 50, and 57.

PÉREZ-CRUZ, F. Kullback-leibler divergence estimation of continuous distributions. In: IEEE. **Information Theory, 2008. ISIT 2008. IEEE International Symposium on**. [S.l.], 2008. p. 1666–1670. Citation on page 46.

PETRIS, G.; PETRONE, S.; CAMPAGNOLI, P. Dynamic linear models. In: **Dynamic Linear Models with R**. [S.l.]: Springer, 2009. p. 31–84. Citations on pages 62, 82, 83, 104, and 121.

PIMENTEL, B. A.; SOUZA, R. M. de. A weighted multivariate fuzzy c-means method in interval-valued scientific production data. **Expert Systems with Applications**, Elsevier, v. 41, n. 7, p. 3223–3236, 2014. Citations on pages 98 and 100.

PINCUS, S. M. Approximate entropy as a measure of system complexity. **Proceedings of the National Academy of Sciences**, National Acad Sciences, v. 88, n. 6, p. 2297–2301, 1991. Citations on pages 36, 42, 45, 83, and 84.

PINCUS, S. M.; GLADSTONE, I. M.; EHRENKRANZ, R. A. A regularity statistic for medical data analysis. **Journal of clinical monitoring**, Springer, v. 7, n. 4, p. 335–345, 1991. Citations on pages 36, 37, and 48.

PLEWNIA, C.; LOTZE, M.; GERLOFF, C. Disinhibition of the contralateral motor cortex by low-frequency rtms. **Neuroreport**, LWW, v. 14, n. 4, p. 609–612, 2003. Citations on pages 40 and 118.

PRADO, R.; MOLINA, F.; HUERTA, G. Multivariate time series modeling and classification via hierarchical var mixtures. **Computational Statistics & Data Analysis**, Elsevier, v. 51, n. 3, p. 1445–1462, 2006. Citation on page 121.

PRADO, R.; WEST, M. **Time series: modeling, computation, and inference**. [S.l.]: CRC Press, 2010. Citations on pages 126 and 127.

PRADO, R.; WEST, M.; KRYSTAL, A. D. Multichannel electroencephalographic analyses via dynamic regression models with time-varying lag–lead structure. **Journal of the Royal Statistical Society: Series C (Applied Statistics)**, Wiley Online Library, v. 50, n. 1, p. 95–109, 2001. Citations on pages 31 and 54.

PRIGOGINE, I. The meaning of entropy. In: **Evolutionary Epistemology**. [S.l.]: Springer, 1987. p. 57–73. Citation on page 35.

PRIORI, A.; BERARDELLI, A.; RONA, S.; ACCORNERO, N.; MANFREDI, M. Polarization of the human motor cortex through the scalp. **Neuroreport**, LWW, v. 9, n. 10, p. 2257–2260, 1998. Citations on pages 39 and 118.

QUEEN, C. M.; SMITH, J. Q. Multiregression dynamic models. **Journal of the Royal Statistical Society: Series B (Methodological)**, Wiley Online Library, v. 55, n. 4, p. 849–870, 1993. Citations on pages 55, 58, 60, 82, and 133.

RAKOTOMAMONJY, A. Surveying and comparing simultaneous sparse approximation (or group-lasso) algorithms. **Signal processing**, Elsevier, v. 91, n. 7, p. 1505–1526, 2011. Citation on page 124.

RAMOS, P. L.; LOUZADA, F.; RAMOS, E. An efficient, closed-form map estimator for nakagami-m fading parameter. **IEEE Communications Letters**, IEEE, v. 20, n. 11, p. 2328–2331, 2016. Citations on pages 168 and 169.

READING, M.; BABYAR, S.; SANTOS-PONTELLI, T.; LEMOS, T.; EDWARDS, D. Parietal-insular-vestibular tdcs for treatment of lateropulsion following stroke. **Brain Stimulation**, Elsevier, v. 1, n. 10, p. e5, 2017. Citation on page 98.

RESTREPO, J. F.; SCHLOTTHAUER, G.; TORRES, M. E. Maximum approximate entropy and r threshold: A new approach for regularity changes detection. **Physica A: Statistical Mechanics and its Applications**, Elsevier, v. 409, p. 97–109, 2014. Citation on page 84.

REVFEIM, K. Approximation for the cumulative and inverse gamma distribution. **Statistica neerlandica**, Wiley Online Library, v. 45, n. 3, p. 327–331, 1991. Citation on page 158.

RICHMAN, J. S.; MOORMAN, J. R. Physiological time-series analysis using approximate entropy and sample entropy. **American Journal of Physiology-Heart and Circulatory Physiology**, American Physiological Society Bethesda, MD, v. 278, n. 6, p. H2039–H2049, 2000. Citation on page 36.

RODGER, J. A. Discovery of medical big data analytics: Improving the prediction of traumatic brain injury survival rates by data mining patient informatics processing software hybrid hadoop hive. **Informatics in Medicine Unlocked**, Elsevier, v. 1, p. 17–26, 2015. Citation on page 111.

RODRIGUES, F. A.; PERON, T. K. D.; JI, P.; KURTHS, J. The kuramoto model in complex networks. **Physics Reports**, Elsevier, v. 610, p. 1–98, 2016. Citations on pages 120 and 132.

ROSSI, S.; HALLETT, M.; ROSSINI, P. M.; PASCUAL-LEONE, A. Safety, ethical considerations, and application guidelines for the use of transcranial magnetic stimulation in clinical practice and research. **Clinical neurophysiology**, Elsevier, v. 120, n. 12, p. 2008–2039, 2009. Citation on page 38.

ROSSINI, P. M.; ROSSI, S. Transcranial magnetic stimulation diagnostic, therapeutic, and research potential. **Neurology**, AAN Enterprises, v. 68, n. 7, p. 484–488, 2007. Citation on page 38.

RUBIN, P.; HOLM, S.; FRIBERG, L.; VIDEBECH, P.; ANDERSEN, H. S.; BENDSEN, B. B.; STRØMSØ, N.; LARSEN, J. K.; LASSEN, N. A.; HEMMINGSEN, R. Altered modulation of prefrontal and subcortical brain activity in newly diagnosed schizophrenia and schizophreniform disorder: A regional cerebral blood flow study. **Archives of General Psychiatry**, American Medical Association, v. 48, n. 11, p. 987–995, 1991. Citations on pages 31, 55, 72, and 112.

SACHS, K.; PEREZ, O.; PE'ER, D.; LAUFFENBURGER, D. A.; NOLAN, G. P. Causal protein-signaling networks derived from multiparameter single-cell data. **Science**, American Association for the Advancement of Science, v. 308, n. 5721, p. 523–529, 2005. Citations on pages 60 and 61.

SANTOS-PONTELLI, T. E.; RIMOLI, B. P.; FAVORETTO, D. B.; MAZIN, S. C.; TRUONG, D. Q.; LEITE, J. P.; PONTES-NETO, O. M.; BABYAR, S. R.; REDING, M.; BIKSON, M. *et al.* Polarity-dependent misperception of subjective visual vertical during and after transcranial direct current stimulation (tdcs). **PloS one**, Public Library of Science, v. 11, n. 3, p. e0152331, 2016. Citations on pages 37, 57, and 98.

SANTOS, T. E.; EDWARDS, D. Non-invasive brain stimulation to treat disorders of human verticality. **Neurologie & Rehabilitation**, v. 25, p. 50–53, 2019. Citations on pages 72, 112, and 127.

SANTOS, T. E.; FAVORETTO, D. B.; TOOSTANI, I. G.; NASCIMENTO, D.; RIMOLI, B. P.; BERGONZONI, E.; LEMOS, T. W.; TRUONG, D. Q.; DELBEM, A. C.; MAKKIABADI, B.; MORAES, R.; LOUZADA, F.; BIKSON, M.; LEITE, J.; EDWARDS, D. Manipulation of human verticality using high-definition transcranial direct current stimulation. **Frontiers in neurology**, Frontiers, v. 9, p. 825, 2018. Citations on pages 16, 20, 31, 32, 36, 37, 45, 50, 54, 57, 66, 78, 90, 99, 101, 117, 118, 119, 120, 127, 131, 132, and 135.

SARKAR, S.; GOEL, N.; MATHUR, B. Performance investigation of nakagami-m distribution to derive flood hydrograph by genetic algorithm optimization approach. **Journal of Hydrologic Engineering**, American Society of Civil Engineers, v. 15, n. 8, p. 658–666, 2010. Citation on page 158.

SCANAGATTA, M.; CAMPOS, C. P. de; CORANI, G.; ZAFFALON, M. Learning bayesian networks with thousands of variables. In: **Advances in neural information processing systems**. [S.l.: s.n.], 2015. p. 1864–1872. Citation on page 60.

SCHEFFER-TEIXEIRA, R.; BELCHIOR, H.; LEAO, R. N.; RIBEIRO, S.; TORT, A. B. On high-frequency field oscillations (> 100 hz) and the spectral leakage of spiking activity. **Journal of Neuroscience**, Soc Neuroscience, v. 33, n. 4, p. 1535–1539, 2013. Citation on page 126.

SCHLÖGL, A.; SUPP, G. Analyzing event-related eeg data with multivariate autoregressive parameters. **Progress in brain research**, Elsevier, v. 159, p. 135–147, 2006. Citation on page 121.

SCHWARTZ, J.; GODWIN, R. T.; GILES, D. E. Improved maximum-likelihood estimation of the shape parameter in the nakagami distribution. **Journal of Statistical Computation and Simulation**, Taylor & Francis, v. 83, n. 3, p. 434–445, 2013. Citation on page 166.

SCUTARI, M. Learning bayesian networks with the bnlearn r package. **arXiv preprint arXiv:0908.3817**, 2009. Citation on page 80.

SHANKAR, P. M.; DUMANE, V.; REID, J. M.; GENIS, V.; FORSBERG, F.; PICCOLI, C. W.; GOLDBERG, B. B. Classification of ultrasonic b-mode images of breast masses using nakagami distribution. **IEEE transactions on ultrasonics, ferroelectrics, and frequency control**, IEEE, v. 48, n. 2, p. 569–580, 2001. Citation on page 158.

SHEKHAWAT, G. S.; SUNDRAM, F.; BIKSON, M.; TRUONG, D.; RIDDER, D. D.; STINEAR, C. M.; WELCH, D.; SEARCHFIELD, G. D. Intensity, duration, and location of high-definition transcranial direct current stimulation for tinnitus relief. **Neurorehabilitation and neural repair**, SAGE Publications Sage CA: Los Angeles, CA, v. 30, n. 4, p. 349–359, 2016. Citation on page 39.

SHEN, Y.; BAINGANA, B.; GIANNAKIS, G. B. Nonlinear structural vector autoregressive models for inferring effective brain network connectivity. **arXiv preprint arXiv:1610.06551**, 2016. Citations on pages 54 and 128.

SHINKAREVA, S. V.; OMBAO, H. C.; SUTTON, B. P.; MOHANTY, A.; MILLER, G. A. Classification of functional brain images with a spatio-temporal dissimilarity map. **Neuroimage**, Elsevier, v. 33, n. 1, p. 63–71, 2006. Citation on page 54.

SIEBNER, H.; PELLER, M.; WILLOCH, F.; MINOSHIMA, S.; BOECKER, H.; AUER, C.; DRZEZGA, A.; CONRAD, B.; BARTENSTEIN, P. Lasting cortical activation after repetitive tms of the motor cortex: a glucose metabolic study. **Neurology**, AAN Enterprises, v. 54, n. 4, p. 956–963, 2000. Citations on pages 40 and 118.

SIEBNER, H. R.; HARTWIGSEN, G.; KASSUBA, T.; ROTHWELL, J. C. How does transcranial magnetic stimulation modify neuronal activity in the brain? implications for studies of cognition. **cortex**, Elsevier, v. 45, n. 9, p. 1035–1042, 2009. Citation on page 39.

SIGGIRIDOU, E.; KOUTLIS, C.; TSIMPIRIS, A.; KUGIUMTZIS, D. Evaluation of granger causality measures for constructing networks from multivariate time series. **Entropy**, Multidisciplinary Digital Publishing Institute, v. 21, n. 11, p. 1080, 2019. Citation on page 79.

SILVA, A. D.; LECHEVALLIER, Y.; CARVALHO, F. de; TROUSSE, B. Mining web usage data for discovering navigation clusters. In: IEEE. **11th IEEE Symposium on Computers and Communications (ISCC'06)**. [S.l.], 2006. p. 910–915. Citation on page 100.

SIMS, C. A. Money, income, and causality. **The American economic review**, JSTOR, v. 62, n. 4, p. 540–552, 1972. Citation on page 77.

SOLO, V. State-space analysis of granger-geweke causality measures with application to fmri. **Neural computation**, MIT Press, v. 28, n. 5, p. 914–949, 2016. Citation on page 77.

SONG, K.-S. Globally convergent algorithms for estimating generalized gamma distributions in fast signal and image processing. **IEEE Transactions on Image Processing**, IEEE, v. 17, n. 8, p. 1233–1250, 2008. Citation on page 158.

SORIA-FRISCH, A.; RIERA, A.; DUNNE, S. Fusion operators for multi-modal biometric authentication based on physiological signals. In: IEEE. **Fuzzy Systems (FUZZ), 2010 IEEE International Conference on**. [S.l.], 2010. p. 1–7. Citations on pages 73 and 113.

SOUZA, L. C.; SOUZA, R. M.; AMARAL, G. J.; FILHO, T. M. S. A parametrized approach for linear regression of interval data. **Knowledge-Based Systems**, v. 131, p. 149 – 159, 2017. ISSN 0950-7051. Citation on page 100.

STAGG, C. J.; BEST, J. G.; STEPHENSON, M. C.; O'SHEA, J.; WYLEZINSKA, M.; KINCSES, Z. T.; MORRIS, P. G.; MATTHEWS, P. M.; JOHANSEN-BERG, H. Polarity-sensitive modulation of cortical neurotransmitters by transcranial stimulation. **Journal of Neuroscience**, Soc Neuroscience, v. 29, n. 16, p. 5202–5206, 2009. Citation on page 40.

SU, L.; WANG, L.; SHEN, H.; FENG, G.; HU, D. Discriminative analysis of non-linear brain connectivity in schizophrenia: an fmri study. **Frontiers in human neuroscience**, Frontiers, v. 7, p. 702, 2013. Citation on page 126.

TEPLAN, M. *et al.* Fundamentals of eeg measurement. **Measurement science review**, v. 2, n. 2, p. 1–11, 2002. Citation on page 99.

TIBSHIRANI, R.; BIEN, J.; FRIEDMAN, J.; HASTIE, T.; SIMON, N.; TAYLOR, J.; TIBSHIRANI, R. J. Strong rules for discarding predictors in lasso-type problems. **Journal of the Royal Statistical Society: Series B (Statistical Methodology)**, Wiley Online Library, v. 74, n. 2, p. 245–266, 2012. Citation on page 122.

TSUI, P.; HUANG, C.; WANG, S. Use of nakagami distribution and logarithmic compression in ultrasonic tissue characterization. **Journal of Medical and Biological Engineering**, WALTER H CHANG, v. 26, n. 2, p. 69, 2006. Citation on page 158.

VENUGOPAL, D.; GOGATE, V. On lifting the gibbs sampling algorithm. In: **Advances in Neural Information Processing Systems**. [S.l.: s.n.], 2012. p. 1655–1663. Citation on page 107.

WANG, H.; GUAN, R.; WU, J. Linear regression of interval-valued data based on complete information in hypercubes. **Journal of Systems Science and Systems Engineering**, v. 21, n. 4, p. 422 – 442, 2012. Citation on page 100.

WANG, N.; SONG, X.; CHENG, J. Generalized method of moments estimation of the nakagami-m fading parameter. **IEEE Transactions on Wireless Communications**, IEEE, v. 11, n. 9, p. 3316–3325, 2012. Citation on page 158.

WERMUTH, N.; LAURITZEN, S. L. On substantive research hypotheses, conditional independence graphs and graphical chain models. **Journal of the Royal Statistical Society: Series B (Methodological)**, Wiley Online Library, v. 52, n. 1, p. 21–50, 1990. Citation on page 125.

WEST, M.; HARRISON, J. **Bayesian forecasting and dynamic models**. [S.l.]: Springer Science & Business Media, 1989. Citations on pages 54, 62, 82, 83, 104, 120, and 121.

WEST, M.; HARRISON, P. J.; MIGON, H. S. Dynamic generalized linear models and bayesian forecasting. **Journal of the American Statistical Association**, Taylor & Francis Group, v. 80, n. 389, p. 73–83, 1985. Citation on page 120.

WHITTAKER, J. **Graphical models in applied multivariate statistics**. [S.l.]: Wiley Publishing, 2009. Citation on page 78.

WHITTLE, P. Estimation and information in stationary time series. **Arkiv för matematik**, Springer, v. 2, n. 5, p. 423–434, 1953. Citation on page 59.

____. **Some recent contributions to the theory of stationary processes**. [S.l.: s.n.], 1954. Citation on page 59.

WIENER, N. **Modern mathematics for the engineer, chapter The theory of prediction**. [S.l.]: MacGrawHill, 1956. Citation on page 78.

WINDHORST, U.; JOHANSSON, H. **Modern techniques in neuroscience research**. [S.l.]: Springer Science & Business Media, 2012. Citations on pages 55, 56, and 57.

WINTER, D. A. Human balance and posture control during ding and walking. **Gait & posture**, Elsevier, v. 3, n. 4, p. 193–214, 1995. Citations on pages 38, 57, 117, and 118.

WIPF, D.; NAGARAJAN, S. **Iterative Reweighted 1 and 2 Methods for Finding Sparse Solutions. UC San Francisco**. [S.l.], 2008. Citation on page 124.

WOJCIK, G. M.; MASIAK, J.; KAWIAK, A.; KWASNIEWICZ, L.; SCHNEIDER, P.; POLAK, N.; GAJOS-BALINSKA, A. Mapping the human brain in frequency band analysis of brain cortex electroencephalographic activity for selected psychiatric disorders. **Frontiers in neuroinformatics**, Frontiers Media SA, v. 12, 2018. Citation on page 126.

YENTES, J. M.; DENTON, W.; MCCAMLEY, J.; RAFFALT, P. C.; SCHMID, K. K. Effect of parameter selection on entropy calculation for long walking trials. **Gait & posture**, Elsevier, v. 60, p. 128–134, 2018. Citation on page 36.

YI, B.-K.; FALOUTSOS, C. Fast time sequence indexing for arbitrary lp norms. In: VLDB. [S.l.], 2000. Citation on page 69.

ZANABRIA, G. G.; SILVEIRA, J. A.; POCO, J.; PAIVA, A.; NERY, M. B.; SILVA, C. T.; ABREU, S. F. A. de; NONATO, L. G. Crimanalyzer: Understanding crime patterns in são paulo. **IEEE transactions on visualization and computer graphics**, IEEE, 2019. Citation on page 76.

ZEEMERING, S. **Sparse estimation: applications in atrial fibrillation**. Phd Thesis (PhD Thesis) — Maastricht University, 2015. Citation on page 122.

ZHANG, W.; CHIEN, J.; YONG, J.; KUANG, R. Network-based machine learning and graph theory algorithms for precision oncology. **NPJ precision oncology**, Nature Publishing Group, v. 1, n. 1, p. 1–15, 2017. Citation on page 77.

ZHAO, X.; ZHOU, X. Modeling gap times between recurrent events by marginal rate function. **Computational Statistics & Data Analysis**, Elsevier, v. 56, n. 2, p. 370–383, 2012. Citations on pages 133 and 179.

ZHOU, J.; HAO, Y.; WANG, Y.; JOR'DAN, A.; PASCUAL-LEONE, A.; ZHANG, J.; FANG, J.; MANOR, B. Transcranial direct current stimulation reduces the cost of performing a cognitive task on gait and postural control. **European Journal of Neuroscience**, Wiley Online Library, v. 39, n. 8, p. 1343–1348, 2014. Citations on pages 31, 38, and 57.

ZOU, C.; FENG, J. Granger causality vs. dynamic bayesian network inference: a comparative study. **BMC bioinformatics**, BioMed Central, v. 10, n. 1, p. 122, 2009. Citation on page 79.

ZUCCOLOTTO, P. Principal components of sample estimates: an approach through symbolic data analysis. **Statistical Methods and Applications**, Springer, v. 16, n. 2, p. 173–192, 2007. Citation on page 100.


ICMC
USP
SÃO CARLOS